A Biomaterials Approach for Therapeutic Angiogenesis

A Thesis Submitted for the degree of Doctor of Philosophy, University College London

Eseelle Kathreen Hendow

Declaration

‘I, Eseelle Kathreen Hendow confirm that the work presented in this thesis is my own. Where information has been derived from other sources, I confirm that this has been indicated in the thesis.’

Acknowledgements

Foremost, I would like to sincerely thank my primary supervisor Professor Richard Day for his continuous guidance, motivation and enthusiasm. His support throughout the years has been invaluable and I could not have asked for a better mentor. Many thanks go to my secondary supervisor, Dr Caroline Pellet-Many, who was instrumental for the progression of this project into pre-clinical work and whose support was always valued.

I am hugely grateful to past and present members of the Applied Biomedical Engineering group for their comradery, encouragement and support throughout the years.

I would also like to thank my family and friends for seeing me through the highs and lows, specifically my partner Dr Oliver Page for his daily encouragement, love and patience, and to my sister Layla Hendow, who undertaking PhD herself, was the best advocate and support I could have wished for.

Finally, I would like to thank the British Heart Foundation for funding this project, without which it would not have been possible.

Abstract

Peripheral arterial disease (PAD) affects over 200 million people worldwide and can lead to limb ischaemia, amputation and death. Therapeutic angiogenesis aims to promote the formation of new blood vessels in order to treat ischaemia. The programming inherent within cells can be utilised to treat diseases at the cellular level. Adipose derived mesenchymal stem cells (ADMSCs) have been shown to secrete pro-angiogenic proteins, thus could have great potential as a therapy for ischemic disease. In addition, biomaterials can effectively deliver therapeutics to a target site and utilise physical characteristics to influence cell behaviour. Surface topography is known to influence cell alignment, morphology and affect cellular expression of growth factors. This work investigated the effect of surface topography on the secretion of angiogenic growth factors from ADMSCs.

Hierarchically structured substrate materials were prepared from poly-DL-lactide-co-glycolide (PLGA) using a thermally induced phase separation (TIPS) process. TIPS materials were characterised using atomic force microscopy to quantify roughness and stiffness, as well as scanning electron microscopy techniques where PLGA processed with TIPS were shown to have higher surface roughness and porosity values. ADMSC proliferation increased on the TIPS-processed substrates compared with the control substrates and the effect of surface topography on the angiogenic secretome of ADMSCs was measured using an *in vitro* model of angiogenesis, proteomic analysis and measurement of vascular endothelial growth factor ($VEGF_{165}$). $VEGF_{165}$ was significantly increased in the supernatants collected from ADMSCs cultured on the TIPS substrate compared with control substrates when normalised for the number of cells. The collected supernatants resulted in increased capillary tubule length, number of capillary junctions and capillary branches in the in vitro angiogenesis assay compared with supernatants collected from control substrates.

This work also investigated the effects of TIPS-processed materials implanted in a pre-clinical model of PAD. Laser Doppler imaging revealed an increase in revascularisation in the ischeamic limbs treated TIPS processed materials compared with control materials. Histology and von Willebrand factor staining revealed evidence of blood vessel formation around the implanted TIPS processed materials.

This study has shown that ADMSCs seeded onto 2D and 3D TIPS-processed PLGA secreted increased quantities of pro-angiogenic factors *in vitro*, and when implanted *in vivo,* TIPS-processed biomaterials improved reperfusion in a pre-clinical model of PAD. These findings open up the opportunity for utilising a unique biomaterial for the treatment of ischemic disease through the promotion of angiogenesis.

Table of Contents

Conferences and Presentations

26/03/15 - BHF Student Conference Cambridge, UK - Attendance

24/04/15 - Division of Medicine Research Retreat London, UK - Attendance

18/05/15 - 21/05/15 - Challenges in Science and Technology of Polymer Materials, Polynova Project, Bulgaria - Poster Presentation

05/09/15 - 10th International Workshop on Cardiovascular Biology and Translational Medicine London, UK – Attendance

18/01/16 - 5th Annual UCL Cardiovascular Science Symposium London, UK – Poster Presentation

24/03/16 - Biological Making Workshop UCL London, UK – Attendance

11/04/16 - BHF Student Conference Glasgow, Scotland – Attendance

20/04/16 - 21/04/16 – UKICRS Conference Cardiff, Wales – Poster Presentation

26/05/16 - Division of Medicine Research Retreat London, UK – Poster Presentation

28/06/16 - 01/07/16 – TERMIS (Tissue Engineering and Regenerative Medicine International Society) EU Conference Upsala, Sweden – Poster Presentation

21/07/16 - Faculty of Medicine Research Retreat London, UK – Poster Presentation and Poster Prize Winner

19/07/16 - Faculty of Medicine Graduate Research Day London, UK – Poster Presentation

16/03/17 - The 6th Annual UCL Cardiovascular Science Symposium 2017 London, UK – Poster Presentation

06/04/17 – 111th Annual meeting of the Association of Physicians, London, UK – Poster Presentation

26/07/17 - 30/06/17 – TERMIS (Tissue Engineering and Regenerative Medicine International Society) EU Conference Davos, Switzerland – Poster Presentation

19/09/17 – 22/03/18 – The Evaluation Exchange Programme, UCL Culture, UCL Public Engagement, UCL Innovation and Enterprise and Aston Mansfield

12/04/18 - BHF Annual 4-year PhD Conference, Edinburgh – Oral Presentation

25/04/18 – UCL Stem Cell Research Symposium London, UK – Poster Presentation and Poster Prize Winner

16/05/18 - Faculty of Medicine Research Retreat London, UK – Poster Presentation

06/06/18 - UCL Seminar on Biomaterials & Tissue Engineering, London UK – Attendance

Publications

Hendow EK, Guhmann P, Wright B, Sofokleous P, Parmar N, Day RM, Biomaterials for hollow organ tissue engineering, Fibrogenesis Tissue Repair, 2016; 9:3.

Guhmann, P., Hendow, E., Maffioletti, S., Cappellari, O., Wells, K., Patrick, S., Day, R. IMPRESS Network Symposium: Delivery of myoblasts in an anchored state for sphincter muscle regeneration, eCM Meeting Abstracts, TERMIS EU, 2017

Hendow E, Pellet-Many C, Day R, Novel biomaterial-based approaches for therapeutic angiogenesis, eCM Meeting Abstracts, TERMIS EU, 2017

Paper in preparation – A Biomaterials Approach for Therapeutic Angiogenesis
Paper in preparation – TIPS Microparticles for Therapeutic Angiogenesis

Figures List

Part I. Chapter 2

Part I. Chapter 2

Part I. Chapter 3

Part I. Chapter 4

Part I. Chapter 5

Figure 5.3: Human angiogenesis proteome profiler array of proteins secreted from ADMSCs seeded onto 7507 TIPS polymer films and 7507 control polymer films. a) A heat map highlighting the pro-angiogenic proteins secreted. b) A heat map highlighting the anti-angiogenic proteins secreted.

Figure 5.4: Quantification of the V2a array from the secretomes from ADMSCs seeded onto PLGA 7507 TIPS polymer films, PLGA 7507 control polymer films, PLGA 7502 TIPS polymer films, PLGA 7502 control polymer films and polystyrene films a) tubule length b) tubule junctions c) tubule branches. (n=1) Where * = P<0.05, ** = P<0.01, *** = P<0.001 and **** = P<0.0001. Ordinary one-way ANOVA = **** (P<0.0001).

Figure 5.5: $VEGF_{165}$ secretion from ADMSCs seeded into cell inserts exposed to the degradation products from PLGA 7507 TIPS polymer films, PLGA 7507 control polymer films, PLGA 7502 TIPS polymer films, PLGA 7502 control polymer films and polystyrene films. (n=1) Two-way ANOVA with Geisser-Greenhouse correction = ** (P=0.0055).

Part I. Chapter 6

Figure 6.1: Laser-Doppler imaging showing the paws of mice that had undergone unilateral femoral artery ligation and superficial femoral artery excision post operatively and at days 14 and 21.

Figure 6.2: SEM images of 5mm 7507 PLGA TIPS polymer implants before a) and after hydrophilisation b). SEM images of 5mm 7507 PLGA control polymer implants before c) and after hydrophilisation d). Images e-g) show the thickness of the 7507 TIPS polymer implants.

Figure 6.3: Laser-Doppler imaging of the paws of mice that had undergone unilateral femoral artery ligation and subsequent implantation of 7507 PLGA TIPS processed films, control 7507 PLGA films and no treatment. Images were taken post-operatively and at days 7, 14 and 21.

Figure 6.4: Quantification of laser-doppler imaging of the paws of mice that had undergone unilateral femoral artery ligation and subsequent implantation of 7507 PLGA TIPS processed films, control 7507 PLGA films and no treatment. Results are shown as perfusion ratio at days 7, 14 and 21. (n=3)

Where * = P<0.05 and *** = P<0.001. Two-way ANOVA with Geisser-Greenhouse correction = * (P=0.0316).

Figure 6.5: H&E staining of tissue sections showing the implantation of PLGA TIPS polymer films and PLGA control polymer films. Red arrows indicate infiltration of cells into the surface of the 7507 TIPS polymer film implant into the hindlimb ischaemia model. Black arrows indicate evidence of blood vessel formation around the 7507 TIPS implant.

Figure 6.6: VWF staining of tissue sections showing the implantation of PLGA TIPS polymer films and PLGA control polymer films into the hindlimb ischaemia model. Black arrows highlight positive staining and indicate evidence of blood vessel formation.

Figure 6.7: H&E stained tissue sections showing collateral blood vessels within the gastrocnemius muscle from each *in vivo* condition a) 7507 TIPS microparticle implantation b-c) 7507 PLGA control microparticle implantation d-e) 7507 TIPS polymer film implantation f-g) 7507 PLGA control polymer film implantation h) granugel only control i) no treatment control j) no ischaemia and no treatment control.

Figure 6.8: Quantification of collaterals found through H&E staining a) outer vessel circumference measurements (µm) Ordinary One-Way ANOVA = **** (P=0.0004) b) lumen circumference measurements (µm) Ordinary One-Way ANOVA = ** (P=0.0034) c) vessel area (μm^2) Ordinary One-Way ANOVA = **** (P=0.0002) d) lumen area (μm^2). (n=5)

Figure 6.9: Quantification of VEGF-A, PDGFA, PEGF, FGF2 and NRP-1 expression (normalised to Actin) from qPCR. (n=1)

Figure 6.10: a) A heat map to show the differences in expression of angiogenic growth factor genes from ischemic tissues implanted with 7507 TIPS polymer film and 7507 control polymer film b) a heat map to show the expression of pro-angiogenic factor genes from ischemic tissues implanted with 7507 TIPS polymer film and 7507 control polymer film c) a heat map to show the expression of anti-angiogenic factors genes from ischemic tissues implanted with 7507 TIPS polymer film and 7507 control polymer film. (n=1)

Part I. Chapter 7

Figure 7.9: $VEGF_{165}$ secretion (pg/mL) from ADMSCs attached to PLGA 7507 TIPS polymer films, PLGA 7507 control films, 7502 TIPS polymer films, 7502 control polymer films and polystyrene polymer films at days 1, 4, 7 and 10 exposed to M1 (Two-way ANOVA with Geisser-Greenhouse correction = **** (P<0.0001)) and M2 (Two-way ANOVA with Geisser-Greenhouse correction = **** (P<0.0001)) phenotype macrophages. (n=5)

Figure 7.10: a) A heat map showing of the secretomes detected from the human angiogenesis proteome profiler array from M1 and M2 macrophages seeded onto 7507 TIPS polymer films and 7507 control polymer films. b) A heat map to show the pro-angiogenic factors from the proteome profiler array c) A heat map to show the anti-angiogenic factors from the proteome profiler array. (n=1)

Figure 7.11: A heat map displaying the proteins detected from the human cytokine proteome profiler array from M1 and M2 macrophages seeded onto 7507 TIPS polymer films and 7507 control polymer films. (n=1)

Part II. Chapter 2

Figure 2.1: SEM images of PLGA 7507 TIPS microparticles and PLGA 7502 TIPS microparticles.

Figure 2.2: SEM images of PLGA 7507 TIPS microparticles, PLGA 7507 control microparticles and polystyrene control microparticles at day 1, 4, 7 and 10.

Figure 2.3: SEM images of PLGA 7507 TIPS microparticles at a) day 1 b) day 4 c) day 7 and d) day 10.

Figure 2.4: a) pH measurements of PLGA 7507 TIPS microparticles.

Figure 2.5: b) Degradation of PLGA 7507 TIPS microparticles as weight percentage loss. (n=5) Weight loss at week 6 was statistically lower (P<0.01 = **) at week 6 from week 3 and at week 30 lower than week 3 (P<0.0001 = ****)

Figure 2.6: NanoCT images a) z-stack of PLGA 7507 TIPS microparticle b) z-stack of PLGA 7502 TIPS microparticle c) 3D reconstruction of PLGA 7507 TIPS polymer film side view d) 3D reconstruction of PLGA 7507 TIPS polymer film surface view e) 3D reconstruction of PLGA 7507 TIPS polymer film.

Figure 2.7: FIB-SEM images of PLGA 7507 TIPS microparticles a) 3µm mill into the radial pore of the microparticle b-f) internal structure of microparticles

Part II. Chapter 3

Figure 3.1: a) undifferentiated ADMSCs monolayer b) fluorescent image of lipidTOX green staining for adipogenic differentiation of ADMSC monolayer c) optical image of alcian blue staining for chondrogenic differentiation of ADMSC monolayer d) optical image of alizarin red staining for osteogenic differentiation of ADMSC monolayer e) fluorescent image of lipidTOX green staining for adipogenic differentiation of ADMSCs from 7507 TIPS microparticles f) optical image of alcian blue staining for chondrogenic differentiation of ADMSCs from 7507 TIPS microparticles g) optical image of alizarin red staining for osteogenic differentiation of ADMSCs from 7507 TIPS microparticles

Figure 3.2: a-c) Light microscopy images of 7507 TIPS microparticles seeded with ADMSCs d-e) Fluorescent images of DAPI stained ADMSCs seeded onto 7507 TIPS microparticles.

Figure 3.3: Optical imaging of ADMSCs seeded onto 7507 TIPS microparticles, 7507 control microparticles and polystyrene control microparticles at days 1, 4, 7 and 10.

Figure 3.4: Alexa Fluor 488 phalloidin and DAPI fluorescent images of ADMSCs seeded onto microparticles in hanging drops. a-b) Cellularised 7507 TIPS microparticles at day 1 c) Cellularised 7507 control microparticles at day 1 d) Cellularised 7507 TIPS microparticles at day 4.

Figure 3.5: Quantification of ADMSCs seeded at concentrations of 1000-8 cells/microparticle onto 7507 TIPS and 7502 TIPS microparticles in hanging drop plates compared to cell only controls calculated using CyQUANT NF cell proliferation assay. (n=5) Two-way ANOVA with Geisser-Greenhouse correction = ** (P=0.0024)

Figure 3.6: ADMSCs seeded at concentrations of 2000-31 cells/microparticle onto 7507 TIPS microparticles in hanging drop plates compared to cell only controls quantified with CellTox Green. (n=3) Two-way ANOVA with Geisser-Greenhouse correction = **** (P<0.0001)

Figure 3.7: PrestoBlue® cell viability assay optimisation experiments a) absorbance readings b) fluorescence. (n=3) Where * = P<0.05, ** = P<0.01 and **** = P<0.0001.

Figure 3.8: ADMSCs seeded at concentrations of 2000-8 cells/particle in hanging drop plates compared quantified with PrestoBlue® viability reagent. Where * = P<0.05, ** = P<0.01, *** = P<0.001 and **** = P<0.0001.

Figure 3.8: PrestoBlue® results of ADMSCs seeded at concentrations of 2000-8 cells/microparticle onto 7507 and 7502 TIPS microparticles in hanging drop plates compared to cell only controls. (n=3) Two-way ANOVA with Geisser-Greenhouse correction = **** (P<0.0001)

Figure 3.9: PrestoBlue® results of ADMSCs seeded onto 7507 TIPS microparticles, 7507 control microparticles and polystyrene control microparticles. (n=8) Two-way ANOVA with Geisser-Greenhouse correction = ** (P<0.0046)

Part II. Chapter 4

Figure 4.1: Quantification of cell numbers with PrestoBlue® cell viability reagent of ADMSCs attached to 7507 TIPS microparticles, 7507 PLGA control microparticles and polystyrene microparticles in hanging drop plate. (n=8) Two-way ANOVA with Geisser-Greenhouse correction = ** (P<0.0046)

Figure 4.2 a) $VEGF_{165}$ secretion (pg/mL) from ADMSCs attached to 7507 TIPS microparticles, 7507 PLGA control microparticles and polystyrene microparticles (n=7) b) Normalised results showing the amount of VEGF (pg/mL) secreted per cell. Two-way ANOVA with Geisser-Greenhouse correction = ** (P<0.00445)

Figure 4.3: A heat map showing all human Angiogenesis Proteome Profiler proteins secreted from ADMSCs seeded onto 7507 TIPS microparticles and 7507 control microparticles in comparison to polystyrene microparticles. (n=2)

Figure 4.4: Heat maps showing human proteome profiler proteins secreted from ADMSCs seeded onto 7507 TIPS microparticles and 7507 control microparticles in comparison to polystyrene microparticles at days 1, 4, 7 and 10.

Figure 4.5: Heat maps showing human pro-angiogenesis proteome profiler proteins secreted from ADMSCs seeded onto 7507 TIPS microparticles and 7507 control microparticles in comparison to polystyrene microparticles at days 1, 4, 7 and 10.

Figure 4.6: Heat maps showing human anti-angiogenesis proteome profiler proteins secreted from ADMSCs seeded onto 7507 TIPS microparticles and 7507 control microparticles in comparison to polystyrene microparticles at days 1, 4, 7 and 10.

Figure 4.7: Quantification of the V2a array from the secretomes from ADMSCs attached to PLGA 7507 TIPS microparticles, PLGA 7507 microparticles, and polystyrene microparticles a) tubule length b) tubule junctions c) tubule branches. (n=1) Where * = P<0.05, ** = P<0.01, *** = P<0.001 and **** = P<0.0001. Ordinary One-way ANOVA = **** (P<0.0001)

Figure 4.8: Quantification of the V2a array from the secretomes from ADMSCs attached to PLGA 7507 TIPS microparticles with the addition of the pro-angiogenic factor VEGF and anti-angiogenic factor PDGF a) tubule length b) tubule junctions c) tubule branches (n=1). Where * = P<0.05, ** = P<0.01, *** = P<0.001 and **** = P<0.0001. Ordinary One-way ANOVA = **** (P<0.0001)

Part II. Chapter 5

Figure 5.1: Quantification of laser-doppler imaging of the paws of mice that had undergone unilateral femoral artery ligation and subsequent implantation of 7507 PLGA TIPS processed microparticles in Aquaform, control 7507 PLGA microparticles in Aquaform, Aquaform only and no treatment. Results are shown as perfusion ratio at days 7, 14 and 21. (n=1)

Figure 5.2: Laser-doppler imaging of the paws of mice that had undergone unilateral femoral artery ligation and subsequent implantation of 7507 PLGA TIPS processed microparticles in GranuGEL, control 7507 PLGA microparticles in GranuGEL, GranuGEL only and no treatment. Images were taken post-operatively and at days 7, 14 and 21.

Figure 5.3: Quantification of laser-doppler imaging of the paws of mice that had undergone unilateral femoral artery ligation and subsequent implantation

of 7507 PLGA TIPS processed microparticles in GranuGEL, control 7507 PLGA microparticles in GranuGEL, GranuGEL only and no treatment. Results are shown as perfusion ratio at days 7, 14 and 21. (n=3) Two-way ANOVA with Geisser-Greenhouse correction = *. (P=0.015)

Figure 5.4: H&E staining of tissue sections showing the implantation of Aquaform gel in the hindlimb ischaemia model.

Figure 5.5: H&E staining of tissue sections showing the implantation of GranuGEL in the hindlimb ischaemia model.

Figure 5.6: H&E staining of tissue sections showing the implantation of PLGA 7507 TIPS microparticles into the hindlimb ischaemia model. Black arrows indicate evidence of blood vessel formation around the 7507 TIPS implant. Blue arrows indicate giant multinucleated cells.

Figure 5.7: H&E staining of tissue sections showing the implantation of PLGA 7507 control microparticles into the hindlimb ischaemia model. Blue arrows indicate giant multinucleated cells.

Figure 5.8: VWF staining of tissue sections showing the implantation of PLGA 7507 TIPS microparticles hindlimb ischaemia model. Black arrows highlight positive staining and indicate evidence of blood vessel formation.

Figure 5.9: VWF staining of tissue sections showing the implantation of PLGA 7507 control microparticles hindlimb ischaemia model.

Figure 5.10: H&E stained tissue sections showing collateral blood vessels within the gastrocnemius muscle from each *in vivo* condition a) 7507 TIPS microparticle implantation b-c) 7507 PLGA control microparticle implantation d) granugel only control e) no treatment control f) no ischaemia and no treatment control.

Figure 5.11: Quantification of collaterals from H&E staining a) outer vessel circumference measurements (µm) b) lumen circumference measurements (µm) c) vessel area (μm^2) d) lumen area (μm^2). (n=5) Ordinary one-way ANOVA = **** (P<0.0001).

Figure 5.12: H&E staining of tissue sections showing the implantation of PLGA 7507 TIPS microparticles into the hindlimb ischaemia model at weeks 1, 3, 6, 12 and 24. (n=1)

Figure 5.13: Quantification of VEGF-A, PDGFA, PEGF, FGF2 and NRP-1 expression from qPCR. (n=1) Where * = P<0.05, ** = P<0.01, *** = P<0.001 and **** = P<0.0001.

Part II. Chapter 6

Figure 6.1: Macrophage Cell Evidence around 7507 TIPS Microparticles implanted into a pre-clinical models of peripheral artery disease.

Figure 6.2: Anti-CD80 Staining on 7507 TIPS Microparticles implanted into a pre-clinical models of peripheral artery disease.

Figure 6.3: Anti-CD163 Staining on 7507 TIPS Microparticles implanted into a pre-clinical models of peripheral artery disease.

Figure 6.4: IL-12 p70 secretion from M1 and M2 phenotype macrophages. (n=5) Where * = P<0.05, ** = P<0.01, *** = P<0.001 and **** = P<0.0001.

Figure 6.5: IL-12 p70 secretion (pg/mL) from M0 macrophages differentiated into M1 (One-way ANOVA = **** (P<0.0001) and M2 phenotype macrophages attached to PLGA 7507 TIPS microparticles at days 1, 4, 7 and 10. (n=5)

Figure 6.6: $VEGF_{165}$ secretion (pg/mL) from M1 and M2 (One-way ANOVA = ** (P=0.001) phenotype macrophages attached to PLGA 7507 TIPS microparticles at days 1, 4, 7 and 10. (n=5)

Figure 6.7: $VEGF_{165}$ secretion (pg/mL) from ADMSCs attached to PLGA 7507 TIPS microparticles at days 1, 4, 7 and 10 exposed to M1 (One-way ANOVA = ** (P=0.0072)) and M2 (One-way ANOVA = * (P=0.033)) macrophage secretomes. (n=5)

Figure 6.8: $VEGF_{165}$ secretion (pg/mL) from ADMSCs attached to PLGA 7507 TIPS microparticles at day 10 in hanging drop plates in ADMSC culture media and exposed to M1 or M2 macrophage secretomes. M1 and M2 cells seeded onto 7507 TIPS microparticles VEGF secretion at day 10. Where * = P<0.05, ** = P<0.01, *** = P<0.001 and **** = P<0.0001. Ordinary one-way ANOVA = **** (P<0.0001)

Tables List

Part I. Chapter 2

Part I. Chapter 3

Part I. Chapter 6

Part II. Chapter 2

Part II. Chapter 3

Supplementary Figures List

Part I. Chapter 5

S5.3: Proteome profiler proteins from ADMSCs on 7507 TIPS and 7507 control polymer films were analysed through STRING Analysis for connections to molecular functions. Images show the connections between the secreted genes and proteins.

S5.4: Proteome profiler proteins from ADMSCs on 7507 control polymer films were analysed through STRING Analysis for connections to biological processes. Images show the connections between the secreted genes and proteins.

S5.5: A table detailing the functions of the proteins included in the human angiogenesis proteome profiler.

S5.6: Images from the V2a array tubules stained with anti-CD31. Images were analysed through Angio.Sys software and tubule length, branches and junctions were quantified.

Part I. Chapter 7

S7.1: STRING data identifying the links between the proteins secreted from M2 macrophages seeded onto 7507 TIPS polymer films. Yellow: Regulation of angiogenesis (5 genes, 2.4e-14 FD). Red: Cellular process (16 genes). Purple: Blood vessel development (5 genes, 4.32e-14 FD). Green: Vasculature development (5 genes, 5.43e-15 FD). Blue: ECM organisation (6 genes, 3.93e-18).

Part II. Chapter 2

S2.1: SEM images of the radial pore on the surface of 7507 TIPS microparticles.

Part II. Chapter 3

S3.1: PrestoBlue® optimisation experiments fluorescence readings of low cell numbers. Where * = $P<0.05$, ** = $P<0.01$, *** = $P<0.001$ and **** = $P<0.0001$.

Part II. Chapter 4

S4.1: $VEGF_{165}$ secretion (pg/mL) per ADMSC seeded onto 7507 TIPS microparticles, 7507 control microparticles and polystyrene microparticles at days 1, 4, 7 and 10.

S4.2: Proteome profiler proteins from ADMSCs on 7507 TIPS microparticles were analysed through STRING Analysis for connections to biological processes. Images show the connections between the secreted genes and proteins.

S4.3: Proteome profiler proteins from ADMSCs on 7507 control microparticles were analysed through STRING Analysis for connections to biological processes. Images show the connections between the secreted genes and proteins.

S4.4: Proteome profiler proteins from ADMSCs on polystyrene microparticles were analysed through STRING Analysis for connections to biological processes. Images show the connections between the secreted genes and proteins.

S4.5: Images from the V2a array tubules stained with anti-CD31. Images were analysed through Angio.Sys software and tubule length, branches and junctions were quantified.

S4.6: Images from the V2a array tubules stained with anti-CD31 where a pro- and anti- angiogenic factor was added to the 7507 TIPS microparticle sampels. Images were analysed through Angio.Sys software and tubule length, branches and junctions were quantified.

Part II. Chapter 5

S5.1 VWF staining of a-b) No treatment control c-d) GranuGEL only control e-f) No ischaemia control

Abbreviations List

A

ADMSCs - Adipose Derived Mesenchymal Stem Cells

ABPI - Ankle-Bronchial Pressure Index

ALI - Acute Limb Ischaemia

AVI - Acute Visceral Ischaemia

C

CAM – Chick Embryo Chorioallantoic Membrane Assay

CCL1/I-309 - Chemokine (C-C Motif) Ligand 1 Inflammatory Cytokine-309

cDNA – Complementary Deoxyribonucleic Acid

CLI - Critical Limb Ischaemia

CVD - Cardiovascular Disease

CXCL1/GROa - Growth Related Alpha Protein Ligand 1

C5/C5a - Complement Component 5/5a

D

DAPI - 4', 6-diamidino-2-phenylindole

DPPIV - Dipeptidyl Deptidase IV

DNA – Deoxyribonucleic Acid

E

ECM - Extracellular Matrix

EGF – Epidermal Growth Factor

EG-VEGF - Endocrine Gland-Derived Vascular Endothelial Growth Factor

ET-1 - Endothelin 1

F

FD – False Discovery Rate

FGF - Fibroblast Growth Factors

G

GA – Glycolic Acid

GDNF – Glial-Derived Neutrophic Factor

G-CSF - Granulocyte-Colony Stimulating Factor

GM-CSF – Granulocyte Macrophage Colony-Stimulating Factor

H

HB-EGF – Heparin-Binding EGF like growth factor

HCL – Hydrochloric Acid

HGF - Hepatocyte Growth Factor

HLI - Hindlimb Ischaemia

H&E – Haemoxylin & Eosin

I

IGF - Insulin Like Growth Factor

IL - Interleukin

INF – Interferon

L

LA – Lactic Acid

LAP – Leucine Aminopeptidase

LPS - Lipopolysaccharide

M

MCP-1 - Monocyte Chemoattractant Protein-1

MEK - 2-Butane/methyl ethyl ketone

MMPs- Matrix Metalloproteinases

MSCs - Mesenchymal Stem Cells

M0 - Macrophages

M1 – Macrophage Type 1 Phenotype

M2 – Macrophage Type 2 Phenotype

M-CSF – Macrophage Colony Stimulating Factor

N

NanoCT - Nano Computed Tomography

P

PAD - Peripheral Arterial Disease

PBS – Phosphate Buffered Serum

PCR - Polymerase Chain Reaction

PDGF- Platelet Derived Growth Factor

PEDF - Pigment Epithelium-Derived Growth Factor

PF4 – Platelet Factor 4

PIGF - Placental Growth Factor

PLC – Polycaprolactone

PLGA - Poly(lactic-co-glycolic acid)

R

RNA – Ribonucleic Acid

T

TGF - Transforming Growth Factor

TIPS – Thermally Induced Phase Separation

TIMP - Tissue Inhibitor of Metalloproteinases

TNF - Tumour Necrosis Factor

TSP – Thrombospondin

U

uPA - Urokinase-Type Plasminogen Activator

V

VEGF - Vascular Endothelial Growth Factors

VEGFR1 – Vascular Endothelial Growth Factor Receptor 1

VEGFR2 – Vascular Endothelial Growth Factor Receptor 2

VWF – Von Willebrand Factor

V2a – Vasculogenesis to Angiogenesis Array

Impact Statement

Cardiovascular disease is a leading cause of mortality worldwide, affecting an estimated 7 million people in the UK, with one in five people over the age of 60 suffering from peripheral arterial disease (PAD). [1-3] There are currently no curative treatments for this epidemic. Therefore, this project aimed to produce a device that can promote angiogenesis through the manufacture of a biomaterial in combination with stem cell therapy. This multidisciplinary research can bridge the gap between engineering and medicine, where the production of a novel biomaterial can be used to address the shortcomings of clinical research. [4, 5] Specifically, despite the recent advances in stem cell therapy for therapeutic angiogenesis, there are issues with retention of cells at the implant site. Biomaterials can overcome this by acting as a delivery vehicle and an anchor for the cells *in vivo,* allowing them to remain at the implant site and have their therapeutic effect. [6, 7] Moreover, the physical characteristics of a biomaterial can be used to promote angiogenesis without the need for chemical modification of the material or genetic modification of the cells. This project focuses on how the surface topography of the biomaterials can be utilised to influence the release of angiogenic growth factors from stem cells.

This research opens up opportunities for future pre-clinical and clinical studies of the administration of cellularised constructs, with research focusing on fully understanding the underlying cellular mechanism of the promotion of angiogenesis from stem cells seeded onto TIPS biomaterials. In addition, future studies can concentrate on determining the optimal construct (acellular or cellular, 2D or 3D biomaterial implants) for *in vivo* therapeutic angiogenesis.

Clinically, the potential impact of this research is great, with the possibility to save lives and improve quality of life; left untreated, the 1-year mortality rate of advanced PAD is 20% and there are strong links to the development of other cardiovascular diseases. The development of a curative treatment would not only impact positively on patients' lives, but it could also prove to be

economically beneficial. It would negate the need for long-term care, pharmaceuticals and treatments, which in aggregate currently cost the National Health Service approximately £200 million per year. [8]

The proposed therapy has various potential clinical applications, from non-invasive administration techniques to the implementation of personalised medicine using autologous stem cells. This technology also opens the prospect of investigation into its use in treating conditions other than PAD, such as myocardial infarction and wound healing; these may be improved or cured through the promotion of angiogenesis.

Chapter 1: Introduction

1.1 Peripheral Arterial Disease

Cardiovascular disease (CVD) is a term referring to the pathosis of the blood vessels or the heart. Disease progression is typically associated with an accumulation of atherosclerotic fatty deposits within the blood vessels, which gradually block the flow of blood. This can lead to the development of peripheral arterial disease (PAD), a cardiovascular disease of the peripheral arteries most commonly affecting the lower extremities. [9] PAD affects over 200 million people worldwide, [10] with 20% of people over the age of 60 in the UK affected. [11] PAD is usually exacerbated by lifestyle choices such as consumption of a high fat diets, smoking and lack of exercise. [12] With an ageing population and a Western obesity epidemic, PAD is becoming more prevalent and sufferers of PAD have an increased risk of developing other cardiovascular diseases. When considering other co-morbidities such as diabetes mellitus and kidney disease, the risk rises further. [13, 14] For example, it is estimated that up to 50% of people with PAD also have coronary artery disease. [15]

In the early stages, PAD can be asymptomatic, but the majority of sufferers will go on to develop symptoms and have a decreased quality of life. Symptoms range from intermittent claudication, paraesthesia, severe pain and tissue loss due to ulcers and gangrene. 10% of sufferers go on to develop limb ischaemia, [16] which falls into three categories of ischaemia; each conferring significant risk of mortality if left untreated. Acute limb ischaemia occurs when there is a sudden cessation of blood flow that severely affects the viability of the effected limb, with the major causes resulting in thrombosis and embolism that come with significant health risks. Critical limb ischaemia (CLI) is defined as occlusion of blood flow to the limbs, often originally presenting as intermittent claudication with the development of ulcers, gangrene and sever pain. For patients with claudication, up to 20% will develop CLI. Conditions such as diabetes can increase the likelihood of this tenfold, as well as being a

leading cause of leg ulcers where PAD exacerbates the wound. If left untreated the risk of amputation ranges from 70-95%, [17] with 1-year a 20% mortality rate. [18] Acute visceral ischaemia (AVI) is a rare but life-threatening condition with 30-day survival rates as low as 28%. AVI can occur when a thrombus forms in an occluded artery, creating an embolus which blocks blood flow resulting in visceral ischaemia of major organs such as the liver, bowels and spleen. This results in life-threatening ischaemia and risks irreversible tissue infarction. [19]

Current primary care treatment plans aim to improve quality of life by managing pain as well as lifestyle changes to reduce the progression of PAD and the risk of additional CVDs. [20] Such plans include cessation of smoking, physiotherapy to improve claudication and pharmacologic agents such as antihypertensives and statins. If these interventions are unsuccessful, surgical revascularisation may become necessary. This involves opening the arterial blockages by balloon angioplasty or bypassing blocked sections of artery using venous grafts. Surgery is only available to a limited cohort of patients, as the choice is dependent factors like co-morbidities and disease severity. Moreover, these operations are often unsuccessful. [21] In emergent cases where blood flow is completely restricted, a cascade of events is triggered within the tissue. The restriction of blood limits tissue perfusion and oxygenation so severely that aerobic metabolism ceases, resulting in the formation of harmful free radicals and reactive oxygen species that break down cell membranes. Apoptosis is activated, and cell necrosis ensues, [22-25] leading to irreversible damage with lower limb amputation being the only lifesaving treatment option. [10]

As there is no curative treatment currently available for PAD, there is a clear need for the development of an alternative therapeutic. Tissue engineering strategies using cell therapy to promote angiogenesis could provide a curative therapy by revascularising the ischemic tissue of patients with PAD and CLI. For an effective cellular treatment, the therapy should be scalable, cost-effective, biocompatible and efficiently delivered. [26] The use of biomaterials could overcome some of these challenges faced by cell therapies. This work

investigated the application of novel polymeric biomaterials, in combination with stem cell therapies, for inducing therapeutic angiogenesis to treat PAD.

1.2 Therapeutic Angiogenesis

Angiogenesis is the formation of new blood vessels from pre-existing vessels and involves a myriad of cell types and growth factors. [27] Therapeutic angiogenesis is a subset of regenerative medicine. The field's purpose is to improve and facilitate angiogenesis to revascularise ischemic tissues. The vast body of research into cell and molecular medicine has opened up more and more opportunities to develop novel therapies for incurable ischemic diseases. By understanding the angiogenic processes and the delivery of growth factors, drugs and/or cells can be used to stimulate and control angiogenesis to treat ischemic diseases. [28] These novel therapies could result in healed tissues, rather than prompting a wound-healing response that would ultimately result in less functional scar tissue. [29] Angiogenesis is initiated by inflammation or hypoxia, where HIF-α is produced. [30, 31] Nitric oxide stimulates vascular endothelial growth factors (VEGF-a, VEGF-b) and basic fibroblast growth factors (FGF-a, FGF-b) which stimulate endothelial cells in the basement membrane of the blood vessel. The stimulated endothelial cells secrete matrix metalloproteinases and additional enzymes that degrade the basement membrane. [32] As the basement membrane degrades, the endothelial cells migrate towards the angiogenic growth factors (primarily VEGF and FGF). [33] The endothelial cells begin to proliferate and deposit basement membrane proteins, forming blood vessel sprouts. The endothelial cells then secrete platelet-derived growth factor (PDGF-B), that recruits multipotent precursor cells to the site. [34] With the addition of transforming growth factor-β (TGF-[β]), precursor cells differentiate into pericytes and halt endothelial cell migration and proliferation. Pericytes surround blood vessels, providing support and stabilisation to the vessel by depositing extracellular matrix (ECM) molecules that inhibit endothelial cell migration. PDGF and TGF-[β] also recruit smooth muscle cells that help provide contractility to the blood vessels. [35-37]

One of the main challenges facing therapeutic angiogenesis is maintaining the dose of a therapy long enough for it to be effective. There are a variety of therapeutic options to treat PAD by stimulating angiogenesis. One of the most widely investigated approaches is the delivery of growth factors. A host of

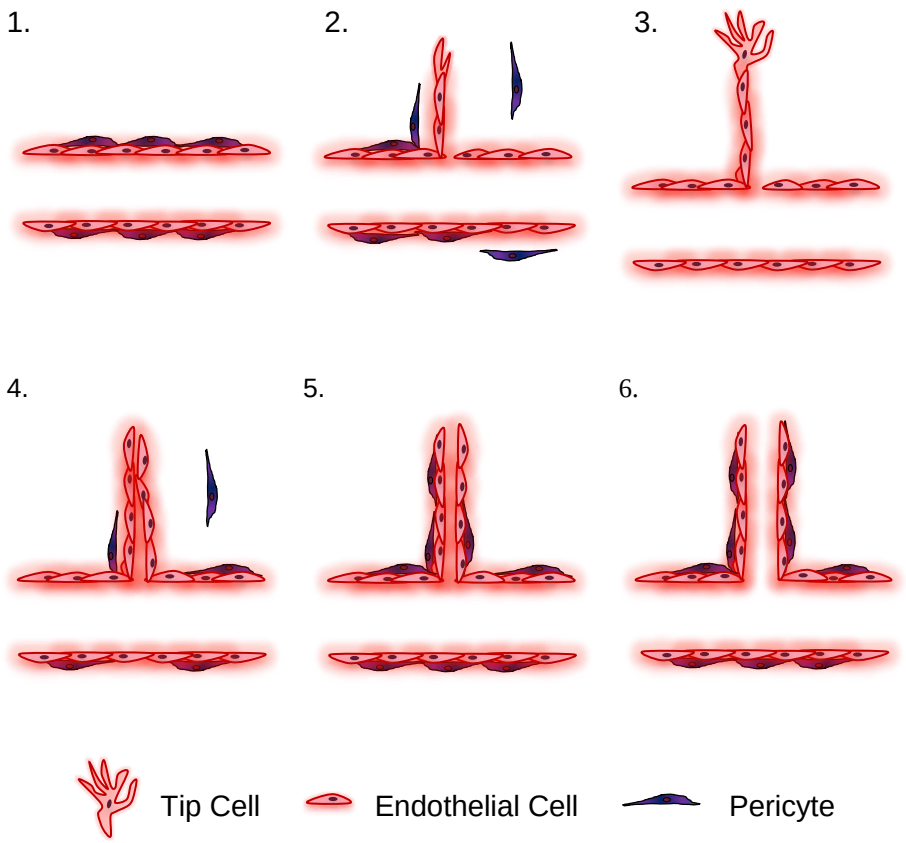

Figure 1.1: Schematic illustrating the main steps in angiogenesis. 1) Pre-existing blood vessel. Angiogenesis induced by hypoxia. 2) Endothelial cell activation stimulated by VEGF-A. Basement membrane begins to degrade and pericytes detach in the presence of Ang-2, VEGF, PDGF and MMPs. 3) Endothelial migration and Tip cell formation in the presence of VEGF-A, PLGF, FGF and MMPs. 4) Endothelial sprout formation, pericyte recruitment VEGF-A, bFGF, HGF, Ang-1/-2. 5) Inhibition of endothelial cell proliferation and lumen formation in the presence of VEGF and FGF. 6) Vessel maturation in the presence of Ang-1 PDGF.

growth factors are essential to drive angiogenesis, with the most prominent being VEGF, PDGF and FGF. The delivery of growth factors for *in vivo* treatment of ischemic disease has often resulted in loss of the therapeutic

agent from the target site. [38] The administration of growth factors for the treatment of PAD has been studied in preclinical and clinical settings, however it has to overcome drawbacks including growth factor stability, long-term efficacy, dose selection and release profiles. [39] Such issues were highlighted in a phase II randomised, double-blind controlled study administering VEGF into patients suffering with intermittent claudication as a result of PAD revealed no improvement in ABI and quality of life of the patients in comparison to control groups. [40] However, the release of growth factors can be controlled through the encapsulation within biomaterials, that upon degradation would release the growth factor slowly over time. Layman *et al.,* 2007, encapsulated FGF-2 in gelatine hydrogels. *In vivo* studies demonstrated improvements in reperfusion and capillary densities in mice treated with FGF-2 gelatine hydrogels in comparison to controls, however this study ended after 4 weeks and did not evaluate *in vivo* FGF-2 levels. [39] In addition, Sun *et al.*, 2005, encapsulated VEGF in PLG for the treatment of PAD, and reported an improvement in revascularisation and capillary density with their constructs in pre-clinical studies. However similarly, the study did not evaluate *in vivo* VEGF levels or address the long-term effects of the treatments. [41] Due to the fast degradation of growth factors (for example, VEGF has a half-life of approximately 30 minutes [42, 43]) and administering higher doses of the growth factor does not always overcome this drawback, as it can result in oncogenic effects, especially with over-administration of VEGF. [44, 45] Alternative sources such as viral vectors or cells can be explored in combination with biomaterials for the treatment of PAD.

Encapsulating the growth factor within biomaterials, to allow for their controlled release upon administration, offers a promising solution to this problem. For example, Kanematsu *et al.,* 2004, injected FGF encapsulated collagen microparticles intramuscularly into mice one week after hindlimb ischemia injury. Results showed increase in capillary density and hindlimb blood flow in comparison to injection of free FGF, hollow microparticles and no treatment, suggesting that controlled release of FGF from microparticles improved reperfusion after induced ischemia. [46] There have also been early stage

human clinical trials involving the administration of growth factors and biomaterials as a treatment for peripheral arterial disease. Marui *et al.,* 2007, ran a clinical trial administering VEGF encapsulated into gelatine microparticles into patients with critical limb ischemia. After 6 weeks, patients reported improvements in pain and claudication. However, there were only seven participants in the study. [47] It is important to consider that the beneficial effects of growth factors are dependent on the correct timing of their expression; matching the release of the growth factor within a delivery device is challenging. [48, 49]

In addition, genes engineered to produce angiogenic factors can be used as a treatment for PAD. There is extensive research investigating VEGF, FGF and hepatocyte growth factor (HGF) within genetic engineering in pre-clinical settings. Liposomal delivery of $VEGF_{165,}$ a specific isoform of VEGF, was achieved by Makinen *et al.*, 2002, and resulted in an increase in function and vascularity in the treated limbs of patients. [50] HGF is also utilised as it has not only been shown to promote angiogenesis, but also to reduce inflammation. [51] Intramuscular delivery of naked HGF plasmids in patients suffering with PAD in a phase 1 clinical trial showed significant improvements in patients' ankle-brachial pressure index (ABPI) and a significant reduction in symptoms associated with PAD. [52] Many studies have reported positive outcomes after therapeutic treatments for PAD often cite ABPI as the sole measure of improvement. ABPI is a ratio of blood pressure at the ankle to blood pressure in the upper arm, where a greater drop in the former compared to the latter is suggestive of PAD. Unfortunately, ABPI is only reliable in patients with severe PAD [11]; Stein *et al.*, 2006, has shown that 46% of patients with PAD had normal ABPI tests. [53] These findings have significant implications when utilised as the primary test for clinical trials for the treatment of PAD.

An alternative way to facilitate tissue regeneration is to allow cells to use their inherent programming and signalling to encourage the host tissue to generate functional tissues. Many different cell types can be utilised for therapeutic angiogenesis, including and not limited to, endothelial cells, [54, 55]

macrophages, [56, 57] pericytes [7, 58] and several stem cell types. [59-64] Cells can be of allogenic or autologous origin. Autologous patient-derived cells can help to avoid inflammation, rejection and the need for immunosuppressive therapy. That being said, some patients' co-morbidities may render use of their own cells' undesirable. By using allogenic cells, large scale-ups, which are often required with tissue engineering applications, become possible. In addition, the development of 'off-the-shelf' products would become a possibility, with treatments more readily available in comparison to autologous cell-based therapies – this would lead to patients receiving therapies much quicker. [65]

Endothelial cells are attractive as an option to facilitate angiogenesis as they are vital for the initiation of normal angiogenesis. Endothelial cells secrete growth factors and drive the formation of blood vessel sprouts. [34] Rufaihah *et al.*, 2011, delivered endothelial cells into the ischemic hindlimbs of mice and found that the there was an increase in perfusion and capillary density compared to saline-only controls. [66] Ishida *et at.,* 2005 harvested peripheral blood mononuclear cells from patient suffering with PAD. The cells were administered intramuscularly into the patients' affected limbs and after 4 weeks improvements in each person's ABPI was seen, as well as improvements in claudication. However, the cell therapy was in conjunction with administration of granulocyte-colony stimulating factor (G-CSF). Without appropriate control groups it cannot be determined to what extent G-CSF versus cell therapy improved patient outcomes. [67]

Within regenerative medicine, pericytes have been extensively studied for the treatment of heart disease, mainly because pericytes can be isolated from cardiac tissue. They are also useful because they can maintain microvascular function when expanded *in vitro* and re-implanted *in vivo*. [68] Cardiac pericytes have been have shown to have similar properties to mesenchymal stem cells, including the ability to differentiate into multiple cell linages. [69] Alvino *et al.*, 2018, were able to show that allogenic cardiac pericytes improved vascularisation by increases in capillary density confirmed by histology along with a reduction in fibrosis, suggesting the cells were immunologically

accepted after transplantation. [58] In addition, other sources of pericytes can be used. Campagnolo *et al.,* 2016, developed a polycaprolactone electrospun scaffold with incorporated peptides and seeded with vascular pericytes. The pericytes provided a source of pro-angiogenic growth factors, which in turn increased endothelial cell density. Therefore this construct has potential to be successfully used as a vascular graft. [70] In addition, Carrabba *et al.,* 2016, studied the effect of pericytes seeded on polycaprolactone/gelatine scaffolds implanted around the femoral artery in a murine model of hindlimb ischemia. Results showed that the cellularised constructs improved revascularisation and arteriogenesis in comparison to controls. [71] However, there is still a need for further research into the definition of pericytes, as well as in the development of a specific identifying cell marker. Furthermore, there is evidence to suggest that pericytes could be involved in the development of heart disease, which could in turn affect therapeutic outcomes of the use of pericytes in cell therapies. [68, 72] There have been numerous studies involving the administration of peripheral blood mononuclear cells for the treatment for PAD, with some reports of improvement in symptoms for patients, though other contradictory results have also been reported. [73]

Stem cell therapies have shown great promise in this field due to their abilities to differentiate and self-renew. Issues regarding their safety *in vivo,* specifically with regards to tumour formation, highlight a shortcoming of their use. Mesenchymal stem cells (MSCs) have been shown to have low tumorigenic [74] and immunogenetic activities, [75] to induce collateral blood vessel formation and to improve symptoms when administered to patients in a randomised clinical trial by Lu *et al.*, 2011. [73] Adipose Derived Mesenchymal Stem cells (ADMSCs) can be readily harvested from adipose tissue in large quantities. They have been shown to secrete bioactive levels of VEGF, HGF, Insulin-like Growth Factor (IGF-1) and FGF, making them an attractive option for therapeutic angiogenesis. [76-79] Therefore, ADMSCs have been widely researched for cell therapy applications. There are two hypothesised mechanisms that explain how ADMSCs improve vascularisation *in vivo*. The first describes the implanted ADMSCs differentiating into cell types that are found in and around blood vessels (e.g. endothelial cells, pericytes). The

second involves ADMSC secretomes (containing bioactive molecules, growth factors and cytokines) that lead to the improvement in vascularisation. [80] There is evidence for both arguments, with Moon *et al.*, 2006, transplanting ADMSCs into a mouse model of PAD. It was found that the mice treated with ADMSCs had significantly higher laser doppler blood reperfusion measurements, which in turn lead to an increase in vascular density and von Willebrand factor expression. [37] Despite these findings, there have been recent studies that have shown that ADMSC secretomes dramatically improve wound healing. [81, 82] In addition, stem cell supernatants have been used for cardiovascular applications with studies showing improvements in cardiac function, [82, 83] growth factor secretion, inflammation and infarct size in *in vivo* studies. Gangadaran *et al*., 2017, also demonstrated that exposing an ischemic hindlimb to stem cell secretomes improves revascularisation of the limb by activating VEGF receptors. [84] Administering the secretomes from ADMSCs *in vivo* reduces the associated risks involved with stem cell transplantation. Safety concerns include stem cell spontaneous differentiation, tumour and metastasis formation. [85] In addition to actively secreting angiogenic growth factors, ADMSCs for treatment within ischemic tissue may be more beneficial over other cell types as it has been extensively shown that ADMSCs have increased survival and angiogenic behaviour in hypoxic conditions. [86] When exposed to hypoxia *in vitro,* VEGF, bFGF and HGF levels are increased, which in turn improves revascularisation. [79, 87, 88] Furthermore, ADMSCs *in vitro* are responsive to angiogenic growth factors. When transplanted from a normoxic to ischemic environment, this could cause a cascade of events leading to promotion of angiogenesis and revascularisation, as there are increases of VEGF secretion in ischemic tissue of patients with PAD as the tissue attempts to initiate angiogenesis. [89, 90] Vu *et al.*, 2017, administered ADMSCs via injection into the rectus femoris muscle of mice with surgically induced hindlimb ischemia. The authors reported that the ADMSCs migrated to the thigh and heal of the mice, and the administration of ADMSCs improved the expression of angiogenesis-related genes, however this effect was also seen in the control PBS group. [91]

Numerous studies have shown that delivering cells by suspension via injection results in minimal retention of cells at the implant site, with up to 90% loss after

24 hours and long-term retention of less than 1%. [4, 77, 92-98] Without an effective way of delivering cells to the target site, the potential of cell therapies remains limited. To overcome these challenges, a biomaterial can be used to act as an anchor for the cells. [58, 87-89] Cells can be seeded onto a biomaterial *in vitro* and then implanted *in vivo,* with the possibility of delivery via minimally invasive methods. By allowing anchorage of dependent cells the opportunity to attach to a surface, this increases the survival of the cells, which would otherwise apoptose if left in suspension. [6, 99] This supports cell attachment, proliferation and survival of the cells *in vivo*, as once the cells are successfully delivered, they are more likely to be retained at the implant site and have their intended therapeutic effect. This would thereby create a more successful cell therapy. [76]

1.3 Biomaterials and Tissue Engineering

Biomaterials are materials that are designed to replace or repair a system or function in the body. [100] They can be produced from natural (e.g. chitosan or hyaluronic acid) or synthetic (e.g. polymers, ceramics or metals) materials and can be used in a variety of different ways. These include metals to replace joints and bones such as the stainless steel Charnley hip replacement, [101] Zirconia ceramic dental implants [102] and polymer drug delivery devices. [103] Certain properties are critical for a biomaterial, including biocompatibility, non-toxicity and appropriate mechanical properties. Additional properties can be achieved through selection of a material and the production process. These include mechanical strength, reproducibility, size, porosity, surface structure, bio-integration ability and degradability (specifically biodegradability). [104] When a material is biodegradable, it negates the need for the removal of said material. Ideally the degradation products would be naturally metabolised by the body, as is the case with poly (lactic-co-glycolic acid) (PLGA) which degrades into lactic acid and glycolic acid. [105] Polymers are often chosen to be used as a biomaterial in conjunction with cells due to their biocompatibility and ability to be modified.

This work primarily focuses on PLGA. PLGA was chosen as it has shown great potential as a biomaterial, with current applications including biodegradable sutures and drug delivery vehicles. [106] PLGA has been used in a variety of tissue engineering applications. For example, Rocha *et al.,* 2009, implanted encapsulated VEGF in PLGA microparticles into a tissue-engineered intestine in order to promote epithelialisation. One study revealed that the microparticles had a sustained release of active VEGF and had increased capillary density and epithelial cell proliferation in large intestinal constructs. [107] R. Ahmadi *et al.,* 2008, showed that smooth muscle cells had superior attachment and delivery on PLGA microparticles over gelatine microparticles to treat faecal incontinence. [108] PLGA has also been utilised in cartilage tissue engineering, with Dai *et al.*, 2010, creating PLGA/collagen meshes with mechanical strength comparable to native cartilage and that successfully culture chondrocytes. [109] PLGA is highly tuneable; the copolymer ratios can be adjusted to alter degradation, mechanical strength and porosity. [110] It has been well established that monomer ratios within PLGA are the driving factor in influencing degradation. Poly (lactic acid) contains methyl side groups that make it more hydrophobic than poly (glycolic acid). The more methyl side groups present the less water the polymer is able to absorb, resulting in less breaks in the ester bonds and slower degradation. [111] In addition the presence of glycolic acid accelerates weight loss of the polymer and thus faster degradation. Therefore, polymers with higher lactic acid and lower glycolic acid contents, such as PLGA 85:15, will degrade much slower than PLGA 65:35. However, there are other properties that affect degradation rate, including molecular weight of the polymer chain, surface area to volume ratio and the inherent viscosity of the polymer. [105] Inherent viscosity is dependent on the molecular weight and relative viscosity of a polymer. Two PLGA polymers can have the same copolymer ratios, but if they have different inherent viscosities, they can behave very differently. The higher the inherent viscosity, the slower the degradation rate of the polymer.

There are a variety of methods for producing polymeric scaffolds, all with different advantages and disadvantages depending on the desired characteristics and applications. For example, water-oil (W/O) or water-oil-

water (W/O/W) emulsion methods are used to produce microparticles with an encapsulated drug in the centre and are especially utilised for water soluble drugs. [112] Unfortunately, these methods are often not appropriate for large scale production. [113] Electrospraying is the process of producing polymer microparticles by subjecting polymer droplets to electrical forces. The droplets become charged and therefore do not clump or coagulate when collected. [114] By varying the processing parameters (voltage, distance between the needle and surface and polymer concentration) the properties of the microparticles can be controlled. To get precisely sized microparticles, the polymer can be jetted with acoustic excitation to enable production of near monodisperse microparticles. [115] In recent years 3D printing has been become increasingly popular for use in tissue engineering. 3D printing is a large and complex field but put simply involves a material (metal, ceramic or polymer) solution being extruded dropwise onto a surface and forming a 3D structure layer by layer. A digital template is often used to control size, geometry and interconnected porosity. [116] One of the greatest advantages of this technology is that it can be used in personalised medicine as structures are made in accordance to exact specifications. For example, 3D printing is particularly beneficial for craniofacial tissue engineering as anatomically accurate prostheses can be produced, improving functional and aesthetic outcomes. [117] 3D-printed atomically accurate models, taken from scans specific to a patient, have also been shown to be useful for surgeons in dental, cardiovascular, oncological and reconstructive surgeries. [118-120] Disadvantages of 3D printing include that it is unable of efficiently produce nano-scale structures, and material properties such as viscosity can influence outcomes (as highly viscous solutions would not be able to pass through the nozzles). Phase inversion or separation [121] is another method used to produced microparticles. The polymer (dissolved in a solvent) is extruded through a nozzle producing polymer droplets, which then undergo a liquid-liquid phase separation. With thermally-induced phase separation (TIPS), this separation occurs due to a large temperature change which can be achieved by freezing the polymer solution in liquid nitrogen. [122] The result is a polymer-rich and polymer-poor phase within the material. The polymer-poor phase is removed by lyophilisation to produce highly porous structures. [123-

125] The TIPS process can also be used to make nano-, micro- or macro-particles, fibres, polymer films and polymer coatings. [126] As with electrospraying, by adjusting polymer concentration, thermal quenching, solvent and copolymer ratios TIPS properties can be controlled. In addition, the quenching temperature and time can influence the material characteristics - if the material is rapidly cooled at a lower temperature, smaller pores will form, as fewer crystals form within the structure and phase separation has less time to occur. [127] One advantage to the TIPS process is its control over porosity. Porosity is a highly desirable property for many regenerative medicine applications, as a scaffold with an interconnected porous structure allows for movement of nutrients as well as cell communication, cell proliferation, cell migration, tissue ingrowth and neovascularisation. Unlike the TIPS process, other methods such as porogen leaching and W/O or W/O/W produce materials with poor interconnectivity. [113] TIPS processed polymers have been utilised in a range of tissue engineering applications. Chen *et al.*, 2018, engineered poly(lactide)/poly(aniline) nano-fibres using TIPS for bone tissue engineering. It was determined that osteogenic differentiation from mesenchymal stem cells was significantly promoted on the TIPS materials. [128] Stem cells have also been successfully differentiated into neural cells on TIPS poly (lactic acid) microparticles. When comparing stem cell survival and differentiation on TIPS microparticles to traditional cell culture, Zare-Mehrjardi *et al.*, 2011, found through histology that the stem cells had successfully infiltrated the TIPS materials and that these samples had an increase in the expression of neural markers as well as neurite outgrowth. [129]

The desired levels of porosity are dependent on the intended use of the scaffold. For example, a scaffold for cartilage tissue engineering would not need to be completely neovascularised, as natural cartilage is avascular and contains no nerves, therefore a less porous scaffold would suffice. [130] However, scaffolds for muscle, bone or cardiovascular engineering would require higher porosity. [131-133] In addition, porosity can strongly influence mechanical properties of the scaffold and these properties are dictated by the tissue in which it is implanted. A material intended to replace cartilage, for example, would need to have sufficient mechanical ability to take high loads

and impacts, which would be reduced with porosity. [134] Vozzi *et al.*, 2018, produced 8 mm x 2 mm scaffolds from polyester urethanes. The scaffolds were cultured with cardiomyocytes and analysed for contractility for 14 days. The authors concluded that the architecture of the TIPS scaffolds sufficiently mimicked the structure of the ECM, allowing for improved contractility and alignment of the cells. However, further studies would be required involving *in vivo* analysis of the construct. [135]

1.3.1 Biomaterials and Cardiovascular Disease

There have been multiple pre-clinical and clinical studies involving the use of cell therapy for the treatment of cardiovascular disease. A meta-analysis of 19 randomised placebo-control clinical trials involving the administration of cell therapies to 837 patients with critical limb ischemia, conducted in 2017 by Rigatto *et al.,* 2017, showed that cell therapy (bone marrow stem cells or mononuclear cells) improved pain, limb perfusion, claudication and wound healing by 59%, as well as reducing the risk of amputation by 37%. [136] This suboptimal reduction in amputation risk could be attributed to the well-documented observation that injecting cells results in poor retention and survival of those cells at the implant site. [127] Biomaterials can be used to act as an anchor for the cells and thus improve the success of cell therapies. [58, 87-89] It has been hypothesised that by mimicking the ECM structure, biomaterials for tissue engineering applications may be more successful.

Hydrogels comprising ECM components (for example: hyaluronic acid, collagen and fibrin) could achieve this. In the treatment of cardiovascular disease, many studies encapsulate growth factors within a hydrogel rather than encapsulating cells. This is perhaps due to issues with cell seeding due to lack of penetration and control over hydrogel formation. [137] However, Tang *et al*., 2011 injected endothelial cells with a hyaluronic based hydrogen before intramuscular implantation in ischemic tissue and observed that by doing this, cells were retained longer at the implant site. Additionally, Katare *et al.,* 2013, encapsulated MSCs in alginate microbeads for the implantation in ischemic hindlimbs of mice. The constructs were shown to promote

reperfusion of the treated limbs, as well as a marked increase in VEGF-A and capillary density. [138] There are however significant challenges facing hydrogel-based tissue engineering. Hydrogels have been shown to have poorer mechanical properties when compared to other biomaterials, making them unsuitable for certain applications. Hydrogels have also been shown to be less successful when multiple cell types are required, so are less promising for more complex tissues. [137] Chow *et al.,* 2017, acknowledged the challenge of achieving effective cell engraftment faced in cell therapy; they proposed encapsulating induced pluripotent stem cell cardiomyocytes in hydrogels combined with erythropoietin to allow cell retention as a treatment for myocardial infarction. They found that combinations of 'hydrogel and erythropoietin', 'hydrogel', 'erythropoietin and cells' and 'cells-only' all improved cardiac function. However, they we unable to show that the hydrogel improved cell retention compared to the 'cell-only' control, suggesting that while the hydrogel only group showed increased ventricular wall thickness, hydrogels may not be the most suitable biomaterial to improve cell retention at the implant site. [139] In addition, Speidel *et al.,* 2017, developed a hydrogel that modulated with heparin binding sites to improve the mechanical properties of the material, specifically to deliver cardiac progenitor/stem cells to infarcted myocardium. [140]

Nanoparticles have also been investigated for the treatment of PAD. They can be functionalised with peptides, drugs or ligands in order to treat specific diseases. Several studies have incorporated growth factors within polymeric nanoparticles (such as VEGF) for the administration into murine models of PAD. [141] However, there are still concerns with the use of nano-scale materials, such as the risk of nanoparticles entering the circulatory system, accumulating in lymph nodes or crossing the blood brain barrier. [142] In order to overcome the safety concerns with nano-scale materials, and the mechanical stability issues with hydrogels, polymer microparticles or patches offer one solution. Kapnisi *et al.*, 2018, reported on the development of a micropatterned cardiac patch with mechanical and conductive properties that aided in the treatment of myocardial infarction. *In vivo* studies revealed the mechanical and conductive properties of the patch matched the myocardium

and did not have any adverse effects on cardiac function, highlighting the importance of mechanical properties. [143] Furthermore, Mirabella *et al.,* 2017, manufactured channelled fibrin patches via 3D printing and seeded them with endothelial cells as a treatment for ischemic disease. The cellularised constructs, unpatterned and acellular substrates were implanted into a murine hindlimb ischemia (HLI) model. After comparing the implanted groups, the authors concluded that the patterned cellularised grafts allowed the most effective bio-integration, which in turn drove the perfusion of the ischemic limb. The authors acknowledged that the procedure required anastomosis and also did not report on the degradability, which in turn raises concerns about the long-term success of the implant. [144, 145]

Mima *et al.,* 2012 coated polylactic acid microparticles with a hydroxyapatite coating to improve bone marrow mononuclear cell attachment. The cellularised construct was implanted into a murine model of peripheral artery disease. The authors concluded that seeding the cells onto the microspheres resulted in improved cell retention at the implant site and a reduction of cellular apoptosis in comparison to the cell-only group. In addition, angiography results showed that mice treated with the cellularised microspheres had improved reperfusion rates and further analysis showed higher intermuscular levels of VEGF and FGF-2. A control group of cellularised polylactic acid microparticles without the hydroxyapatite coating could have been included to assess the effect of the coating and the direct contact to polylactic acid on the cells. [146] The use of PLGA microparticles have been widely explored in the tissue engineering field. [105, 147-151] Huang *et al.*, 2012, reported that PLGA microparticles seeded with bone marrow derived stem cells injected into infarcted rat myocardium resulted in improved retention at the implant site, improvements in cardiac function and stem cell engraftment. [152] Hoareau *et al.*, 2018 demonstrated that combining cell therapy (stromal vascular cells) with PLGA microparticles for the treatment of CLI induced significant improvements in revascularisation and necrosis in pre-clinical studies compared to cell-only therapy, which did not aid in recovery rates. [153] In addition, Saif *et al*., 2010, encapsulated VEGF, Ang-1 and HGF in different combinations along with the addition of vasculogenic progenitor cells and

evaluated their effect on neovascularisation *in vitro* and *in vivo.* They found that the combination of growth factors slowly released by the degradation of the microparticles and the cell therapy improved neovascularisation. The authors describe their choice to use PLGA microparticles over hydrogels as they are highly tuneable, can be chemically modified and provide mechanical support to the tissue. [154]

Despite an extensive search, little can be found on the use of PLGA microparticles in combination with ADMSCs for the treatment of PAD. The majority of studies focus on either the encapsulation of angiogenic growth factors within microparticles, [46, 47, 154-156] genetically modified stem cells to express increased quantities of growth factors, [156-159] the delivery of cell/hydrogel constructs [137, 138, 160] or for bone tissue engineering. [161-165] For example, Paterson *et al.*, 2018, developed highly porous polymeric microparticles that had increased *in vitro* angiogenic activity with the ability to support cell proliferation and ingrowth for use in bone tissue engineering. [166] Clearly there is scope for further research into the use of PLGA microparticles with ADMSCs to promote angiogenesis as a therapy for PAD.

1.4 Effect of Biomaterial Physical Properties on Cell Behaviour

Research into the effect of biomaterial physical properties on cell behaviour is vast. Topography, stiffness, plasticity, hydrophobicity and mechanics are just a mere selection of the properties of a material that can not only be manipulated but affect cell behaviour intentionally or otherwise. Traditionally, cells are cultured and expanded in 2D tissue culture. This has been adequate to study cells in the past, making it easier and more efficient for expansion and investigation into cell interactions. However, 2D surfaces do not accurately represent cell environments *in vivo,* and it has been well established that cells behave differently in 2D culture in comparison to 3D culture. Changes include spreading, morphology, differentiation and survival. [167] However, the addition of topographic features, such as grooves, pores, pits cell attachment can be increased even on 2D surfaces, as they can become representative of 3D microenvironments. This can positively influence cell behaviour in terms of

the direction of growth, spreading, proliferation, adhesion and differentiation of cells. [167, 168] Increasing surface roughness at the macro and nanometre scale can lead to more efficient cell attachment, which is essential for the success of many implants and tissue engineering constructs. [169]

It has been shown that surfaces which diverge further from ECM features and mechanics more drastically affect cell fate. [170] When exploring the effect of the ECM on biomaterials for therapeutic angiogenesis, material characteristics focus on either the biological cues the ECM provides, or on endothelial cell interactions with the ECM. This is because the ECM, and the degradation of the basement membrane by endothelial cells, play a critical role in angiogenesis. [32] However, it has been proffered that by mimicking the physical characteristics of the ECM, cell behaviour can be controlled. The ECM is porous, rough and has micro- and nano-scale topological features. [171-173] The influence of the ECM on cell attachment and proliferation is thought to be due to the topological features causing clustering of the cells' integrins. This results in changes to cellular actin cytoskeletal organisation [174] and thus the shape of the cells, as shown by Gilber *et al*., 2014. [175] Cell shape changes can guide cell proliferation, as well as influence stem cell differentiation and cell survival, as rounded cell shape can trigger apoptosis. [175, 176] Cells have been shown on many occasions to follow patterns of surfaces. If these patterns are in conjunction with the cell's preferred shape, this can be beneficial. Jang *et al*., 2010, showed the neurite filopodia outgrowth was improved along long ridges and grooves compared to smooth surfaces. [177] Stiffness, or the rigidity of a material, heavily influences cell behaviour. Once a cell attaches to a material, the stiffness will exert a certain amount of strain on the cell which can influence cell proliferation, differentiation and cell survival. [178] In general, cells attached to stiffer surfaces will have more organised, stiff cytoskeletons and stronger integrin and focal adhesion bonds than cells attached to softer surfaces. This results in an increase in proliferation. [179] In addition, Bellas *et al.*, 2014 reported that VEGF secretion from endothelial cells was increased when these cells were cultured on stiffer surfaces, due to activation of GATA2 and Rho pathways. [175] Pluripotent stem cells cultured on stiff surfaces will preferentially differentiate into

osteocytes in comparison to adipogenic and chondrogenic linages which prefer softer surfaces. [180, 181] Studies have shown that it is possible to differentiate stem cells into cardiomyocytes on various biomaterials. [182, 183] However, it has also been shown that cardiomyocyte differentiation is possible in suspension, [60] with stiffness influencing contractility of the cells, rather than affecting the differentiation. [184, 185] It is widely reported that mesenchymal stem cells, such as bone marrow-derived or adipo-derived, can be differentiated into adipo-, neuro-, chondro- and osteo-lineages. [186] Many factors can influence the differentiation of stem cells. *In vitro*, this involves the addition of specific supplements to cell culture medium. [187, 188] However, many researchers have observed the spontaneous differentiation of stem cells. Through research, it has been discovered that the characteristics of the material which cells are cultured on influence their differentiation abilities. It has been shown that stiffer substrates promote the differentiation into osteogenic lineages, whereas softer substrates result in differentiation into adipocytes and neurons. [181]

As previously mentioned in Section 1.3, there are numerous investigations into the use of biomaterial and cell therapy strategies for therapeutic angiogenesis in bone tissue engineering applications. This includes the study of how surface topography and physical properties of biomaterials can affect the angiogenic behaviour of cells. [161-165] Despite the extensive research into PLGA as a promising biomaterial and ADMSCs as an angiogenic cell therapy discussed in this chapter, little is known about the effect of surface topography of PLGA biomaterials on the secretion of angiogenic growth factors from ADMSCs. This work will investigate the effect of the unique hierarchical topography of TIPS processed PLGA on the secretion of angiogenic growth factors from ADMSCs for the treatment of PAD.

1.5 Hypothesis

The hypothesis of this project is as follows: ‘Hierarchical textured surface topographies promote the secretion of angiogenic growth factors for therapeutic angiogenesis’.

Part I. Evaluation of TIPS-Processed Films

1. Introduction

Thermally induced phase separation (TIPS) was previously discussed and outlined in Section 1.3. It was used to fabricate constructs with unique topographical features where the processing parameters were tuned to produce polymer constructs with different physical characteristics.

Briefly, the TIPS method was used to process polymers through subjecting polymers, in this case primarily PLGA dissolved in solvent, to a large temperature change, which resulted in materials with highly porous structures. This produced biocompatible materials, as the toxic solvent was removed during the lyophilisation stage of processing, as well as PLGAs inherent biocompatibility as its degradation products are lactic acid and glycolic acid, which are naturally metabolised and excreted from the body. [105] The TIPS process is highly tuneable; it can be used with a range of polymers and solvents and parameters such as polymer compositions, drop height and quenching time can be adjusted. With this comes further influence over the materials properties, as for example adjusting the porosity of a material can ultimately influence its degradation rate, mechanical integrity and *in vivo* behaviour. [122]

Part I.

Chapter 2: Preliminary Evaluation of TIPS-Processed Films

2.1 Introduction

This chapter describes the fabrication of a range of different TIPS polymer films and reports the physical characterisation of the materials using various microscopy techniques, roughness and stiffness measurements. ADMSCs were seeded onto TIPS processed polymer films and preliminary biological characterisation experiments were performed. Cellular behaviour was assessed through LIVE/DEAD staining and angiogenic growth factor secretion, with the view to select a polymer formulation to be studied further.

2.2 Methods

2.2.1 Polymer Solution Preparation

To produce polymer solutions 1 g of PLGA 5010 (PURASORB PDLG 5010, 50/50 DL-lactide/glycolide copolymer, inherent viscosity 1.0 dl/g, Corbion Biomaterials, Gornchem, Netherlands), PLC 7015 (PURASORB PLC 7015, 70/30 L-lactide/caprolactone copolymer, 1.5 dl/g Corbion Biomaterials, Gornchem, Netherlands), PLGA 7502-A (PURASORB PDLG 7502 Acid terminated, 75:25 DL-lactide/glycolide copolymer, inherent viscosity 0.2 dl/g, Corbion Biomaterials, Gornchem, Netherlands), PLGA 7502 (PURASORB PDLG 7502, 75:25 DL-lactide/glycolide copolymer, inherent viscosity 0.22 dl/g, Corbion Biomaterials, Gornchem, Netherlands) and PLGA 7507 (PURASORB PDLG 7507, 75:25 DL-lactide/glycolide copolymer, inherent viscosity 0.70 dl/g, Corbion Biomaterials, Gornchem, Netherlands) were dissolved in 10 mL dimethyl carbonate (DMC) (anhydrous >99%, D152927, Sigma Aldrich, UK) to produce 10 wt% solutions and 0.5 g of polymer dissolved in 10 mL DMC in 50 mL Falcon tubes (352070, BD Biosciences, USA) to produce 5 wt% solutions. Samples were mixed using magnetic stirring for 18 hours at room temperature. As polystyrene could not be dissolved in DMC, an alternative solvent with low toxicity was chosen. 1 g and 0.5 g of polystyrene (174950, ThermoFisher, UK) was dissolved in 10 mL 2-Butane/methyl ethyl ketone (MEK) (anhydrous >99%, 445468, Sigma, UK) in 50 mL Falcon tubes (352070, BD Biosciences, USA) using magnetic stirring for 18 hours at room temperature to produce 10 wt% and 5 wt% solutions.

Polymer Name	Lactic Acid %	Inherent Viscosity (dl/g)
PLGA 5010	50	1.00
PLGA 7502-A	75	0.20
PLGA 7502	75	0.22
PLGA 7507	75	0.70
PLC 7015	70	1.50

Table 2.1: Summary of polymer compilations used to produce polymer films.

2.2.2 TIPS Film Material Preparation

13 mm diameter 0.16 mm thick D263 M Borosilicate cover glasses (631-0150, VWR, UK) were coated in the polymer solutions (as prepared in Section 2.2.1) by holding individual coverslips with tweezers and manually submerging them into the polymer solution. Excess solution was discarded by holding the coverslip at a 90^{o}C angle and dabbing the edge on a paper towel. The coated coverslips were then immediately immersed into 200 mL of liquid nitrogen in a 100 mm diameter stainless steel container (Endecotts, Fisher Scientific, 12348069, UK) to induce phase separation. In order to ensure the residual DMC did not exceed its melt temperature (2-4^{o}C), that would dissolve the polymer coating, the samples were immediately transferred to a -80^{o}C freezer before being transferred to a freeze-dryer (Edwards Freeze-dryer, EF03, Edwards, West Sussex, UK). Once under vacuum, the samples were lyophilised for 18 hours to allow the sublimation of residual DMC from within the material.

2.2.3 Control Film Material Preparation

PLGA 7502 (PURASORB PDLG 7502, 75:25 DL-lactide/glycolide copolymer, inherent viscosity 0.22 dl/g, Corbion Biomaterials, Gornchem, Netherlands) and PLGA 7507 (PURASORB PDLG 7507, 75:25 DL-lactide/glycolide copolymer, inherent viscosity 0.70 dl/g, Corbion Biomaterials, Gornchem, Netherlands), PLGA 5010 (PURASORB PDLG 5010, 50/50 DL-lactide/glycolide copolymer, inherent viscosity 1.0 dl/g, Corbion Biomaterials, Gornchem, Netherlands) and PLC 7015 (PURASORB PLC 7015, 70/30 L-lactide/caprolactone copolymer, 1.5 dl/g Corbion Biomaterials, Gornchem, Netherlands) 10 wt% polymer solutions were prepared as in Section 2.2.1. 13 mm diameter 0.16 mm thick D263 M Borosilicate cover glasses (631-0150, VWR, UK) were coated as described in Section 2.2.2. Coated cover glasses were placed flat onto non-adhesive sheets (DY992, R&D, UK). The coated cover glasses were left to completely dry for 72 hours in a fume hood. For the polystyrene control 13 mm x 0.2 mm cell culture treated sterile Thermanox plastic coverslips (174950, ThermoFisher, UK) were used.

2.2.4 High-Resolution Imaging Using Scanning Electron Microscopy

Scanning Election Microscopy (SEM) was used to examine the ultrastructural features of polymer films. The samples were mounted onto aluminium stubs via carbon tabs and allowed to completely dry. Prior to imaging, each sample was sputter coated with gold/palladium alloy in an argon atmosphere. Samples were imaged using a Jeol 7401 high resolution field emission SEM at a range of magnifications (x200-x3000).

2.2.5 Surface Texture Analysis Using Atomic Force Microscopy

Atomic force microscopy (AFM) was used to quantify the surface roughness and stiffness of polymer films. Images were taken with a JPK Nanowizard atomic force microscope (JPK Instruments, Germany) fitted with a Respa-10 etched silicone probe or a MSNL-10 6 cantilever 0.01-0.5 N/M sharp nitride level probe (Bruker, UK). The AFM and cantilevers were calibrated before imaging. To calibrate the microscope the cantilever tip was aligned to the laser, the photodiode was centred and was ensured to have a full range of motion. Images were acquired in liquid tapping mode in PBS (P5493-1L, Sigma, UK). A 50 μm x 50 μm area of each sample was measured with 3-5 scans per sample at 512 x 512 pixels. From these images, the average roughness values were obtained using JPK analysis software source (JPK Instruments, Germany). The cantilevers were calibrated for stiffness measurements by creating force curves for the sensitivity and spring constants, where peaks in the curves corresponded to the force required on the cantilever for stiffness measurements. 63 points within the scanned sample were measured producing individual force curves and average results were obtained. The cantilevers were replaced every 6-8 scans and re-calibrated before each use.

2.2.6 Surface Texture Analysis Using Dektak XT Surface Profilometry

Dektak XT Surface Profilometer (Bruker, USA) was used to measure the surface roughness of 7507 PLGA TIPS, 7502 PLGA TIPS, 5010 PLGA TIPS, 7507 PLGA control, 7502 PLGA control, 5010 PLGA control and polystyrene polymer films. The Dektak profilometer used stylus contact to measure the average roughness of the polymer films while also providing 2D profiles and

3D maps of the scanned area. The samples were loaded onto the scan stage and the door of the machine was closed to avoid the effects of noise pollution, vibrations and dust that can interfere with the measurements. Samples were measured at ambient temperature and dry conditions. Once loaded the stylus made contact with the sample to establish the baseline point, from this hills and valleys 50% above and 50% below the baseline were measured. The maximum range of 1A/6.55 µm vertical resolution and 1 µm step height was selected. Due to the brittle nature of the PLGA and its low deformation point, the lowest stylus tracking force of 1 mg was selected, with the exception of 5 mg for PLC TIPS films (that has relatively higher stiffness in comparison to PLGA). [189] The maximum scan length of 2000 µm was selected, due to the large diameter of the polymer films. Using the live video display the location of measurement was chosen at three random points on the surface of each polymer film to produce average measurements of surface roughness.

2.2.7 Adipose-Derived Mesenchymal Stem Cell Culture

Cell cultures were carried out using aseptic techniques and in a class II laminar flow hood. StemPro™ human adipose derived stem cells (ADMSCs) were purchased from ThermoFisher (single non-diabetic donor from human lipoaspirate tissue, $1x10^6$ cells/mL in MesenPRO RS™ medium at 1 passage, R7788-115, ThermoFisher, UK). MesenPRO RS™ medium (12746-012, Thermofisher, UK) was prewarmed in a 37ºC water bath. MesenPro RS™ Growth supplement (R7788-110, Thermofisher, UK) was added to 500 mL of the basal medium with 5 mL 200 mM L-Glutamine (25030081, Gibco, UK). The ADMSCs were rapidly thawed in a 37ºC water bath and added to 10 mL complete MesenPro RS™ medium in a 30 mL centrifuge tube (60.9922.212, Sarstedt, Germany). The cell suspension was then centrifuged for 5 minutes at 1000 rpm. The media was discarded, and the cell pellet resuspended in 12 mL of MesenPro RS™ media and seeded into a T75 cell culture flask (156499, ThermoFisher, UK) at a density of $2 x10^5$ cells/cm^2.

The growth of cells were monitored using light microscopy and cells were passaged once they reached 60-80% confluency. The culture medium was

removed using sterile 10 mL pipettes, ensuring it did not disturb the cell monolayer. 5 mL of 1X PBS was added to the flask to gently wash the cells. This was removed and discarded. 0.25% sterile filtered Trypsin-EDTA (pH 7.0 -7.6, T4049, Sigma, UK) solution was thawed and added to the monolayer of cells. The T75 flask was closed and placed back into the incubator. After 2-5 minutes the flasks were removed from the incubator and checked under a light microscope to evaluate cell detachment. The flasks were returned to the laminar flow hood, and 10 mL of complete MesenPro RS^{TM} media was added to neutralise the trypsin-EDTA. This solution was then transferred to a sterile 30 mL centrifuge tube (60.9922.212, Sarstedt, Germany) and centrifuged at 1000 rpm for 5 minutes. The media was discarded, and the cell pellet was resuspended in 1 mL complete media. To determine cell number and viability, the NucleoCounter NC-200 automated cell counter (Chemometec, Denmark) was used. 200 μL of the cell suspension was transferred to a sterile 1.5 mL microcentrifuge tube (E1415-1500, StarLab, UK) and loaded into pre-calibrated Via1-Cassettes containing acridine orange and DAPI. The cassette was placed into the NucleoCounter and cell population and viability were calculated as a result of the acridine orange signal. For all experiments, only ADMSCs between passages 4 and 7 were used. If passaging was not required, the media of the cells was replaced every 2-3 days. The culture media was removed ensuring not to disturb the cell monolayer. 5 mL of 1X PBS (prewarmed to 37 ^{o}C) was added to the flask to gently wash the cells. This was removed and discarded. 12 mL of prewarmed complete MesenPro RS^{TM} media was added to the flask. The flask was placed into an incubator at 37^{o}C/5% CO_2 until passaging or additional media changes were required.

2.2.8 Cellularising Polymer Constructs

TIPS and control polymer films were placed into sterile low attachment 24 well plates (CLS3527, Sigma, UK) and UV sterilised for 1-2 hours. Polymer films were hydrophilised by combining 1 mL of 70% absolute ethanol (E10600/05, Fisher Scientific, UK) to 4 mL MesenPro RS^{TM} reduced serum medium. 0.5 mL of the ethanol/media was added to each film. The plate was placed onto a plate shaker and samples were incubated at 37^{o}C 5% CO_2 with gentle

agitation overnight. Polymer films were washed with pre-warmed 1X PBS and seeded with $1x10^5$ cells/well P4-P7 ADMSCs in complete MesenPro RS™ reduced serum medium. Plates were incubated at 37°C 5% CO_2. 0.45 mL supernatants were collected at days 1, 4, 7 and 10, frozen and replaced with 50 mL fresh medium.

2.2.9 Assessing Cell Viability with LIVE/DEAD Staining

LIVE/DEAD viability assay is fluorescence based, that uses calcein-AM that enters cells and is converted to fluoresce green by esterases present in live cells and EthD-1 dye that can only pass through the disrupted membranes of dead cell cells and fluoresces red. The assay can be used to assess viability by simply counting the live and dead cells. [190] LIVE/DEAD staining was used to assess the cell viability of ADMSCs seeded density of $1x10^5$ cells/well in complete MesenPro RS™ media onto 7507 PLGA TIPS polymer films, 7502 PLGA TIPS polymer films, 5015 TIPS polymer films, 7502-A TIPS polymer films, PLC TIPS polymer films, polystyrene TIPS films, 7507 control polymer films, 7502 PLGA control polymer films and polystyrene films at 10 wt% and 5 wt%. The culture media was removed, and the polymer films were gently washed with 1 mL 1X PBS (P5493-1L, Sigma, UK). Control samples were also produced by seeding cells onto glass coverslips and killed with 70% methanol for 30 minutes. 20 µL of 2 mM EthD-1 stock was added to 10 mL sterile 1X PBS (P5493-1L, Sigma, UK) and vortexed to make a 4 uM concentration. 5 µL 4 mM calcein AM stock was added to create the complete LIVE/DEAD dye. 500 µL of the dye was added directly to the coverslips and cells and incubated for 40 minutes avoiding direct light. To visualise the dead cells a Texas Red dye filter at 528-617 nm was used and for the live cells a fluorescein bandpass filter at 494-517 nm was used with Olympus TIRF inverted microscope (The Confocal Imaging unit, Rockefeller Building, UCL, London).

2.2.10 Preliminarily Evaluation of the Angiogenic Effects of TIPS Polymer Films

A DuoSet Human FGF basic (bFGF) enzyme-linked immunosorbent assay (ELISA) (DY233B, R&D Systems, UK) was used to determine the amount of angiogenic growth factor bFGF that was released into the supernatants from ADMSCs seeded onto TIPS and control polymer films (n=5). The capture antibody was reconstituted to 120 μg/mL in 1X PBS (P5493-1L, Sigma, UK) and diluted to the working concentration of 1.0 μg/mL in 1X PBS. 100 μL was added to each well of a Nunc-Immuno MicroWell 96 well plate (M9410, Sigma, UK). Plates were sealed (DY992, R&D, UK) and incubated overnight at room temperature. Wash buffer was prepared as 0.05% Tween-20 (P1379, Sigma, UK) in 1X PBS (P5493-1L, Sigma, UK). Each well was washed with wash buffer three times and blotted to remove excess liquid. Reagent diluent was prepared as 1% bovine serum albumin (05482, Sigma, UK) in 1X PBS (P5493-1L, Sigma, UK) and 0.2 μm filtered. Plates were blocked with 300 μL of reagent diluent for 2 hours at room temperature then washed. The bFGF standard was reconstituted to 100 ng/mL in reagent diluent and diluted to a working concentration of 2000 pg/mL in reagent diluent and serial dilutions were prepared up to 7.81 pg/mL. Samples were centrifuged and 100 μL were added to each well in triplicate, along with the bFGF standards and incubated at room temperature for 2 hours and washed. The detection antibody was reconstituted to 6.0 μg/mL in reagent diluent and diluted to the working concentration to 100 ng/mL. 100 μL of detection antibody was added to each well, incubated at room temperature for 2 hours and washed. The Streptavin-HRP was diluted at a ratio of 1:200 in reagent diluent and 100 μL was added to each well. The plate was sealed, protected from light, incubated for 20 minutes at room temperature and washed. The substrate solution was prepared by adding equal volumes of colour reagent A (H_2O_2) and colour reagent B (Tetramethylbenzidine) (DY994, R&D, UK) immediately before addition. 100 μL of the substrate solution was added to each well. The plate was sealed, protected from light, incubated for 20 minutes at room temperature and 50 μL of 2 N H_2SO_4 was added to each well to stop the reaction and further colour development. The plate was then immediately read

using a microplate reader (Fisher Scientific, UK) at wavelength 450 nm with correction set to 540 nm.

2.2.11 Statistical Analysis

The data was imputed into GraphPad Prism 8 software (GraphPad Software, USA) for analysis and presented as mean values with error bars depicting the standard deviation. To analyse two or more groups with one variable, ordinary one-way ANOVA tests were used. For two or more groups with two or more variables a repeated-measured ANOVA was used with Geisser-Greenhouse correction applied. For comparison between two groups the data was first tested for normality through a Kolmogorov-Smirnov test. If normally distributed, a parametric unpaired Welch Student *t*-test was performed. If not normally distributed, a nonparametric Wilcoxon Student *t*-test was performed. P values of <0.05 indicated statistical significance and were shown as *, with P<0.01 = **, P<0.001 = *** and P<0.0001 = ****.

2.3 Results

2.3.1 Ultrastructural Imaging of Polymer Films Using Scanning Electron Microscopy

SEM was used to visualise the topography of the TIPS and control polymer films. SEM uses accelerated electron beams that scan samples to create images with higher magnification and resolution than conventional optical microscopes. The electron beam interacts with the sample to produce secondary electrons that are detected, creating detailed images which allow for the study of surface topographies. [191] A range of polymers were processed using TIPS, including PLGA 5010 at 10 wt% and 5 wt%, PLGA 7502 at 10 wt%, PLGA 7502-A at 10 wt% and 5 wt%, PLGA 7507 at 10 wt% and 5 wt%, PLC 7015 at 10 wt% and 5 wt% and polystyrene at 10 wt% and 5 wt% that were all imaged under SEM.

Imaging revealed that PLGA polymers that underwent TIPS processing had produced highly porous and rough surfaces (Figure 2.1). TIPS processed PLGA 5010 had much lower visible porosity and roughness compared with TIPS PLGA 7502, TIPS PLGA 7502-A and TIPS PLGA 7507 films. Reducing the weight percentage of PLGA 5010 in DMC from 10 wt% to 5 wt% greatly increased the porosity and the interconnectivity of pores on the surface of the TIPS films. Images in Figure 2.1 of TIPS processed 7502-A showed surfaces with high porosity, with pore sizes ranging from nanometre to micron. PLC 7015 had the highest inherent viscosity (1.5 dl/g) and the largest pores could be seen at x3000 magnification. Images show that polystyrene did not produced the distinctive topography that PLGA polymers had formed after TIPS processing. PLGA 5010 10 wt%, PLGA 7502 10 wt%, PLGA 7507 10 wt% and polystyrene 10 wt% control surfaces were produced and imaged using the same conditions as the TIPS films. SEM images show that smooth surfaces were created with no visible pores seen.

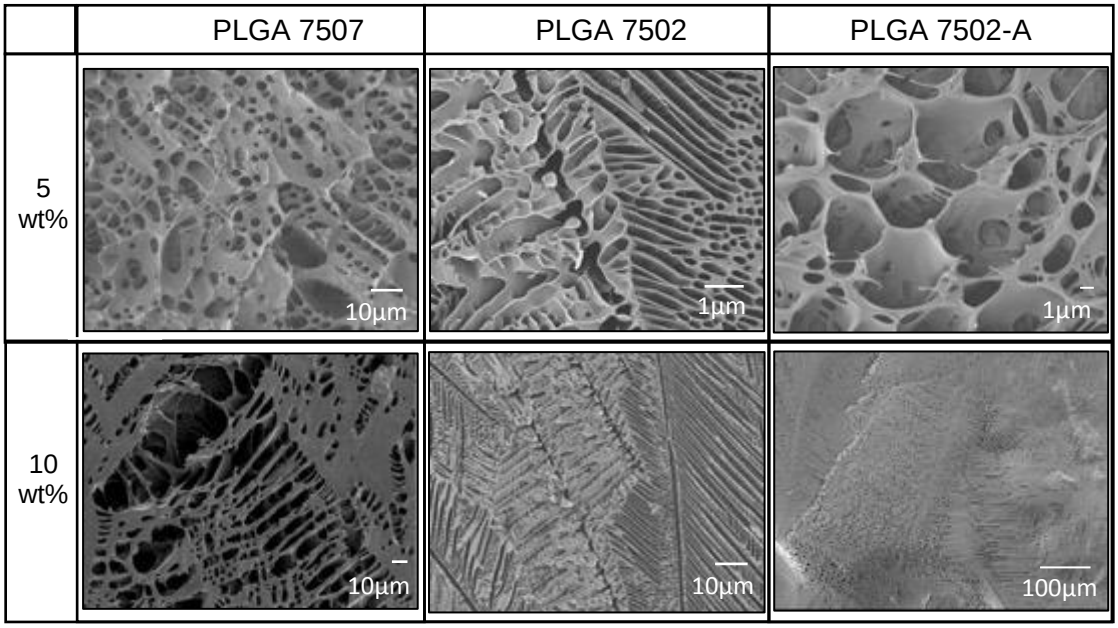

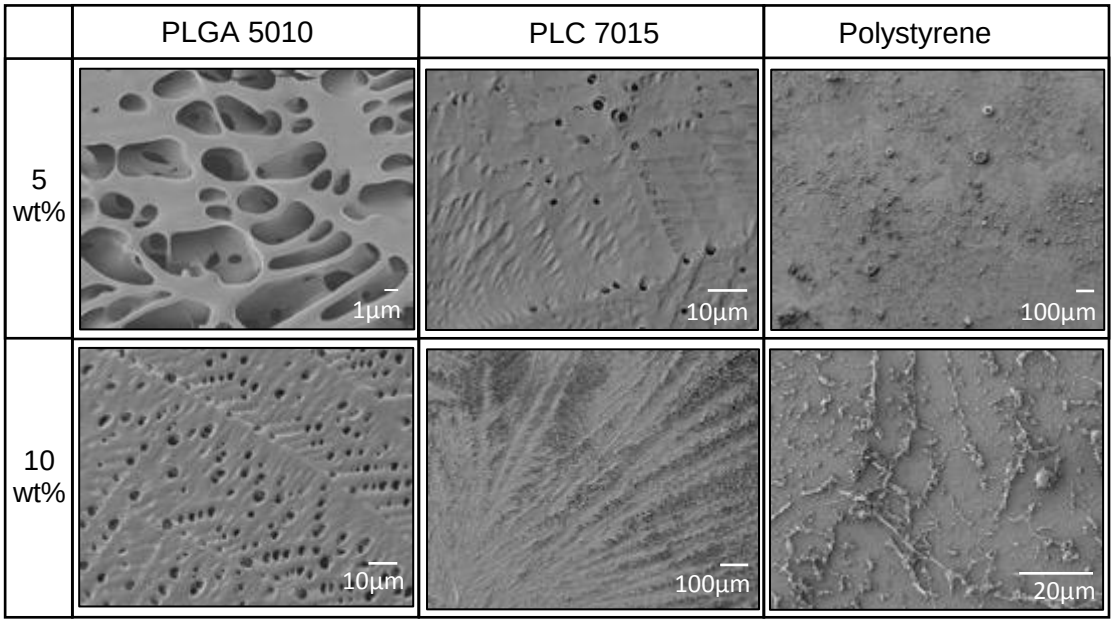

Figure 2.1: SEM images of TIPS processed PLGA 7507, PLGA 7502, PLGA 5010, PLGA 7502-A, PLC 7015 and Polystyrene at 5 wt% and 10 wt%.

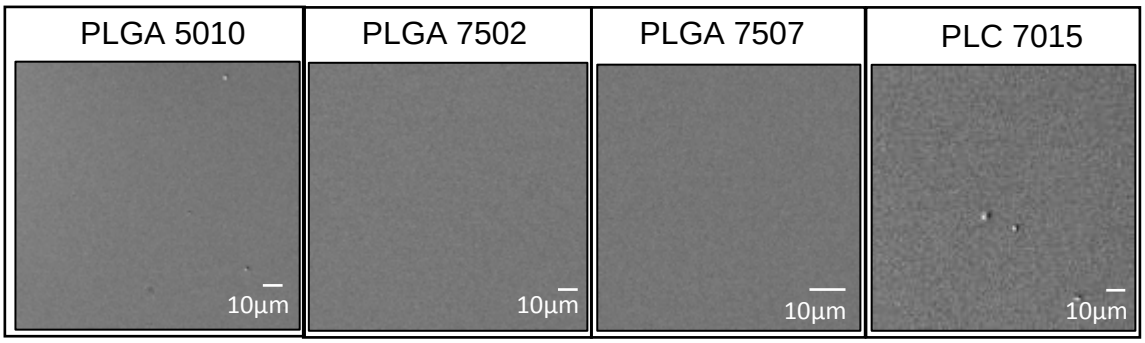

Figure 2.2: SEM images of control PLGA 5010, PLGA 7502, PLGA 7507 and PLC 7015 polymer films.

2.3.2 Surface Texture Analysis

2.3.2.1 Surface Roughness Measurements using Atomic Force Microscopy

AFM was used to quantify the roughness of the polymer films. AFM scans samples by measuring the forces (van der Waals, electrostatic, magnetic and capillary forces) between the cantilever tip and the sample, which is reconstructed into an image of the surface by plotting these results against the position of the tip against the sample. From this the topography of a sample can be calculated. [192, 193] With the preliminary screen of TIPS processed polymer films, Figure 2.3 revealed that films produced with 5 wt% solutions had significantly higher surface roughness compared with between their 10 wt% counterparts. With the highest roughness values detected from PLGA 5010 and PLGA 7507 5wt% TIPS films.

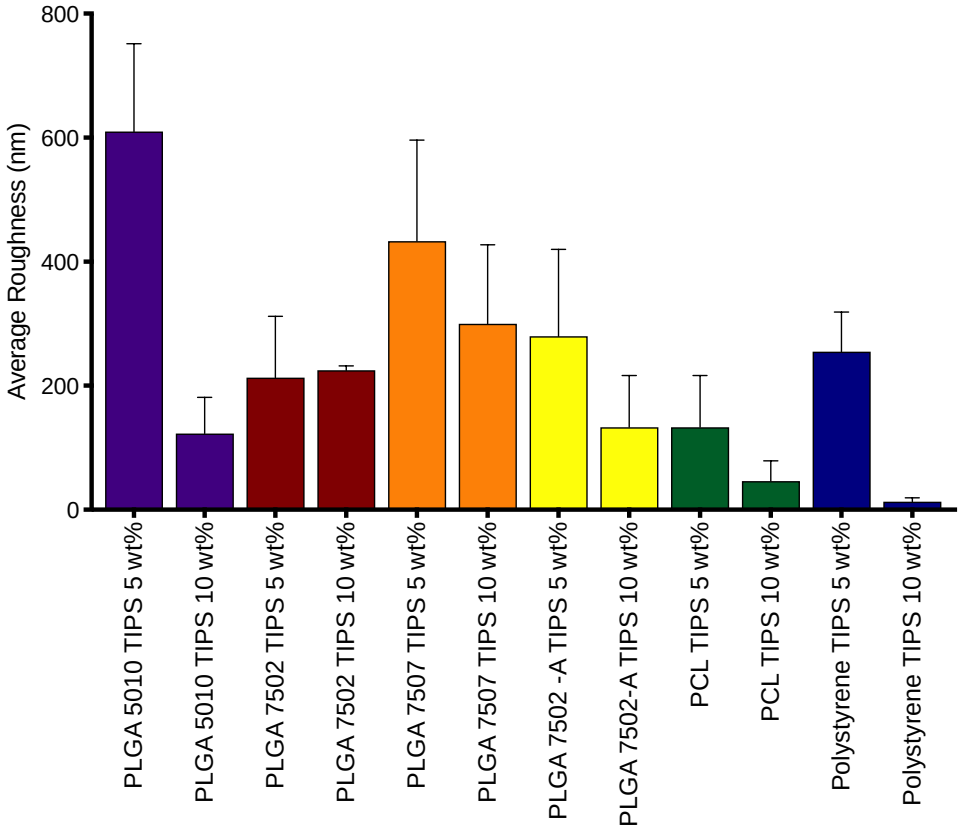

Atomic Force Microscopy Average Roughness. Ordinary One-way ANOVA = **** (P<0.0001).

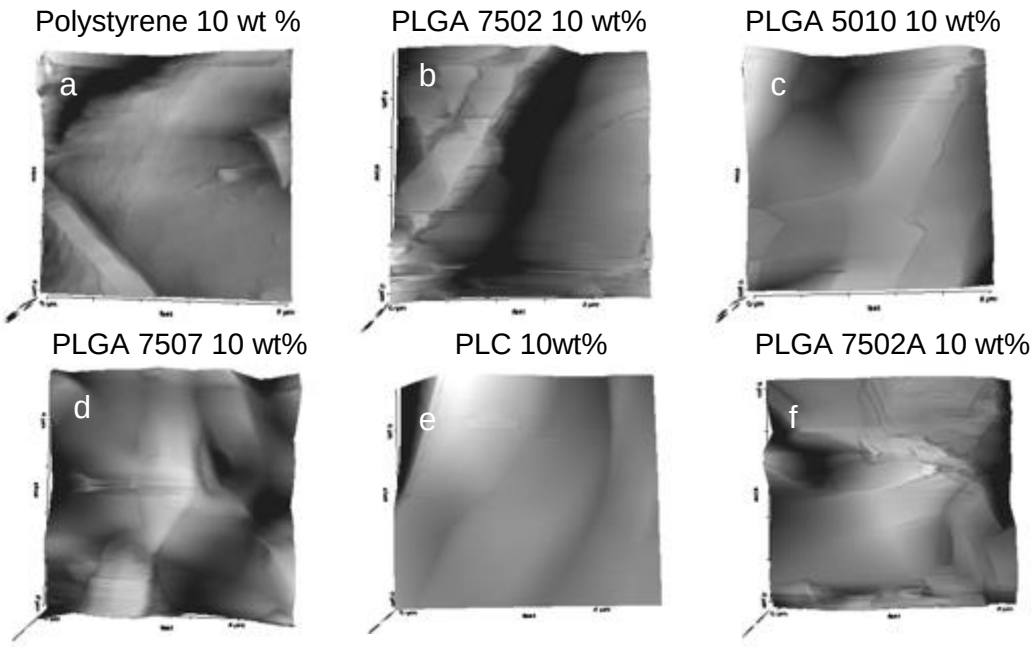

Figure 2.4: AFM images of TIPS processed polymer films at 10 wt%. a) Polystyrene b) PLGA 7502 c) PLGA 5010 d) PLGA 7507 e) PLC f) PLGA 7502A.

2.3.3 Dektak Surface Profilometry Roughness Measurements

Dektak surface profilometry was used to measure surface roughness of polymer films. Figure 2.5 shows that polymer controls also had higher roughness values to polystyrene surfaces. 7502 TIPS polymers had higher average roughness values compared to 7507 TIPS polymer films (6270 nm ±764.48, 1870 nm ±71.1 respectively).

2.3.3 Assessing Cell Viability

A LIVE/DEAD assay was used to investigate any toxic effect of the biomaterial polymer films on ADMSCs. Imaging revealed the highest proportion of live cells on PLGA 7502 10 wt%, PLGA 7507 10 wt% and PLGA 5010 10 wt%. The fewest live cells and the majority of dead cells were seen on PLGA 5010 5 wt%, PCL 5 wt% and PLGA 7502-A 5 wt% (representative images shown in Figure 2.6).

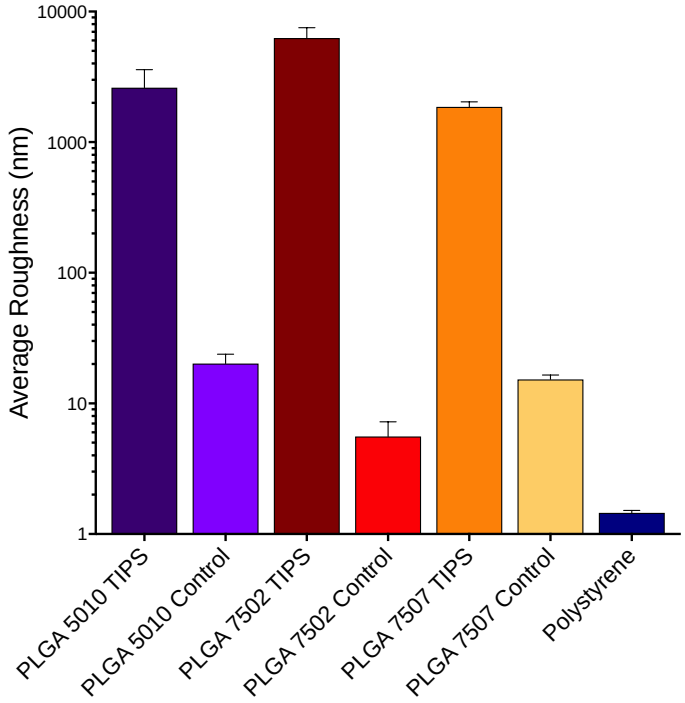

Figure 2.5: Dektak Surface Profilometry Average Roughness Results. (n=3) Ordinary one-way ANOVA = **** (P<0.0001)

2.3.4 Preliminarily Evaluation of the Angiogenic Effects of TIPS Polymer Films

The secretomes from ADMSCs seeded onto PLGA 5010, 7502, 7502-A and 7507 and PLC (5wt % and 10 wt%) TIPS processed films were measured for the angiogenic growth factor bFGF at days 1 and 5. Results show that the 10 wt% formulations of TIPS-processed PLGA 7507, PLGA 5010, PLGA 7502 and PLGA 7502-A polymer films led to increased amounts of bFGF in the supernatant compared with the 5 wt% formulations (Figure 2.7). PLGA 7507 10 wt%, PLGA 5010 10 wt%, PLGA 7502 10 wt% had the highest bFGF levels after 5 days. Some of the TIPS film samples, such as PLC 5wt%, PLGA 7502A 5wt% and PLGA 5010 5wt% had reduced amounts of bFGF in the supernatant after 5 days compared with bFGF levels at day 1.

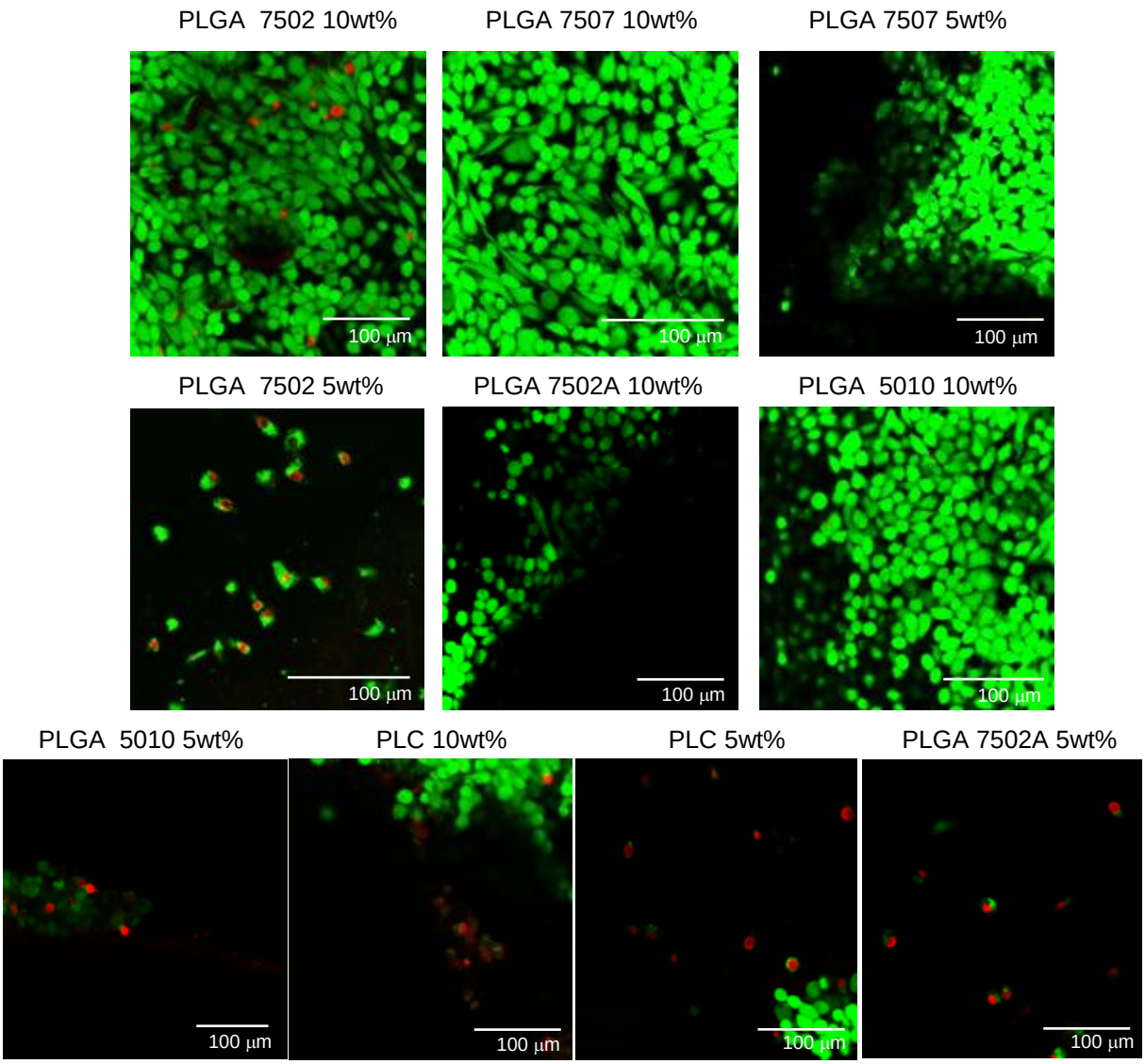

Figure 2.6: LIVE/DEAD representative fluorescent images of TIPS processed polymer films.

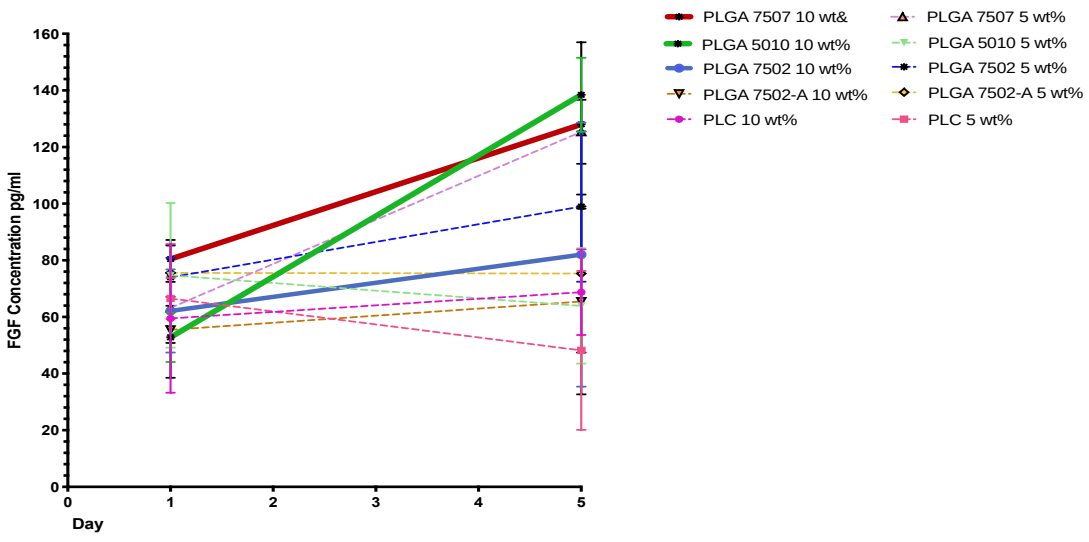

Figure 2.7: bFGF secretion from ADMSCs over 5 days when attached to TIPS polymer films. (n=3)

2.4 Discussion

To determine the optimal biomaterial for use as an angiogenic therapy, a range of polymer films were manufactured using the TIPS process at 5 wt% and 10 wt%. Four different formulations of PLGA with varying lactic acid contents and inherent viscosities (summarised in Table 2.1) were investigated as well as PLC that was chosen as an alternative degradable polymer to PLGA, and polystyrene was investigated as a non-degradable polymer. Physical parameters including roughness and porosity were characterised. Polymer films were first imaged using SEM to evaluate the surface topography and revealed distinct differences between different compilations of PLGA TIPS processed polymers, with PLGA formulations forming more porous surfaces compared to PLC and polystyrene TIPS processed films. As SEM is mainly a qualitative tool, AFM and Dektak profilometry were employed to quantify surface roughness of the polymer surfaces.

TIPS polymer coatings produced from 5 wt% solutions produced polymer films with higher porosity compared with 10 wt% solutions due to the increase in solvent in the 5 wt% solution. During the TIPS process, the solvent was frozen and removed by sublimation during lyophilisation. This removal of the solvent resulted in the unique hierarchical and porous structure of the TIPS materials. Figure 2.1 shows TIPS processed polystyrene did not produce TIPS surfaces or high porosity, and unlike any of the other samples, small microparticles were seen in the images. This could be a reaction of the different solvent (MEK) with the polymer to the liquid nitrogen. Roughness measurements reveal that the 5 wt% polystyrene films had similar average roughness to PLGA and PLC TIPS polymer films, but the 10 wt% TIPS processed polystyrene films had very low roughness levels. Figures 2.1 and 2.4 show TIPS surfaces formed from different compositions of PLGA were rougher and more porous compared with PLC. PLC is a copolymer of lactic acid and ε-caprolactone and is a biodegradable polymer with a much slower degradation rate in compared with PLGA (2-4 years), due to the more complex chemical structure taking longer to break down (Figure 2.8). In addition, PLC has been shown to have

increased flexibility and has been shown to have poor cell adhesion due to poor hydrophilicity in comparison to PLGA. [194, 195] Quantification of surface roughness using AFM (Figure 2.3) exhibited that PLC 5 wt% had the lowest average roughness compared to PLGA 5 wt% compositions, and the same trend was seen with the 10 wt% PLC group. The reduced surface roughness observed is associated with the low porosity of PLC, highlighted in SEM images (Figure 2.1).

The difference in roughness between PLC and PLGA can also be attributed to the higher solubility of PLGA in DMC. During TIPS processing two distinct phases were formed: a polymer rich and a solvent rich phase. Subsequent lyophilisation resulted in the sublimation of the solvent resulting in the formation of a porous and rough structure. Polymers with higher solubility disperse more evenly within the polymer solution and phase separation takes longer than with polymers with lower solubility, resulting in a more dense structure and rougher surface topographies. [196, 197] PLC had a high inherent viscosity (1.5 dl/g) and 70% lactic acid content and therefore had a very slow degradation rate. This characteristic was deemed not suitable for this proposed application as ideally *in vivo* a material would degrade as new tissues form. In addition, the continued presence of a material *in vivo* could result in a prolonged immune response and adverse side effects such as failure of the implant. Therefore, from this, coupled with the low surface roughness and porosity, PLC was not brought forward into further studies.
7502-A is a copolymer comprising of 75% lactic acid and 25% glycolic acid with an additional acid terminated side group (COOH). The addition of COOH caused the polymer to become more hydrophilic and degrade faster in the presence of water, which was further increased by a low inherent viscosity of 0.2 dl/g. SEM images in Figure 2.1 of TIPS processed 7502-A and roughness measurements (Figure 2.3) revealed that average roughness was similar to TIPS 7502 films, suggesting that the addition of the acid terminated side group did not affect the roughness of the material produced using the TIPS process. However, due to the fast degradation rate, this material was very difficult to handle as it would disintegrate and showed low mechanical integrity. This suggested that it would not be suitable for the proposed application, as the

device would need to be able to withstand delivery and implantation into a load bearing limb. [198]

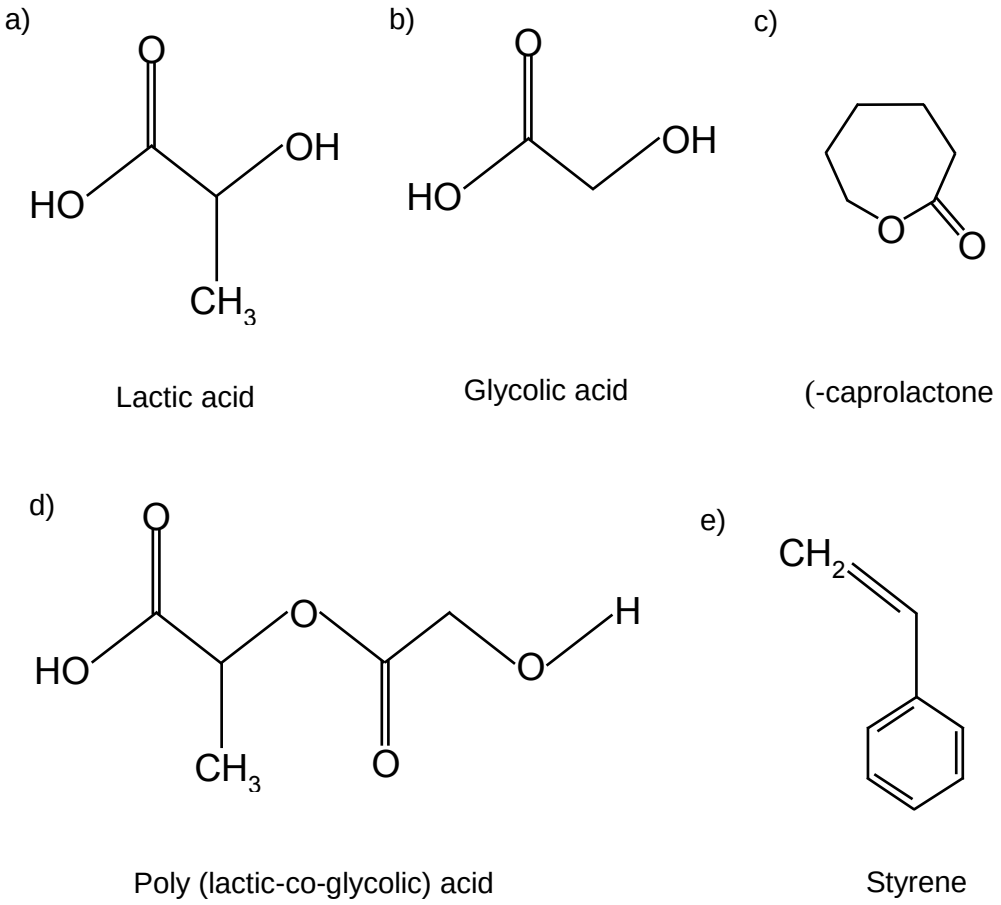

Figure 2.8: Molecular structure of a) lactic acid, b) glycolic acid, c) (-caprolactone, d) Poly (lactic-co-glycolic acid) and e) styrene.

Dektak surface profilometry was used to quantify surface roughness of PLGA 7507 TIPS films, PLGA 7507 control films, PLGA 7502 TIPS films, PLGA 7502 control films, PLGA 5010 TIPS films, PLGA 5010 control films and polystyrene control films. Results displayed in Figure 2.5 reveal that TIPS processed polymers had significantly higher roughness than controls, with PLGA 7502 TIPS having higher average roughness compared with PLGA 7507 TIPS, which were also reflected in AFM measurements (Figure 2.3). The divergences between the measurements obtained from AFM and Dektak surface profilometry instruments can be seen as much higher values obtained from the Dektak profiler. This is due to the conditions in which measurements

were taken. Dektak profilometry was performed in dry conditions, whereas AFM was conducted in liquid that produced conditions more representative of intended biological use. This exposure to liquid would have initiated degradation, resulting in lower roughness measurements. Therefore, it can be proffered that measurements taken with AFM are more representative, however what these two different techniques have highlighted is how quickly the roughness of these polymers can change. This is an important consideration when selecting which polymer composition to use as one of the aims of this study was to assess how cells respond to TIPS processed surfaces, where materials may appear rough in initial measurements (and images) but may not maintain their topography once exposed to aqueous conditions.

The difference in behaviour of the various PLGA compilations can be largely attributed to the inherent viscosity and lactic acid content. Inherent viscosity affects the degradation of the polymer as it is dependent on molecular weight, and the lower the inherent viscosity, the faster the degradation resulting in a less rough surface. For example, PLGA 7507 and PLGA 7502 have a lactic acid content of 75%, but inherent viscosities if 0.7 dl/g and 0.22 dl/g respectively. This caused significant differences in the roughness (Figures 2.4 and 2.5), porosity (Figure 2.1) and thus degradation rate of the polymer films. Whereas co-polymers with a lower lactic acid content such as PLGA 5010 (50%) degraded quicker than PLGA 7507 (composed of 75% lactic acid) as increased lactic acid content results in a less hydrophilic polymer that cannot absorb as much water. Water drives the hydrolysis of ester bonds that break the polymer chain resulting in degradation. [105] Despite having high average roughness values (Figures 2.4 and 2.5) the fast degradation rate of PLGA 5010 made the handling very difficult due to the fragility of the polymer, and long-term cellular studies unfeasible.

To facilitate cell attachment to the films the polymers had to be hydrophilised, as PLGA is highly hydrophobic and a hydrophilic surface is necessary to facilitate cell attachment. By hydrophilising the surfaces, the proteins found in cell culture medium (e.g. fibronectin and vitronectin) that are hydrophobic can

attach to the material and thus cells can successfully attach and survive. [199, 200] Hydrophobicity, along with surface topography and chemistry can strongly influence biocompatibility of the material. Lee *et al.*, 1998, showed that creating materials with moderate hydrophilicity achieved superior serum adsorption and fibroblast, endothelial and ovary cell attachment. [201] Hydrophilisation was achieved by exposing the materials to absolute ethanol as it has been previously shown that ethanol can successfully hydrophilise TIPS microparticles, [202] as well as larger PLGA scaffolds. [203] Furthermore, it is hypothesised that the addition of ethanol can contribute to the sterilisation of the materials, which is vital to avoid contamination and infection in downstream studies.

Preliminary biological characterisation of cellularised polymer films involved evaluating biocompatibility of the materials through a LIVE/DEAD assay and measuring the expression of the angiogenic growth factor bFGF from the cells. Representative images in Figure 2.6 demonstrate that there were considerably more cells on PLGA 7507 10 wt% and PLGA 7502 10 wt% polymer films, suggesting that these formulations of PLGA allowed for superior cell attachment and survival after 24 hours. This is due to the higher surface roughness and porosity of the PLGA polymer films compared to PLC, that facilitated cell attachment. Despite the high surface roughness and porosity of PLGA 7507-A, this polymer film did not support cell attachment, most likely due the fast degradation rate of the material upon exposure to liquid and poor mechanical integrity, making PLGA 7507-A less suitable for the proposed application.

To further assess the activity of the cells attached to polymer films, bFGF secretion into supernatants was measured. bFGF is a potent growth factor that is involved in angiogenesis. Specifically, bFGF stimulates endothelial cells to secrete matrix metalloproteinases and additional enzymes that degrade the basement membrane, that allows for the migration of endothelial cells and thus blood vessel formation. [32] bFGF ELISA results (Figure 2.7) show that the highest secretion of bFGF were from ADMSCs seeded onto PLGA 7507 10 wt%, PLGA 7502 10 wt% and PLGA 5010 10 wt%, suggesting that these

formulations of PLGA not only support cell attachment, but the cellular secretion of bFGF. In comparison, ADMSCs seeded onto PLC and PLGA 7502-A formulations had lower levels of bFGF detected, most likely due to the fewer cells that had attached to the surfaces, therefore they were not brought forward into further studies.

From the physical and biological characterisation results it was decided to take PLGA 7507 10 wt% and PLGA 7502 10 wt% polymer films into further studies due to their superior pro-angiogenic behaviour and unique surface topographies.

2.5 Summary

From preliminary studies evaluating different TIPS-processed polymers through physical and biological characterisation it was determined that PLGA 7507 and PLGA 7502 would be studied further in comparison to smooth PLGA controls to evaluate how surface topography effects cellular behaviour. In addition, smooth polystyrene controls were included to evaluate the effect of PLGA and its degradation on cellular behaviour. Physical characterisation of 2D polymer films with SEM, AFM and Dektak profilometry revealed that the TIPS process had produced highly porous and rough surfaces. AFM analysis highlighted differences between different formulations of PLGA, with TIPS processed PLGA 7507 polymer films being rougher and stiffer than PLGA 7502 TIPS polymer films. LIVE/DEAD imaging illustrated superior cell attachment and survival on PLGA 7507 TIPS and PLGA 7502 TIPS polymer films, which in turn resulted in an increase in bFGF secretion. PLGA 7507 TIPS and 7502 TIPS polymer films were investigated further in subsequent chapters.

Part I.

Chapter 3: Preparation of TIPS Processed Substrates

3.1 Introduction

This chapter is focused on the fabrication of TIPS polymer films from two formulations of PLGA; 7507 and 7502, selected from the findings outlined in section Part I. Chapter 2. The polymer films were characterised using various microscopy techniques where roughness and stiffness measurements were reported, with a view to determine parameters of the TIPS processed materials that may influence them in the application as a scaffold for therapeutic angiogenesis.

3.2 Methods

3.2.1 Polymer Solution Preparation

Solutions of PLGA 7502 and PLGA 7507 were prepared as described in Chapter 2 Section 2.2.1.

3.2.2 TIPS Film Material Preparation

The preparation of TIPS films was described in Chapter 2 Section 2.2.2.

3.2.3 Control Film Material Preparation

The preparation of control films was described in Chapter 2 Section 2.2.3.

3.2.4 High-Resolution Imaging Using Scanning Electron Microscopy

SEM was described in Chapter 2 Section 2.2.4.

3.2.5 Surface Texture Analysis Using Atomic Force Microscopy

AFM was described in Chapter 2 Section 2.2.5.

3.2.6 Internal Structure Analysis using X-ray Nano Computed Tomography

NanoCT was used to analyse the internal structure of TIPS processed materials. The Xradia Versa XRM-520 nanoCT system was used to visualise the internal structure of 7507 TIPS polymer films. A 5 mm circular segment from the 13 mm 7507 TIPS polymer films was taken using a biopsy punch (A615110, Agar Scientific, UK). An area of 510 μm x 510 μm from the polymer film was taken with 1401 projections and 57 seconds exposure time with bin set at 1. A reference image was taken and used to normalise the final scan.

3.2.7 Statistical Analysis

Statistical Analysis methodology was described in Chapter 2 Section 2.2.11.

3.3 Results

3.3.1 Ultrastructural Imaging of Polymer Films Using Scanning Electron Microscopy

The 10 wt% PLGA 7507 TIPS, PLGA 7502 TIPS, PLGA 7507 control, PLGA 7502 control and polystyrene polymer films underwent a degradation study and were imaged under SEM. Polymer films were imaged at day 1, 4, 7, 10 and 21. Figure 3.1 displays evidence that the TIPS treated polymers degraded over time, with a loss in porosity and roughness. The control PLGA films had few physical differences from day 0 to 21, indicating that any biological effects seen from cells attached to the control surfaces over time would not be from changes in surface topography. PLGA 7502 TIPS film visibly lost physical features such as roughness and porosity after 1 day, which was quicker in comparison to with to 7507 TIPS films, which still had visible pores at day 10. The TIPS processed films had topographies similar to control films after 21 days. As polystyrene is a non-degradable material, there were no visible signs of degradation at any of the tested time-points.

3.3.2 Surface Texture Analysis

3.3.2.1 Atomic Force Microscopy Roughness Measurements

The 10 wt% PLGA 7507 TIPS, PLGA 7502 TIPS, PLGA 7507 control, PLGA 7502 control and polystyrene polymer films underwent a degradation study and were examined under AFM for roughness and stiffness. The results show that the TIPS polymer films were significantly rougher than the smooth controls, in particular polystyrene which had overall the lowest roughness measurements. PLGA 7502 TIPS films had the highest roughness at day 0 (440 ±277 nm), however due to its fast degradation rate this decreased significantly over time (at day 10 55 ±28 nm). PLGA 7507 TIPS also had a high roughness at day 0 (225 ±74 nm) with a much slower degradation rate

over time (at day 10 140 ±10 nm). This quantification of roughness corresponds to the images in Figure 3.1.

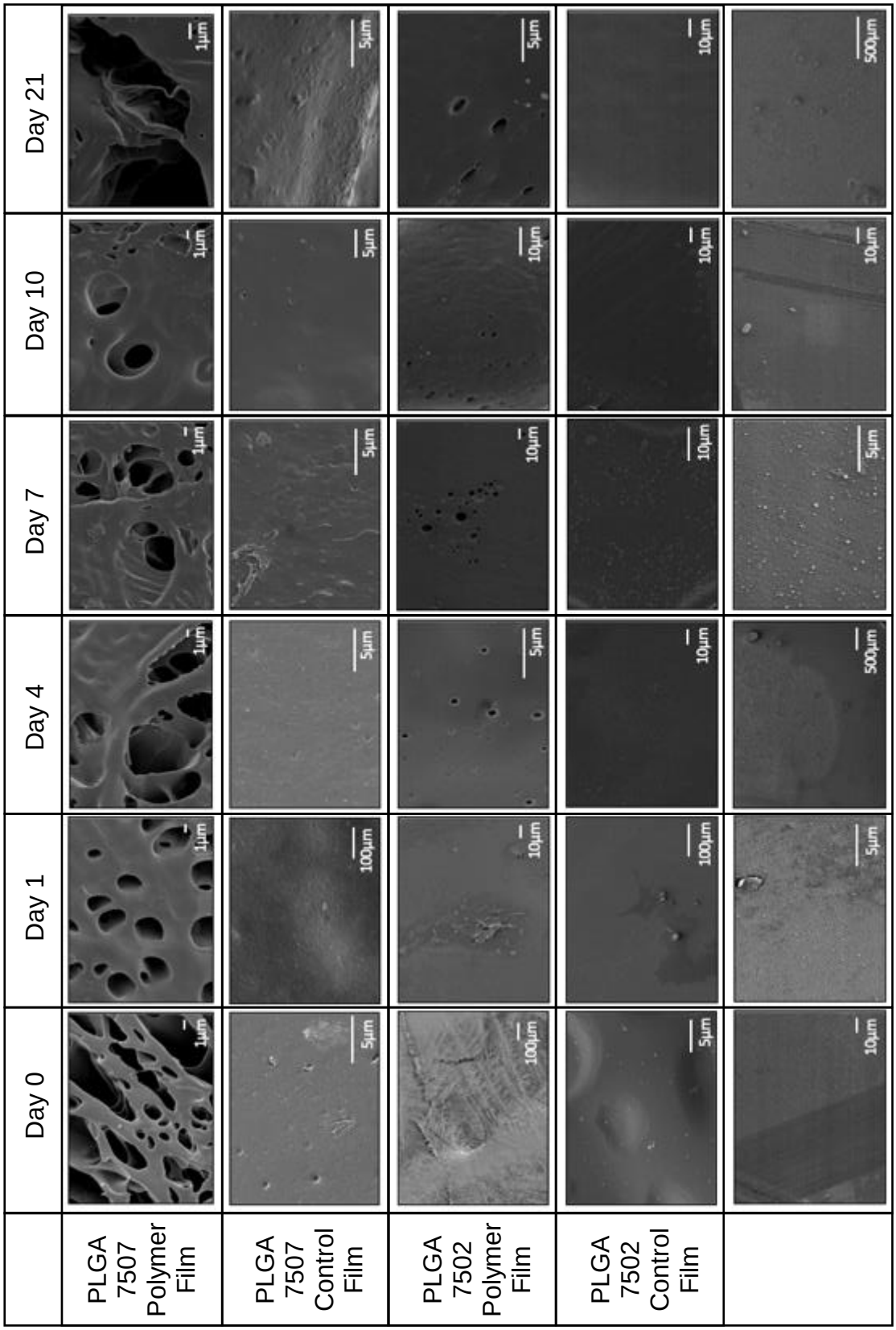

Figure 3.1: SEM images showing the degradation of PLGA 7507 TIPS films, PLGA 7507 control films, PLGA 7502 TIPS films, PLGA 7502 control films and polystyrene control films at days 0, 1, 4, 7, 10 and 21.

(nm)	Day 0	Day 1	Day 4	Day 7	Day 10
PLGA 7507 TIPS	225	414	319	226	138
PLGA 7507 Control	109	231	63	228	2.3
PLGA 7502 TIPS	440	664	443	1011	55
PLGA 7502 Control	69	49	28	10	0.6
Polystyrene	6.6	4.5	8.1	6.7	5.1

Table 3.1: AFM Average roughness measurements of polymer films in nm. (n=5)

	Day 0	Day 1	Day 4	Day 7	Day 10
PLGA 7507 TIPS		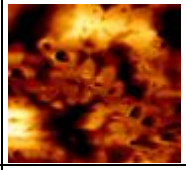	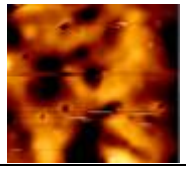	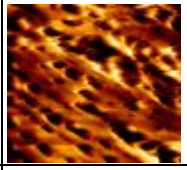	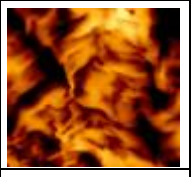
PLGA 7507 Control	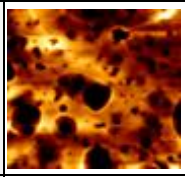	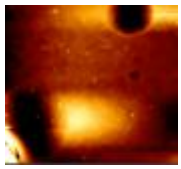	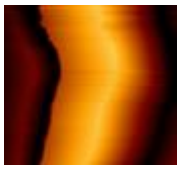	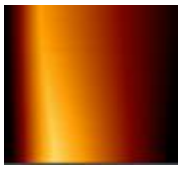	
PLGA 7502 TIPS		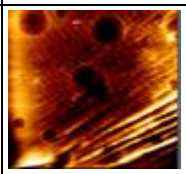		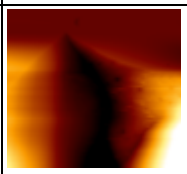	
PLGA 7502 Control	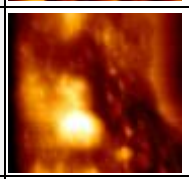	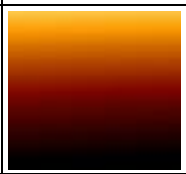	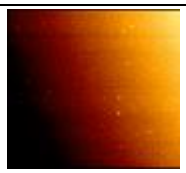	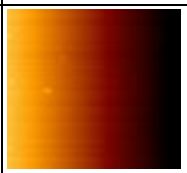	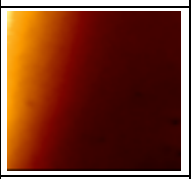
Poly-styrene	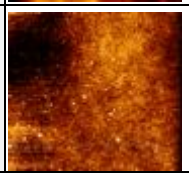	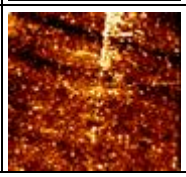	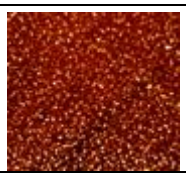	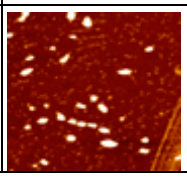	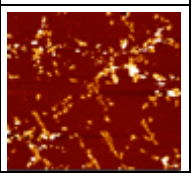

Figure 3.2: AFM images of 7507 TIPS polymer films, 7507 control films, 7502 TIPS polymer films, 7502 control films and polystyrene films at days 0, 1, 4, 7 and 10. Scale: 50 µm x 50 µm.

3.3.2.2 Determining Polymer Film Substrate Stiffness

AFM was used to measure the stiffness of PLGA 7507 TIPS, PLGA 7502 TIPS, PLGA 7507 control, PLGA 7502 control and polystyrene polymer films. Polystyrene had significantly higher stiffness measurements (Table 3.2). The stiffness of polystyrene films did not considerably change over time as it is a non- degradable material, and stiffness can be affected by degradation. PLGA structures fabricated using the TIPS process had higher stiffness measurements compared to control polymers, with 7507 TIPS films having the highest stiffness measurements of the PLGA samples tested (4575 ±1344.5 MPa at day 0). All PLGA samples stiffness values decreased as the material degraded.

	Day 0	**Day 1**	**Day 4**	**Day 7**	**Day 10**
PLGA 7507 TIPS	4.6 GPa	1.7 GPa	0.9 GPa	0.8 GPa	0.2 GPa
PLGA 7507 Control	0.1 KPa	0.1 KPa	6.0 Pa	0.1 Pa	0.1 Pa
PLGA 7502 TIPS	1.2 MPa	0.7 MPa	0.6 MPa	0.4 MPa	0.2 MPa
PLGA 7502 Control	1.2 Pa	0.6 Pa	0.6 Pa	0.6 Pa	0.05 Pa
Polystyrene	2.1 GPa	3.7 GPa	3.3 GPa	2.8 GPa	2.9 GPa

Table 3.2 AFM Average stiffness (MPa) measurements of polymer films. (n=5)

3.3.3 Investigating the Internal Structure of TIPS Films

The internal structure of PLGA 7507 TIPS polymer films were studied using X-ray NanoCT techniques. Reconstructed images (Figure 3.3) reveal that for

TIPS processed polymers had interconnected porous networks beyond the surfaces of the samples.

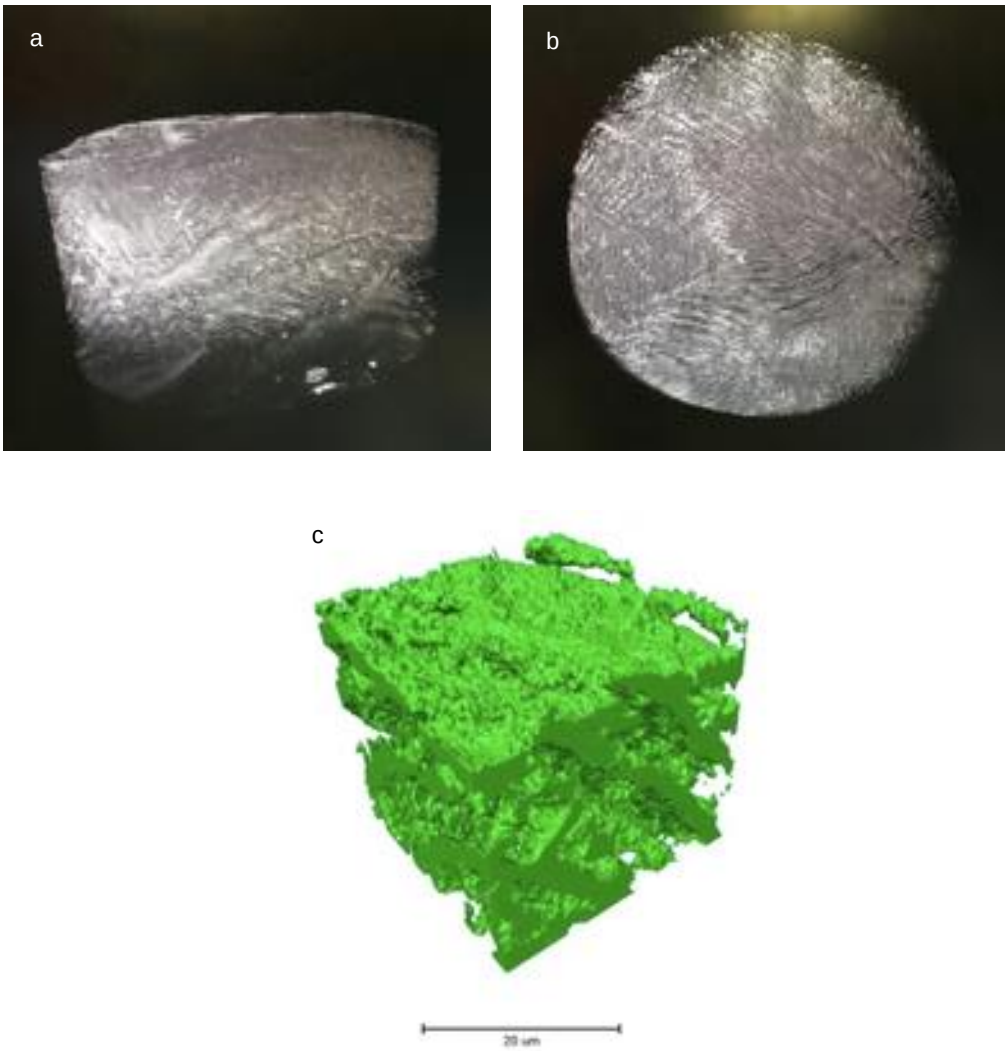

Figure 3.3: NanoCT images a) 3D reconstruction of PLGA 7507 TIPS polymer film side view b) 3D reconstruction of PLGA 7507 TIPS polymer film surface view c) 3D reconstruction of PLGA 7507 TIPS polymer film.

3.4 Discussion

Exploring 2D polymer film surfaces provided advantages such as reproducibility and ease of manufacture. In addition, vital characterisation methods such as AFM and Dektak profilometry were only possible on 2D surfaces, therefore to investigate TIPS processed PLGA with these techniques, 2D films were produced.

As SEM is mainly a qualitative tool, AFM was utilised to quantify surface roughness and the stiffness of the polymer surfaces. PLGA 7507 TIPS films, PLGA 7507 control films, PLGA 7502 TIPS films, PLGA 7502 control films, and polystyrene control films were investigated. SEM images (Figure 3.1) revealed that PLGA 7502 TIPS polymer films lost topographical surface features over time which were quantified through average roughness measurements (Table 3.1). This effect can be attributed to the exposure of PLGA 7502 to PBS, which triggered the degradation of the polymer (through hydrolysis), driven further by its low inherent viscosity. The high porosity of the material also increased degradation rate, as porosity increases surface to volume ratios, which in turn drives degradation. [204] TIPS PLGA 7507 polymer films showed signs of degradation with a loss of surface roughness and porosity seen, albeit at later time points due to the slower degradation rate of the PLGA 7507 formulation in comparison to PLGA 7502 (Figure 3.1). PLGA 7502 control, PLGA 7507 control and polystyrene control films had little topographical surface features and thus average roughness measurements did not significantly change over time. Therefore, cellular behaviour changes seen on these surfaces would not be in a response to changes in topography. Confirmation of the smooth surfaces of the control films was vital in order to accurately compare the response of the cells on the TIPS surfaces to smooth surfaces.

In addition to quantifying roughness, AFM also measured the stiffness of the polymer films. The stiffness of a material dramatically influences cell behaviour in terms of survival, attachment, proliferation, migration and differentiation. It

has been shown that cells on stiffer surfaces attach more strongly through focal adhesions and differentiate more readily (depending on the cell type). [205] Although, a balance has to be achieved, as very stiff surfaces, such as tissue culture plates, can result in changes in morphology such as unwanted rounding of cells. [178] The observation that TIPS-processed materials had a higher elastic modulus compared with control materials was also observed by Cao *et al.*, 2006, where highly porous networks were shown to have increased elastic moduli. [206, 207] Even as the 7507 and 7502 TIPS processed polymer films began to degrade, the stiffness was higher than 7507 PLGA and 7502 PLGA control polymer films, due to the continued presence of porosity, highlighted in stiffness results (Table 3.2). All the samples stiffness values decreased from day 0 to 1, where in this time the materials had been hydrophilised as they would be to facilitate cell attachment before *in vitro* cell culture experiments. This effect was also seen in experiments by Wu *et al.,* 2004, where it was shown that hydrophilising polymer scaffolds resulted in a decrease in Young's modulus. [208] In addition, the decrease in Young's modulus can be attributed to the initiation of degradation. It has been shown that different formulations (7507 and 7502) of smooth PLGA did not affect the stiffness, [209] as seen in the stiffness measurements of the control polymer films. This suggests that the TIPS structure effected the stiffness of the materials, with the increase in stiffness seen promoting cell attachment and proliferation. [178]

Furthermore, it has also been widely acknowledged that surfaces that have stiffnesses comparable with the ECM result in improved cell responses. [178, 205, 210, 211] The stiffness of ECM *in vivo* varies greatly, with muscle tissue stiffness between 0.8-0.4 MPa and bone approximately 100 GPa. [212, 213] Cells respond to the stiffness of a material, for example stiffer surfaces have been shown to promote osteogenic differentiation of stem cells, as bone inherently has high stiffness. [214-216] Consequently, it is vital to tune material properties for the desired outcome. Therefore, the lower stiffness of PLGA could prove to be more advantageous for ADMSC survival and pro-angiogenic behaviour over stiffer polymers such as polystyrene.

NanoCT imaging (Figure 3.3) displayed that TIPS polymer films had an interconnected porous structure beyond the surface, suggesting that porosity would remain even as the material began to degrade. A scaffold with a highly porous interconnected structure, such as polymers processed with TIPS, is advantageous for tissue engineering applications as it allows for cell and tissue infiltration, cell proliferation and nutrient diffusion. [217, 218]

3.5 Summary

Two distinct PLGA based polymer films were produced through TIPS processing. Physical characterisation revealed that 7507 TIPS polymer films were rougher, stiffer and degraded more slowly than PLGA 7502 TIPS polymer films. NanoCT imaging revealed that TIPS processed polymer films had an interconnected porous structures beyond the surface, indicating the potential for prolonged porosity, mechanical integrity and enhanced cellular infiltration *in vivo*. From these findings the TIPS processed polymer films were investigated further for their effect on ADMSC attachment, proliferation and angiogenic behaviour.

Part I.

Chapter 4: *In Vitro* Biological Characterisation of TIPS-Processed Films

4.1 Introduction

It has been established that delivering cells in suspension for cell therapy applications results in poor retention at the implant site. [5, 77, 92-94] Because of this, implanted cells are not able to elicit their full therapeutic effect, and any therapeutic potential seen *in vitro* are rendered redundant. Therefore, it is vital to explore delivery techniques that allow for improved cell retention. The proposed method is to utilise biomaterials. Biomaterials can support cell attachment, proliferation and anchor the cells at the implant site. [86] However, before this stage, it must be established that cellularising TIPS-processed polymers is possible and how the cells respond to the biomaterial. TIPS-processed polymers could offer superior cell attachment and proliferation in comparison to traditional 2D tissue culture surfaces due to the rough topography achieved during processing more accurately representing the ECM, where the ECM is vital for cellular attachment, alignment, proliferation and survival. [135] It has been shown that the addition of micro-topographical features (that mimic the ECM) onto 2D polymer surfaces can facilitate cell attachment and regulate cell shape. [219, 220] Therefore, this chapter explored the cellularisation of TIPS PLGA polymer films that have been shown to have unique rough topographies, and the optimisation of assessing cell viability and proliferation with a view to investigate how the cells respond to the TIPS polymer films in subsequent chapters.

4.2 Methods

4.2.1 Adipose-Derived Mesenchymal Stem Cell Culture

ADMSC cell culture was described in Chapter 2 Section 2.2.7.

4.2.1.1 Adipose-Derived Mesenchymal Stem Cell Growth

Cell growth time and log phase was determined for ADMSCs at passage 2 by seeding 2 x10^5 cells/cm^2 in a T75 cell culture flask. Each flask was trypsinised and cell numbers calculated (as described in Chapter 2 Section 2.2.7) every 24 hours. Results were plotted on a log-linear scale.

4.2.2 Cellularising TIPS Polymer Films

Polymer films were cellularised with ADMCSs as described in Chapter 2 Section 2.2.8.

4.2.3 Assessing Cell Viability Using LIVE/DEAD Staining

The LIVE/DEAD staining protocol was described in Chapter 2 Section 2.2.9.

4.2.4 Quantifying Cells Attached to Polymer Films

4.2.4.1 Quantifying Cell Numbers with CyQUANT NF Cell Proliferation Assay

CyQUANT NF assay (C35006, Molecular Probes, UK) procedure for adherent cells was followed. The dye was prepared by first diluting the provided x5 HBSS stock buffer to x1 HBSS buffer with deionised water. 22 µL of CyQUANT NF dye reagent (protected from light) was added to 10 mL x1 HBSS buffer to make the dye solution. First, a standard curve for cells attached to polymer films was produced. In a sterile 24 well plate serial dilutions of ADMSCs from 200,000 cells/well in 0.5 mL of complete MesenPro RS^{TM} medium was added to each well to 195 cells, in triplicate including a media only control. The plates were incubated at 37^{o}C 5% CO_2 for 24 hours to allow cell attachment to the surface. The culture medium was removed, and the samples were gently washed twice with 500 µL of 1X PBS (P5493-1L, Sigma, UK). 500 µL of the

prepared CyQUANT NF dye solution was added to each well and the plate was incubated for 1 hour. 100 µL of each sample was transferred to a black wall/clear flat bottom 96 well tissue culture plate (CC691, Appleton Woods, UK) in triplicate (n=8). The fluorescence intensity was measured using a fluorescence microplate reader (TECAN SPECTRAFLUOR Fluorescence and Absorbance microplate reader, BETAFTC program, Tecan, Switzerland) at 485 nm excitation and 530 nm emission detection and a standard curve produced. From the standard curve, cell numbers attached to polymer films were interpolated using linear regression analysis. Once the polymer films were cellularised, 0.5 mL of the supernatants were removed and CyQUANT NF used to quantify cell numbers.

4.2.4.2 Quantifying Cell Numbers with PrestoBlue® Cell Viability Reagent

PrestoBlue® cell viability reagent (A13261, Molecular Probes, UK) was used to calculate cell number of ADMSCs seeded onto polymer films (n=8). Polymer films were seeded with 1 x 10^5 ADMSCs and PrestoBlue® Cell viability reagent was added to the samples of interest at a ratio of 1:10 to culture media. Plates were incubated for 4 hours at 37^{o}C 5% CO_2 avoiding exposure to direct light. 100 µL supernatants were transferred into a black wall/clear flat bottom 96 well tissue culture plate in triplicate. The plate was then read using fluorescence plate reader at 560/612nm.

4.2.5 Statistical Analysis

Statistical Analysis methodology was described in Chapter 2 Section 2.2.11.

4.3 Results

4.3.1 Adipose-Derived Mesenchymal Stem Cell Culture

To determine the cell doubling time and log time of ADMSCs a growth curve was created. It was it was vital to not over-passage ADMSCs, as this can lead to unwanted differentiation. Figure 4.1 revealed that low passage (P2) ADMSCs came quickly (approximately 60 hours) out of the lag growth phase and into the log growth phase, where a steady rate of cell proliferation continued for 64-526 hours. From these findings ADMSCs were cultured for at least 64 hours before use in experiments and were not used after 21 days of culture. This is in accordance with the supplier's instructions. [221]

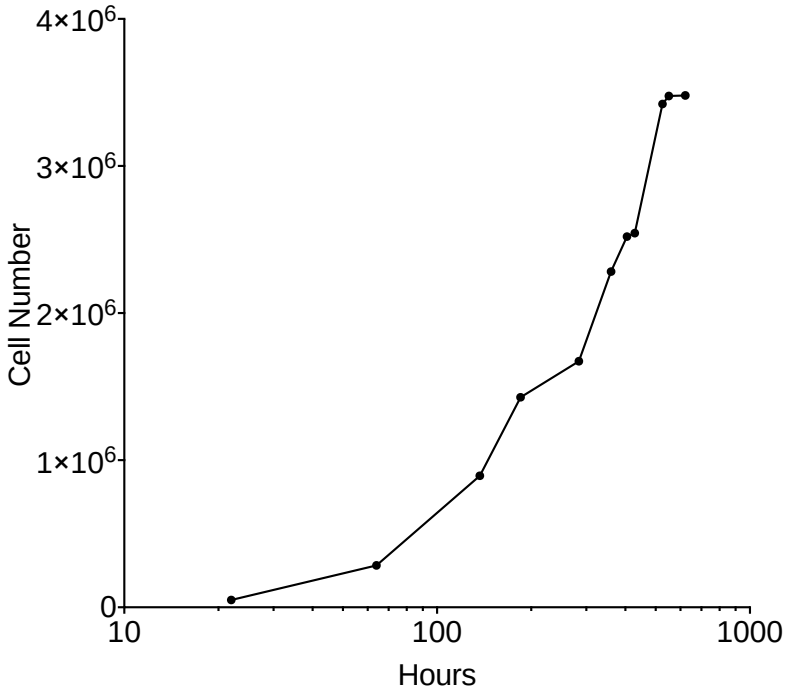

Figure 4.1: Graphical representation of ADMSC growth rate. (n=1)

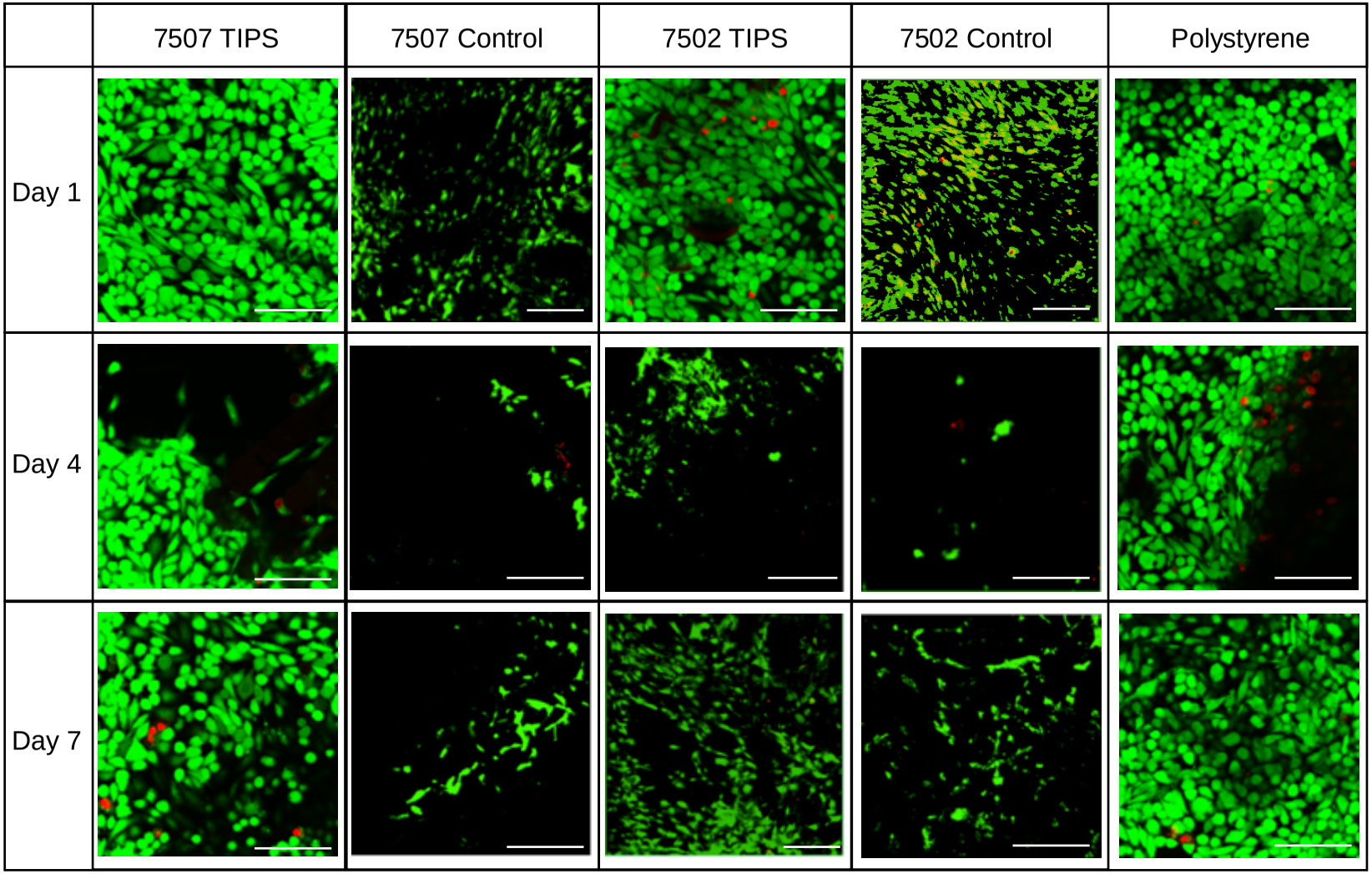

Figure 4.2: LIVE/DEAD fluorescent images of TIPS processed polymer films and controls at days 1, 4 and 7. Scale bars 100 μm

4.3.2 Assessing Cell Viability with LIVE/DEAD Staining

A LIVE/DEAD assay was used to investigate any toxic effect the biomaterial surfaces on ADMSCs and if there was a change in cellular viability over time. LIVE/DEAD images in Figure 4.2 suggest that after 7 days there was a decrease in cell numbers, with fewer cells adhered to 7507 TIPS films, 7507 control films, 7502 TIPS films and 7502 polymer films, with 7507 control and 7502 control films having the highest loss of cells. Images show that cells successfully survived on polystyrene smooth films. Only a few dead cells could be seen on any of the surfaces, suggesting that the polymer films and their degradation products did not promote cell death.

4.3.3 Determining Cell Number and Measuring Cellular Proliferation

Several different cell proliferation assays were investigated for their ability to accurately determine the number of cells attached onto polymer films.

CyQUANT NF dye binds to cellular nucleic acids and measures DNA content via fluorescence, which is directly proportional to cell number. $1x10^5$ cells were seeded onto each polymer film and 24 hours after seeding CyQUANT NF dye was used to measure cell numbers. Figure 4.3 shows that 7507 TIPS films had significantly higher cell attachment over 7507 polymer control and polystyrene films (5.6×10^5 cells/well, 1.3×10^5 cells/well, 3.1×10^5 cells/well respectively). ADMSCs seeded onto 7507 TIPS polymer films had significantly higher cell numbers compared with 7507 control films up to day 7, including significantly higher cell numbers compared to 7502 TIPS and polystyrene polymer films at day 4 (5.5×10^5 cells/well and 3.6×10^5 cells/well respectively).

PrestoBlue® cell viability reagent was also used to determine the ADMSC cell numbers on 7507 TIPS polymer films, 7507 control polymer films, 7502 TIPS polymer films, 7502 control polymer films and polystyrene control films over 10 days. 7507 TIPS polymer films had increased cell attachment 24 hours

after seeding (1 x 10^5 cells/well). After 7 days 7507 TIPS polymer films had higher cell numbers than controls and 7502 TIPS films. This trend continued up to day 10. The cell numbers did not significantly increase from day 1 to 10, suggesting that the films may have been saturated at day 1.

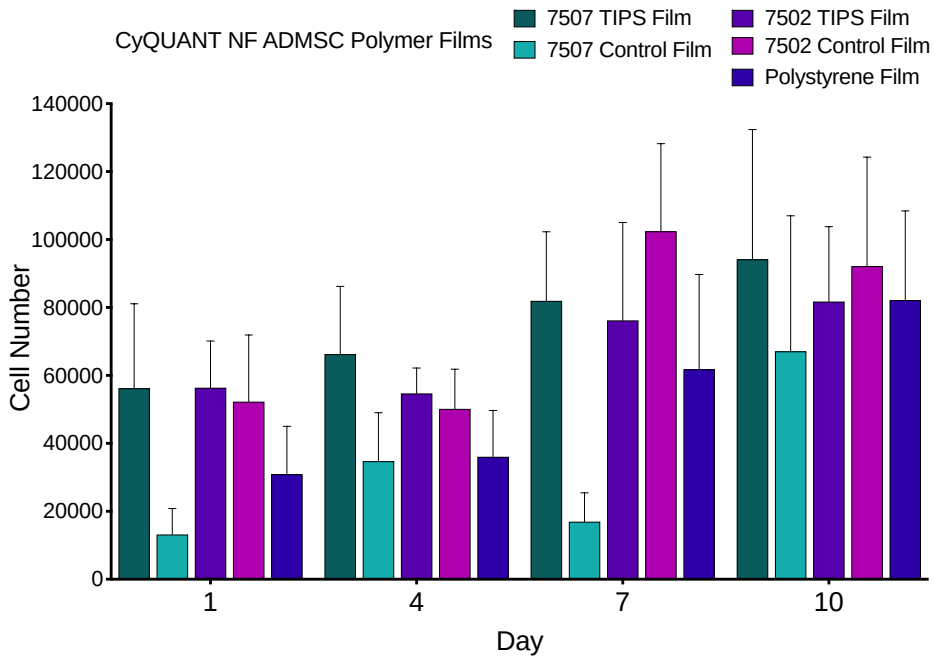

Figure 4.3: ADMSC cell numbers on polymer films at days 1, 4, 7 and 10 quantified with CyQUANT NF cell proliferation assay. (n=8) Two-way ANOVA with Geisser-Greehouse correction = *** (P=0.001)

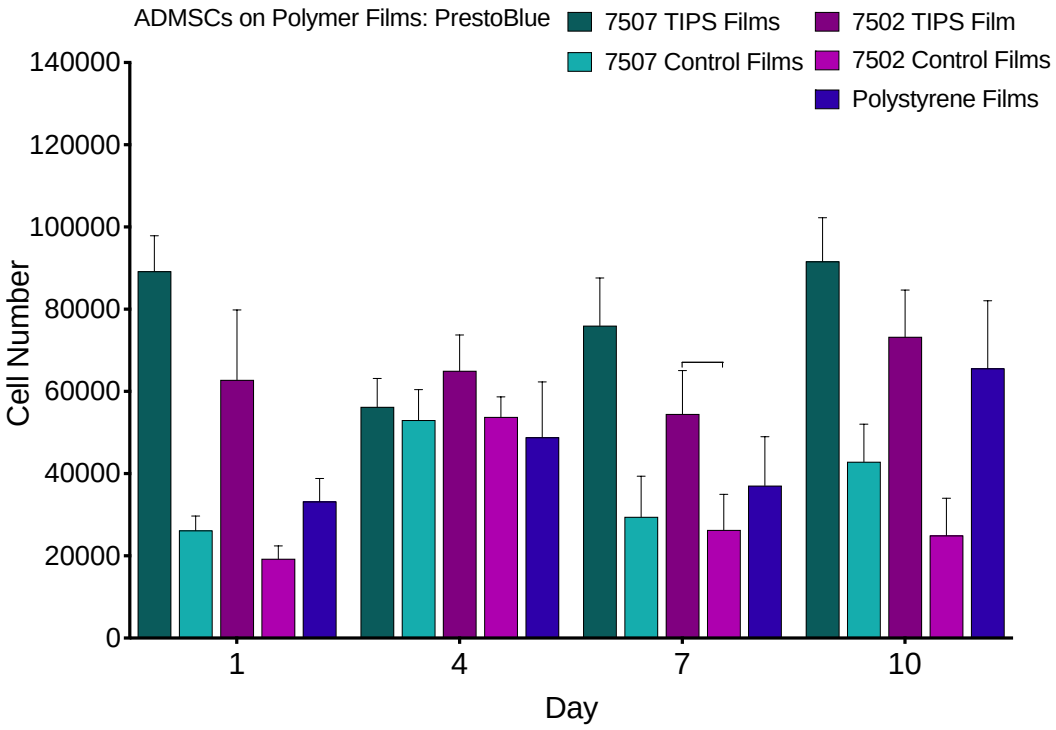

Figure 4.4: ADMSC cell numbers on polymer films at days 1, 4, 7 and 10 quantified with PrestoBlue cell viability assay. (n=8) Two-way ANOVA with Geisser-Greehouse correction = *** (P=0.001)

4.4 Discussion

Studies first focused on the doubling time of ADMSCs as it has been shown that doubling time and prolonged cell culture correlates with decreased self-renewal, differentiation ability of stem cells as well as the decreased expression of stem cell markers such as Sox2 and Oct4. [222, 223] The doubling time of ADMSCs was also determined to ensure the cells used throughout the project remained plastic and had not reached senescence and had full regenerative potential. From Figure 4.1 ADMSCs were cultured for at least 64 hours before use in experiments and were not used after 21 days of culture.

To assess the ADMSCs survival beyond 24 hours and the effect of polymer films on ADMSCs in culture up to day 7, LIVE/DEAD fluorescent imaging (Figure 4.2) was used to image cells attached to PLGA 7507 and 7502 TIPS films, as well as smooth 7507 and 7502 control polymer films and polystyrene films. Polystyrene was included to act as a non-degradable polymer control, as well as to replicate conventional 2D tissue culture conditions. LIVE/DEAD imaging revealed that cells successfully attached to both 7507 and 7502 TIPS surfaces and higher numbers were visible on the TIPS and polystyrene surfaces compared with the smooth control surfaces resulting in more live cell (calcein-AM -green) staining visible. Cellularised PLGA 7507 TIPS films had fewer numbers of live cells visible at day 7 in comparison to day 1. Both the 7507 and 7502 control polymer films had fewer live cells visible at day 1, which decreased through to day 7. This observation is due to poorer cell attachment on the smoother surfaces. Mesenchymal stem cells are an adherent cell type, therefore must achieve attachment to survive. [6] Cells attach to surfaces through transmembrane cell adhesion proteins called integrins. As well as being crucial for cell attachment, shape and survival, integrins can activate signalling pathways within cells. In turn, this can be affected by the ECM, roughness and stiffness of a material. [224] It has been widely reported that cell attachment to surfaces can be dramatically influenced by surface properties, with rougher surfaces facilitating adherence. [225-228] It is proffered that this is because a rougher surface more closely resembles the

architecture of the ECM (where cells would attach in *in vivo* conditions). [172, 229, 230] However polystyrene control was shown to have good cell attachment and survival through the time points. Previous imaging and characterisation had shown polystyrene films to have low surface roughness and porosity (Part I. Chapter 3). As with tissue culture surfaces, the polystyrene films were modified to allow for superior cell attachment, [231] therefore the observed cell attachment and survival seen in Figure 4.2 was expected. Polystyrene was included as a non-degradable control and a comparison to 2D tissue culture as the proposed therapeutic was intended to involve a degradable material. This would negate the need for removal surgeries (and the associated complications) and would reduce the risk of a prolonged immune response that can negatively impact an implant.

To quantify the observed cell attachment seen through LIVE/DEAD imaging, cell numbers and the proliferation of cells on the polymer films was measured through exploring a variety of different assays. CyQUANT NF cell proliferation assay was used to assess the number of cells seeded onto polymer films. The fluorescent CyQUANT NF dye binds to nucleic acids (A-T) in cellular DNA and as such, was used to quantify cell number and proliferation. The assay had many advantages, including fast running time (1 hour), no cell lysis required, high sensitivity and was compatible with high-throughput screening. However, as CyQUANT NF was DNA based assay, the die bound to live and dead cells, although this is more of a concern for counting cells in suspension, where the dead cells are less easily removed. [232] CyQUANT NF was successfully used to detect cell numbers on polymer films, however an alternative assay was investigated that only detected live cells. PrestoBlue® cell viability assay is a resazurin based assay that can be used to determine cell numbers as a function of their metabolic activity. Resazurin is reduced to resorufin in metabolically active cells, resulting in a colour change that can be measured by absorbance or fluorescence. The assay is non-toxic to cells, allowing for the tested cells to be used for further experimentation and has been shown to have excellent sensitivity. [190, 233] When comparing cell numbers from CyQUANT NF and PrestoBlue®, there was a large difference in the number of cells detected on 7507 TIPS polymer films at day 1, with 8.92×10^4 cells/well

detected with PrestoBlue® and 5.6 x 10^4 cells/well with CyQUANT NF. As each polymer film was seeded with 1 x 10^5 cells, these results suggest that PrestoBlue® more accurately detected cell numbers. PrestoBlue® is a very sensitive assay, capable of detecting as few as 12 cells/well, [234] whereas CyQUANT NF has a detection limit of 100 cells. [235] In addition, the number of cells detected on 7507 TIPS polymer films had a large error when read with CyQUANT NF at day 10 ($\pm$3.7 x 10^4 cells/well) compared with PrestoBlue® ($\pm$0.98 x 10^4 cells/well), further suggesting the inaccuracy of the CyQUANT NF assay. There were also large discrepancies between the number of ADMSCs detected on control PLGA groups depending on the assay used. At days 7 and 10, CyQUANT NF detected much higher cell numbers on PLGA 7502 control polymer films (10.3 x 10^4 cells/well and 9.2 x 10^4 cells/well respectively) in comparison to PrestoBlue® measurements (5.5 x 10^4 and 2.5 x 10^4 cells/well respectively). Due to the superior sensitivity and accuracy of PrestoBlue®, this assay was used to determine cell numbers and proliferation in further experiments.

A limitation of the TIPS polymer films was that when exposed to cell culture conditions (cell culture media, 37^{o}C, 5% CO_2), some of the films would lift from the glass coverslip, most likely due to the porosity of the PLGA weakening the attachment to the glass. This was undesirable as the ADMSCs could have been responding to the smooth underside of the TIPS polymer films, therefore effecting the observed results. This obstacle was overcome by utilising the polystyrene films (Chapter 2 Section 2.2.3, Thermanox plastic coverslips, 174950, Thermofisher, UK) where the TIPS polymer did not lift off, most likely due to the hydrophilic nature of the polystyrene facilitating attachment of the PLGA. Therefore, TIPS films in this project were prepared by coating polystyrene coverslips.

4.5 Summary

This chapter explored the cellularisation of 7507 and 7502 TIPS polymer films. Increased numbers of ADMSCs were seen in LIVE/DEAD fluorescent imaging of PLGA 7507 TIPS films. Cell numbers were quantified through two different assays, where optimisation resulted in PrestoBlue® cell viability reagent being chosen as the most suitable method for determining cell numbers. The superior cell attachment on 7507 TIPS polymer films seen was due to the increased roughness and stiffness of PLGA 7507 TIPS materials in comparison to PLGA 7502 and smooth PLGA controls determined in Part I. Chapter 3. The angiogenic behaviour of ADMSCs attached to PLGA 7507 TIPS and 7502 TIPS polymer films were studied in subsequent chapters.

Part I.

Chapter 5: Investigation of the Biological Mechanism Responsible for the Observed *In Vitro* Pro-Angiogenic Effect of TIPS Polymer Films Adipose-Derived Mesenchymal Stem Cell Substrates

5.1 Introduction

Cell therapy involves the use of cells to facilitate tissue regeneration as a curative treatment for many diseases. [236] Using cells in a clinical setting is not a new concept. Bone marrow transplants, for instance, have been used as a cancer treatment for over 60 years. [237] Nevertheless, cell therapy is a developing field with over 200 cell therapy based products currently available or undergoing development for regulatory approval, with the use of stem cells as a cell therapy in clinical trials increasing from 7% in 2016 to 8% in 2017, and recent advances in immunotherapy involving use of a patient's own cells are successfully used to treat certain cancers. [238, 239] The underlying mechanisms accountable for tissue regeneration using current cell therapy approaches are still being elucidated and there are still many areas of cell therapy under investigation.

In order to facilitate angiogenesis through cell therapy, ADMSCs were selected. It is understood that ADMSCs have inherent pro-angiogenic properties, given their ability to secrete pro-angiogenic growth factors *in vitro* and *in vivo.* These include VEGF, FGF and PDGF. [76-79, 240] Thus, in conjunction with the fact they are easily isolated in large quantities through enzymatic digestion of lipoaspirates, [241] survive in harsh, hypoxic conditions, [242] and demonstrate anti-inflammatory effects, [243] they have been chosen to facilitate therapeutic angiogenesis in numerous preclinical trials for the treatment of cardiovascular diseases. There have been numerous reports showing improved perfusion following ischemic hindlimb injuries, [89, 90] increased cardiac function [82, 83] and angiogenic growth factor secretion [84] after the administration of ADMSCs. ADMSCs have been investigated in clinical trials, where the safety of mesenchymal stem cell implantation has been shown, [244] with a 5-year follow-up study by Lee *et al.*, 2010, where the administration of two doses of 50 million stem cells to 16 patients (who had suffered from ischaemic stroke) were shown to have no long-term negative side effects associated with stem cell transplant. In addition, the treated patients had significant improvements in recovery and clinical outcomes. [245] ADMSCs have been investigated specifically for the treatment of critical limb ischaemia, a serious consequence of PAD. Administration of ADMSCs into patients have resulted in improvements in claudication, chronic pain and wound healing, with formations of collateral blood vessels and networks confirmed by angiography after 2-6 months. [242, 246]

This chapter explored the *in vitro* pro-angiogenic effect of ADMSCs cultured on TIPS processed substrates and the biological mechanism responsible for this response. To achieve this, the angiogenic response were studied using *in vitro* angiogenesis assays and angiogenic protein profiling of ADMSCs seeded onto TIPS polymer films.

5.2 Methods

5.2.1 Quantifying Adipose Derived Mesenchymal Stem Cells Numbers

Cell numbers were measured using PrestoBlue® cell viability reagent as described in Chapter 4 Section 4.2.4.2 at days 1, 4, 7 and 10.

5.2.2 Assessing In Vitro Angiogenic Activity of Cellularised TIPS Polymer Films

5.2.2.1 Measuring $VEGF_{165}$ Secretion Using Enzyme-linked Immunosorbent Assay

A DuoSet Human $VEGF_{165}$ enzyme-linked immunosorbent assay (ELISA) (DY293B, R&D Systems, UK) was used to determine the amount of $VEGF_{165}$ released into the supernatants from ADMSCs seeded onto polymer films (n=9). The capture antibody was reconstituted to 120 μg/mL in 1X PBS, (P5493-1L, Sigma, UK) and diluted to the working concentration of 1.0 μg/mL in 1X PBS. 100 μL was added to each well of a Nunc-Immuno MicroWell 96 well plate (M9410, Sigma, UK). Plates were sealed with adhesive plate sealers (DY992, R&D, UK) and incubated overnight at room temperature. Wash buffer was prepared as 0.05% Tween-20 (P1379, Sigma, UK) in 1X PBS (P5493-1L, Sigma, UK). Each well was washed by aspirating with wash buffer three times and blotted to remove excess liquid. Reagent diluent was prepared as 1% bovine serum albumin (05482, Sigma, UK) in 1X PBS and 0.2 μm filtered. Plates were blocked with 300 μL of reagent diluent for 2 hours at room temperature then washed. $VEGF_{165}$ standard was reconstituted to 100 ng/mL in reagent diluent and diluted to the working concentration of 4000 pg/mL in reagent diluent and serial dilutions were made up to 7.81 pg/mL. 100 μL of standards and samples were added to wells in triplicate, incubated at room temperature for 2 hours and washed. The detection antibody was reconstituted to 6.0 μg/mL in reagent diluent and diluted to the working concentration to 100 ng/mL. 100 μL of detection antibody was added to each well, incubated at room temperature for 2 hours and washed. The Streptavin-HRP was diluted at a ratio of 1:200 in reagent diluent and 100 μL was added

to each well. The plate was sealed, protected from light, incubated for 20 minutes at room temperature and washed. The substrate solution was prepared by adding equal volumes of colour reagent A (H_2O_2) and colour reagent B (Tetramethylbenzidine) (DY994, R&D, UK) and 100 μL was added to each well. The plate was sealed, protected from light, incubated for 20 minutes at room temperature. 50 μL of 2 N H_2SO_4 was added to each well to stop the reaction and further colour development. The plate was then read using a microplate reader (Fisher Scientific, UK) at wavelength 450 nm with correction set to 540 nm.

5.2.2.2 Screening for Angiogenic Proteins from Adipose-Derived Mesenchymal Stem Cells on TIPS Surfaces

Human proteome profiler angiogenesis array kit (ARY007, R&D Systems, UK) was used to profile 55 different angiogenesis related proteins from the supernatants of ADMSCs attached on TIPS and control polymer films. The membranes were handled with flat tipped tweezers at the edges to avoid destruction of the membrane or contamination. To block the membranes array buffer 7 was added to each well of a 4-well multi-well dish and incubated for one hour at room temperature on a rocking plate shaker. The supernatants from ADMSCs seeded onto PLGA 7507 TIPS films, PLGA 7507 control films and polystyrene films from each time point were pooled, and a total of 1 mL for each sample was transferred to a microfuge tube (T9661, Sigma, UK). 0.5 mL of array buffer 4 was added to each sample with 15 μL reconstituted detection antibody cocktail (reconstituted with 100 μL dH_2O) and incubated at room temperature for 1 hour. Each membrane was washed in 20 mL of 1x Wash Buffer for 10 minutes on a rocking plate shaker three times. The samples were added to individual membranes and incubated overnight at 4^oC on a plate shaker in constant motion. The membranes were washed three times. Streptavin-HRP was diluted in array buffer 5 to the working concentration of 1:40, added to the membranes and incubated for 30 minutes on a rocking plate shaker. The membranes were washed three times. The first membrane was removed from the wash container. Excess wash buffer was drained from the membrane by blotting the lower edge onto paper towels. The

membrane was placed on the bottom sheet of a plastic sheet protector with the identification number facing up. 1 mL of the provided Chemi Reagent Mix was pipetted evenly onto the membrane. The top plastic sheet protector was placed on top of the membrane. This was incubated for 1 minute at room temperature. Excess Chemi Reagent Mix was removed and the membrane was wrapped in 1 layer of Suran wrap (FIL1040, LabShop, UK). The membrane was placed in an autoradiography film cassette with the identification number facing up. This process was repeated with the remaining membranes. In a dark room, the membranes were exposed to X-ray film (34090, Thermo Scientific, UK) for 1, 5, 10, 30 and 60 minutes for optimal film exposure. X-ray films were processed in an X-ray Film Auto Processor (Gmedi Co, GAP-201). To analyse the results, the films were scanned in greyscale with a calibrated optical density tablet and safe as a TIFF file. In ImageJ, the optical density tablet was analysed and calibrated. The optical density values that corresponds to each step was inputted. From this, the intensity of each of dot on the membranes were calculated using the 'plot lanes' function. This was repeated for all the exposed dots. Each dot on the membrane corresponded to a different angiogenesis related protein. Results were also analysed using STRING protein-protein interaction network database. [247]

5.2.2.3 In Vitro Evaluation of Angiogenesis

Vasculogenesis to angiogenesis array (Va2) (ZHA-4000, Cellworks, UK) was used to quantify the effects of conditioned media from ADMSCs on TIPS and control polymer films on *in vitro* angiogenesis.

Complete seeding medium was prepared by adding the seeding medium supplement to the V2a seeding medium (ZHA-1960, Cellworks, UK). 0.5 mL of the complete medium was added to each well of the provided 24 well plate and placed in an 37ºC/5% CO_2 incubator for 30 minutes to pre-equilibrate. A co-culture of cryopreserved human umbilical vein endothelial cells (500,000/vial, ZHC-2102, Cellworks, UK), human dermal fibroblasts (1,000,000/vial, ZHC-5102, Cellworks, UK) and early passage human

umbilical endothelial cells from multiple donors (500,000/vial, ZHC-2301, Cellworks, UK) was provided. The cells were rapidly thawed in a 37ºC water bath and added to 12 mL V2a seeding medium. 0.5 mL of the cell suspension was added to each well resulting in a final concentration of 8.3 x 10^4 cells/mL. The plate was incubated at 37ºC with 5% CO2 humidified atmosphere for 24 hours to allow cell attachment. Complete growth medium was prepared by adding the growth medium supplement to the V2a growth medium (ZHA-1970, Cellworks, UK). For the positive control, VEGF (2 μg/mL, ZHA-1300, Cellworks, UK), the was thawed and 11µl was added to 10.989ml V2a growth medium. For the negative control, 220µl of Suramin (1 mM) was added to 10.780ml growth medium. A growth medium only control was also included. Test compounds were prepared by mixing equal volumes of complete V2a growth medium to the conditioned media. The media was aspirated from the well and using a serological pipette 0.5 mL of growth medium containing test or control materials was gently added down the side of the well. Extra care was taken not to disrupt the cell monolayer. Plates were incubated at 37ºC with 5% CO2 humidified atmosphere. The process of media changes of the entire plate was repeated every 2-3 days for 14 days. After 14 days, the cells were fixed and stained for the endothelial cell marker CD31.

Each well was washed with a wash buffer prepared by combining 500 mL of deionized water, 100 mg potassium chloride (7447-40-7, Sigma, UK), 100 mg potassium phosphate monobasic (7778-77-0, Sigma, UK), 4 g sodium chloride (7647-14-5, Sigma, UK), 600 mg sodium phosphate dibasic (7558-79-4, Sigma, UK). To fix the cells, 0.5 mL ice cold 70% ethanol was gently added to each well and incubated at room temperature for 30 minutes. Blocking buffer was prepared by dissolving 5 g of bovine serum albumin (>96%, 05482, Sigma, UK) in 500 mL of wash buffer. Wells were blocked by with 0.5 mL of pre-prepared blocking buffer. 35 µL of mouse anti-human CD31 antibody (ZH-1225, Cellworks, UK) was diluted in 14 mL blocking buffer and 0.5 mL was added to each well. Samples were incubated at 37°C for 60 minutes. The wells were washed with blocking buffer. 28µl of the secondary goat anti-mouse IgG AP conjugate antibody was added to 14 mL blocking buffer and 0.5 mL was

added to each well. Samples were incubated at 37°C for 60 minutes. The wells were washed with deionized water. 0.5 mL of the BCOP/NBT substrate was added to each well for 10 minutes to allow the colour development of the tubules. The wells were washed with deionized water and allowed to air dry before imaging. The wells were imaged under a Lecia light microscope. AngioSys 2.0 Image Analysis Software (ZHA-5000, Cellworks, UK), was used for semi-automated analysis of the images by measuring the number of tubules, junctions, the total tubule length, and the mean tubule length.

5.2.3 Evaluating the Effect of Polymer Film Degradation Products on the Secretion of VEGF from Adipose Derived Mesenchymal Stem Cells

PLGA 7507 TIPS, PLGA 7502 TIPS, PLGA 7507 control, PLGA 7502 control and polystyrene films were placed into a 24 well plate (CLS3473-24EA, Corning, UK) with 0.5 mL complete MesenPro RS™ medium. 1.0 µm cell inserts (353104, Falcon, UK) were placed into each well. 20,000 ADMSCs in 0.5 mL media was seeded into each insert. Supernatants were taken from the coverslips at days 1, 4, 7 and 10 and replaced with 0.5 mL fresh media. The pH of the supernatant was measured using a digital microprocessor pH meter. The pH meter was first calibrated using pH 4 (4.01 HI 5004-01, Envo Global, NZ) and pH 7 (7.01 HI 5007-12, Envo Global, NZ). VEGF secretion was measured using VEGF ELISA (DY293B, R&D, UK)

5.3 Results

5.3.1 Evaluating the VEGF Secretion in Relation to Cell Proliferation

The number of ADMSCs on polymer films were investigated Part I. Chapter 4, where it was shown that there were increased numbers of ADMSCs on 7507 TIPS polymer films after 10 days in comparison to 7502 TIPS polymer films and control polymer films.

The VEGF secretion from the ADMSCs seeded onto polymer films were determined by $VEGF_{165}$ ELISA. Results show that for ADMSCs attached to 7507 TIPS films, 7507 control films and polystyrene films, ADMSCs had increased levels of $VEGF_{165}$ released from days 1 to 10. Whereas PLGA 7502 TIPS and 7502 control films had an increase after 4 days, but $VEGF_{165}$ release from the ADMSCs remained consistent (73,300 ±11,300 pg/mL and 25,000 ±9,000 pg/ml at day 10 respectively). $VEGF_{165}$ ELISA results were normalised to cell number (Figure 5.1) to determine the amount of $VEGF_{165}$ secreted per cell and if $VEGF_{165}$ concentration was dependent on cell numbers. Results show that ADMSCs seeded onto PLGA 7507 control films, 7502 TIPS films and 7502 control polymer films remained consistent throughout the timepoints had showed no significant differences in secretion. However, cells seeded onto 7507 TIPS polymer films showed significantly higher levels of $VEGF_{165}$

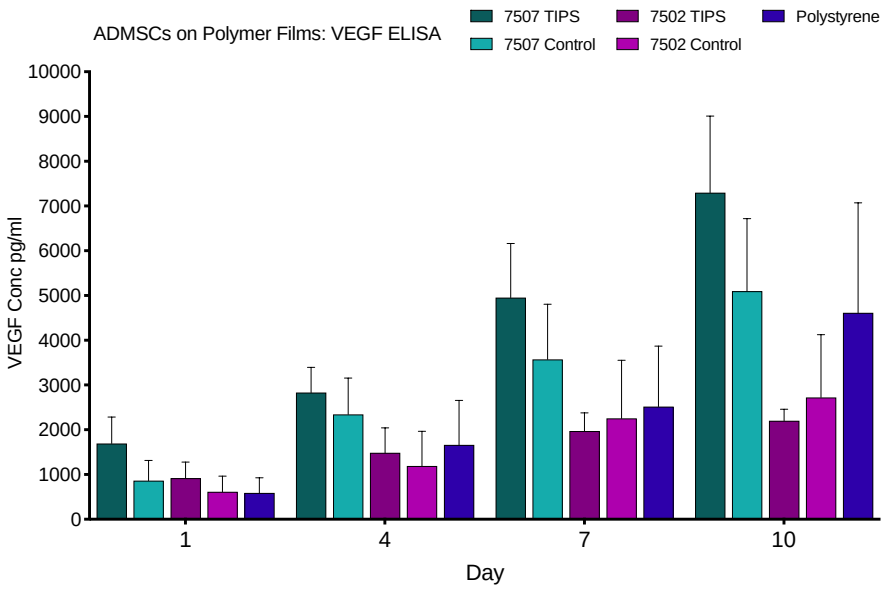

b)

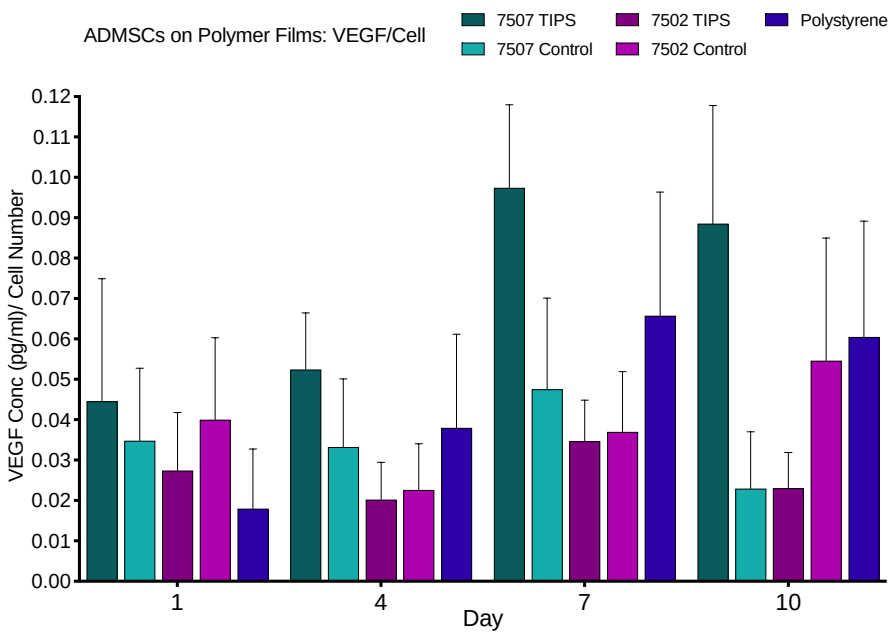

Figure 5.1: a) $VEGF_{165}$ secretion of ADMSCs on 7507 TIPS films, 7507 PLGA control films, 7502 TIPS films, 7502 PLGA control films and polystyrene films at days 1, 4, 7 and 10. (n=9) Two-way ANOVA with Geisser-Greenhouse correction = **** (P<0.0001) b) Normalised results showing the amount of VEGF (pg/mL) secreted per cell. Two-way ANOVA with Geisser-Greenhouse correction = * (P=0.0237).

per cell compared to 7502 TIPS and polystyrene polymer films, with a large increase in $VEGF_{165}$ secretion after 7 days. (7507 TIPS; 0.1 ±0.02 pg/mL/cell, 7507 control; 0.05 ±0.02 pg/mL/cell, 7502 TIPS; 0.04 ±0.01 pg/mL/cell, 7502 control; 0.04±0.01 pg/mL/cell and polystyrene; 0.07 ±0.03 pg/mL/cell).

5.3.2 Screening for Angiogenic Proteins Secretion from Adipose-Derived Mesenchymal Stem Cells

A human proteome profiler array that detects 55 different angiogenic-related proteins was used to screen the supernatants from ADMSCs seeded onto 7507 TIPS, 7507 control and polystyrene polymer films. Results presented show proteins that had a two-fold increase/decrease when compared to polystyrene films (Figure 5.2). Interestingly, ADMSCs secreted different levels of proteins depending on if they were seeded onto TIPS or smooth 7507 PLGA

films. For example, when seeded onto 7507 TIPS polymer films, ADMSCs secreted more of the pro-angiogenic factors; Angiopoeitin-1 and -2, artemin, VEGF-C and interleukin (IL)-1b, and less anti-angiogenic thrombospondin (TSP)-1/-2, Serpin B5, leucine aminopeptidase (LAP) and tissue inhibitor of metalloproteinases (TIMP) -4 than when seeded onto 7507 control films. In addition, cells secreted 19 more pro-angiogenic proteins when seeded onto PLGA films compared with polystyrene films, and 5 anti-angiogenic proteins were down regulated when cells were seeded onto PLGA films compared to polystyrene films. The proteins highlighted in the array were further analysed using STRING database. [247] From this, pathways involved in biological processes such as regulation of angiogenesis (11 genes, false discovery 5.9e-13), regulation of cell locomotion (17 genes, false discovery 8.5e-16), response to stimulus (20 genes, false discovery 8.6e-05) and angiogenesis were detected (11 genes, false discovery 3.8e-11).

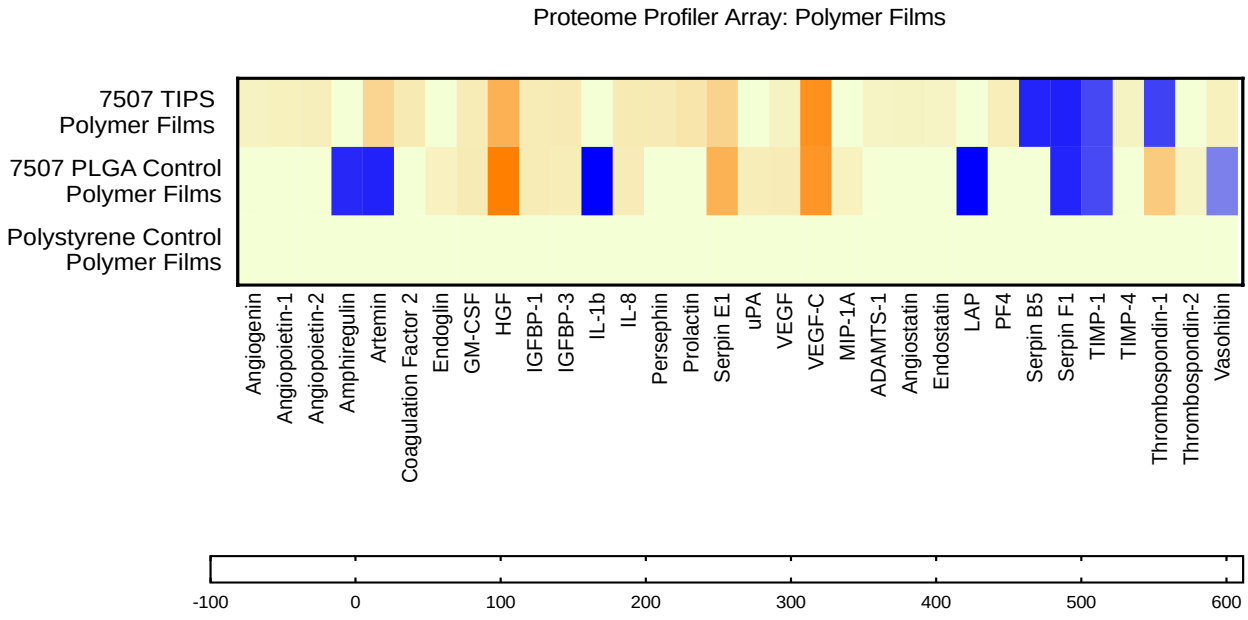

Figure 5.2: Human Angiogenesis Proteome Profiler array of proteins secreted from ADMSCs seeded onto 7507 TIPS polymer films and 7507 control polymer films. (n=2)

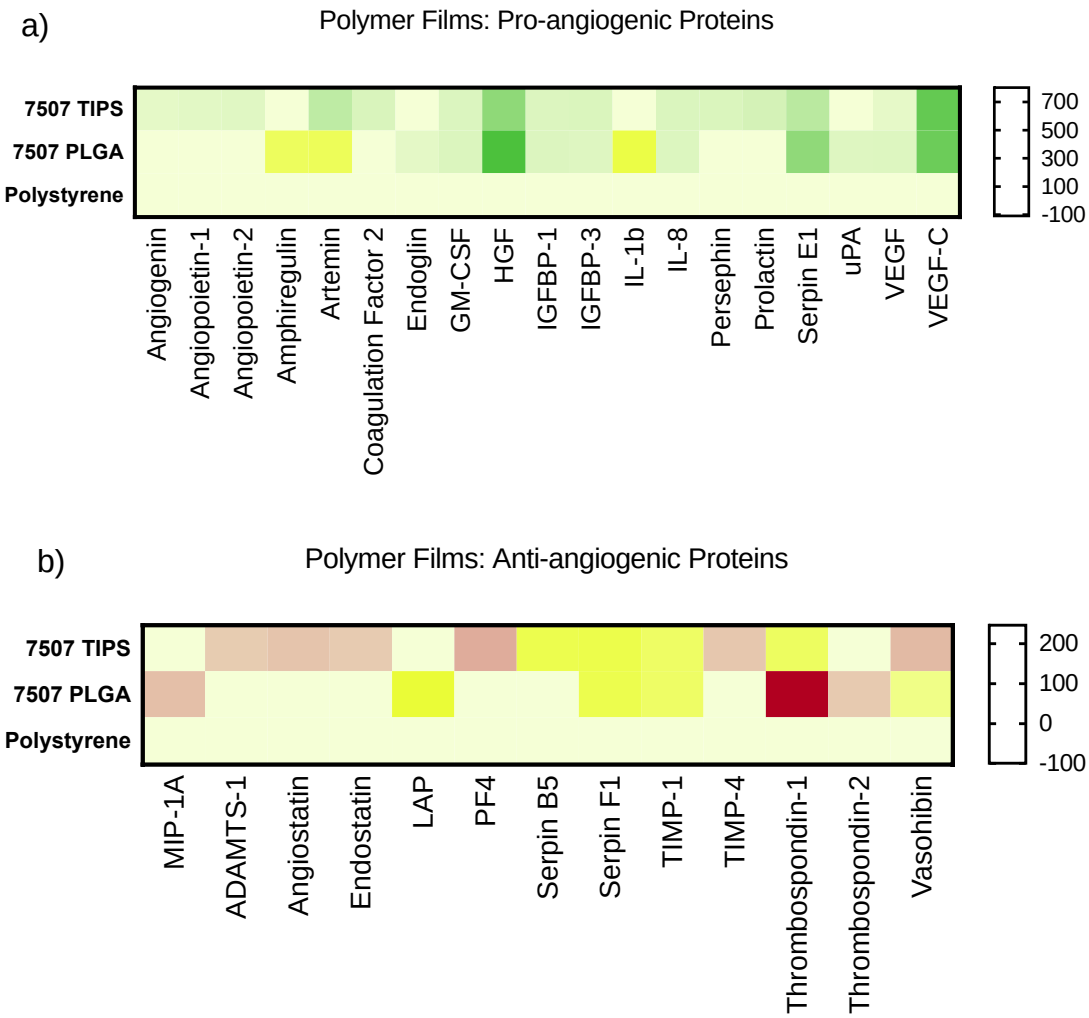

Figure 5.3: Human Angiogenesis Proteome Profiler array of proteins secreted from ADMSCs seeded onto 7507 TIPS polymer films and 7507 control polymer films. a) A heat map highlighting the pro-angiogenic proteins secreted. b) A heat map highlighting the anti-angiogenic proteins secreted.

5.3.3 In Vitro Evaluation of Angiogenesis Using a Vasculogenesis to Angiogenesis Array

The V2a array (Figure 5.4) were used to assess the effect of the conditioned media containing the supernatants of ADMSCs seeded onto 7507 TIPS, 7507 control, 7502 TIPS, 7502 control and polystyrene films on angiogenesis *in vitro* via the growth of tubules from a co-culture of endothelial cells and fibroblasts. After 14 days, samples were stained for PECAM-1, imaged and

analysed using Angio.Sys.2.0 software. Results are shown graphically, comparing the average length of the tubules, the junctions and branches. A positive control of VEGF, negative control of Suramin and a media only control were included in the experiment. As expected, the VEGF control had the highest number of branches/length/junctions and the Suramin had inhibited angiogenesis and blocked the growth of tubules. 7507 TIPS had significantly

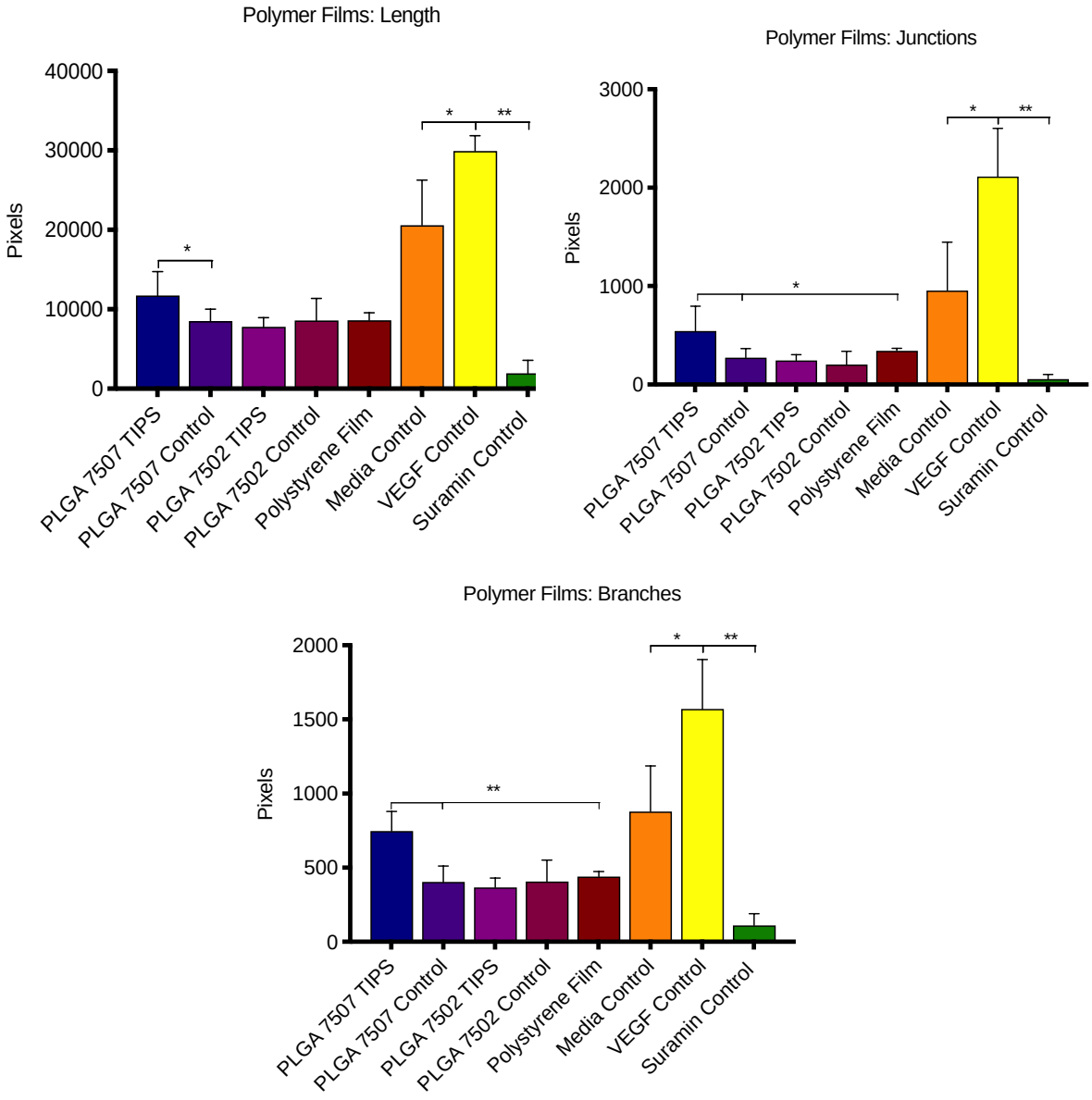

Figure 5.4: Quantification of the V2a array from the secretomes from ADMSCs seeded onto PLGA 7507 TIPS polymer films, PLGA 7507 control polymer films, PLGA 7502 TIPS polymer films, PLGA 7502 control polymer films and polystyrene films a) tubule length b) tubule junctions c) tubule branches. (n=1) Where * = P<0.05, ** = P<0.01, *** = P<0.001 and **** = P<0.0001. Ordinary one-way ANOVA = **** (P<0.0001).

higher average length of tubules compared to 7507 control polymer films, as well as a higher number of junctions and branches to polystyrene films. The co-cultures exposed to conditioned media from samples grown on 7502 TIPS and 7502 control polymer films showed no significant differences in tubule formation.

An experiment to determine how the degradation products of the polymer films effect the secretion of angiogenic growth factors from ADMSCs was performed. Cell inserts were placed over polymer films and seeded with ADMSCs. The leached media on the films were taken and measured for $VEGF_{165}$ concentration using $VEGF_{165}$ ELISA. Figure 5.5 shows that $VEGF_{165}$ secretion increased through the time points with 7507 TIPS polymer films had significantly higher VEGF concentrations compared to 7507 control films at days 1, 4 and 7, with higher $VEGF_{165}$ secretion at day 10 than all the samples. When comparing these results to polystyrene, a non-degradable material (therefore it is assumed there are no degradation products effecting the ADMSCs), there is significantly higher $VEGF_{165}$ release from 7507 TIPS polymer films and no significant difference between PLGA control films and 7502 TIPS polymer films.

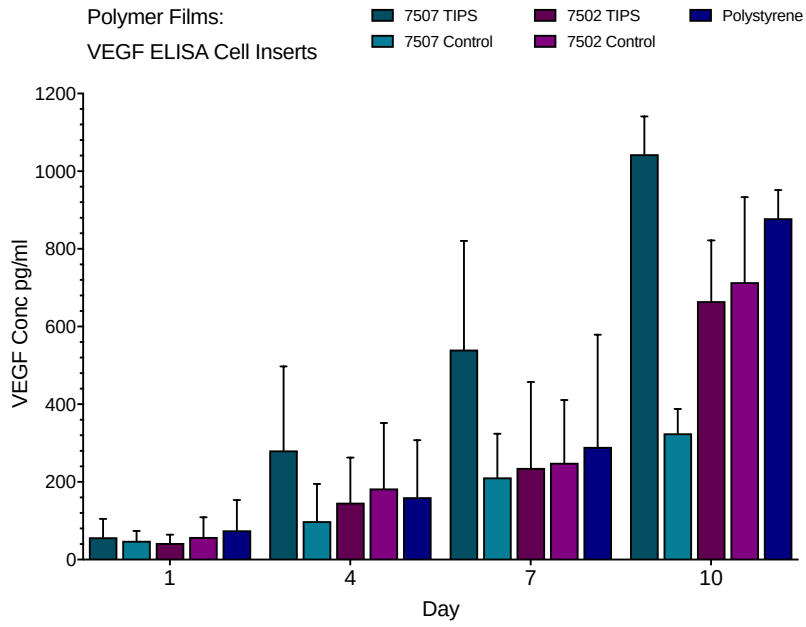

Figure 5.5: $VEGF_{165}$ secretion from ADMSCs seeded into cell inserts exposed to the degradation products from PLGA 7507 TIPS polymer films, PLGA 7507 control polymer films, PLGA 7502 TIPS polymer films, PLGA 7502 control polymer films and polystyrene films. (n=1) Two-way ANOVA with Geisser-Greenhouse correction = ** (P=0.0055).

5.4 Discussion

VEGF is arguably the most crucial growth factor in the angiogenic process. [248-250] VEGF is produced by tumour cells, macrophages, platelets, [251] fibroblasts, bone marrow derived cells, endothelial cells, [252] pericytes, smooth muscle cells and mesenchymal stem cells. [253] VEGF and its receptors play a critical role in angiogenesis by inducing vascular leakage, inducing vasodilation, endothelial cell migration, gene expression and tubule formation. When discussing VEGF in angiogenesis, it most often refers to a subset of VEGF known as VEGF-A, as there are seven members of the VEGF family, with VEGF-A, VEGFR1, VEGFR2 playing prominent roles in angiogenesis. Whereas VEGF-C, VEGF-D and VEGFR3 are involved in vasculogenesis (the formation of blood vessels *in utero*). [254] VEGF-A has a considerable effect on endothelial cells, as it binds to two binding sites on vascular endothelial cells, VEGF receptor 1 (VEGFR1) and VEGF receptor 2 (VEGFR2). [255, 256] VEGF-A is critical in developmental angiogenesis, as it has been shown in VEGF-A +/- and VEGF-A -/- knockout mice do not survive beyond day 11 *in utero*. [257] It has also been demonstrated that VEGFR2 knock-out mice do not develop organised blood vessels and do not survive beyond 9 days *in utero*. [258] Attachment of VEGF to VEGFR2 prompts endothelial cell proliferation by activation of the Raf/Mek/Erk pathway. [256]

Within VEGF-A, there are additional subdivisions known as isoforms formed from alternative splicing of the VEGF-A gene. [259] Each isoform behaves differently, for example $VEGF_{165}$ enhances VEGFR-2 signalling and $VEGF_{189}$ is bound to the ECM. $VEGF_{165}$ is the predominant isoform of VEGF-A and has been shown to have the highest pro-angiogenic activity. [256, 260, 261] Consequently, $VEGF_{165}$ concentration was selected to be measured as a primary indicator of angiogenic activity and was first measured with ELISA. The results of the $VEGF_{165}$ ELISAs were normalised to cell number from the PrestoBlue® cell viability results to determine $VEGF_{165}$ secretion per cell and it should also be noted that the MesenPro RS medium utilised for ADMSC cell culture contained bFGF, EGF, HGF and PDGF.

This was to assess if the increase in $VEGF_{165}$ secretion throughout the timepoints and the higher levels on PLGA 7507 TIPS polymer films was due to an increase in cell proliferation, or an increase secretion from the ADMSCs. The normalised data (Figure 5.1) showed that PLGA TIPS 7507 polymer films had significantly higher $VEGF_{165}$ levels per cell in comparison to 7507 smooth control films at days 4, 7 and 10. As the primary difference between 7507 TIPS and control microparticles was the structure, (and subsequent mechanical characteristics differences) this property could be key in causing the change in $VEGF_{165}$ secretion from ADMSCs. There was no significant difference between $VEGF_{165}$ secretion from ADMSCs seeded on 7507 control films at day 1 and day 10. TIPS 7507 polymer films $VEGF_{165}$ secretion per cell significantly increased up to day 7, where it remained constant up to day 10. This difference seen between the 7507 TIPS and control polymer films suggest that the TIPS topography and structural characteristics had an effect on the secretion and synthesis of $VEGF_{165}$ from ADMSCs. There was no significant difference between days 1 and 10 for PLGA 7502 TIPS and control, suggesting that the 7502 compilation of PLGA did not affect the secretion of $VEGF_{165}$ from ADMSCs over time, despite the differences in topography and structure between the TIPS and control surfaces. This response could be due to the fast degradation rate of PLGA 7502, with the 7502 TIPS surfaces losing surface features such as roughness quickly (as seen in the characterisation of polymer films using AFM and SEM in Part I. Chapter 2). The $VEGF_{165}$ secretion from ADMSCs seeded onto polystyrene films also showed a statistically significant increase from day 1 to 10. This is likely as polystyrene films are tissue culture treated, therefore facilitate cell adhesion and have been shown to improve cell proliferation and function. [262] VEGF synthesis is initiated by hypoxia or oxidative stress in ADMSCs, through an increase in the activation of the p38 MAPK pathway. Mechanical and chemical stimuli also influence VEGF synthesis, where ADMSCs were shown to increase VEGF production in response to shear stress by Bassaneze *et al.,* 2010. In addition the presence of TNF-a has been shown to increase VEGF production from ADMSCs. [263] Therefore, the response of the ADMSCs to the TIPS surfaces could have influenced the synthesis of VEGF. As ELISA measures VEGF release, the synthesis and/or intercellular storage of VEGF can be measured

through measuring mRNA content (western blotting and PCR) and flow cytometry. [264, 265]

In order to elicit a pro-angiogenic effect *in vivo,* studies have shown that concentrations of 0.05-0.6 pg/mL of VEGF/cell is sufficient to stimulate angiogenesis, [266-268] with ADMSCs naturally secreting approximately 0.003-0.04 pg/mL of VEGF per cell. [269, 270] Figure 5.1b shows a $VEGF_{165}$ detection of 0.04 ±0.03 to 0.1 ±0.02 VEGF pg/mL/cell on 7507 TIPS polymer films which therefore would be capable of promoting angiogenesis *in vivo* as well as showing that attachment to TIPS processed 7507 PLGA surfaces enhanced the $VEGF_{165}$ secretion per cell compared with standard tissue culture conditions.

An experiment to assess the effect of the polymer film degradation products (lactic acid and glycolic acid) on the secretion of $VEGF_{165}$ from ADMSCs revealed that there was an increase in $VEGF_{165}$ secretion from ADMSCs exposed to 7507 TIPS polymer films, and no difference between PLGA 7502 TIPS films, PLGA 7502 and 7507 control films and the non-degradable polystyrene films. This suggests that the PLGA degradation products do not negatively affect the secretion of angiogenic growth factors from ADMSCs and that in fact 7507 TIPS polymer films promoted the secretion of angiogenic growth factors, advocating their use for therapeutic angiogenesis. This may have been a response to a change in pH that would occur from the degradation of PLGA, where pH has been shown to influence angiogenesis, with acidic conditions influencing cellular VEGF secretion through the ERK1/2/MAPK signalling pathway. [271]

The samples were analysed further using an angiogenic proteome profiler array that was able to detect 55 different angiogenic related proteins. The array was used to assess if there was an effect of the different materials on the secretion of angiogenic growth factors, to highlight any other key proteins (other than VEGF) secreted and to aid in highlighting a possible pathway for the mechanism of action of growth factor release from ADMCSs on TIPS surfaces. Since the majority of proteins were detected in the array, Figure 5.3

displayed results with a two-fold increased or decreased expression compared with polystyrene films. This allowed for a more manageable assessment of the results and to focus on proteins with a significant difference in expression.

In order to further evaluate the data from the proteome profilers, the identified proteins were inputted into the 'STRING' database. STRING is part of the ELIXIR core data resource and provides information on known and predicted protein-protein interactions. The database covers nearly 10 million proteins from over 2000 organisms. [247] From this resource it was possible to make links between the proteins, specifically how the proteins link to mechanisms of action or pathways, with the number of linked genes and false discovery rates given. False discovery rate (FR) describes the percentage of a group of declared positive results that are negative. It takes into account the number of errors among a rejected null hypothesis. It is particularly useful for controlling how many false rejections are made when making multiple comparisons, such as with genomic data. [272] Figure 5.3 presents the pro-angiogenic and anti-angiogenic proteins detected from ADMSCs seeded onto 7507 TIPS polymer films and 7507 control polymer films. The data shows not only that multiple angiogenic proteins were expressed from the samples, but also differences between these groups. The proteins were inputted into the string database and multiple biological processes were revealed, such as regulation of cell migration, vascular development and angiogenesis (see supplementary Figures S5.2 - 5.4). From this analysis, there were more proteins linked to biological processes from the 7507 TIPS film samples compared with the 7507 PLGA control films, with lower false positives. For example, there were 10 genes linked to angiogenesis (with 2.27e-11 false discovery rate) for 7507 TIPS polymer films compared to 6 genes (with 6.44e-5 false discovery rate) for 7507 control polymer films. From this it can be said that there is a stronger association with the proteins secreted from the ADMSCs seeded onto the TIPS polymer films with angiogenesis compared to the PLGA 7507 smooth films, and that utilising TIPS polymer films increases the pro-angiogenic behaviour of ADMSCs. Further information into the pro- and anti-angiogenic effects of the proteins included in the angiogenic proteome profiler array are summarised in Supplementary Table S5.5.

An effective way to assess the effect of compounds or potential therapies on angiogenesis before *in vivo* experiments is to utilise *in vitro* assays. Since the 1970's chick embryo chorioallantoic membrane assays (CAM) have been used to evaluate angiogenesis in the lab. CAM involves the addition of the compound of interest into a chick embryo. The subsequent embryonic blood vessel development is monitored and analysed. Drawbacks include the ethics involved with the use of an animal embryo and the multiple assays required for consistent results, the effect on angiogenesis can only be monitored for a few days and the embryo can elicit an inflammatory response that can affect the results. [273] To overcome these limitations, an alternative assay was chosen. The vasculogenesis to angiogenesis array (V2a) provided advantages such as the ability to test multiple compounds in one plate, was carried out over two weeks, involved a co-culture of human cells that were able to show angiogenic activity by incorporating many angiogenic processes including endothelial cell migration, proliferation and the formation tubule structures. [66] The V2a array was used to evaluate the effect of the conditioned media from ADMSCs attached to 7507 TIPS films, 7507 control films, 7502 TIPS films, 7502 control films and polystyrene films on the tubule formation on a co-culture of endothelial cells and fibroblasts as a measure of *in vitro* angiogenesis. After 14 days of periodic addition of conditioned media, tubules were stained with PECAM-1/CD31, imaged and analysed using Angio.Sys 2.0 software, where the number/pixel density of total length, junctions and branches were quantified. The V2a kit included three internal controls. A positive control of the pro-angiogenic factor VEGF that would increase endothelial tubule formation, a negative control of suramin, that is thought to inhibit angiogenesis by preventing binding of VEGF by blocking the KDR receptors and also blocks FGF receptors preventing binding of FGFs and [274, 275] a media only control to identify any effects the media may have on the tubule formation. The provided software measured the number of tubules, mean tubule length, number of junctions and mean number of branches, which was translated as a measurement of angiogenesis. Figure 5.4 shows that the positive and negative controls behaved as expected, with more tubules formed with the addition of VEGF and significantly less formed with the addition of suramin. The results indicated that the secretomes of ADMSCs seeded onto

TIPS polymer films substrates resulted in increased *in vitro* angiogenesis compared with PLGA controls and thus has shown that the exposure to the TIPS-structure positively influences the promotion of angiogenesis.

As previously discussed, characteristics such as topography, stiffness, porosity and hydrophobicity of a material influence cell behaviour. [201, 207, 225, 276] Stiffness and roughness of the polymer films were characterised in Chapter 3, where it was shown that PLGA 7507 TIPS films had higher stiffness values and a slower degradation rate that resulted in rougher surfaces after 10 days compared to PLGA 7502 TIPS films and smooth PLGA films. It has been reported that cells more readily attach to rougher and stiffer surfaces; [205, 219, 220] this chapter has shown that ADMSCs not only successfully attach and survive on TIPS surfaces, but also display pro-angiogenic behaviour through an increase in VEGF secretion and activation of biological processes including regulation of cell migration, vascular development and angiogenesis. The synthesis of VEGF from ADMSCs has been shown to be influenced by many factors including oxidative stress, hypoxia and chemical and mechanical stimuli. [277] This is particularly promising for the proposed application of cellularised TIPS constructs to treat ischemic disease through the promotion of angiogenesis. By implanting a material in which cells readily attach and proliferate, the cells can remain at the target site to have their therapeutic effect. In addition, the pro-angiogenic behaviour of ADMSCs seeded onto TIPS polymer films suggest that these constructs could conceivably successfully induce angiogenesis in pre-clinical and clinical settings.

5.5 Summary

This chapter investigated the angiogenic effect of cellularised TIPS polymer constructs.

Previous chapters have reported that the TIPS process produced films with a dramatically different structures to the control films, that in turn altered the degradation, stiffness and roughness of the material. This chapter has subsequently highlighted that 7507 TIPS polymer films had superior pro-angiogenic behaviour compared to PLGA 7502 TIPS films and smooth control films. This occurred through increased secretion of VEGF and the promotion of biological processes such as regulation of cell migration, vascular development and angiogenesis. Therefore, PLGA 7507 TIPS-processed substrates were investigated further through pre-clinical studies and also as an alternative 3D microparticle delivery device in Part II.

5.6 Supplementary Information

S5.1 $VEGF_{165}$ secretion (pg/mL) per ADMSC seeded onto TIPS and control polymer films at days 1, 4, 7 and 10. $VEGF_{165}$ secretion per cell was higher from ADMSCs seeded onto 7507 TIPS polymer films, with the highest secretion at day 7. There were significantly lower levels of $VEGF_{165}$ secreted from cells attached to control films.

pg/mL/cell	Day 1	Day 4	Day 7	Day 10
7507 TIPS polymer films	0.045	0.052	0.097	0.089
7507 control polymer films	0.035	0.033	0.048	0.023
7502 TIPS polymer films	0.028	0.020	0.035	0.023
7502 polymer control	0.040	0.023	0.037	0.055
Polystyrene polymer films	0.018	0.038	0.066	0.061

S5.2 Proteome profiler proteins from ADMSCs on 7507 TIPS polymer films were analysed through STRING Analysis for connections to biological processes. Images show the connections between the secreted genes and proteins. The detected genes had strong connections to regulation of locomotion, angiogenesis, regulation of cell migration, blood vessel and vascular development.

Biological Processes:

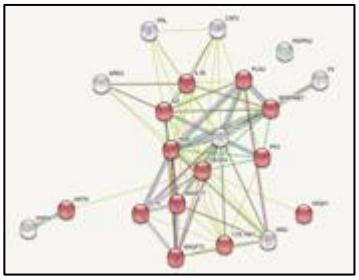

Regulation of locomotion
(13 genes, 5.6e-11 FR)

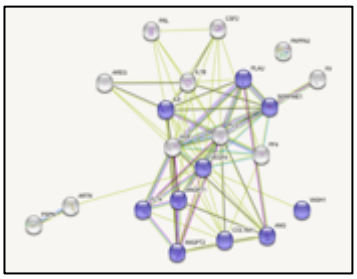

Angiogenesis.
(10 genes, 2.27e-11 FR)

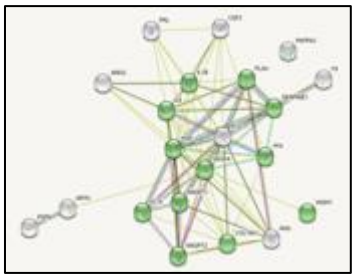

Regulation of Cell Migration
(12 genes, 1.85e-10 FR).

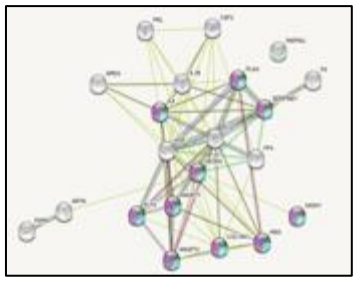

Blood vessel and vascular development
(10 genes, 1.06e-10 FR)

S5.3 Proteome profiler proteins from ADMSCs on 7507 TIPS and 7507 control polymer films were analysed through STRING Analysis for connections to molecular functions. Images show the connections between the secreted genes and proteins. TIPS polymer films had 15 genes connected to receptor binding in comparison to control polymer films where only 6 genes were connected to receptor binding.

Molecular Function:
Receptor Binding: TIPS

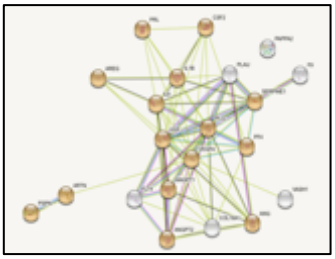

(15 genes, 5.78e-12 FR)

Control

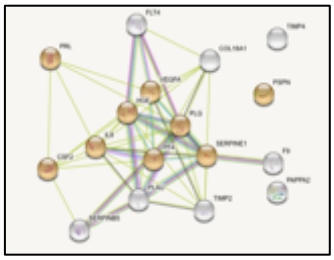

(6 genes, 1.49e-4 FR)

S5.4 Proteome profiler proteins from ADMSCs on 7507 control polymer films were analysed through STRING Analysis for connections to biological processes. Images show the connections between the secreted genes and proteins. The detected genes had connections to angiogenesis, regulation of cell migration and blood vessel and vascular development. There were less proteins connected to these biological processes, with the control polymer films in comparison to TIPS polymer films.

Biological Processes:

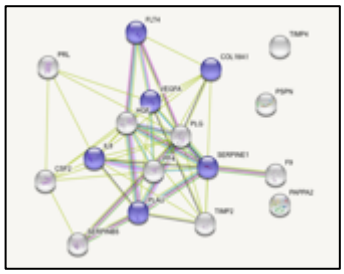

Angiogenesis
(6 genes, 6.44e-5 FR)

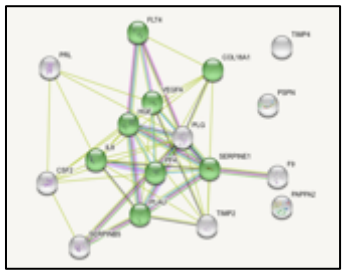

Regulation of Cell Migration
(8 genes, 4.43e-10 FR)

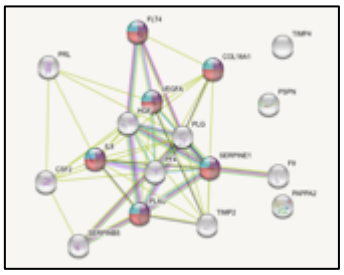

Blood vessel and vascular development
(6 genes, 1.68e-4 FR)

S5.5 A table detailing the functions of the proteins included in the human angiogenesis proteome profiler.

Name	Function	Description	Ref
Activin A	Promotes	Activin-A is a member of the TGF-b family. It regulates endothelial cell proliferation.	[278]
ADAMTS-1	Inhibits	ADAMTSs are a group of proteases that bind to the ECM. The anti-angiogenic activity of ADAMTS-1 is mediated through TS motifs and is connected to TSP1 and TSP2.	[279]
Angiogenin	Promotes	The protein encoded by ANG gene is a very strong potent mediator of new blood vessel formation.	[280]
Angiopoietin -1	Promotes	Angiopoietin-1 plays an important role in vascular development and angiogenesis. It binds to an endothelial cell-specific tyrosine-protein kinase receptor.	[280]
Angiopoietin -2	Promotes	Ang-2 works with VEGF to facilitate cell proliferation and migration of endothelial cells. Ang-2 binds the endothelial-specific receptor tyrosine kinase 2.	[281]

Angiostatin	Inhibits	Angiostatin is a specific angiogenesis inhibitor. It blocks tumour angiogenesis.	[282]
Amphiregulin	Promotes	AR is an epidermal growth factor receptor ligand that enhances angiogenesis by increasing VEGF-A levels.	[265]
Artemin	Promotes	ARTN modulates endothelial cell behavior and promotes angiogenesis.	[283]
Tissue Factor III	Promotes	Enables cells to initiate the blood coagulation cascades. TF and VEGF expression mutually enhance each other and has been shown to be critical for VEGF expression. VEGF causes TF promoter activation and gene up-regulation.	[284, 285]
CXCL16	Promotes	CXCL16 induces angiogenesis via ERK, Akt, p38 pathways and HIF-1α modulation.	[286]
DPPIV/ CD26	Promotes	DPPIV has roles in ECM degradation, cancer invasion, endothelial cell sprouting, cell migration and angiogenesis.	[287]
EGF	Promotes	Epidermal growth factor binds to EGF-receptors, that code for a transmembrane receptor tyrosine kinase that regulates angiogenesis.	[288]
EG-VEGF	Promotes	Endocrine gland derived VEGF is mainly expressed in the placenta and is a potent angiogenic factor stimulating endothelial cell proliferation, migration and sprouting.	[289]
Endoglin/ CD105	Promotes	Endoglin is a receptor for TGF-b. It is expressed in proliferating endothelial cells and is regulated by HIF-1a.	[290]
Endostatin	Inhibits	Endostatin is a fragment of collagen XVIII, a proteoglycan/collagen found in vessel walls and basement membranes that inhibits angiogenesis.	[291, 292]
		Endothelin-1 is a vasoactive peptide. It has roles in effecting pericytes, endothelial cells, increases	

Endothelin-1	Promotes	the secretion of VEGF and HIP-1a. It also stimulates fibroblasts to produce pro-angiogenic factors.	[293]
FGF acidic	Promotes	FGF1 promotes proliferation in endothelial, fibroblasts and stem cells. Been shown to exert pro-angiogenic effects on endothelial cells and are involved in the organisation of endothelial cells into tubules.	[294]
FGF basic	Promotes	FGF2 promotes proliferation in endothelial, fibroblasts and stem cells. Involved in the organisation of endothelial cells into tubules.	[294]
FGF-4	Promotes	Involved in myogenic cell migration and proliferation of stem cells. FGF4 has been linked to FGF1 and FGF2 in the promotion of angiogenesis.	[294]
FGF-7/KGF	Promotes	Keratinocyte growth factor acts on microvascular endothelial cells and epithelial cells. It stimulates proliferation and activates MAPK.	[295]
GDNF	Promotes	Glial-derived neurotrophic factor mediates endothelial cell network formation independent of VEGF.	[296]
GM-CSF	Promotes	GMCSF induces vessel sprouting and endothelial cell survival. It has been shown to accelerate inflammatory responses.	[297]
HB-EGF	Promotes	Heparin binding-EGF regulates angiogenesis through P13K, MAPK and eNOS pathways by influencing VEGF.	[298]
HGF	Promotes	HGF promotes angiogenesis stimulating endothelial cell proliferation and migration.	[299, 300]
IGFBP-1	Promotes	IGFBP-1 modulates the biological activities of IGF-1 proteins. IGFs Induce proliferation,	[301]

		migration, and differentiation of endothelial and smooth muscle cells.	
IGFBP-2	Promotes	Increases the production of genes related to VEGF production, endothelial cell migration and angiogenesis.	[302]
IGFBP-3	Promotes	IGFBP-3 promotes endothelial cell motility. It up-regulates VEGF and MMPs. IGFBP-3 positively regulates angiogenesis through involvement of IGF-IR signalling and SphK/S1P activation.	[303]
IL-1 beta	Promotes	IL-1B is produced by activated macrophages and stimulates IL-2 release, B-cell maturation and proliferation, and fibroblast growth factor activity. IL-1 proteins are involved in the inflammatory and proangiogenic responses.	[304]
CXCL8/ IL-8	Promotes	IL-8 binds to CXCR2 receptors on endothelial cells and activates the angiogenic ERK/PK3 pathway.	[305]
LAP	Inhibits	TGF-1b inhibits proliferation of epithelial cells and VEGF.	[306]
Leptin	Promotes	Activates angiogenesis through a leptin receptor in endothelial cells. Leptin also regulates MMPs and TIMPs.	[307]
CCL2/ MCP-1	Promotes	Mediates TGF-beta signalling via Smad3/4 that is involved with stimulating smooth muscle cell migration towards endothelial cells.	[308]
CCL3/MIP-1 alpha	Promotes	CCL3 promotes VEGF-A expression and endothelial progenitor cell migration.	[309]
MMP-8	Promotes	MMPs are involved in the breakdown of ECM and tissue remodelling. MMP-8 converts Ang-1 to Ang-2, which increases endothelial cell proliferation/migration-related gene expression.	[310]

MMP-9	Promotes	MMP promotes VEGF and VEGF receptor-2 binding, resulting in increased capillary vessel density.	[311]
NRG1-beta1	Promotes	NRG-1 is an epidermal growth factor present in the cardiac microvascular endothelium. NRG-1 has been shown to be vital for angiogenesis.	[312]
Pentraxin 3	Inhibits	PTX3 blocks FGF receptor 2 and inhibits FGF exerting its angiogenic activity.	[313]
PD-ECGF	Promotes	Platelet derived endothelial cell growth factor promotes endothelial cell proliferation and motility. PD-ECGF is primarily expressed from platelets and placenta.	[314]
PDGF-AA	Promotes	PDGF-AA is most highly expressed in the heart, muscle and pancreas. It regulates angiogenesis by regulating FGF-2 levels.	[315]
PDGF-AB/ PDGF-BB	Promotes	PDGF-B is expressed by pericytes and endothelial cells. It is vital for the maturation of the vascular wall and also is enhanced by VEGF.	[315]
Persephin	Promotes	Persephin is a protein belonging to the GDNF family and promotes neuronal survival. Persephin is and related to Artemin and TNF-b. GDNF interacts with MAPK, P13K/AKT and ERK pathways that promote angiogenesis.	[316, 317]
CXCL4/ PF4	Inhibits	PF4 inhibits angiogenesis by interacting with angiogenic growth factors, activates CVCR3 receptors and integrin binding.	[318]
PlGF	Promotes	Placental Growth Factor-1 is active in angiogenesis, as well as in the stimulation, proliferation, and migration of endothelial cells. It signals through receptor VEGFR-1.	[319]
Prolactin	Promotes	Prolactin induces phosphorylation of ERK1/2 and STAT5 that induces tube formation of endothelial	

		cells. It releases pro-angiogenic factors via leukocytes and epithelial cells.	[320, 321]
Serpin B5/ Maspin	Inhibits	Maspin inhibits angiogenesis by halting endothelial cell migration towards bFGF and VEGF to limit mitogenesis and tube formation.	[322]
Serpin E1/ PAI-1	Inhibits	Serpin E1 inactivates VEGF receptor 2 and blocks VEGF binding and signalling.	[323]
Serpin F1/ PEDF	Inhibits	PEDF inhibits angiogenesis by blocking Ang-2 signalling in endothelial cells. PEDF binding causes cleavage of VEGF-R1 and blocks VEGF signalling.	[324]
TIMP-1	Inhibits	TIMP-1 inhibits specifically ADAM10 and MMP-9. MMPs degrade the basement membrane and TIMPS effect cell growth, differentiation, migration and apoptosis.	[325]
TIMP-4	Inhibits	TIMP-4 inhibits multiple MMPs and ADAM17/28/33. TIMP-4 reduces microvascular density and inhibits neovascularization.	[325, 326]
Thrombo-spondin-1	Inhibits	TSP1 has anti-angiogenic activity. It is a matricellular glycoprotein that influences cellular phenotype and the structure of the ECM. These effects are important components of the tissue remodelling that is associated with angiogenesis.	[327]
Thrombo-spondin-2	Inhibits	TSP2 can inhibit angiogenesis by limiting proliferation and inducing apoptosis of endothelial cells. It can inhibit the remodeling of the ECM.	[328]
uPA	Promotes	uPA helps increase vascular permeability by supporting endothelial cell proliferation and migration with VEGF. It can interact with EGF and PDGF receptors during angiogenesis, affecting proliferation and survival of endothelial and smooth muscle cells.	[329]

Vasohibin	Inhibits	Vasohibin is a negative feedback regulator of angiogenesis produced by endothelial cells. It is expressed in endothelial cells to stop angiogenesis.	[330]
VEGF	Promotes	VEGF induces angiogenesis by initiating the degradation of the ECM, it regulated endothelial cell migration and tubule formation. TGF-β, EGF and PDGF-BB induce VEGF-A mRNA expression.	[331, 332]
VEGF-C	Promotes	VEGF-C binds to VEGFR3. VEGF-C mRNA levels increase in response to pro-angiogenic PDGF, EGF, TGF-β and IL-1β.	[333]

S5.6: Images from the V2a array tubules stained with anti-CD31. Images were analysed through Angio.Sys software and tubule length, branches and junctions were quantified. Images show that more tubules had formed from 7507 TIPS polymer film samples in comparison to 7507 control films, 7502 TIPS and control films. Images of internal controls revealed VEGF promoted tubule formation and suramin blocked tubule formation.

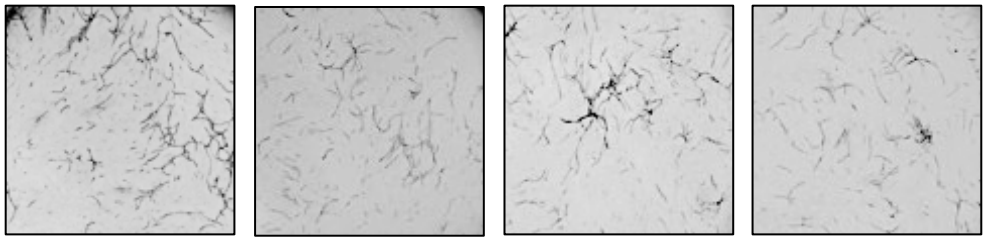

7507 TIPS polymer film | 7507 control polymer film | 7502 TIPS polymer film | 7502 control polymer film

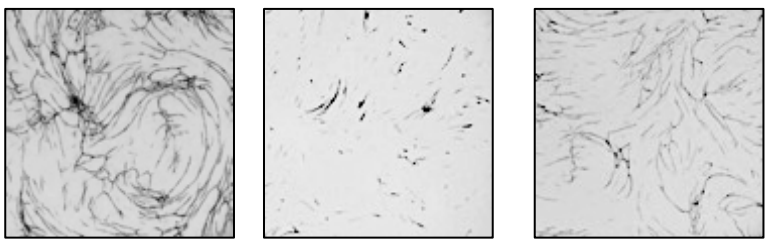

VEGF control | Suramin control | Media control

Part I.

Chapter 6: Pre-Clinical Evaluation of Acellular TIPS-Based Materials

6.1 Introduction

6.1.1 Pre-Clinical Models of Peripheral Artery Disease

Peripheral artery disease (PAD) is caused by a reduction or cessation of blood flow in the peripheral arteries, often resulting in ischaemia of the lower extremities. If left untreated a deadly complication termed critical limb ischaemia can develop. [10] With no curative treatments for PAD currently available and *in vitro* studies limited to early stage research due to difficulties replicating living organisms in the lab, it is vital to be able to reproduce diseases *in vivo* in order to effectively develop new treatments. To achieve this in a pre-clinical setting, the hindlimb ischaemia model is often utilised by obstructing blood flow to the lower extremities with surgical intervention. The hindlimb ischaemia model has been established in a range of animals, including mice, [334] rats, [335] rabbits, [336] pigs [337] and to sheep. [338] There are multiple methods to induce ischaemia, and the selection of the most appropriate procedure is dependent on the animal's age, gender, strain, the level and severity of ischaemia required, and the treatment investigated. For example, Niiyama *et al.*, 2009, reported that the age of an animal significantly affected recovery times. With young mice recovering much quicker than older mice, where older mice are more suited for angiogenic studies as any differences between treated and control groups would have time to be seen. [334] Animal strain must also be considered when selecting the method to

induce ischaemia. Helisch *et al.*, 2006, showed that the genetics of a mouse can impact the formation of collateral vessels, and thus reperfusion time. Therefore, animals that are genetically modified (where blood vessel formation is affected) would need to be subject to a procedure that is able to effectively induce ischaemia, without causing complete necrosis of the foot, and experiments would need to be optimised before further studies. [339, 340] Procedures to induce ischaemia can involve femoral artery ligation, femoral artery excision, dissection of the femoral artery and vein, electrocoagulation of the iliac artery and/or femoral artery. [334, 340-342] To optimise the method that was able to induce ischaemia in mice immediately without causing necrosis, two methods were investigated. Firstly, unilateral femoral artery ligation and, secondly, unilateral artery excision. Both were evaluated through laser doppler imaging.

6.1.2 Tissue Engineering Strategies for the Treatment of Ischemic Disease

The hindlimb ischaemia model has been used to investigate the effect of many therapies for the treatment of PAD. Treatments range from gene therapies to promote the secretion of pro-angiogenic growth factors, [50] cell therapies with the delivery of stem cells and endothelial cells, [66, 71, 84, 91] angiogenic growth factor delivery, most commonly VEGF, FGF or PDGF [46], drug delivery, [343] biomaterials in combination with cell therapies [138, 146, 344] and hydrogel based biomaterials alone [345] for the treatment of PAD. There have been successes in the delivery of cell therapies for the treatment of ischemic disease: Frangogiannis *et al.*, 2018, conducted a review that examined the delivery of a range of cell types for the treatment of PAD to patients who were not able to receive revascularisation surgery. They concluded that cell therapy was a promising treatment for PAD as many clinical trials reported improvements in rest pain, blood flow and wound healing, as well as lower amputation rates. Despite these results, some clinical trials did not report a difference between groups receiving the therapy and placebo, highlighting the need for improvements to cell therapy

approaches. [73] Studies have shown that delivery of cells via suspension results in up to a 90% cell loss from the implant site after 24 hours and long-term cellular retention is less than 1%. [4, 5, 77, 92-94] Without an effective way of delivering cells to the target site the potential of ischemic treatments remains futile. To overcome these challenges, a biomaterial can be utilised to facilitate cell therapies by acting as an anchor for the cells, support proliferation and survival of the cells. From this, the cells can remain at the implant site and have the opportunity to have their therapeutic effect. [68, 90, 346-348]

The *in vitro* pro-angiogenic response seen from ADMSCs seeded onto 7507 PLGA TIPS polymer films through the increased secretion of VEGF and *in vitro* capillary formation in Chapter 5 opens up the possibility of utilising TIPS-processed ADMSC substrates for the treatment of PAD. Before this, the response, safety and delivery of the polymer films *in vivo* must be determined in the relevant pre-clinical model. This chapter explores the use of the hindlimb ischaemia model as a pre-clinical model of peripheral artery disease. Once established, this model was then utilised to investigate the *in vivo* response to TIPS biomaterials through the subsequent implantation and assessment with laser doppler imaging and histology.

6.2 Methods

6.2.1 Inducing Ischaemia in a Pre-Clinical Model of Peripheral Arterial Disease

Before surgery all tools and surgical drapes were autoclaved at 121^{o}C for 15 minutes. New and disposable surgical cap, clothes, shoe covers, and gloves were worn. Aseptic technique was always followed. Female 2-3 months old c57bl/6 mice were anaesthetised in an anaesthesia chamber, with 1-3% Isoflurane (PRI001325-EA, SAS, USA) and 2 L/min oxygen flow. The anaesthesia chamber was cleaned before and after each use using 70% ethanol. The mouse was placed in the supine position away from the surgical table and connected to a continuous flow of isoflurane and oxygen where both limbs were extended and shaved using an electric shaver. A protective gel was placed over both eyes of the mouse to prevent drying (Puralube vet ointment). The mouse was then transferred to the surgical table and placed in the supine position on a draped heated pad to prevent heat loss from the animal. Using an aesthetic facemask, the mouse was connected to a continuous flow of 1-3% isoflurane with 2 L/min oxygen flow. The right hindlimb was extended and secured with autoclave tape and the skin cleaned with an antiseptic wash. A microscope was used for a clearer view of the hindlimb during the surgery. An incision approximately 1 cm in length was made in the skin above the femoral arterial bundle with scissors. Using fine forceps, the subcutaneous fat was removed from the thigh muscle and the neurovascular bundle was exposed.

6.2.1 Evaluation of Methods to Induce Hindlimb Ischaemia.

To determine the optimal hindlimb ischaemia model two different approaches were evaluated: unilateral femoral artery ligation and superficial artery excision. Unilateral femoral artery ligation (n=2) was performed by separating the femoral nerve from the femoral artery and vein at the proximal position near the groin and above the superficial epigastric artery. A non-absorbable 7-0 silk suture (7733D, Ethicon, USA) was passed through the separated artery and vein and tied twice to occlude blood flow, whilst keeping the nerve

unaffected. The second method, superficial artery excision, involved gently separating the nerve from the femoral artery and vein, ligating the femoral artery once at the common femoral artery site and again at the superficial femoral artery site using non-absorbable 7-0 silk sutures (7733D, Ethicon, USA). The artery was cut below the suture the and excised (n=2). Between surgeries all instruments were wiped clean and re-sterilised using a hot bead steriliser (Premier Deluxe Model B) at 250^{o}C for 10-30 seconds and allowed to cool before re-use. All incisions were closed with 3-4 5-0 coated Vicryl absorbable sutures (J409G, Ethicon, USA) and cleaned, then animals were placed into a recovery chamber until consciousness was regained. All incision sites were checked after 24 hours to ensure the sutures had not broken and for signs of infection or suffering. If the sutures had broken, the animal was anaesthetised, and the wound was re-sutured with 5-0 coated Vicryl absorbable sutures. The animals were monitored every 6-7 days. The efficiency of the surgeries was assessed by laser doppler imaging immediately after surgery, and the blood reperfusion was measured weekly up to 21 days with laser doppler imaging.

6.2.2 Blood Flow Evaluation Using Laser Doppler Imaging

To assess if hindlimb ischaemia had been induced during surgery, the mouse was placed in the prone position on a heated pad and connected to a continuous flow of 1-3% isoflurane and 2 L/min oxygen via an aesthetic facemask. The heated pad was covered with a non-reflective surface to minimise the backscattered light that can interfere with the laser doppler measurements. The laser doppler (moorVMS-LDF, UK) was connected to a laptop (Dell) with the moorVMS-LDF software. A live image of the mouse was taken and from this an area was selected for imaging. Laser doppler images were taken of the paws. Once completed, the anaesthetic mask was removed and the mouse was transferred to a recovery chamber until consciousness was regained. This process was repeated after each surgery was completed.

At days 7, 14 and 21 mice were anaesthetised in an anaesthesia chamber with 1-3% Isoflurane and 2 L/min oxygen flow. The mouse was then transferred to

a heated pad with a non-reflective surface, placed in the prone position and connected to a continuous flow of isoflurane and oxygen. Laser doppler images were taken of the paws. The mouse was then moved to the supine position, limbs extended and imaged again. The mouse was placed into a recovery chamber until consciousness was regained. A region of interest was highlighted and analysed using Moor software. The median values were taken from the experimental and control regions of interest and the untreated limb of each animal was used as the control.

6.2.3 Polymer Film Implantation into the Hindlimb Ischaemia Model

Before surgeries, polymer films were prepared as outlined in section 6.2.1. Implants were created by producing a 5 mm circular segment from the 13 mm prepared polymer films using a biopsy punch (A615110, Agar Scientific, UK) to create circular and replicable samples. The samples were imaged under SEM as described in Section 2.2.4 to assess the structure of the implant, as well as to measure the thickness of the films. Unilateral femoral artery ligation was used in c57bl/6 mice. Once ischaemia had been induced, 7507 TIPS polymer films were implanted over the occluded bundle (n=3) and this was repeated with 7507 control polymer films. (n=2) No treatment controls were also included. (n=2). All incisions were closed with 3-4 coated Vicryl absorbable sutures (J409G, Ethicon, USA). All incision sites were checked after 24 hours to ensure the sutures had not broken. If this had occurred, the sites were re-sutured as outlined in Section 6.2.1. The efficiency of the surgeries were assessed by laser doppler imaging immediately after surgery, and the blood reperfusion was measured weekly up to 21 days with laser doppler imaging. The surgeries were repeated three times.

6.2.3 Evaluation of Implanted TIPS-Based Materials

6.2.3.1 Preparing Microscope Slides Using TESPA

3-triethoxysilylpropylamine (TESPA) was used to functionalise glass surfaces with alkoysilane molecules to induce a positive charge. This allowed for enhanced attachment of sectioned tissues. Clean glass slides (631-1551, VWR, UK) were incubated in acetone (20065.362, VWR, UK) for 5 minutes at

room temperature. Slides were then placed in 2% TESPA (440140, Sigma, UK) in acetone for 5 minutes at room temperature. The slides were then washed twice in deionized H_2O for 5 minutes and left to dry at room temperature for 18-24 hours.

6.2.3.2 Histological Analysis of Tissues

Animals were culled using the established schedule I method of 5 minutes exposure to CO_2 from 30% to 70% and confirmation of death by cervical dislocation. The lower limbs were dissected, and tissues were immersed in 4% formalin solution (HT501128, Sigma-Aldrich, UK) for 48 hrs or RNALater (AM7020, ThermoFisher, UK) and placed in -20^{o}C freezer for long term storage. RNALater is a solution developed to stabilise and protect RNA within tissues without having toxic effects and allowing long-term storage of tissues. It has been shown to have comparable RNA as fresh tissue and samples stored in conventional methods such as freezing in liquid nitrogen. [349] After fixation in formalin and before tissue dehydration and embedding, the gastrocnemius muscle was dissected from the femoral bone and placed into a histology cassette (18000-130, VWR, USA). Samples were then placed into 70% ethanol for 1 hour, 95% ethanol for 1 hour, 100% ethanol for 1 hour, 1½ hours, overnight and again for 1 hour. Samples were drained and placed into Histo-clear (AGR1345, Agar Scientific, UK) for 1 hour and again for 2 hours. Finally, samples were placed into 58°C Paraplast X-tra wax (P3808, Sigma, UK) for 1 hour and again for 2 hours. 15 mm x 15 mm disposable moulds (3804016, Lecia, UK) were used to embed the samples. The base of the mould was filled with warm wax (approximately to 5 mm deep). The cassette containing the tissue was removed from the wax and the lid discarded. The tissue was transferred into the mould, ensuring that the proximal portion of the tissue was facing down. Once the wax had begun to solidify, wax was poured over the tissue and the bottom of the cassette was placed on top. Once the wax was completely cooled and hardened the paraffin block was removed out of the mould. Blocks were stored at -10^{o}C. Tissues were sectioned using a microtome. First, a water bath was pre-warmed to 37^{o}C. A blade was placed onto the microtome (and replaced every ten blocks). The block was placed

into the microtome where the block was aligned in the vertical plane. The block was cut down to the desired tissue plane. The microtome dial was set to cut 5 µM and five sections of paraffin ribbons were cut and picked up with forceps. The ribbons were floated on the surface of the 37ºC water bath. The sections were then collected at approximately a 30^{o} angle using Superfrost Plus Adhesion microscope slides (J1810AMNT, ThermoFisher, UK) or TESPA slides. Sections were pressed between filter paper (grade 303, 150 mm, 516-0295, VWR, UK) soaked with 70% ethanol. The block was cut 100 µm and another five 5 µM sections were cut. After this, blocks were refrozen because as the wax began to melt the sections would not cut properly due to the low melting point of the wax. Slides were dried and stored at room temperature.

6.2.3.3 Haematoxylin and Eosin staining of Tissue Sections

Before Haematoxylin and Eosin (H&E) staining, samples were de-waxed and rehydrated. Slides were placed into a slide rack and incubated in Histo-clear (AGR1345, Agar Scientific, UK) for 5 minutes twice and blotted for excess reagent. Slides were then incubated in 100% ethanol for 5 minutes twice, once in 95% ethanol for 5 minutes, once in 80% ethanol for 5 minutes and finally in deionized water for 2 minutes. Slides were blotted to removed excess water and immersed in haematoxylin for 3 minutes. Slides were then rinsed in alkaline tap water for 5 minutes to neutralise the acid. Slides were fast dipped into acid alcohol 20 times (1mL hydrochloric acid and 50 mL 70% ethanol) and immersed in tap water. For eosin staining, 1% eosin stock solution was prepared by combining 4 g eosin Y (E4009, Sigma, USA) with 80 mL distilled water and 320 mL 95% ethanol. Eosin Y working solution was prepared by combining 100 mL eosin Y stock solution to 300 mL 80 ethanol and 2 mL glacial acetic acid (537020, Sigma, USA). Slides were plunged into the working eosin solution for 30 seconds then immediately transferred into 95% ethanol for 5 minutes. Slides were then dehydrated by incubating in 95% ethanol for 5 minutes for a total of three times, two incubations in 100% ethanol for 5 minutes each and twice in Histo-clear for 5 minutes. Slides were then mounted with 0.5 mL DPX mountant (44581, Sigma, UK) and covered with a

glass coverslip (AGL463450, Agar Scientific, UK). Slides were images using a Nanozoomer 2.0-HT (Hamamatsu, UK).

6.2.3.4 Immunohistochemical Staining of Tissue Sections

Immunohistochemistry to stain for von Willebrand factor (VWF) was carried out. Slides were warmed for 20 minutes at 60ºC then de-waxed and rehydrated using serial dilutions of ethanol and Histo-clear (AGR1345, Agar Scientific, UK) outlined in section 6.2.3.2. Slides were incubated for 1 hour in 0.1% Triton (T8787, Sigma, UK) diluted in 1X PBS. Sections were washed twice in 1X PBS for 5 minutes. Antigen retrieval was performed by using Trypsin Enzymatic Antigen Retrieval solution (ab970, Abcam, UK). Trypsin buffer was warmed to 37ºC and combined with the trypsin stock at a ratio of 1:1. 200–400 µl of the solution was pipetted onto each slide and incubated at 37ºC in a humidified chamber for 10 minutes. The slides were washed twice in 1X PBS. To quench endogenous peroxidase activity, which may lead to high background staining, sections were incubated in 0.3% hydrogen peroxide for 20 minutes. (10ml H_2O_2 in 300 mL Methanol). The slides were washed twice in 1X PBS. To stain for VWF, VECTASTAIN Elite ABC HRP kit (Peroxidase, Sheep IgG) (PK-6106, Vector Laboratories, USA) was used. To prevent non-specific binding of the antibody to the tissues, each section was blocked. 200 µL of Vectorstain blocking serum sheep IgG stock was added to 1 mL 1X PBS. 200–400 µl of blocking solution was pipetted onto each slide. Slides were incubated for 1 hour at room temperature in a humidified chamber. Sheep primary antibody to Von Willebrand Factor (VWF, Ab11713, Abcam, UK) was first optimised with dilutions of VWF at 1:1000, 1:500, 1:250, 1:100 and 1:25 in 1X PBS. 200–400 µL was pipetted onto each slide. Slides were incubated overnight at 4°C in a humidified chamber. The slides were transferred to a slide rack and washed twice in 1X PBS for 5 minutes. Biotinylated secondary antibody was prepared by adding 150 µL of the normal blocking serum stock and 50 µL of the biotinylated antibody stock to 10 mL of 1X PBS. 200–400 µL of the solution was pipetted onto each slide. Slides were incubated for 1 hour at room temperature in a humidified chamber. The slides were transferred to a slide rack and washed twice in 1X PBS for 5 minutes. 15 minutes before use

VECTASTAIN Elite ABC reagent was prepared. 200 µL of reagent A was added to 10 mL 1X PBS which and mixed thoroughly, then 200 µL of reagent B was added. Before incubation with VECTASTAIN ABC reagent sections were washed twice in 1X PBS for 5 minutes. 200–400 µL of the solution was pipetted onto each slide and sides were incubated for 30 minutes at room temperature in a humidified chamber. Slides were then transferred to a slide rack and washed twice in 1X PBS for 5 minutes. To develop the stain, one of each SigmaFAST tablet was dissolved in 10ml deionized water (Sigma, 1002031992). One slide was removed from the 1X PBS, wiped down and placed under a microscope. 1 mL peroxidase substrate solution was added, and stain development was monitored. Slides were not exposed to peroxidase substrate for more than 10 minutes. Once the stain had developed slides were immersed in 1X PBS, then deionized water to stop the stain developing further. This was repeated for all the slides. The sections were counterstained with hematoxylin as described in section 6.2.3.3. Slides were images using a Nanozoomer 2.0-HT (Hamamatsu, UK). It was determined that 1:1000 dilution was optimal. Slides were also stained for endothelial cell marker anti-CD31 (ab28364, Abcam, UK) at dilutions 1:10, 1:25, 1:50, 1:100, 1:250, 1:500 with VECTASTAIN Elite ABC HRP kit (Peroxidase, Rabbit IgG) (PK-6101, Vector Laboratories, UK).

6.2.4 Evaluation of Arteriogenesis

H&E stained sections were evaluated for evidence of arteriogenesis by manually identifying arterial bundles within the gastrocnemius tissue. Sections from the same position from the tissue were selected and imagedusing a Nanozoomer 2.0-HT (Hamamatsu, UK). The arteries within these bundles were measured by manually drawing around the outer and inner lumen in the NPD.view2 software which provided measurements. From the circumference measurements the area of the lumen and artery wall were calculated using the equations in Table 6.1

1. $R_o = C_o \div 2\pi$		
2. $R_i = C_i \div 2\pi$		
3. $A_t = \pi R_o^2$		
4. $A_i = \pi R_i^2$		
5. $A_o = A_a - A_i$		
A_o = Outer Area	C_o = Outer Circumference	R_o = Outer Radius
A_i = Inner Area	C_i = Inner Circumference	R_i = Inner Radius
A_t = Total Area		

Table 6.1: Equations used to calculate circumference measurement of blood vessels from H&E stained tissue sections.

6.2.5 Evaluation of Angiogenesis Related Gene Expression from Ischemic Limbs Treated with TIPS-Based Materials

6.2.5.1 Extracting RNA From Tissues for Evaluation of Gene Expression

6.2.5.1.1 Method 1 Using RNeasy Mini Kit (74104, Qiagen, UK)

Harvested tissue from previously described surgeries were stored in RNALater and placed in -80^{o}C freezer for long term storage. It was essential to first decontaminate the work station of RNA by simply spraying all tools and work surfaces with RNaseZap (AM9780, ThermoFisher, UK). 10-30 mg of tissue was added to 700 µL of Buffer RLT lysate solution and 20 µL 2 M dithiothreitol (DTT) was loaded into a QIAshredder homogenizer spin column (79654, Qiagen, UK) held in a 2 mL RNase free collection tube. The samples were centrifuged for 2-3 minutes and the supernatant was transferred to a micro-centrifuge tube. 70% cold ethanol was added to the sample at a ratio of 1:1 and pipetted thoroughly. 700 µL of the sample was added to a RNease spin column in a 2 mL collection tube and spun for 20 seconds. The flow through was discarded. 700 µL of Buffer RW1 was added to the RNeasy spin

column to wash the membrane. The buffer RPE was reconstituted with 4 times as much 99% ethanol. 500 µL of the buffer was added to the spin column and centrifuged for 20 seconds. An additional 500 µL of the buffer was added to the spin column and centrifuged for 2 minutes to remove excess RPE buffer the column. The spin column was placed into a RNase free collection tube and 50 µL RNase-free water was pipetted directly onto the column membrane with care taken to not touch the sides of the column. The column was spun for 1 minute and RNA concentration of the flow through was measured using Nanodrop 8000 UV Visible Spectrophotometer (Thermo, UK).

6.2.5.1.2 Measuring RNA Quality and Concentration with NanoDrop 8000 UV Visible Spectrophotometer

Samples were kept on ice before and during measurements. Before measurements the wells on the stage of the NanoDrop spectrophotometer was cleaned with a dry microfiber tissue (07-301-002, ThermoFisher, UK) to remove dust. 2 µL of RNAse free H_2O was pipetted onto the first well on the stage. The stage lid was gently closed. The NanoDrop software was opened and RNA analysis selected. To calibrate the system, the calibration setting was selected and run. Once complete, the lid was lifted and the RNAse free H_2O wiped away with a microfiber tissue. 2 µL of the sample was pipetted onto the first well on the stage. Once the measurement was complete the 260/280 ratio, 260/230 ratio, concentration of RNA (ng/µL) and a spectroscopy graph (absorbance vs wavelength) was provided. The sample was wiped away with a microfiber tissue and this process was repeated for all samples.

6.2.5.1.3 Method 2 Using Monarch Total RNA MiniPrep Kit (T2010S, Moncarch, UK)

The work station was decontaminated of RNA by spraying all tools and work surfaces with RNaseZap (AM9780, ThermoFisher, UK). 10-30 mg of tissue was extracted from the region of interest from the mouse limbs stored in RNALater and was placed into an RNase-free microcentrifuge tube (AM12425, Invitrogen, UK). Monarch DNA/RNA protection reagent was diluted to 1x solution with nuclease free water. 1x DNA/RNA protection reagent was

added to each microcentrifuge tube was added at a ratio of 1mg to 100 µL. To ensure higher RNA yields tissues were mechanically homogenized. Proteinase K was reconstituted with 250 µL Proteinase K Resuspension Buffer. For every 300 µL of protection reagent added to the sample, 30 µL of Proteinase K Reaction buffer and 30 µL Proteinase K was added. Samples were vortexed and incubated in a waterbath at 55^{o}C for 10 minutes. Samples were then vortexed and centrifuged for 2 minutes at 16,000xg and the supernatants were transferred to new microcentrifuge tubes. RNA Lysis buffer was added to the supernatants at a ratio of 1:1. Samples were vortexed for 10 seconds. gDNA removal columns were added to RNase free collection tubes. 800 µL of the sample was added to the removal column and centrifuged for 30 seconds. Any remaining sample were added to the removal column and centrifuged again. The flow through was saved and the removal column was discarded. In order to precipitate the RNA, an equal volume of cold 99% ethanol was added to the sample and thoroughly mixed by repeated pipetting. The sample was transferred to an RNA Purification Column fitted with a RNase free collection tube. The sample was centrifuged for 30 seconds and the flow-through was discarded. RNA wash buffer was reconstituted with 6.4 mL 99% ethanol. To enzymatically remove any residual gDNA, 500 µL of RNA wash buffer was added to the column and the sample was spun for an additional 30 seconds and the flow through discarded. 75 µL of DNase reaction buffer was added directly to the matrix of the column and 5 µL of DNase 1 previously reconstituted with 55 µL nuclease free water. After 15 minutes incubation at room temperature 500 µL RNA Priming buffer was added, the sample was centrifuged for 30 seconds and the flow through discarded. This process was repeated with 500 µL wash buffer and spun for 2 minutes. The column was transferred to a RNase-free microcentrifuge tube. 100 µL nuclease-free water was added directly to the column matrix taking extra care not to touch the sides of the column. The sample was centrifuged for 30 seconds to elute the RNA. RNA was concentration and purity were measured using NanoDrop 8000 UV Visible Spectrophotometer (Thermo, UK) and stored in a -80^{o}C freezer.

6.2.5.2 Reverse Transcription of RNA to cDNA Synthesis

To create cDNA from the extracted RNA and eliminate genomic DNA, the RNA was reverse transcribed using QuantiTect Reverse Transcription Kit (205310, Qiagen, UK). RNA concentrations were calculated from NanoDrop Spectrophotometer. All reagents were kept on ice to avoid RNA degradation before use. RNA samples were removed from the -80ºC freezer and thawed on ice. To eliminate genomic DNA, 2 µL of x7 gDNA Wipeout Buffer was added to a MicroAmp Fast 0.1 mL 8-Tube Strip (4358293, Thermo, UK). 72.74 ng of RNA was added to each tube and adjusted to a total of 14 µL with RNase-free H_2O. The samples were incubated for 2 minutes at 42ºC and placed on ice. In a separate tube, 1 µL Quantiscript Reverse Transcriptase, 4 µL x5 Quantiscript RT Buffer and 1 µL RT Primer Mix was combined. This solution was added to the 14 µL from the DNA elimination reaction to a total of 20 µL. Samples were incubated for 15 minutes at 42ºC, then 3 minutes at 95ºC and stored at -20ºC before further use.

6.2.5.3 Design of Oligonucleotide Primers for Quantitative Polymerase Chain Reaction

Oligonucleotide primers were designed to be 20 base pairs long, with a melting temperature between 66-72ºC, desalted with a coupling efficiency of 99% with GC contents between 45-55%. Primers were reconstituted with nuclease free water to a concentration of 100 uMole. Once primers were checked and passed self-annealing, Heparin formation and GC clamp tests, they were purchased from Invitrogen, UK. The primers designed were VEGF-A, FGF2, PDGFRA, PEGF and NRP-1 (summarised in Table 6.2). Murine actin (Mmu Actb) was used as a reference gene.

Primer Name	Forward (5'-3')	Tm	Reverse (5'-3')	Tm
Murine Vascular Endothelial Growth Factor A (VEGF-A)	CAG GCT GCT GTA ACG ATG AA	47	CTC ACC AAA GCC AGC ACA TA	47
Murine Basic Fibroblast Growth Factor (FGF2)	AGC GGC TCT ACT GCA AGA AC	49	GCC GTC CAT CTT CCT TCA TA	47

Murine Platelet Derived Growth Factor Receptor Alpha (PDGFRA)	TGG CAT GAT GGT CGA TTC TA	45	CGC TGA GGT GGT AGA AGG AG	51
Murine SerpinF1 (PEGF)	AAG ACG ACC CTC CAG CAT TT	47	AGG GGC AGG AAG AAG ATG AT	47
Murine Neurophilin-1 (NRP-1)	AAC CCA CAT TTC GAT TTG GA	49	TTC ATA GCG GAT GGA AAA CC	48

Table 6.2: Summary of Primers designed for qPCR.

6.2.5.4 Relative Quantitative Polymerase Chain Reaction to Evaluate Angiogenesis Related Gene Expression from Ischemic Limbs Treated with TIPS-Based Materials

Relative quantitative polymerase chain reaction (qPCR) was used to amplify the full coding sequences of VEGF-A, FGF2, PDGFRA, PDGF and NRP-1 in order to detect and quantify the expressions of the genes. All reagents and samples were thawed and kept on ice. 10 µL 2x Brilliant II SYBR Green QPCR (600882, Aligent, UK), 8 µL RNase-free H_2O, 0.5 µL reverse primer, 0.5 µL forward primer and 1 µL of the cDNA were thoroughly mixed and added to a well in a MircoAmp Optical 96-well reaction plate (10411785, Fisher Scientific, UK), two blank control wells were included and the plates were sealed with well caps (MicroAmp 8-Cap Strip, N8011535, ThermoFisher, UK). This was repeated with all samples and forward and reverse primers. Actin (Mmu Actb) was used as a reference gene. Agilent Mx3005P qPCR system was used to analyse the samples. Before samples were placed into the reader, the plates were centrifuged for 30 seconds. The thermal profile was set to run one cycle at 95^{o}C for 5 minutes, then the samples were exposed to 95^{o}C for 10 seconds and 57^{o}C for 7 seconds for 40 cycles. Finally, samples were run once at 95^{o}C for 1 minute, 55^{o}C for 30 seconds and 95^{o}C for 30 seconds.

6.2.6 Profiling for Angiogenic Growth Factors from Ischemic Limbs Treated with TIPS-Based Materials

Qiagen RT^2 Angiogenic Growth Factors Array (PAHS-072Z, Qiagen, UK) was used to profile 84 angiogenic related growth factors from the limbs with induced hindlimb ischaemia and treated with acellular TIPS and control polymer films. RNA was extracted (Section 6.2.5.1.3) from control limbs and limbs implanted with 7507 TIPS polymer films after hindlimb ischaemia. The reagents of the RT^2 first strand kit (330401, Qiagen, UK) were thawed and centrifuged. To eliminate DNA, 2 µg Buffer GE was added to 150 ng of RNA and made up to a total volume of 10 µL with RNase-free water. This solution was thoroughly mixed by pipetting, then incubated for 5 minutes at 42ºC and placed on ice. To created cDNA, to each tube 10 µL of reverse transcription mix (4 µL 5x Buffer BC3, 1 µL Control P2, RE3 Reverse Transcriptase Mix and 3 µL RNase-free water) was added. The samples were incubated at 42ºC for 15 minutes, 95ºC for 5 minutes and placed on ice. 1350 µL of the RT^2 SYBR Green ROX qPCR Mastermix (330520, Qiagen, UK) was combined with 1248 µL RNase-free water and 102 µL of the cDNA synthesis reaction. To the RT2 PCR Array 96 well plate (330231, Qiagen, UK) 25 µL of the prepared solution was added to each well and pipetted up and down to ensure thorough mixing, avoiding bubble formation. Each well was sealed. Before samples were placed into the reader, the plates were centrifuged for 30 seconds. The thermal profile was set to run 1 cycle at 95ºC for 10 minutes, then the samples were exposed to 95ºC for 15 seconds, 55ºC for 35 seconds and 72ºC for 30 seconds for 40 cycles.

6.3 Results

6.3.1 Pre-Clinical Evaluation of Acellular TIPS-Based Materials

6.3.1.1 Hindlimb Ischaemia Model

Two methods were used to induce hindlimb ischaemia in c57/bl6 mice to determine the most appropriate method to block blood flow to the lower limb, whilst avoiding complete necrosis and amputation of the extremity. Unilateral femoral artery ligation and superficial femoral artery excision were performed and laser doppler images were taken immediately after surgeries and then at days 7 and 21. Images were evaluated and quantified. Results revealed that unilateral femoral artery ligation had induced ischaemia immediately, with no necrosis developing as reperfusion returned to the limb after 21 days. Superficial femoral artery excision did not induce ischaemia in the limbs, as seen in Figure 6.1 and remained unchanged through the timepoints.

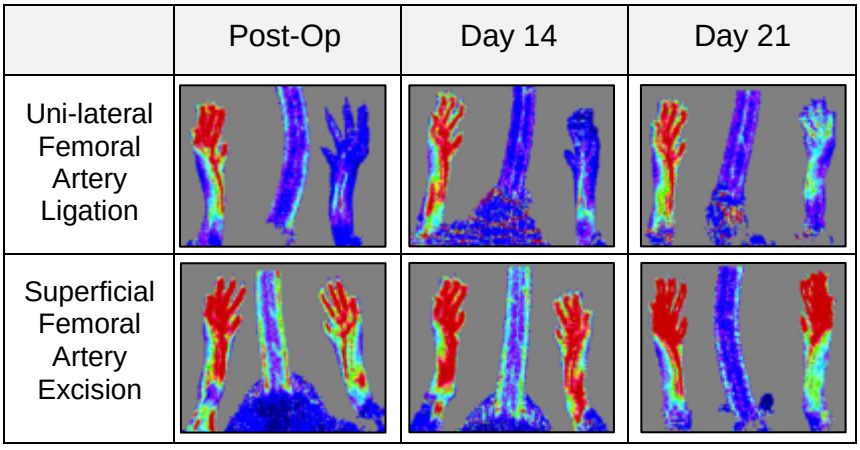

Figure 6.1: Laser-doppler imaging showing the paws of mice that had undergone unilateral femoral artery ligation and superficial femoral artery excision post operatively and at days 14 and 21.

Therefore, unilateral femoral artery excision was selected as the method that most effectively induced hindlimb ischaemia and was used in all further *in vivo* experiments. Laser doppler imaging was first used post-operatively to confirm that ischaemia had been induced in the treated limbs. It was used weekly for

3 weeks to analyse the progression of reperfusion in the hindlimbs and paws. Images were analysed using moorVMS-LDF software for quantitative results. Results were plotted as perfusion ratio, where the untreated limb of each animal acted as the treated limbs control.

6.3.2 Implantation of Biomaterials

Before the implantation of polymer films, they were prepared from 13mm films produced in Part I. Section 2.2.3. Polymer films were hydrophilised as described in Part I. Section 2.2.8. 5mm polymer films were imaged to assess the integrity of the films after cutting and hydrophilisation. Figure 6.2 shows that the biopsy punch had successfully cut the 7507 TIPS and control polymer films without damaging the integrity of the film. Images show that hydrophilisation did not affect the 7507 control polymer films. There were visible differences in the edges of the7507 TIPS and PLGA control polymer films before and after hydrophilisation. Hydrophilised polymer films had more frayed edges; most likely due to degradation. Figures 5.2 e-g show representative images with the thickness of the 7507 TIPS polymer films measured. Average thickness was 1.41 µm. Hindlimb ischaemia was induced in C57/bl6 mice and either 5mm 7507 TIPS or 7507 control polymer films were immediately implanted into the ischaemic limb.

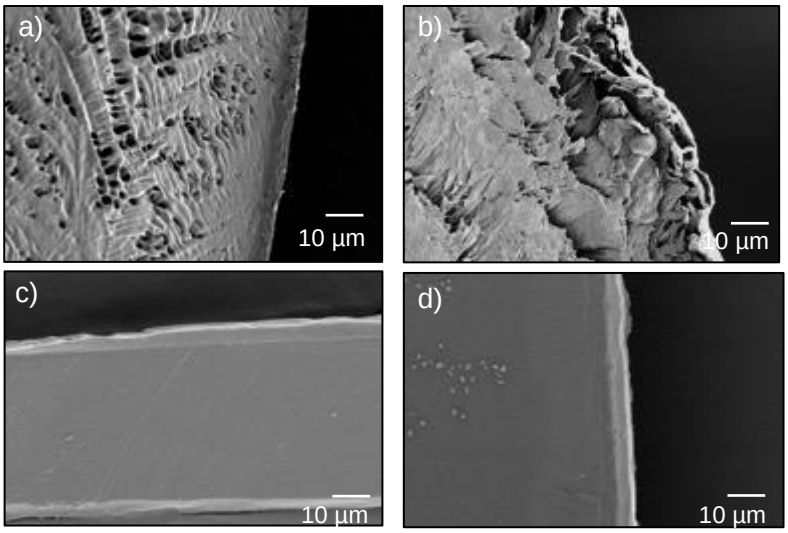

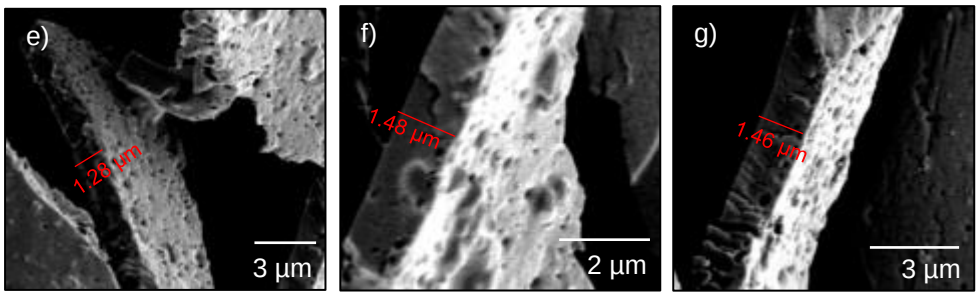

Figure 6.2: SEM images of 5mm 7507 PLGA TIPS polymer implants before a) and after hydrophilisation b) SEM images of 5mm 7507 PLGA control polymer implants before c) and after hydrophilisation d) Images e-g) show the thickness of the 7507 TIPS polymer films.

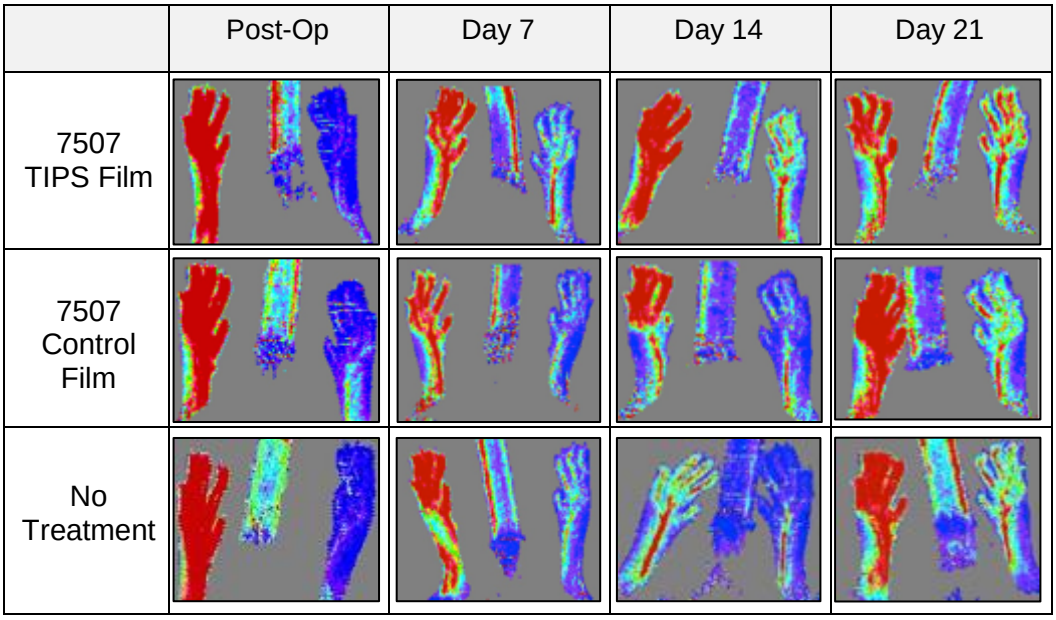

Figure 6.3: Laser-doppler imaging of the paws of mice that had undergone unilateral femoral artery ligation and subsequent implantation of 7507 PLGA TIPS films, control 7507 PLGA films and no treatment. Images were taken post-operatively and at days 7, 14 and 21.

The animals' limbs were imaged using laser doppler immediately after surgeries and at days 7, 14 and 21. Figure 6.3 shows that ischaemia was induced after surgeries and after 7 days, there was no significant difference in the reperfusion of limbs between all groups. After 14 days, mice with the 7507 TIPS polymer film implant had significantly higher reperfusion rates compared to the control implant (0.95±0.2 and 0.35 ±0.3 respectively). This effect continued to 21 days with a further increase in perfusion ratio with the 7507 TIPS polymer films (0.9 ±0.16) compared to 7507 control polymer films and a no treatment control (0.32 ±0.09 and 0.56 ±0.2 respectively).

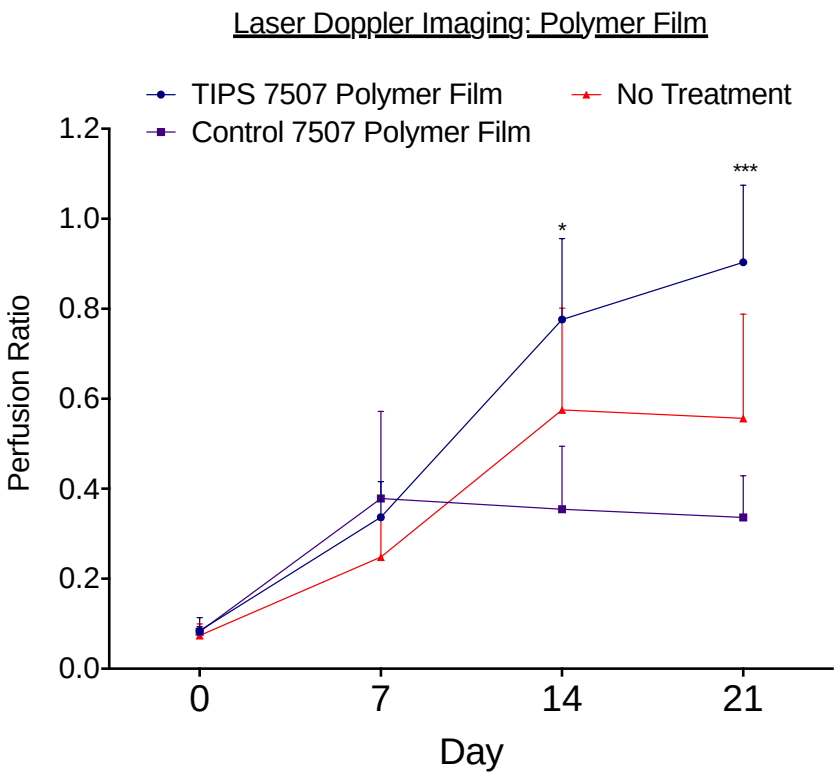

Figure 6.4: Quantification of laser-doppler imaging of the paws of mice that had undergone unilateral femoral artery ligation and subsequent implantation of 7507 PLGA TIPS processed films, control 7507 PLGA films and no treatment. Results are shown as perfusion ratio at days 7, 14 and 21. (n=3) Where * = P<0.05 and *** = P<0.001. Two-way ANOVA with Geisser-Greenhouse correction = * (P=0.0316).

6.3.3 Histological Analysis

The hindlimbs were harvested, fixed, embedded and sectioned as described in section 6.2.3.2. Sections were stained with haemoxylin and eosin (H&E) as described in section 6.2.3.3. Haemoxylin is a basic stain that binds to negatively charged substances and thus stains the nuclei of a cell purple. Eosin is a negatively charged stain that binds to positively amino acids and stains the cytoplasm of cells pink. [350] Tissue sections (Figure 6.5) show that the implanted polymer films remained at the implant site. The texture of the TIPS processed material is visible in images 6.5a, b and c, revealing that after 21 days the hierarchical texture of the material was still present.

Haemoxylin stain shows attachment and infiltration of cells into the surface of the 7507 TIPS polymer film implant, indicated by red arrows in image 6.5a. There is also evidence of blood vessel formation around the 7507 TIPS

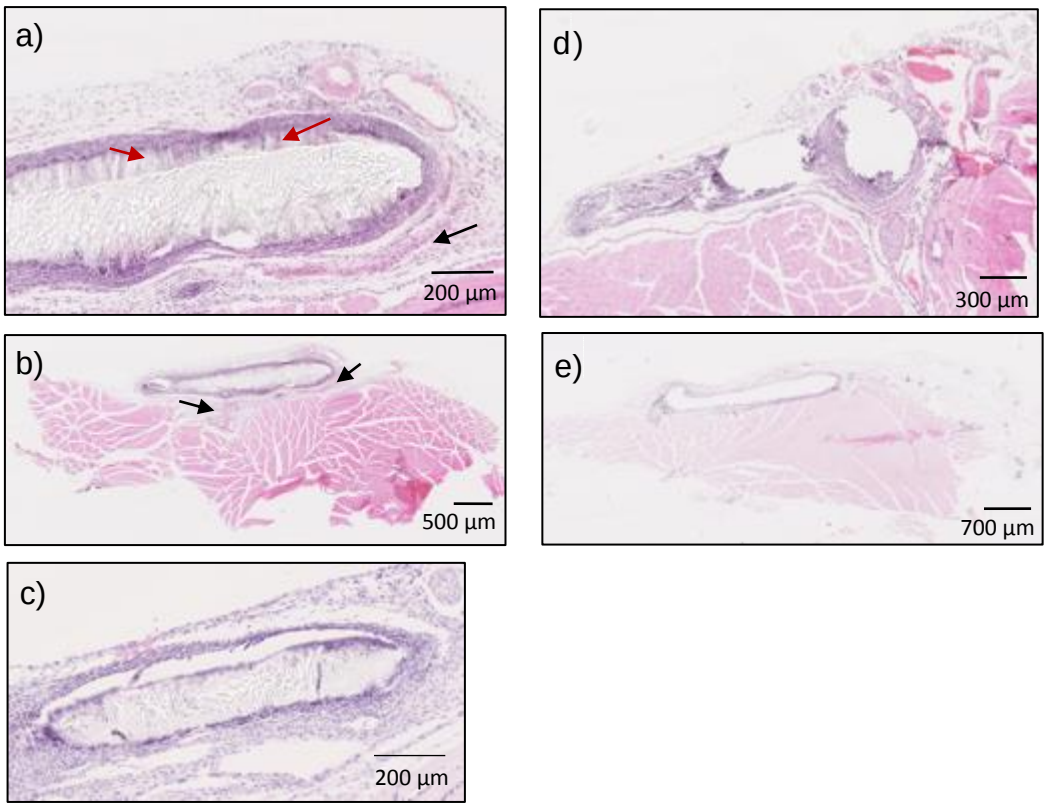

Figure 6.5: H&E staining of tissue sections showing the implantation of a-c) PLGA TIPS polymer films and d-e) PLGA control polymer films into the hindlimb ischaemia model. Red arrows indicate infiltration of cells into the surface of the 7507 TIPS polymer film implant. Black arrows indicate evidence of blood vessel formation around the 7507 TIPS implant.

implant, as indicated in image 6.5a and 6.5b in black arrows. The evidence of blood vessels was investigated further using immunohistochemistry staining for von Willebrand factor (VWF). Positive VWF staining can be seen around 7507 TIPS polymer film implant, as well as around the 7507 control, indicated by black arrows. The presence of more blood vessels seen around the TIPS implant may account for the increased reperfusion seen in the laser doppler imaging and quantification (Figure 6.4).

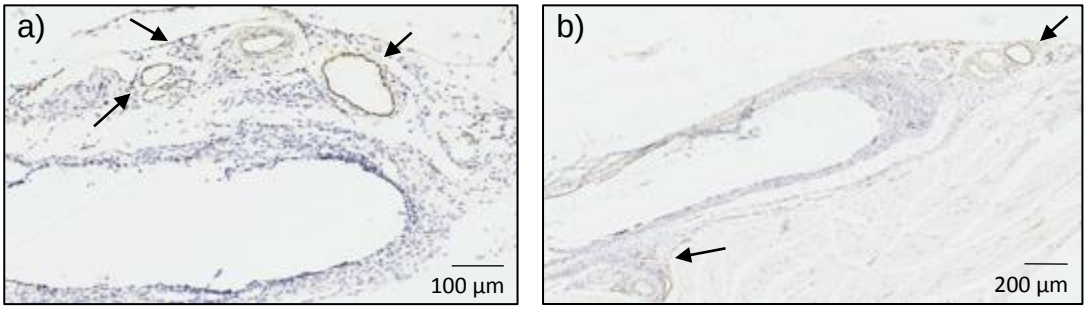

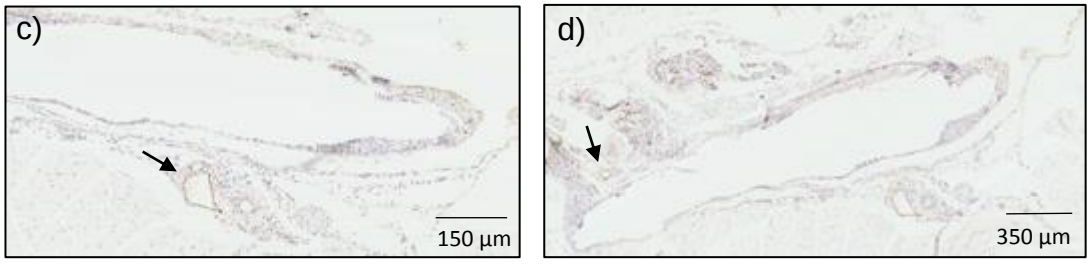

Figure 6.6: VWF staining of tissue sections showing the implantation of a-b) PLGA TIPS polymer films and c-d) PLGA control polymer films into the hindlimb ischaemia model. Black arrows highlight positive staining and indicate evidence of blood vessel formation.

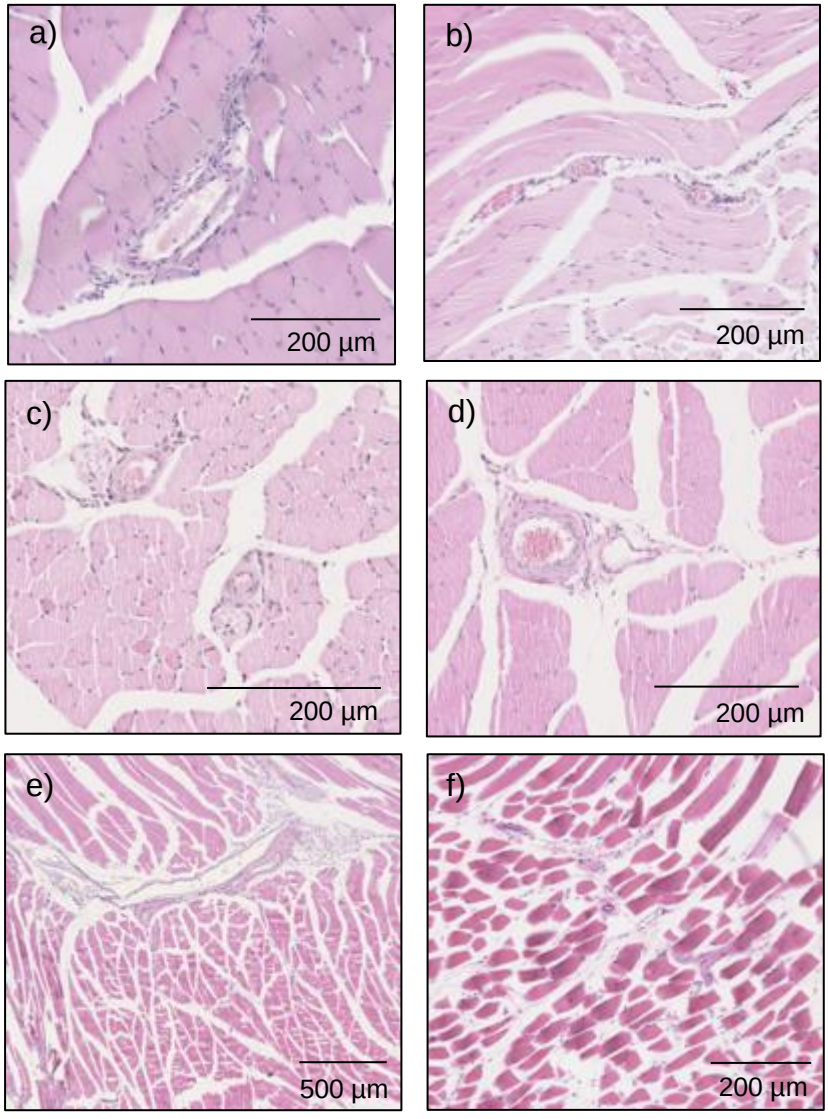

Figure 6.7: H&E tissue sections showing collateral blood vessels within the gastrocnemius muscle a-b) 7507 TIPS polymer film implantation c-d) 7507 PLGA control polymer film implantation e) no treatment control f) no ischaemia and no treatment control.

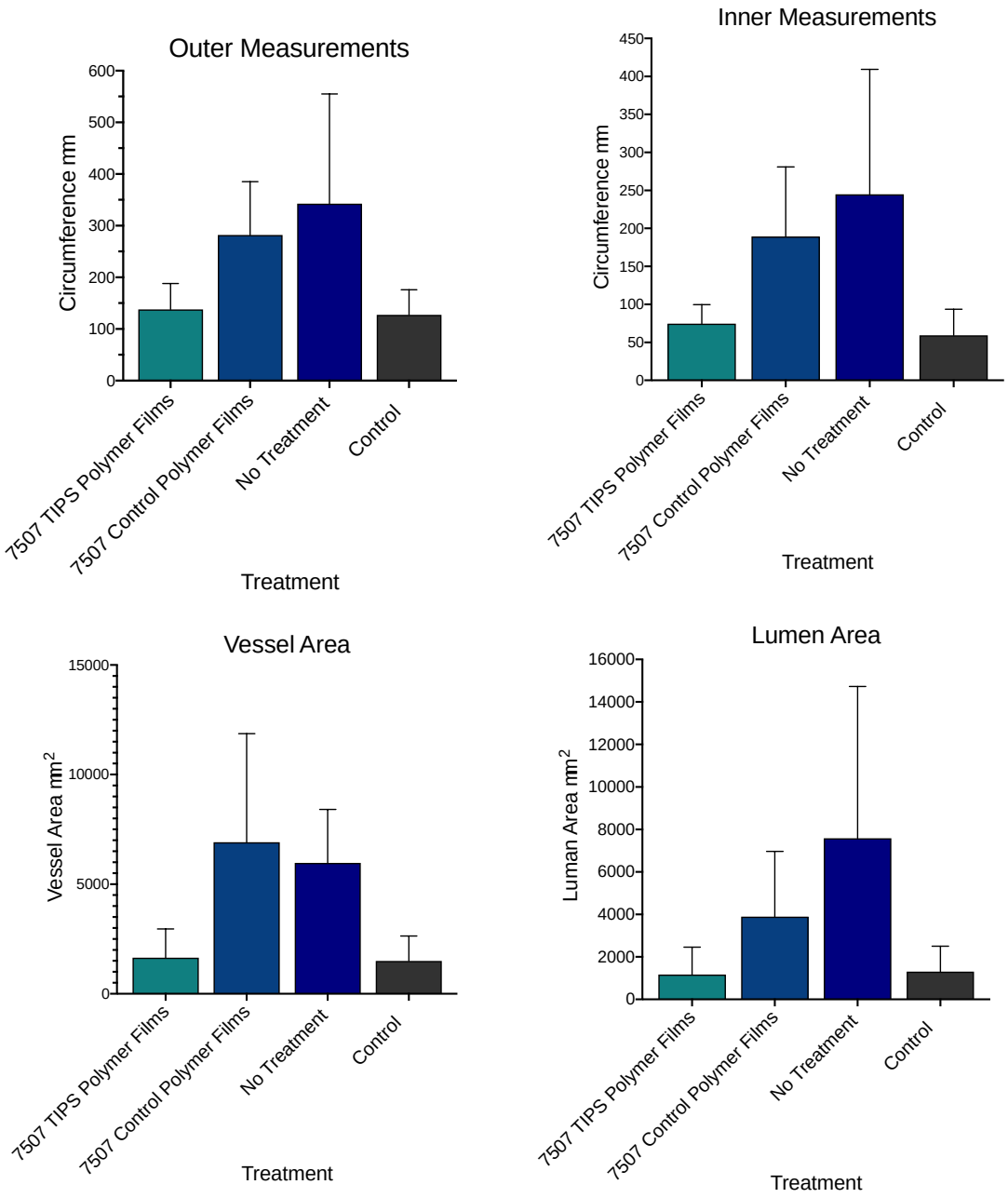

Figure 6.8: Quantification of collaterals found through H&E staining a) outer vessel circumference measurements (µm) Ordinary One-Way ANOVA = **** (P=0.0004) b) lumen circumference measurements (µm) Ordinary One-Way ANOVA = ** (P=0.0034) c) vessel area (µm^2) Ordinary One-Way ANOVA = **** (P=0.0002) d) lumen area (µm^2). (n=5)

H&E stained sections were also examined for evidence of arteriogenesis. This was achieved by identifying collateral blood vessel formation in the gastrocnemius muscle and quantifying the vessel area, lumen area and vessel area/lumen area. Figure 6.7 shows images of representative collaterals and Figure 6.8 shows the quantification of blood vessel measurements from limbs treated with TIPS polymer films had significantly smaller collateral vessel size compared with PLGA polymer films and no treatment controls. There was a

significant difference in both the vessel area and lumen area between ischemic limbs with no treatment and non-ischemic controls. There was no significant difference in vessel area and circumference measurements between TIPS polymer films and non-ischemic controls vessels (n=3). Results show that ischemic limbs with no treatment had significantly larger collateral vessel size and lumen size.

6.3.4 Analysis of In Vivo Gene Expression

Samples that had undergone ischemic surgery and treated with TIPS polymer films were analysed for the expression of VEGF-A, FGF2, PDGFRA, PEDF and NRP1. In order to extract RNA, 30 mg of tissue (stored in RNAlater) from around the occluded vessel was harvested. RNA was extracted using Qiagen RNeasy Mini Kit. RNA concentration and quality were measured using Nanodrop spectrophotometer. Unfortunately, the levels and quality of the RNA was very poor, as indicated by 260/280 and 260/230 ratios, therefore an alternative method had to be adopted. Monarch Total RNA MiniPrep kit was used as it contained an additional gDNA removal and RNA protection step. With this method, RNA was successfully extracted and qPCR performed. The results were normalised to the reference gene (Actin) and show (Figure 6.9) that were no significant differences in gene expression between groups. These experiments require further optimisation and protocol development.

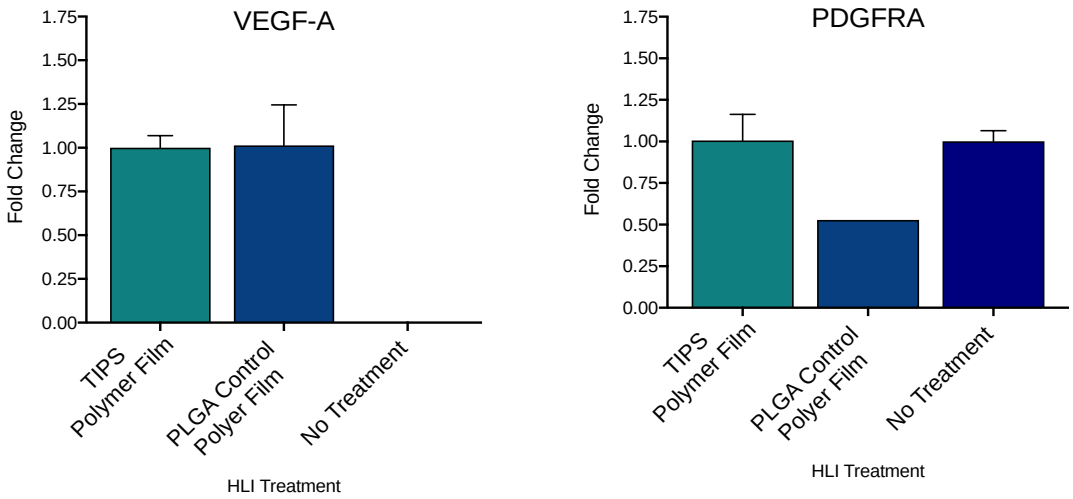

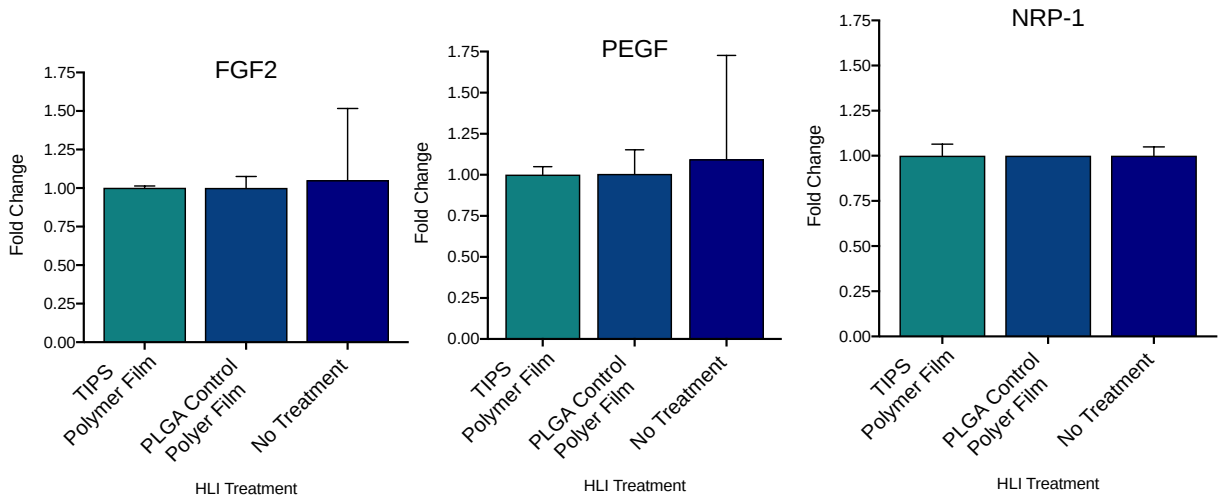

Figure 6.9: Quantification of VEGF-A, PDGFA, PEGF, FGF2 and NRP-1 expression from qPCR (n=1).

A Qiagen RT^2 array was used to screen 84 genes associated with angiogenic growth factors. Murine hindlimbs treated with 7507 TIPS and control polymer films were prepared as described in 6.2.3. Results are displayed in Figure 6.10 as a heat map of genes with a 10% increase/decrease in expression compared to reference genes plotted. In addition, the results are shown as pro-angiogenic genes (green heat map) and anti-angiogenic factors (red heat map). The results show that there were differences between the expression profiles between TIPS and control samples. For example, 7507 TIPS had higher expression of VEGFA, Rasa1, Angpt1/4, FGF2, to name a few.

The most significant difference found was the expression of Wars2. There are also differences between the expression of anti-angiogenic factors including Angptl1, Cga, Col4a3, Ifnb1, Timp3/4 and Amot. String analysis of factors promoted on TIPS polymer films compared to control polymer films showed connections to several biological processes including regulation of vascular development (7 genes, 1.8e-06 FD), blood vessel development (8 genes, 3.4e-06 FD), vascular development (8 genes, 4.27e-06 FD) and cardiovascular system development (9 genes, 5e-06 FD).

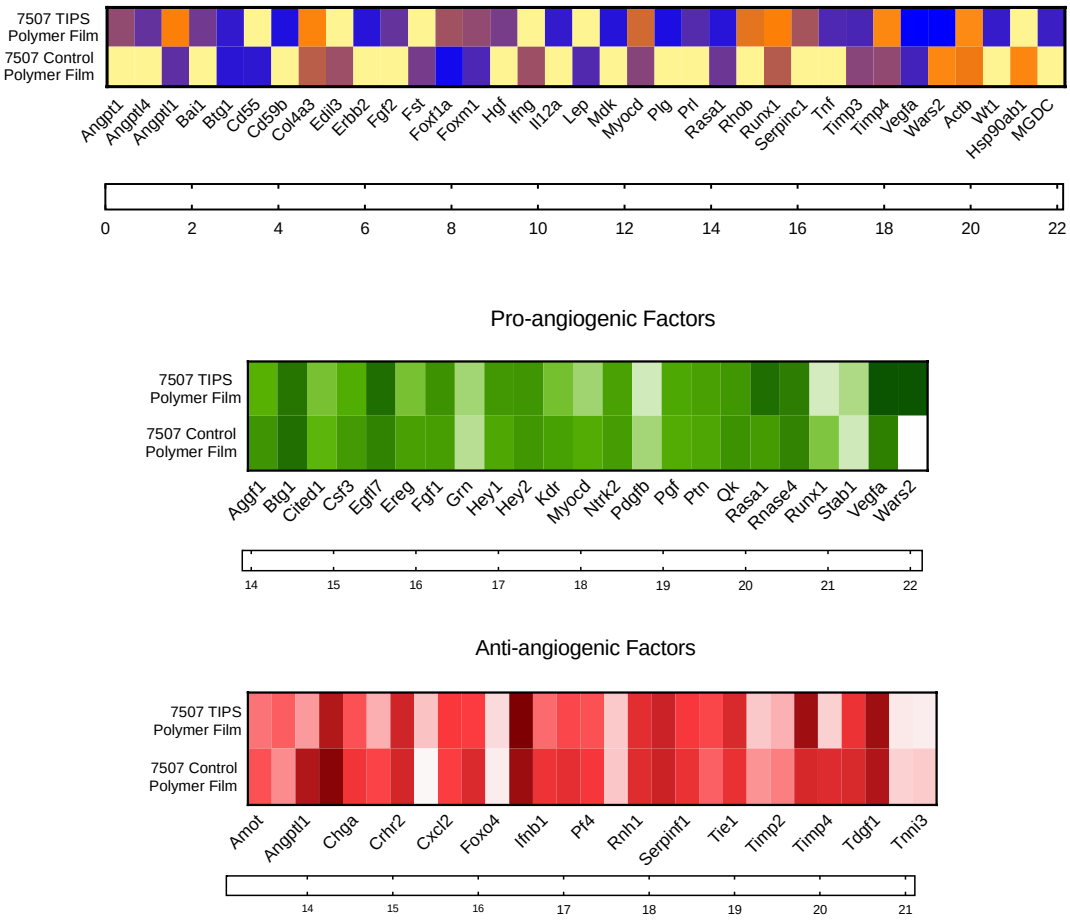

Figure 6.10: a) A heat map to show the expression of angiogenic growth factor genes from ischemic tissues implanted with 7507 TIPS polymer film and 7507 control polymer film b) a heat map to show the pro-angiogenic factor genes from 7507 TIPS polymer film and 7507 control polymer film groups c) a heat map to show the anti-angiogenic genes from ischemic tissues implanted with 7507 TIPS polymer film and 7507 control films (n=1).

6.4 Discussion

The hindlimb ischaemia model has been established as a useful pre-clinical model to investigate potential therapies for PAD. [66, 71, 91, 146, 334-337, 342, 344] There are multiple procedures that induce hindlimb ischaemia and the method of induction is dependent on factors including, the animal age, gender, strain, and the treatment investigated. For the purpose of this study mice were chosen due to their small size that contributed to their low cost of housing, smaller quantities of expensive materials/therapeutics required and fast surgery (and recovery from surgery) times. Mice were also chosen throughout the pre-clinical studies as species to species variability can also affect the outcomes of studies, as species will vary in blood vessel structure, vessel formation and collateral presence. Water *et al.*, 2004, reported on the differences between species collateral vascular networks, with mice more closely resembling human anatomy compared with rats. [351] The use of mice also opens up further investigative potential due to their ability to be genetically modified, which is especially useful for exploring genetic therapies. This also includes the possibility to study human cells/derived treatments on immunodeficient mice. [352] To date, the hindlimb ischaemia model continues to be the most studied method to study PAD. [334, 339, 342, 353-355] It has many advantages such as fast surgery times (approximately 30 minutes per mouse), low risk of complications, it is reproduceable, incorporation of therapeutics is possible (depending on the administration/therapy required) and ischaemia is induced immediately, as confirmed by laser doppler imaging (Figure 6.3). [334]

As with many *in vivo* models, there are discrepancies with the disease it replicates and the disease pathosis that cannot be accounted for. For example, PAD often develops because of atherosclerosis, fatty deposits forming in the arteries that block blood flow, [9] and is associated with generalised atherosclerosis and the development of other cardiovascular diseases. [15] This is extremely difficult to replicate in an *in vivo* setting, especially with small animal surgery. However, Madeddu *et al.*, 2006,

identified an alternative technique to the hindlimb ischaemia model via the induction of thrombus, or spontaneous plaque rupture, that was used to study atherosclerosis induced PAD. This was achieved with apolipoprotein E deficient mice on high cholesterol diets, thrombin injection, iron trichloride, adenovirus administration or mechanical disruption of the endothelial surface of the arteries. [353] Such techniques could be incorporated into pre-clinical experiments in the future to more accurately replicate PAD In an experimental setting.

Whilst it is important for models to be reproduceable in an experimental environment, it is not representative of how PAD would naturally present and progress, with each patient having differences in disease progression, severity and symptoms, which in turn are exacerbated by patient specific co-morbidities such as hypertension and diabetes. [340] The disadvantage of using murine models was the ability of the mice to naturally revascularise and heal after hindlimb ischaemia induction after three weeks, as shown in the no treatment control groups (Figures 6.1 and 6.3). [341] This limited the therapeutic window of therapies and made long-term studies infeasible. Therefore, the findings from the murine hindlimb ischaemia model should be taken as proof of concept, and aid the development of further pre-clinical and clinical studies. [356]

It was vital that the first surgeries that were undertaken were to assess the most appropriate method to induce ischaemia with the mice that were to be used for the implantation experiments. Two different methods of varying severity were used to induce ischaemia; unilateral femoral artery ligation and superficial femoral artery excision. Post-operative laser doppler images (Figure 6.1) revealed that unilateral artery ligation was successful in inducing hindlimb ischaemia but in contrast superficial artery excision did not cease blood flow to the paws. Despite the fact that this method has been established to be one of the most effective to inducing ischaemia, [357] in this case it was not severe enough for the c57/BL6 mice. The blood flow was most likely redirected into the deep femoral artery to allow the perfusion of the limb despite the excision of the artery. In contrast, the high ligature performed with

unilateral artery ligation avoided the redirection of blood flow and induced ischaemia immediately. With this method, revascularisation seen after 21 days which was in accordance with the established time-frame of the natural revascularisation of murine hindlimbs that have undergone ischemic surgery. [341] No necrosis was observed in any of the limbs and thus limb amputation was not necessary. For the purpose of this study, complete necrosis was not required as the proposed therapy would aim to induce angiogenesis before the patients PAD was so severe that amputation was required. In addition, it was also deemed unnecessarily severe as it would directly impact on the quality of life of the mice with a view to follow the guidance of 'the three R's' (replace, reduce, refine).

The implantation of acellular polymer films were first investigated due to the high numbers of variables that exist with a dual therapy (cells and biomaterials). These include cell dose, administration (e.g. intramuscular, systemic), optimal cell conditions (passage, *in vitro* culture time, seeding densities onto biomaterials etc.). TIPS 7507 polymer films were implanted into the hindlimb ischaemia model in order to assess how the materials behaved *in vivo* in terms of their ability to be implanted and remain at the implant site, their degradation behaviour and the host response to the materials. 7507 TIPS and control films were prepared and were imaged under SEM (Figure 6.2). Images displayed that polymer films remained intact after cutting into 5mm disks and hydrophilisation. Quantification of laser doppler imaging (Figure 6.4) revealed that there was a significant difference in the reperfusion rate of the mice treated with the 7507 TIPS polymer films. After 14 and 21 days, the mice treated with the 7507 TIPS polymer films had much higher reperfusion rates, where the 7507 control film groups did not differ from the no treatment control, which after 21 days had not improvement in perfusion ratios from day 7. Doppler is a well-established method to assess reperfusion of ischemic limbs, [341, 358] however, factors such as anaesthesia, temperature, oxygenation, hair (that attenuates the doppler signal) can influence results. [359] Therefore, to investigate the reperfusion response further, the tissues were harvested and processed through histological analysis. Sectioning and H&E staining revealed that the polymer films had successfully remained at the implant site

after 21 days, without the use of a fixative or sutures. However prolonged studies investigating the full degradation of the polymer films are required to fully understand how the material degrades, the lifetime of the implant and the *in vivo* response to the degration. There was also evidence of cellular infiltration within the implant, that would have aided in its ability to remain at the implant site. Sections of the control polymer film were obtained, but were not as intact as the TIPS films, which may be an artefact of the sectioning procedure (that can tear the material) or elude to the weaker structural integrity of the control film compared with the TIPS polymer film. This could account for the difference in response seen from the TIPS and control materials, as materials that have improved mechanical integrity can support the host tissue, which in turn can improve regeneration. [360]

H&E staining is a well-established staining technique that is often the first stain used to identify cells, tissues and diseases due to its reliability, ability to be used with multiple different tissues and fixatives. [350] Blood vessel formation can be identified through H&E staining, with Kim *et al.*, 2015, used H&E staining to identify blood vessels within tissue sections. [361] Clustering of cells stained positive for eosin around the TIPS processed implants suggest the formation of blood vessels (Figure 6.5), however staining for specific cell types such as endothelial cells is a more conventional method for identifying blood vessels. CD31/PECAM is one of the most common used immunohistochemical stains, it is specifically used to stain for endothelial cells, and thus for blood vessel formation. CD31 is a cell adhesion molecule found on endothelial cell intracellular junctions, as well as inflammatory cells and plasma cells. [362] After optimisation, anti-CD31 had positively stained the lumen of blood vessels in control slides. Despite attempts to optimise the protocol through antigen retrieval methods, quenching endogenous peroxidase activity, incubation times and varying the concentration of the primary antibody, the staining was unsuccessful when applied to sections of interest. Therefore, an alternative stain was investigated. Von Willebrand factor (VWF) is synthesised in endothelial cells and is therefore present in the plasma and Weibel Palade bodies of endothelial cells, it is also found in the matrix of blood vessel walls and therefore is a tool for investigating blood

vessel formation. [362, 363] Figure 6.6 shows positive VWF staining indicating the formation of blood vessels around the implant, suggesting that TIPS films promoted blood vessel formation in comparison to smooth controls. Likely through the integration to the host tissue, facilitated by the rough topography and interconnected porous structure of the TIPS materials. To further evaluate the VWF staining, the number of capillaries can be quantified as a ratio of capillary density to myofibers. This quantification between treated groups could account for the differences in reperfusion rates seen between the ischemic limbs, as an increase in capillary to muscle fibres would allow an increase in blood perfusion of the muscle. [364] Higher capillary to myofiber ratios have been linked to an increase in angiogenesis and reperfusion of ischemic limbs in pre-clinical and clinical studies. [365-367]

There are several biological processes that result in the formation of blood vessels. Vasculogenesis only occurs in embryonic development and results in the formation of the vascular network from *de novo* production of endothelial cells. [368, 369] Angiogenesis is the formation of capillaries from pre-existing vessels and occurs in ischemic or hypoxic conditions. Arteriogenesis is the formation and enlargement of arteries from pre-existing arterioles. Arteriogenesis can cause the revascularisation of a limb through increasing blood flow to collateral arteries without angiogenesis occurring, and occurs when there is an increase in shear stress. [369, 370] Limbourg *et al.*, 2009, reported that both arteriogenesis and angiogenesis are vital for the reperfusion of ischemic tissue and that arteriogenesis can be evaluated from the morphological assessment of collateral arteries in smooth muscle. [369] Angiogenesis can be quantified through many methods including quantifying the number of capillaries in the gastrocnemius muscle through immunohistochemical stains as well as observing muscle perfusion and vasodilation through angiography. [369, 371-373]

Preliminary work investigating the extent of arteriogenesis [374] shown in Figures 6.7 and 6.8 indicated that TIPS polymer films had smaller vessel and

lumen diameters compared with controls. This suggested that the implantation of control polymers resulted in an increase in arteriogenesis in comparison to TIPS PLGA implants. When taking into account that the implantation of 7507 TIPS polymer films resulted in an increase in reperfusion of the treated ischemic limb, and the positive VWF staining, it could be proffered that reperfusion in ischemic limbs treated with 7507 TIPS polymer films was not due to arteriogenesis, but angiogenesis. Conversely, these results suggest that the slight reperfusion seen after 21 days in control limbs is due to arteriogenesis. However, to fully assess arteriogenesis blood vessels should be perfused with a vasodilation solution to avoid collapse [369, 375] and the number of arterioles would need to be calculated, where arterioles can be identified through smooth muscle actin staining. [376]

To measure vasodilation further surgery is often required, with stimulating probes implanted to stimulate the gracilis anterior muscle. Blood flow and pressure can be measured, as well as profunda diameters from subsequent imaging. [373, 377] High resolution ultrasound can also be used to measure real-time vasodilation, most commonly after the addition of a stimulus. [378, 379] Vasodilation most commonly occurs due to an increase in nitric oxide. Nitric oxide has been shown to have roles in both arteriogenesis and angiogenesis by increasing capillary formation and endothelial cell migration. [380] It has been shown that nitric oxide is present within ischemic hindlimbs 14 days after surgery and could contribute to increases in reperfusion and blood flow seen within this time frame. [381-383] Davis *et al.*, 2004, hypothesised that the stress the endothelial cells within the blood vessels are exposed to through hindlimb ischaemia surgery causes an increase in nitric oxide production through an increase in mRNA expression from binding of nuclear factor kappa B to a endothelial nitric oxide promotor region. [384] To assess if vasodilation effects the increase in reperfusion seen with the implantation of TIPS-processed materials, further assessment of mice would be required through imaging so not to subject the mice to further surgeries, which in itself may affect *in vivo* responses observed through causing inflammation.

To analyse the gene expression from tissues qPCR was used. qPCR is a sensitive and precise method to quantify nucleic acids through the amplification and detection of DNA targets. [385] It was utilised to analyse the expression of VEGF-A, PEDF, NRP-1. PDGFRA and FGF2, which were chosen as they are not only key angiogenic proteins but also were highlighted in the proteome profiler array in Part I. Chapter 4. RNA quality and quantity were assessed through Nanodrop UV spectrophotometer readings. The Nanodrop analysed samples by measuring surface tension and fibre optics. [386] Samples were exposed to UV light at 260 nm, as this is the average wavelength that successfully penetrates DNA and RNA. The UV light is absorbed by the RNA and using Beer-Lambert law the absorbed light is related to the absorbance rate, and thus the concentration of RNA within a sample. Quality of RNA was given as absorbance ratios of 260/230 and 260/280. [387, 388] For pure RNA both 260/280 and 260/230 ratios should be between 1.8-2.2. There are many reasons why samples would produce impure ratios. Low 260/230 ratios could be cause by DNA, phenol (from extraction) or carbohydrate contamination of the sample, buffer carryover, inefficient degradation of RNA or insufficient precipitation with ethanol. Low 260/280 ratios often indicate the sample is contaminated with proteins or phenol. In addition, pH can affect ratios, with extremes in pH causing degradation of molecular bonds and thus the destruction of RNA/DNA. [389, 390] The RNeasy mini kit was not successful, producing low quantities of RNA and impure ratios. Therefore, an alternative kit (Monarch total RNA mini prep kit) was used that involved an additional DNA removal step. This resulted in purer RNA ratios and an overall higher yield of RNA. Primers for qPCR were designed as described in Section 6.2.5.3 No definitive conclusions could be drawn from qPCR results as unfortunately, due to time constraints as well as a limited number of samples resulted in replica qPCR experiments infeasible. Ideally the qPCR would be optimised, and further testing performed. Optimisation would be achieved through determining optimal primer concentrations, RNA concentrations, formation of a standard curve, optimal annealing temperature determined and testing the primers for purity and primer-dimer potential with gel electrophoresis and SYBR Green I analysis. [391, 392]

The angiogenesis growth factor array from Qiagen was able to detect 86 genes related to angiogenic growth factors. Due to the high cost of each array, only two groups were able to be assessed. RNA extracted from 7507 TIPS polymer films were chosen due to the significant increase in reperfusion ratio seen from laser doppler imaging in Figure 6.4 and compared to 7507 control polymer film implantations, with a view to highlight any possible differences the implantation of TIPS-processed materials had to control smooth materials on the expression of angiogenic-related genes. STRING analysis of genes promoted from the TIPS polymer film group (Figure 6.10) showed links to multiple biological processes including blood vessel development, vascular development and cardiovascular system development with Wars2 associated in all three processes, which was the gene with the most significant difference in expression found with a high expression from 7507 TIPS polymer films compared with 7507 control polymer film. Wars2 or mitochondrial tryptophanyl-tRNA synthetase is implicated in angiogenesis through responding to TNF-α and VEGF. Wars2 promotes endothelial cell migration, proliferation and capillary formation and the inhibition in zebrafish results in diminished heart function and vessel deformities. [393-395] Further analysis into the implications of Wars2 on the promotion of angiogenesis in a preclinical model of angiogenesis treated with the implantation of TIPS-processed materials is required.

The premise for the presented work was to perform a proof of concept study with the view to implant cellularised constructs into the hindlimb ischaemia model to further evaluate the angiogenic effects of ADMSCs and TIPS PLGA polymer films. The unique surface topography and structure of TIPS polymer films had shown a pro-angiogenic response without the addition of biological agents or cells. As such, acellular polymer films were evaluated further with qPCR techniques, and the administration of injectable acellular 3D TIPS microparticles was explored in Part II. Chapter 5.

6.5 Summary

Pilot studies investigating the effect of TIPS-processed polymer films *in vivo* were investigated. Evaluation of laser doppler imaging determined that the implantation of PLGA 7507 TIPS polymer films into a preclinical model of PAD increased the reperfusion of the ischemic limb after 21 days compared with controls. Histological analysis revealed that the polymer films remained at the implant site, indicating that future studies involving the implantation of cellularised constructs, the cells should be able to remain at the implant site and have their therapeutic effect.

Preliminary studies into evaluating the extent of arteriogenesis had shown that there was more evidence of arteriogenesis with control groups compared with TIPS-processed substrates, indicating that the increase in revascularisation seen within the TIPS treated groups was from the formation of capillaries through angiogenesis.

The implantation of TIPS polymer films into the hindlimb ischaemia model was analysed further through angiogenic growth factor gene expression compared with the control PLGA film implantation. Analysis of genes promoted from the TIPS polymer film group highlighted links to multiple biological processes including blood vessel development, vascular development and cardiovascular system development.

The unique surface topography and structure of acellular TIPS based PLGA biomaterials could not only provide support to the host tissue but also facilitate native cell infiltration, recruitment of cells, and thus the activation of pathways that result in capillary formation and illicit a pro-angiogenic response without the addition of biological agents or cells through the host tissue response to the nano and micro surface characteristics. These findings open up the possibility of utilising unique TIPS-processed biomaterials for the treatment of PAD.

Part I.

Chapter 7: Investigation of a Putative Biological Mechanism Responsible for the *In Vivo* Pro-Angiogenic Effect of Acellular TIPS Polymer Films

7.1 Introduction

7.1.1 The Immune Response to Biomaterials

It is well established that implantation of a material or foreign object into the body will result in a host immune response. [396] The need to investigate the immune response of biomaterials stems from the adverse effects it can cause, from pain to tissue destruction to complete failure of an implant. [397]

When a material or device is introduced in the body, the injury caused results in the initiation of the coagulation cascade where proteins in the blood and ECM absorb onto the surface of the biomaterial, that in turn activates an innate immune response. The innate immune response is governed largely by neutrophils, mast cells and monocytes, that migrate to the injury site and secrete inflammatory cytokines including tumour necrosis factor (TNF-α), interferon (INF)-γ, interleukin (IL)-4/-8/-13/-16 and monocyte chemoattractant protein-1 (MCP-1). This response is acute, lasting from hours to days. If this response persists, chronic inflammation develops. The chronic immune response is dictated by macrophages. Monocytes at the injury site differentiate into macrophages and circulating macrophages are recruited to the site due to the prolonged expression of TNF-α, IL-4 and IL-13. Macrophages attach onto the surface of the implant (as they are unable to phagocytose the material) and fuse to form foreign body giant cells. From this, the inflammation

can be resolved or the foreign body giant cells deposit matrix proteins that encapsulates the material and forms granulation tissue. The extent of the acute and chronic inflammatory response is dependent on the implant or injury, with a biomaterial reaction usually lasting two to three weeks. If the reaction persists, fibrous capsule formation occurs that can lead to the failure of the implant or infection. Opportunities exist to control this response via the polarisation of macrophages. [396-403]

Macrophages polarise into two distinct phenotypes depending on the cytokines and growth factors present. It has been shown that the type of macrophage influences the remodelling of the tissue surrounding the implant. Classically activated or type 1 macrophages (M1) result in tissue fibrosis and alternatively activated or type 2 macrophages (M2) result in tissue regeneration. [397] M1 macrophages are considered to be pro-inflammatory and are activated by lipopolysaccharides (LPS), INF-γ, TNF-α and granulocyte macrophage colony-stimulating factor (GM-CSF). [404] M1 macrophages secrete pro-inflammatory cytokines including IL-1/-6/-8/-12/-23 which drive the inflammatory response and ultimately result in fibrous scar tissue formation or infection. Polarisation into M2 macrophages occurs in the presence of IL-4/-10/-13, macrophage colony stimulating factor (M-CSF) and adenosine. [404] M2 cells can resolve the foreign body reaction by secreting numerous pro-angiogenic growth factors including TGF-β, PDGF and VEGF that can recruit a host of cell types to induce wound healing and angiogenesis. [405, 406]

In response to a biomaterial, macrophages can accelerate the degradation of a biomaterial through the secretion of reactive oxygen species and acidic factors, which in turn can reduce the mechanical integrity of the material. [407] It is vital that the degradation rate of a material coincides with the rate of remodelling and ECM production in order for the implant to have its therapeutic effect. As the immune response has been shown to resolve with the elimination of the material, it is also important that an implant is not present for longer than needed.

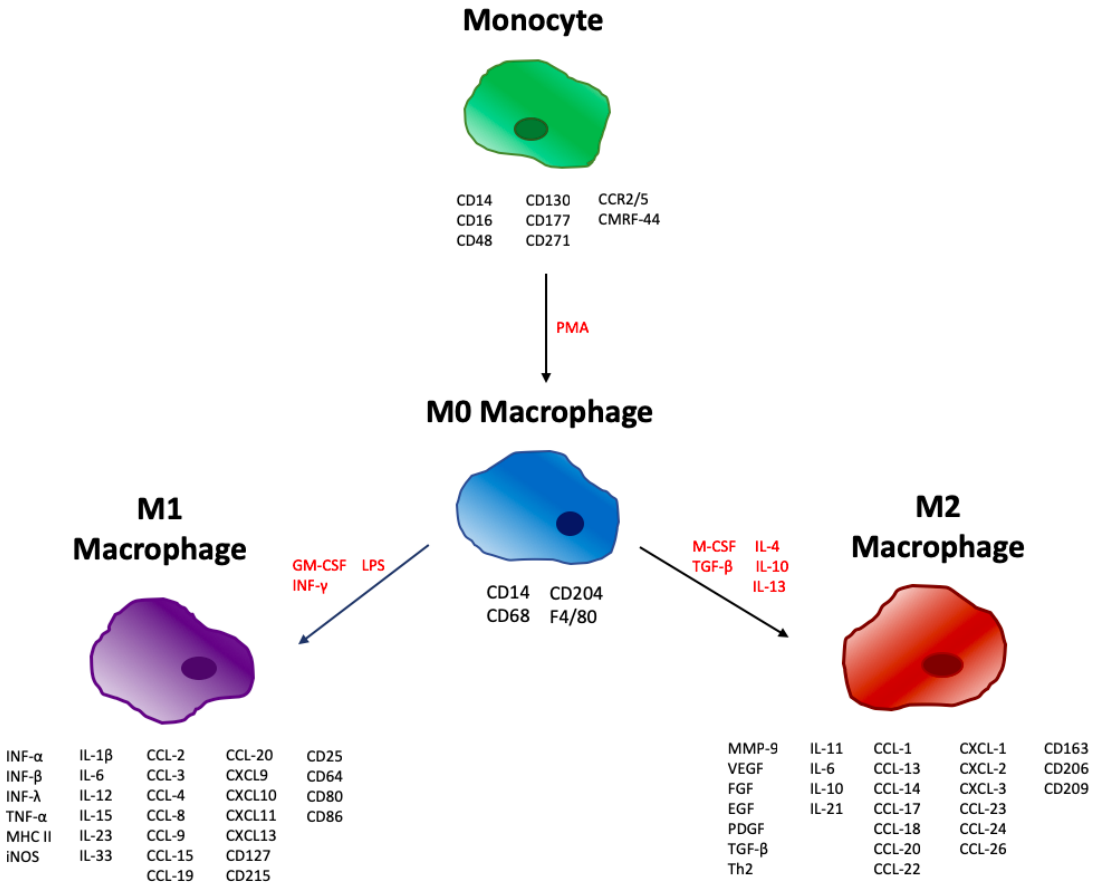

Figure 7.1: Schematic detailing the secretomes (black) and factors that induce differentiation (red) of monocytes, M0 macrophages, M1 macrophages and M2 macrophages.

As the immune response to a biomaterial can dictate its success or failure, many studies have focused on adapting materials to modulate the immune reaction. Physical properties of a material including its hydrophobicity and surface chemistry can influence the immune response through the initial absorption of proteins on the surface. [396, 402] Yu *et al*., 2011, demonstrated that modifying materials with polyethylene glycol to produce more hydrophilic surfaces resulted in less protein adsorption and less successful attachment of macrophages to the materials and thus a reduced immune response. [408] Substrate stiffness can regulate macrophage polarisation where surfaces with high stiffnesses have been shown to increase pro-inflammatory M1 behaviour. [409-411]

The surface topography of a material has also been shown to influence immune cell activation and cytokine secretion through cell attachment and

morphology. The influence of micro and nano surface features on biomaterials on macrophages has been widely studied. [412-414] For example, Chen *et al.*, 2010, reported that surface gratings in the micro range resulted in a reduced inflammatory response compared to nano sized features or smooth control surfaces. [415] Furthermore, Waterfield *et al.*, 2010, found that when macrophages attached to materials with different surface topographies, different pathways were activated. Where the NFkB pathway (that regulates the immune response) was more highly activated from cells attached to smoother surfaces. [416]

7.1.2 Macrophages and Angiogenesis

Macrophages play numerous roles angiogenesis. M2 macrophages secrete the pro-angiogenic factors; IL-8, bFGF, PDGF and VEGF. [405, 406] Jetten *et al.*, 2014, found that M2 macrophages increased *in vitro* angiogenesis through increased expression of FGF2, insulin-like growth factor-1 and chemokine ligand 2 and *in vivo* angiogenesis through increased endothelial cell recruitment. [417] M2 macrophages also secrete matrix metalloproteinases (MMPs). Within angiogenesis, MMPs contribute to the degradation and remodelling of the basement membrane, aid pericyte and endothelial cell recruitment. [418] The role of M1 macrophages are predominately pro-inflammatory and work to eliminate foreign bodies from the body through the secretion of reactive oxygen species and nitric oxide. [419] However, nitric oxide has been shown to initiate angiogenesis in hypoxic environments through the stimulation of HIF-1a, VEGF and the regulation of endothelial cells. [420] Therefore the presence of M1 cells at the implant site can in turn lead to the promotion of angiogenesis.

These findings open up the possibility of utilising the *in vivo* macrophage response to biomaterials to promote angiogenesis. Hence, studies into the immune response of TIPS-processed materials were performed through the examination of *in vivo* implanted acellular TIPS polymer films and the examination of the *in vitro* response to M0/M1/M2 macrophages.

7.2 Methods

7.2.1 Histological Analysis of Tissue Sections

Hindlimb ischaemia was induced in c57/bl6 mice and implanted with TIPS-processed polymer films as described in Part I. Section 6.3.1. Tissues were processed and H&E stained as described in Part I. Section 6.2.3.2.

Slides were stained for M2 macrophages with anti-CD163 (ab182422, Abcam, UK) at a dilution of 1:500 in PBS (P5493-1L, Sigma, UK) and M1 macrophages with anti-CD80 (ab64116, Abcam, UK) at a dilution of 1:50 in PBS with VECTASTAIN Elite ABC HRP kit (Peroxidase Rabbit IgG) (PK-6101, Vector Laboratories, UK) following the immunohistochemistry protocol outlined in Part I. Section 6.2.3.4.

7.2.2 THP-1 Cell Culture

Complete RPMI-1640 media (R5886, Sigma, UK) with HEPES modification was prepared with the addition of sodium pyruvate (S8636, Sigma, UK), 0.05 mM 2-Mercaptoethanol (ES-007-E, Sigma, UK), 1 mM pyruvate (S8636, Sigma, UK), 200 nM L-glutamine (G7513, Sigma, UK) and 10% fetal bovine serum (heat inactivated, E.U. approved, south American origin, 10500064, Life Technologies, UK). Human monocytic THP-1 cells at passage 3 were rapidly thawed in a 37^{o}C water bath and cultured in 20 mL of complete RPMI-1640 media in suspension for 1 week in an incubator at 37^{o}C and 5% CO_2. Cells were passaged up to P10 and re-seeded at a density of $4x10^5$ cells/mL.

7.2.3 Differentiation of THP-1 Cells into Macrophages

To differentiate the THP-1 cells into macrophages (M0), $4x10^5$ cells/mL cells were incubated with 150 nM (1mg/mL) phorbol 12-myristate 13-acetate (PMA, P8139, Sigma, UK) for 24 hours in complete RPMI-1640 medium at 37^{o}C/5% CO_2. Cells were then incubated in RPMI-1640 complete medium for 48-72 hours at 37^{o}C/5% CO_2.

7.2.4 Differentiation of Macrophages into Classical Macrophage Type 1 Phenotype

To differentiate M0 to classical type 1 macrophages (M1), $4x10^5$ cells/mL M0 cells were incubated with 20 ng/mL recombinant human IFN-γ (300-02, Peprotech, UK) and 10 pg/mL LPS (L2630, Sigma, UK) in 15 mL of complete RPMI-1640 medium and incubated at 37°C and 5% CO_2 for 48 hours.

7.2.5 Differentiation of Macrophages into Alternative Macrophage Type 2 Phenotype

To differentiate M0 to alternative type 2 macrophages (M2), $4x10^5$ cells/mL M0 cells were incubated with 20 ng/mL recombinant human IL-4 (200-04, Peprotech, UK) and 20 ng/mL recombinant human IL-13 (200-13, Peprotech, UK) in 15 mL of complete RPMI-1640 medium at 37°C/5% CO_2 for 48 hours.

7.2.6 Cellularising TIPS Polymer Films

M0, M1 and M2 cells were detached from T75 flasks through trypsinisation described in Part I. Section 2.2.7. 7507 PLGA TIPS films, 7507 PLGA control films, 7502 PLGA TIPS films, 7502 PLGA control films and polystyrene films were prepared as described in Part I. Section 2.2.2 and hydrophilised as in Part I. Section 2.2.8.

To evaluate the effect of polymer films on the behaviour of macrophages, polymer films were seeded with 1×10^6 M1 or M2 cells in 0.5 mL M1 or M2 differentiation medium in an ultra-low attachment 24 well plate (CLS3473, Corning, UK) (n=5). The supernatants were removed from each well at days 1, 4, 7 and 10, frozen and replenished with 0.5 mL fresh differentiation media.

To assess how the polymer films effected the differentiation of M0 cells, polymer films were seeded with 1×10^6 M0 cells in 0.5 mL in complete RMPI-1640 media and cultured for 24 hours in an ultra-low attachment 24 well plate (CLS3473, Corning, UK) (n=5). After 24 hours the media was removed and M1 or M2 media was added. The supernatants from each well were removed

at days 1, 4, 7 and 10, frozen and each well was replenished with 0.5 mL fresh differentiation media.

ADMSCs were cultured as described in Part I. Section 2.2.7. To investigate the effect of M1 and M2 supernatants from ADMSCs seeded polymer films, $1x10^6$ P6 ADMSCs in 0.5 mL MesenPRO^{TM} complete media was seeded onto polymer films in an ultra-low attachment 24 well plate (CLS3473, Corning, UK) and cultured for 24 hours (n=5). After 24 hours the MesenPro RS^{TM} media was removed and 0.5 mL supernatants of M1 or M2 cells was added. The supernatants from each well were removed at days 1, 4, 7 and 10, frozen and each well was replenished with 0.5 mL M1 or M2 supernatants.

7.2.7 Assessing Macrophage Behaviour on TIPS Polymer Films

Human Interleukin 12 (IL-12 p70) Enzyme-linked Immunosorbent Assay (ELISA) (DY293B, R&D Systems, UK) was used confirm M1 and M2 differentiation and the amount of IL-12 p70 released into the supernatants from cells seeded onto 7507 PLGA TIPS, 7507 PLGA control, 7502 PLGA TIPS, 7502 PLGA control and polystyrene polymer films (n=5).

The capture antibody was reconstituted to 480 μg/mL in 1X PBS (P5493-1L, Sigma, UK) and diluted to the working concentration of 4.0 μg/mL in 1X PBS. 100 μL was added to each well of a Nunc-Immuno MicroWell 96 well plate (M9410, Sigma, UK). Plates were sealed (DY992, R&D, UK) and incubated overnight at room temperature. Wash buffer was prepared as 0.05% Tween-20 (P1379, Sigma, UK) in 1X PBS (P5493-1L, Sigma, UK). Each well was washed with wash buffer three times and blotted to remove excess liquid. Reagent diluent was prepared as 1% bovine serum albumin (05482, Sigma, UK) in 1X PBS (P5493-1L, Sigma, UK) and 2% goats' serum (16210064, Gibco, NZ) and 0.2 μm filtered. Plates were blocked with 300 μL of reagent diluent for 2 hours at room temperature then washed. The IL-12 p70 standard was reconstituted to 400 ng/mL in reagent diluent and diluted to a working concentration of 2000 pg/mL. Serial dilutions were prepared up to 7.81 pg/mL. Samples were centrifuged and 100 μL were added to each well in triplicate, along with the standards and incubated at room temperature for 2 hours and

washed. The detection antibody was reconstituted to 6 μg/mL in reagent diluent and 2% heat activated normal goats' serum (16210064, Gibco, NZ) and diluted to the working concentration of 100 ng/mL. 100 μL of detection antibody was added to each well, incubated at room temperature for 2 hours and washed. The Streptavin- HRP was diluted at a ratio of 1:40 in reagent diluent and 100 μL was added to each well. The plate was protected from light, incubated for 20 minutes at room temperature and washed. The substrate solution was prepared by adding equal volumes of colour reagent A (H_2O_2) and colour reagent B (Tetramethylbenzidine) (DY994, R&D, UK) immediately before addition. 100 μL of the substrate solution was added to each well. The plate was protected from light, incubated for 20 minutes at room temperature and 50 μL of 2 N H_2SO_4 (339741, Sigma, UK) was added to each well to stop the reaction and further colour development. The plate was then immediately read using a microplate reader (Fisher Scientific, UK) at wavelength 450 nm with correction set to 540 nm.

$VEGF_{165}$ ELISA (DY293B, R&D Systems, UK) was used to determine the concentration of $VEGF_{165}$ in the supernatants from M0, M1, M2 and ADMSCs seeded onto 7507 PLGA TIPS, 7507 PLGA control, 7502 PLGA TIPS, 7502 PLGA control and polystyrene polymer films (n=5). The methodology was described in Part I. Section 5.2.2.1.

7.2.8 Screening for Cytokine Secretion from Adipose-Derived Mesenchymal Stem Cells Using Human Proteome Profiler Angiogenesis Array

Human Cytokine Array (ARY005B, R&D, UK) was carried out using the methodology described in Part I. Section 5.2.2.2 with cytokine array membrane (898260, ARY005B, R&D, UK) and a cytokine specific detection Antibody Cocktail (898261 ARY005B, R&D, UK).

7.2.9 Statistical Analysis

Statistical Analysis was performed as described in Part I. Section 2.2.11.

7.3 Results

7.3.1 Histological Analysis of Tissue Sections

Figure 7.2 shows H&E stained tissue sections from Part I. Chapter 6 where ischaemia was induced in the hindlimbs of c57bl/6 mice and implanted with 7507 TIPS polymer films. Black arrows indicate the formation of multinucleated giant cells at the surface of the TIPS film implant, arising from the fusion of macrophages. [421] In order to identify whether the cells were M1 phenotype, sections were stained using antibody directed against CD80 and to identify if the cells were M2 phenotype, anti-CD163 was used. Immunohistochemical staining (Figure 7.3) shows evidence of positive anti-CD163 staining around the 7507 TIPS polymer film implants. There was also evidence of positive anti-CD163 macrophage infiltration into the TIPS material as seen in Figure 7.3a. Staining for M1 macrophages with anti-CD80 showed no evidence of positive staining (Figure 7.4).

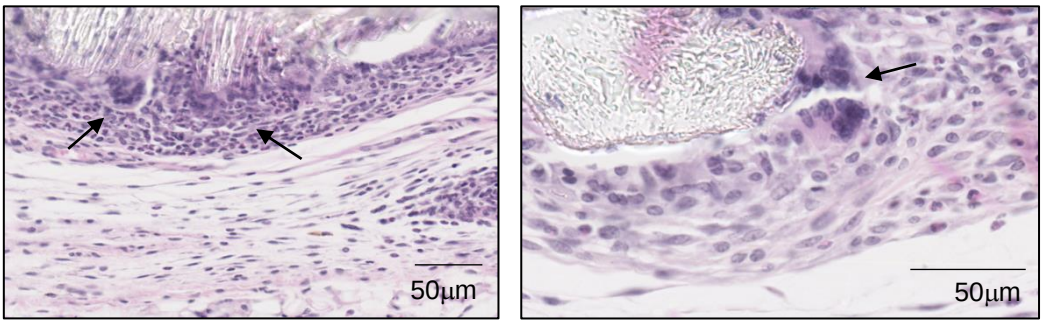

Figure 7.2: H&E staining tissue sections from 7507 TIPS Polymer Films implanted into a pre-clinical models of peripheral artery disease.

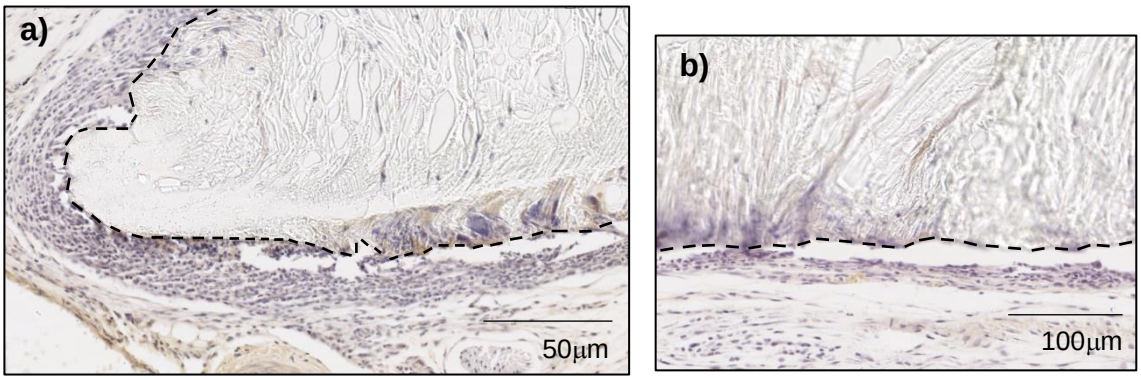

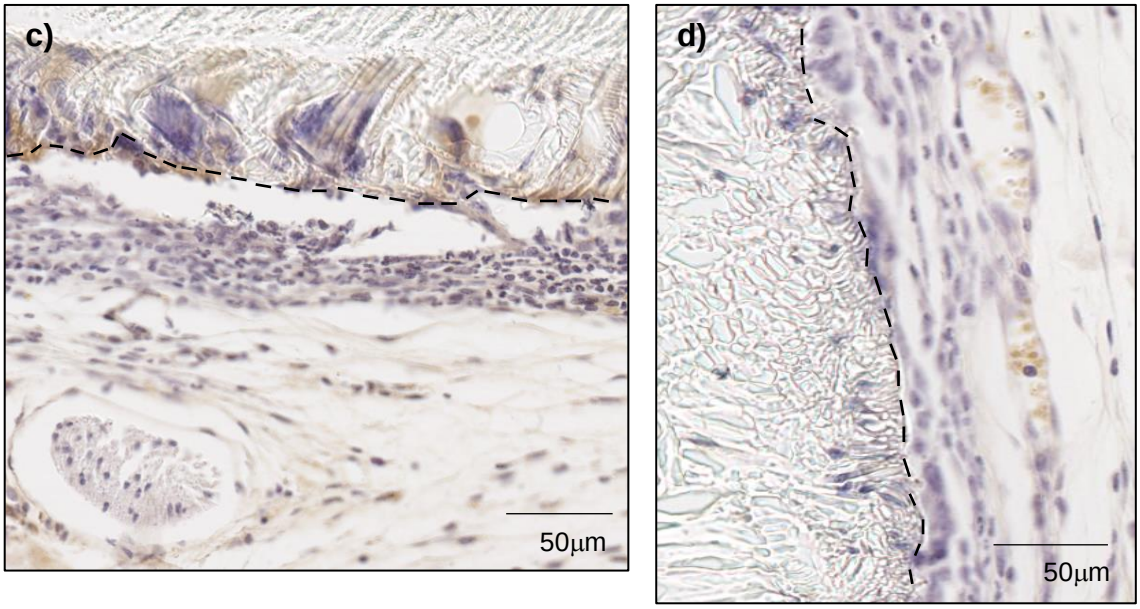

Figure 7.3: Anti-CD163 staining of 7507 TIPS Polymer Films into a pre-clinical models of peripheral artery disease. Dotted line indicates implant/tissue boundary.

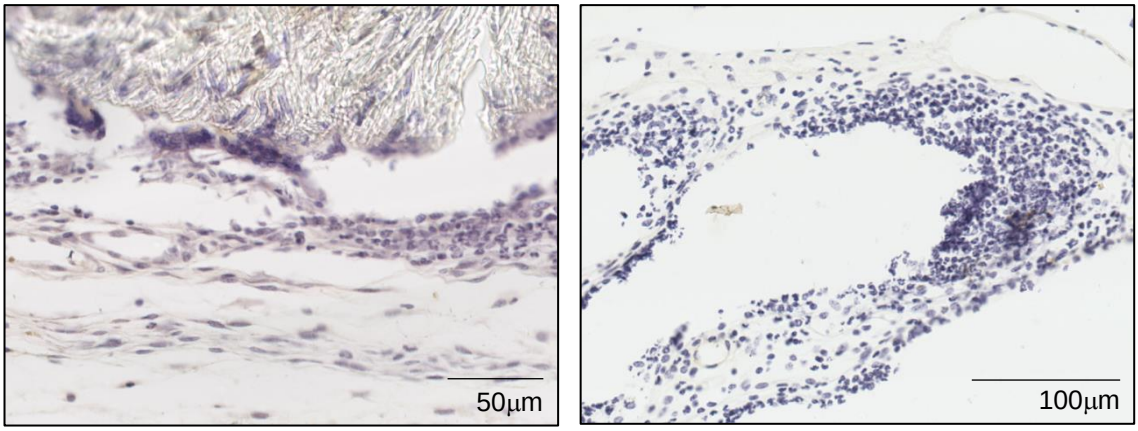

Figure 7.4: Anti-CD80 staining on 7507 TIPS Polymer Films into a pre-clinical models of peripheral artery disease.

7.3.2 Differentiation of THP-1 Cells into Macrophages

To ascertain if the differentiation of M0 macrophages into M1 and M2 macrophages was successful an IL-12 p70 ELISA was used as M1 macrophages express high levels of IL-12. Figure 7.5 revealed that M1 macrophages secreted significantly higher levels of IL-12 in comparison to M2 cells, confirming that the protocol established successfully differentiated M0 macrophages into M1 and M2 phenotypes.

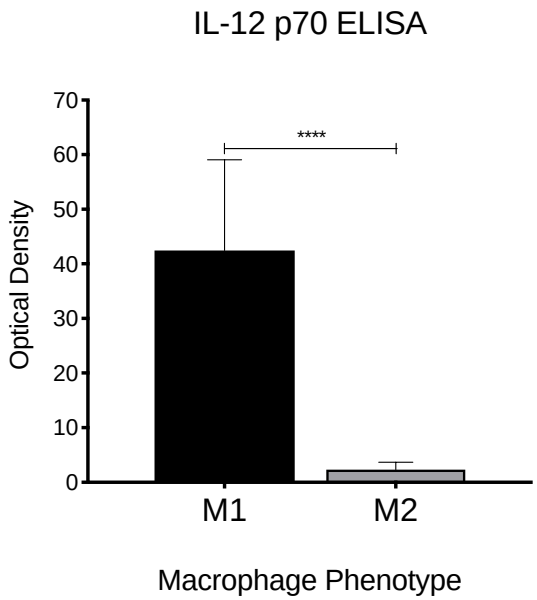

Figure 7.5 : IL-12 p70 ELISA from supernatants from M1 and M2 phenotype macrophages. (n=5) Where * = P<0.05, ** = P<0.01, *** = P<0.001 and **** = P<0.0001.

7.3.3. Assessing Macrophage Behaviour on TIPS Polymer Films

M0 macrophages were seeded on 7507 PLGA TIPS, 7507 PLGA control, 7502 PLGA TIPS, 7502 PLGA control and polystyrene films. The M0 cells were incubated either M1 or M2 macrophage differentiation medium to assess how the materials affected the ability of the cells to differentiate. The supernatants from each sample was measured for IL-12 p70 levels. Figure 7.6 shows M1 macrophages secreted higher levels of IL-12, with a significant increase in secretion from cells seeded onto 7507 TIPS processed films after 10 days. There were low IL-12 levels from M2 cells seeded onto all the polymer films with no significant difference between the time points.

The supernatants were also measured for $VEGF_{165}$ levels. $VEGF_{165}$ secretion from M1 macrophages seeded onto polymer films did not significantly vary between days 1 to 10. At day 4, TIPS PLGA films had higher VEGF levels compared to polystyrene (556.27 ±18.09 pg/mL), with 7507 TIPS (812.39 ±4.14 pg/mL) having higher concentrations than 7502 TIPS (556.52 ±43.7

pg/mL). This trend continued through days 7 and 10. M2 macrophages had significantly higher $VEGF_{165}$ secretion on days 7 and 10, predominantly when seeded onto TIPS processed films (7507 PLGA TIPS; 1858.77 ±19.55 pg/mL and 7502 PLGA TIPS 1308.97 ±65.08 pg/mL on day 7).

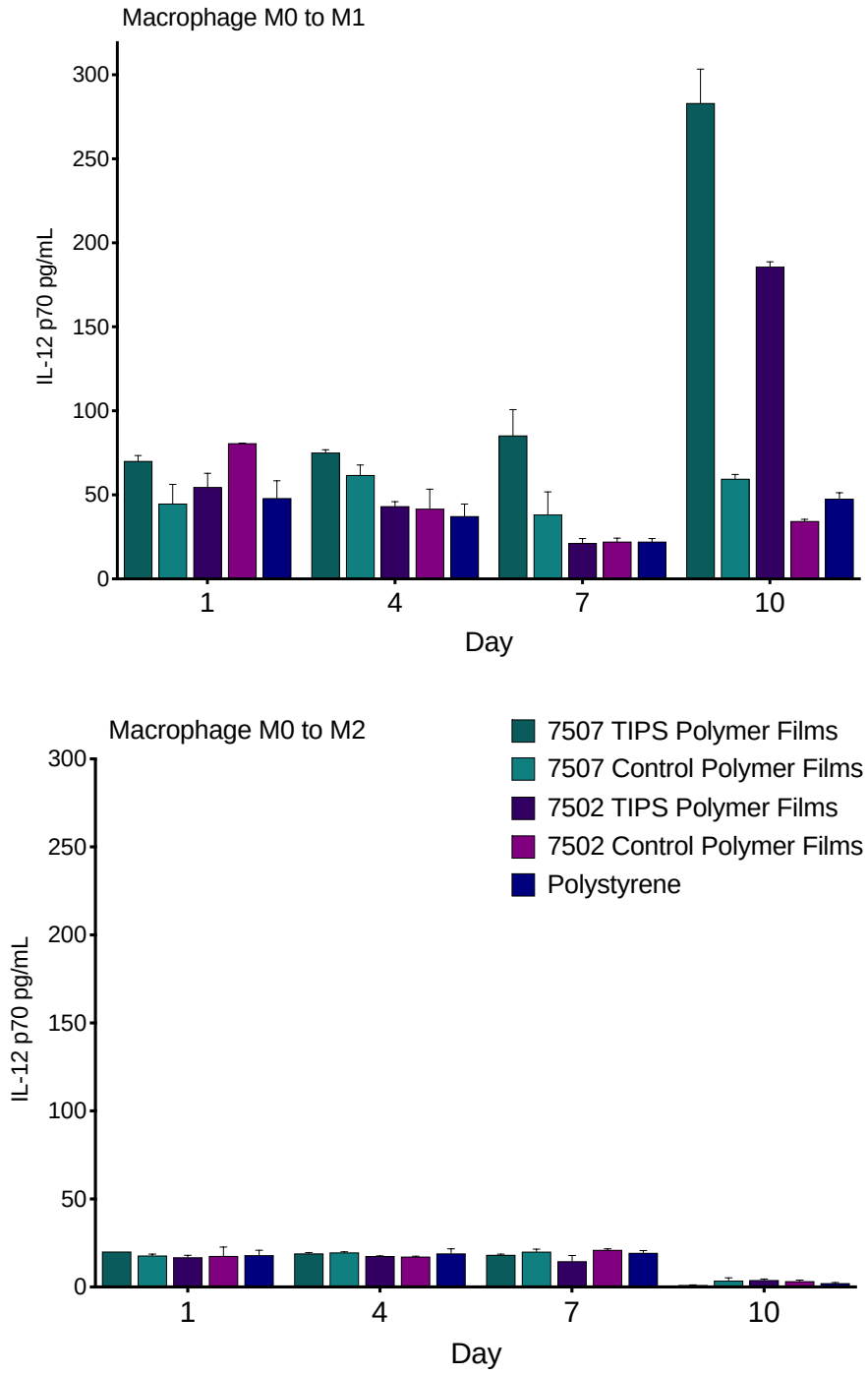

Figure 7.6: IL-12 p70 secretion from M0 macrophages differentiated into M1 and M2 phenotype macrophages seeded onto PLGA 7507 TIPS polymer films, PLGA 7507 control films, 7502 TIPS polymer films, 7502 control polymer films and polystyrene polymer films for 1, 4, 7 and 10 days. (n=5) Two-way ANOVA with Geisser-Greenhouse correction = * (P<0.05)

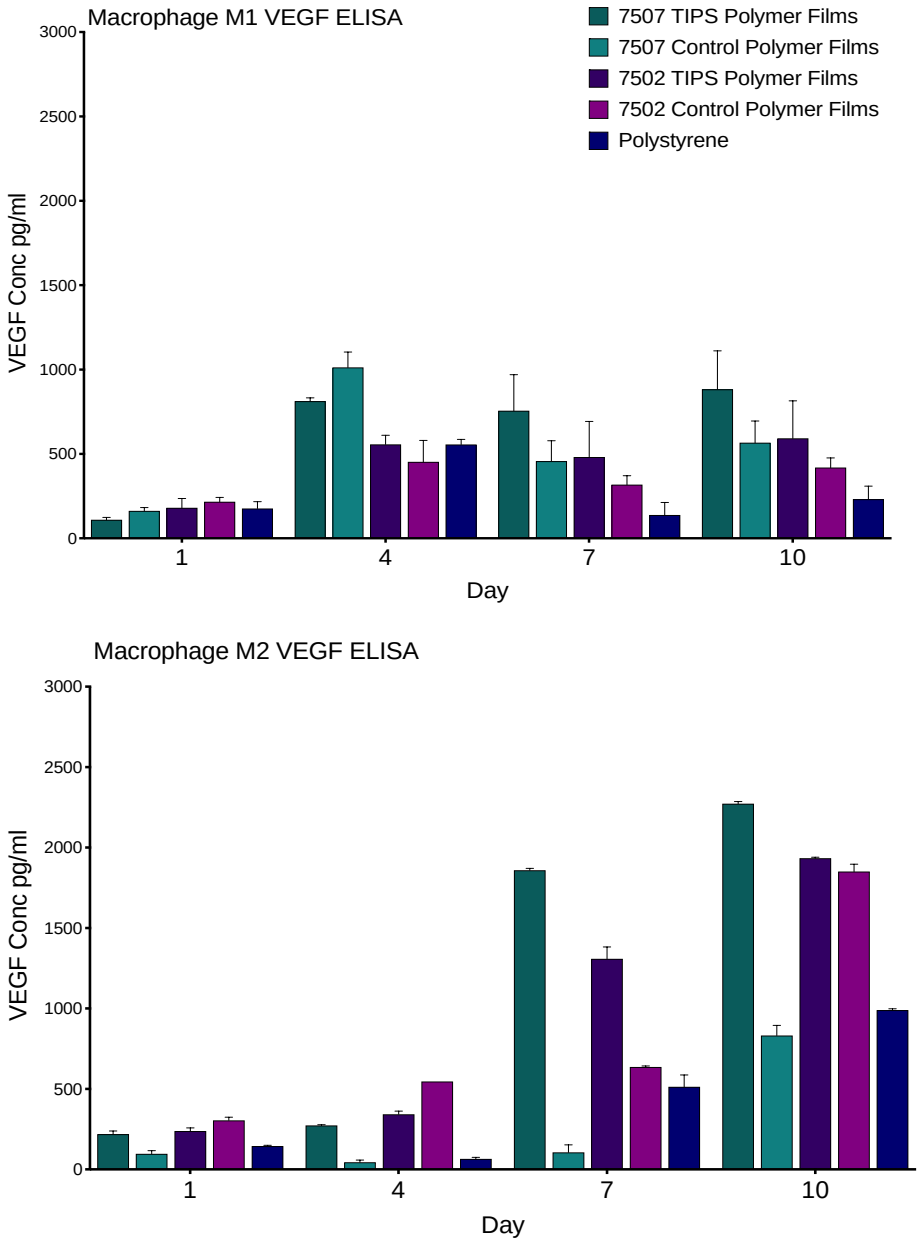

Figure 7.7: $VEGF_{165}$ secretion from M1 (Two-way ANOVA with Geisser-Greenhouse correction = * (P=0.0192)) and M2 (Two-way ANOVA with Geisser-Greenhouse correction = **** (P<0.0001)) phenotype macrophages attached to PLGA 7507 TIPS polymer films, PLGA 7507 control films, 7502 TIPS polymer films, 7502 control polymer films and polystyrene polymer films at days 1, 4, 7 and 10. (n=5)

M0 macrophages were differentiated into M1 and M2 types on polymer films. Figure 7.6 shows $VEGF_{165}$ levels secreted from the differentiated M1 and M2 cells. The secretion of $VEGF_{165}$ from M0 differentiated to M1 macrophages on the polymer films had elevated $VEGF_{165}$ levels from M2 macrophages, with

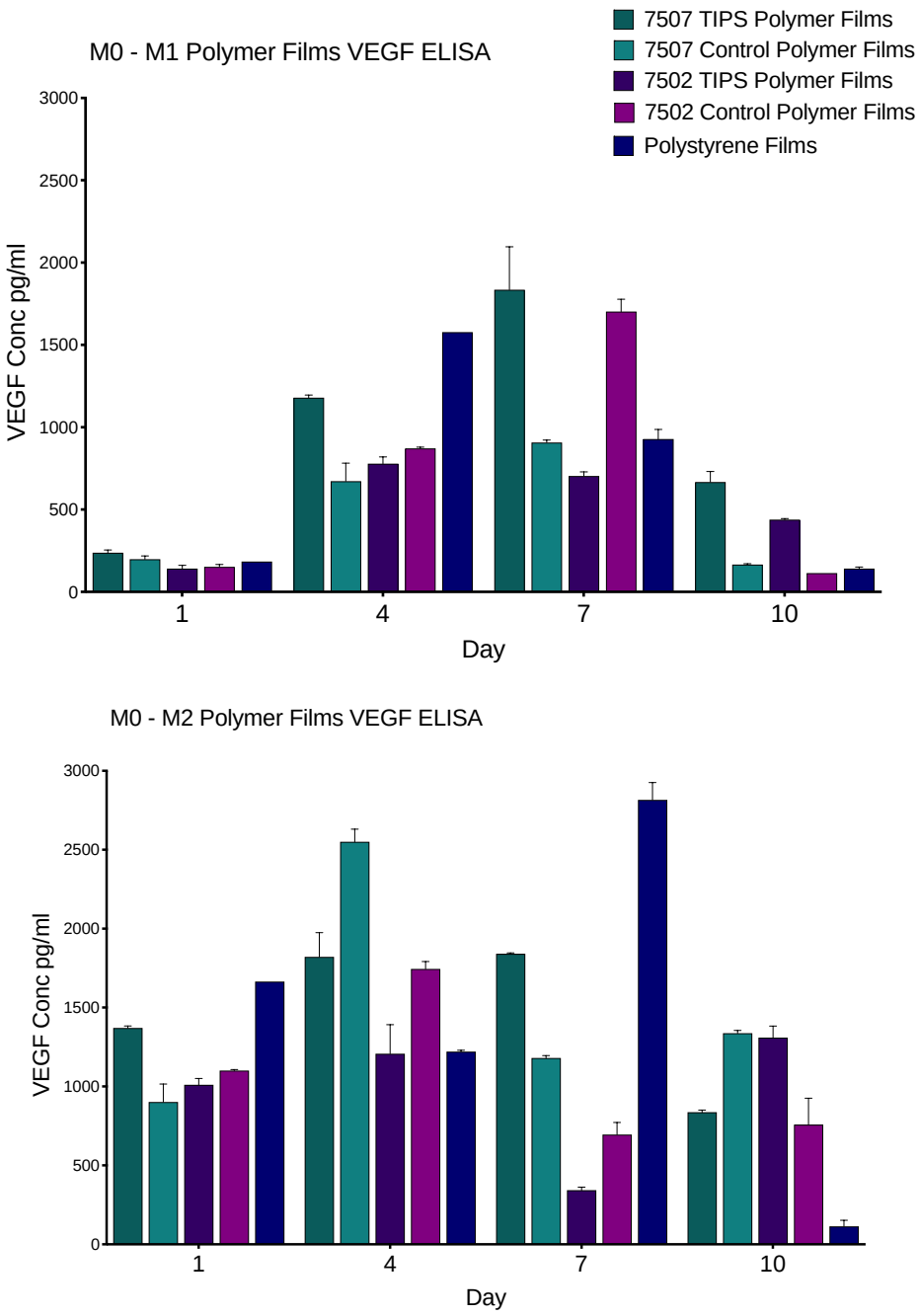

Figure 7.8 $VEGF_{165}$ (pg/mL) secretion from M0 macrophages differentiated into M1 (Two-way ANOVA with Geisser-Greenhouse correction = **** (P<0.0001)) and M2 (Two-way ANOVA with Geisser-Greenhouse correction = **** (P<0.0001)) phenotype macrophages seeded onto PLGA 7507 TIPS polymer films, PLGA 7507 control films, 7502 TIPS polymer films, 7502 control polymer films and polystyrene polymer films at days 1, 4, 7 and 10. (n=5)

the highest levels of $VEGF_{165}$ detected on polystyrene films (2815.1 ±94 pg/mL). To assess how exposure to macrophage secretomes affected the polymer cellularised with ADMSCs, polymers were seeded with ADMSCs as

described in Chapter 4 Section 4.2.2 and exposed to the conditioned media from M1 or M2 cells.

When exposed to TCP-1 derived M1 and M2 secretomes ADMSCs seeded onto TIPS and control PLGA films expressed much higher levels of $VEGF_{165}$ than macrophages alone. ADMSCs seeded onto polystyrene expressed significantly less $VEGF_{165}$ in comparison to PLGA TIPS and control films shown in Figure 7.9. M1 and M2 conditioned media on the $VEGF_{165}$ secretion from ADMSCs seeded on 7502 PLGA TIPS and control films after 7 days, however at the earlier timepoints there was a higher level of $VEGF_{165}$ detected from samples exposed to both types of macrophage in comparison to ADMSCs alone. $VEGF_{165}$ levels at day 7 on 7507 TIPS films showed ADMSCs seeded under standard culture conditions have higher $VEGF_{165}$ secretion (4954 ±1167 pg/mL) compared to ADMSCs exposed to M1 (2461.15 ±36.28) and M2 secretomes (3082.77 ±42.87) with the increase of ADMSC $VEGF_{165}$ levels increasing at day 10 (7300.62 ±1642.87 pg/mL). The same difference can be seen with 7507 control PLGA films at day 10. Interestingly, as with 7502 polymer films, there were higher levels of $VEGF_{165}$ from ADMSCs exposed to macrophages. For example, 7507 TIPS exposed to M2 secretomes expressed 3059.12 ±587.96 pg/mL compared to 1696.95 ±528.06 pg/mL ADMSCs alone.

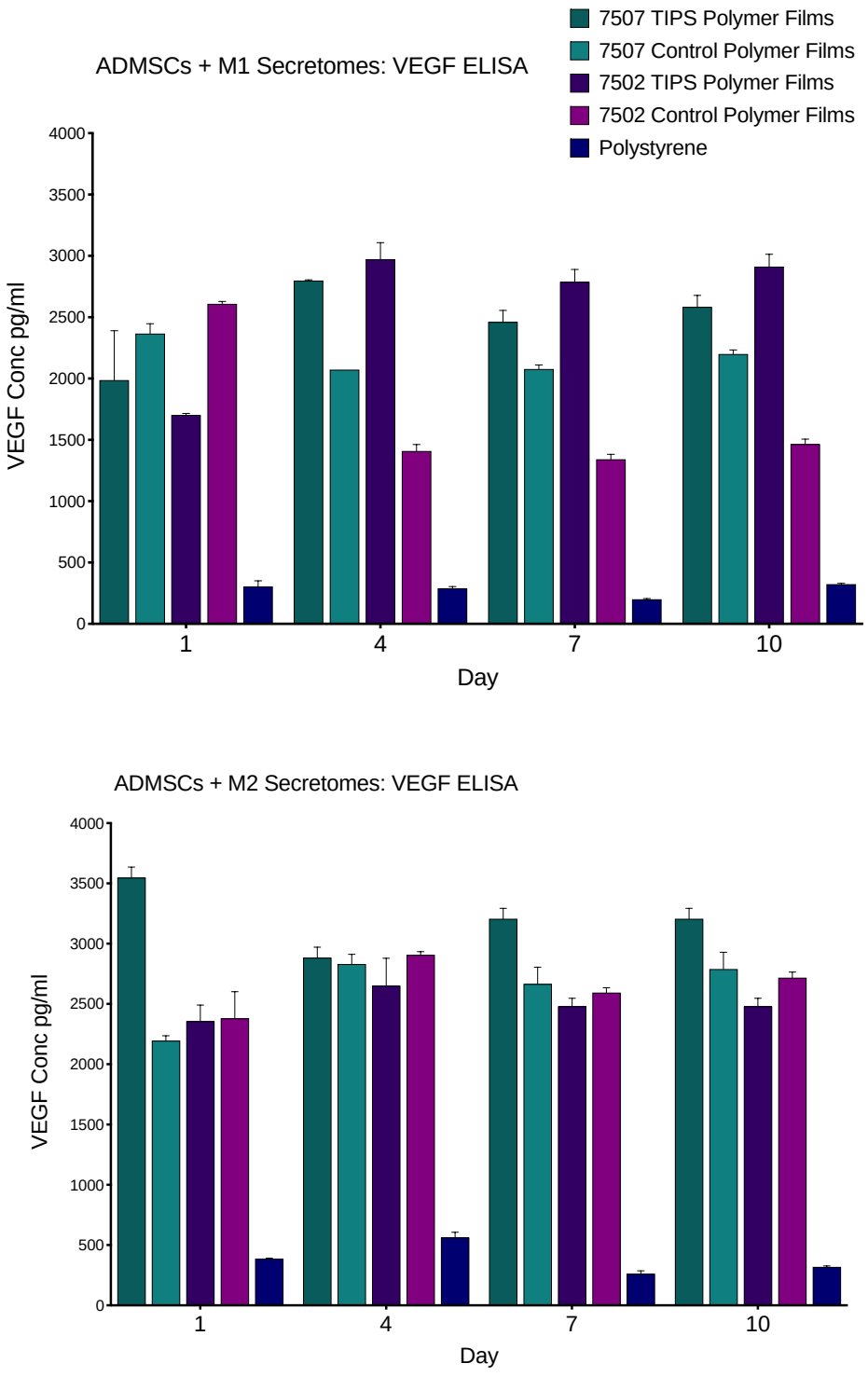

Figure 7.9 $VEGF_{165}$ secretion (pg/mL) from ADMSCs attached to PLGA 7507 TIPS polymer films, PLGA 7507 control films, 7502 TIPS polymer films, 7502 control polymer films and polystyrene polymer films at days 1, 4, 7 and 10 exposed to M1 (Two-way ANOVA with Geisser-Greenhouse correction = **** (P<0.0001)) and M2 (Two-way ANOVA with Geisser-Greenhouse correction = **** (P<0.0001)) phenotype macrophages. (n=5)

In order to investigate the potential angiogenic secretomes of M1 and M2 cells when interacting with TIPS polymer films, an angiogenic proteome profiler was carried out. There were many differences in expression of angiogenic proteins between samples from TCP-1 derived M1 and M2 macrophages seeded onto 7507 TIPS and 7507 control polymer films, as well as between M1 and M2 macrophages. For example, pro-angiogenic factors FGFR2, MCP-1, MIP-1A, MMP-9 were found in increased quantities on TCP-1 derived M1 cells seeded on 7507 TIPS polymer films compared to M1 on 7507 control polymer films (Figure 7.10). In addition, M2 cells on 7507 TIPS surfaces had higher dipeptidyl peptidase IV (DPPIV), endothelin 1 (ET-1), MMP-8, PDGF-AA, placental growth factor (PIGF), Prolactin, Serpin E1 and urokinase-type plasminogen activator (uPA) levels compared to M2 control samples. When examining the differences between M1 and M2 type macrophages, M2 on TIPS surfaces had increased levels of endocrine gland-derived vascular endothelial growth factor (EG-VEGF), Endoglin, IGFB-1/-2/-3, MMP-8, PDGF-AA, PIGF, Prolactin, Serpin E1 and uPA compared to M1, and M2 on control surfaces had higher levels of ANG, FGFR2, IGFB-1/-2, MIP-1, MMP-8, PDGF-AA, Persephin, Prolactin and uPA M2 control compared to M1 seeded on control surfaces. In addition, there were also differences in anti-angiogenic protein levels. Higher levels of CXCL16 and TIMP-1 were found with samples from control materials in comparison to TIPS polymer films. Also, there were increased quantities of Endostatin, Serpin F1 and TSP-1 from samples seeded with M2 macrophages.

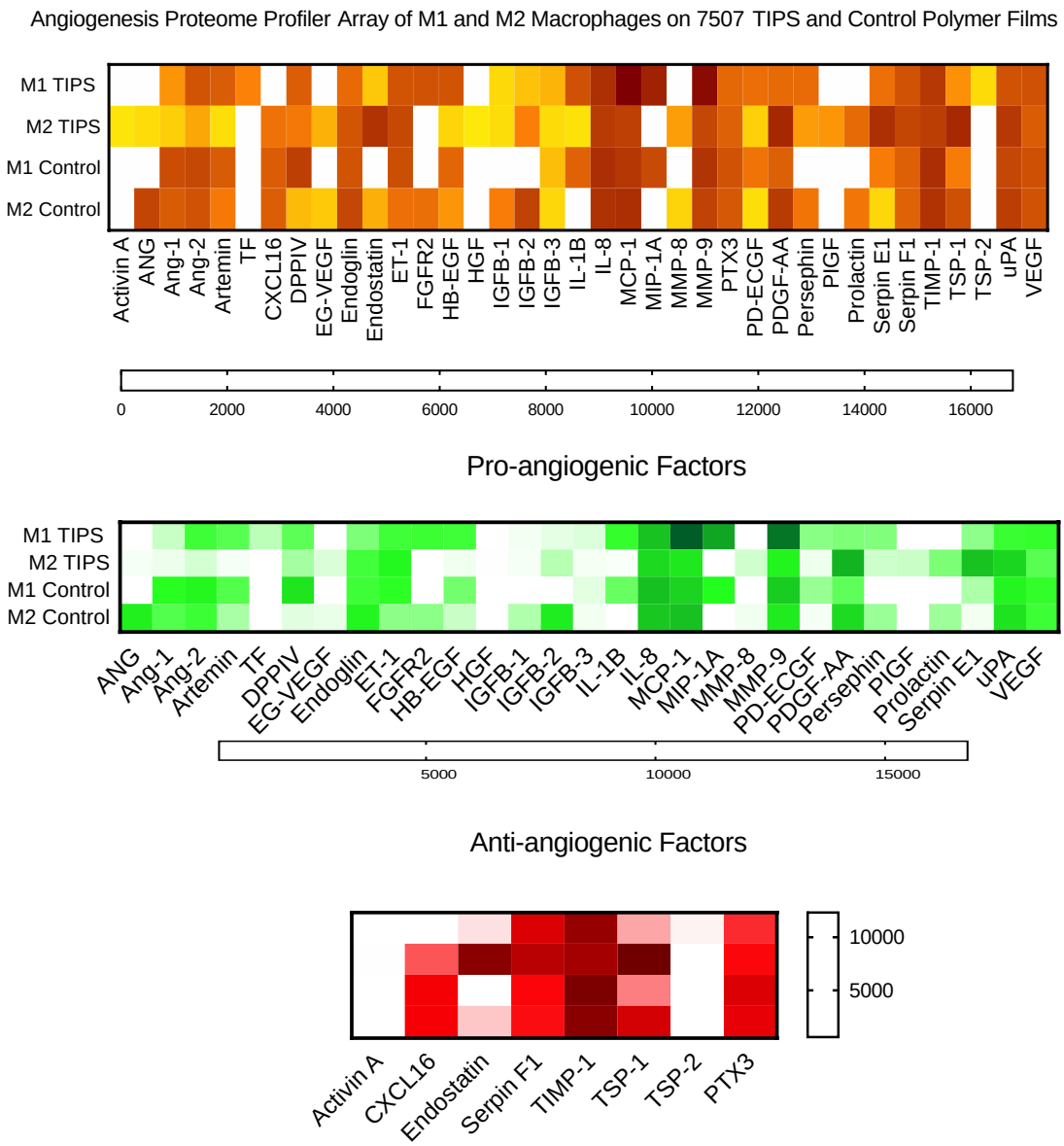

Figure 7.10: a) A heat map showing of the secretomes detected from the human angiogenesis proteome profiler array from M1 and M2 macrophages seeded onto 7507 TIPS polymer films and 7507 control polymer films. b) A heat map to show the pro-angiogenic factors from the proteome profiler array c) A heat map to show the anti-angiogenic factors from the proteome profiler array. (n=1)

A separate profiler was also performed on 7507 TIPS and control polymer films to assess the cytokine release profiles (Figure 7.11). When comparing M2 macrophage samples, there was an increase in expression of growth-related alpha protein ligand 1 (CXCL1/GROa) and G-CSF, and a decrease in chemokine (C-C motif) ligand 1 inflammatory cytokine-309 (CCL1/I-309),

CD40 and IL-4 on samples from cells seeded onto 7507 TIPS polymer films in comparison to 7507 smooth control surfaces. In addition, there were higher levels of chemokine (C-C motif) ligand 2/monocyte chemoattraction protein 1 (CCL2/MCP-1), complement component 5/5a (C5/C5a), CXCL1, G-CSF, GM-CSF and IL-5 cytokines from M1 macrophage samples in comparison M2 macrophage samples.

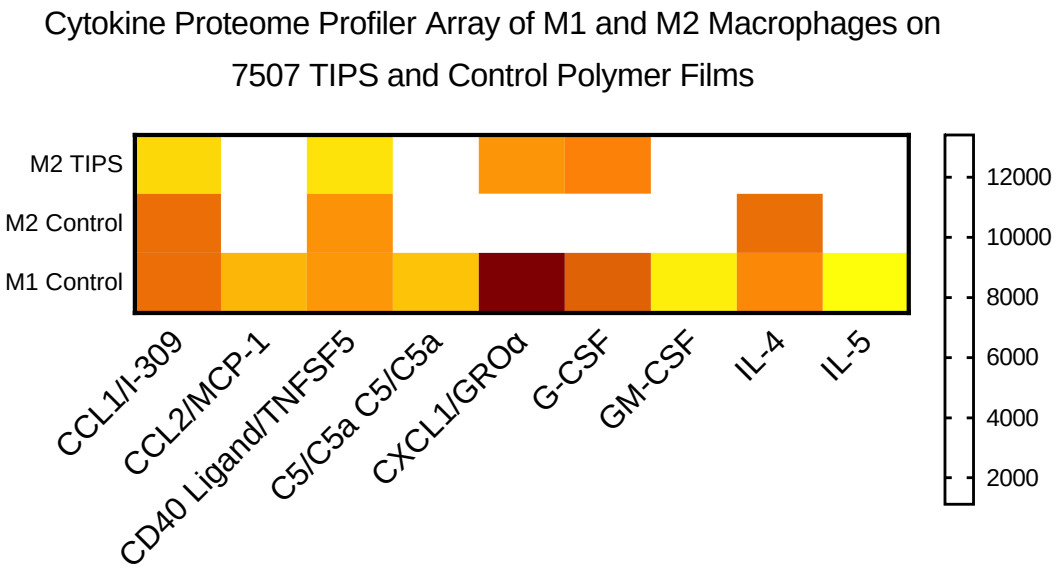

Figure 7.11: A heat map displaying the proteins detected from the human cytokine proteome profiler array from M1 and M2 macrophages seeded onto 7507 TIPS polymer films and 7507 control polymer films. (n=1)

7.4 Discussion

7507 PLGA TIPS polymer films were implanted into a pre-clinical model of PAD. H&E stained tissue sections revealed the presence of multinucleated giant cells around the implants in Figure 7.2. Immunocytochemistry was used in an attempt to identify these cells in order to further understand the *in vivo* response to TIPS polymer films.

Macrophages differentiate into at least two phenotypes in response to different signalling molecules and materials, where M1 type macrophages are primarily involved in the pro-inflammatory response and M2 type macrophages have roles in resolving inflammation, would healing and angiogenesis. [422]

Tissue sections were stained for M1 cells using anti-CD80. Figure 7.4 revealed negative staining for anti-CD80, suggesting that the macrophages present around the TIPS polymer implants were not M1 pro-inflammatory cells. Figure 7.3 displayed some evidence of positive anti-CD163 staining around the TIPS polymer implants. This suggested that the immune response associated with the implantation of the TIPS polymer film was being resolved through the presence of M2 macrophage response, rather than an immune response dominated by M1 macrophages. To confirm this, alternative stains for M1 and M2 macrophages can be used.

Laser doppler imaging from Part I. Section 3.3.2 revealed that the implantation of TIPS polymer films into the hindlimb ischaemia model resulted in an increase in reperfusion in comparison to controls as well as blood vessel formation around the implant. This response could have been supported by the presence of M2 macrophages, that have been shown to secrete angiogenic growth factors (VEGF, FGF, EGF and PDGF) that promotes endothelial migration and subsequent blood vessel formation. [417, 423] To investigate the effect of M1 and M2 macrophages further, *in vitro* experiments were performed to examine the effect of TIPS-processed polymer films on macrophage behaviour.

Figure 7.5 revealed that M0 macrophages successfully differentiated into M1 and M2 phenotypes through the increased secretion of the M1 marker IL-12 p70 from M1 cells (where THP-1, M0 and M2 cells do not express IL-12 p70). [424] The results in Figure 7.6 show that the TIPS and control polymer films did not inhibit the differentiation of the macrophages. It was important to establish this, as despite aiming to reduce and resolve a pro-inflammatory response (through M2 differentiation), M1 cells are considered necessary to reduce the risk from infection from surgery. [425, 426] Interestingly, after 10 days there was significantly higher levels of IL-12 from M1 cells seeded onto 7507 TIPS polymer films, suggesting that the cells were proliferating at a higher rate compared to the other polymer film groups, where it has been shown (Part I. Section 4.3.3) that TIPS surfaces promote cell proliferation. However, cell proliferation assays would need to be employed to confirm this. Alternatively, the surface of the 7507 TIPS films stimulated a stronger M1 cell response after 10 days. It has been shown that materials with high porosity can influence macrophage behaviour. [427-430] Materials with high porosity result in an increased immune response *in vivo* through the formation of a fibrin capsule. This appears to be a negative response, however despite this, it has been shown that the porous materials are associated with the resolution of this pro-inflammatory response to a greater extent than smooth materials through tissue remodelling of initiated by M2 cells behaviour. [431-435] Therefore, the pro-inflammatory response associated with 7507 TIPS polymer films can be resolved more quickly and may even have an increased pro-angiogenic compared to smooth control films.

The secretion of $VEGF_{165}$ from M2 macrophages was significantly higher than M1 macrophages found after 7 days when seeded onto 7507 TIPS polymer films in comparison to smooth polymer controls (Figure 7.7). This behaviour can be attributed to the porosity of the 7507 TIPS polymer films. Porosity has been shown to promote M2 macrophage differentiation and pro-angiogenic behaviour through the secretion of $VEGF_{165}$. [436, 437] The $VEGF_{165}$ ELISA results also revealed that polymer films seeded with M1 macrophages secreted $VEGF_{165}$, despite that M1 macrophages have not been shown to produce $VEGF_{165}$. Therefore, the detection of $VEGF_{165}$ could have arisen from

the M1 macrophages differentiating into M2 macrophages as a response to the attachment to the polymer films. The same effect was seen in Figure 7.8, where macrophages were differentiated into M1 phenotype after being seeded onto the polymer films. This response could be useful for therapeutic angiogenesis as the TIPS PLGA 7507 polymer films could reduce a pro-inflammatory response *in vivo* and promote angiogenesis through the differentiation of M1 into M2 macrophages. Macrophages have been shown to spontaneously differentiate into different phenotypes from exposure to different conditions, [438, 439] where the exposure to the unique surface topography of TIPS-processed surfaces could have provided an environment that promoted M2 differentiation. The differentiation of M1 macrophages occurs through the inhibition of the Pi3K pathway and subsequent activation of the NF-κB pathway, that results in nitric oxide expression. [440] Whereas M2 macrophages are activated in the presence of TGF-β and IL-10, that promotes the activation of the Pi3K and thus Akt pathways that causes a reduction in LPS activation and subsequent formation of M2 macrophages. [441, 442] The inhibition or activation of the Pi3K pathway can also be influenced by inflammatory stimuli and growth factors. [443, 444] The increase in M2 cells could be from M0 responding to TIPS surfaces and releasing factors that activates Pi3K pathway and promotes the formation of M2 macrophages.

M2 macrophages seeded onto polystyrene films had low levels of $VEGF_{165}$ secretion in comparison to TIPS and control PLGA films (Figure 7.7). Rostam *et al.*, 2016, studied the impact of surface modification of polystyrene and found that polystyrene modified to be hydrophobic promoted differentiation into M1 macrophages. [445] The polystyrene films used were tissue culture modified and therefore exhibited enhanced cell attachment. This would have resulted in an increased pro-inflammatory response and subsequent reduced VEGF expression, highlighting the advantage of utilising biodegradable PLGA films over polystyrene films.

Part I. Chapter 5 revealed that ADMSCs seeded onto 7507 TIPS polymer films exhibited pro-angiogenic properties *in vitro*. To investigate how the secretomes from M1 and M2 macrophages effected ADMSC angiogenic behaviour, 7507 TIPS, 7507 control, 7502 TIPS, 7502 control and polystyrene polymer films were cellularised with ADMSCs, exposed to M1 or M2 secretomes and $VEGF_{165}$ concentrations were measured.

The $VEGF_{165}$ secretion from ADMSCs seeded onto polystyrene films exposed to M1 and M2 macrophage secretomes were significantly lower than the TIPS and control PLGA polymer films throughout the time points. This effect can be attributed to the difference in physical properties between polystyrene and PLGA. For example, porosity has been shown to influence macrophage behaviour [427-430] and the smooth surface of the polystyrene films in this study had a decreased pro-inflammatory immune response (Figure 7.6), which in turn resulted in a reduction in the resolution of inflammation through the secretion of $VEGF_{165}$ (Figure 7.7 and 7.9). In addition, the degradability of the material influenced the behaviour of macrophages. Polystyrene is a non-degradable polymer, therefore the immune response would be prolonged in comparison to degradable polymers such as PLGA, where the response resolved as the material degraded. [446, 447] Polystyrene was also shown to be much stiffer than PLGA through AFM measurements (AFM results, Part I. Chapter 3). Sadtler *et al.*, 2019, showed that stiffer scaffolds implanted *in vivo* resulted in an decreased expression of M2 marker anti-CD206, suggesting that stiffer materials downregulated tissue repair. [448] Therefore the high stiffness of polystyrene contributed to the lower activity of M2 macrophages and thus highlighting the benefits of using materials with lower stiffness values such as PLGA.

Figure 7.9 revealed that there were higher $VEGF_{165}$ levels secreted from ADMSCs exposed to M2 secretomes in comparison to M1 secretomes. When exposed to M1 secretomes there were higher levels of $VEGF_{165}$ secreted from ADMSCs seeded onto 7507 TIPS and 7502 TIPS polymer films in comparison to smooth control surfaces. This effect could be attributed to the fact that M2 cells secrete $VEGF_{165}$ and the $VEGF_{165}$ measured was a combination of the

$VEGF_{165}$ produces from the M2 cells and ADMSCs. Alternatively, additional pro-angiogenic growth factors within the M2 secretome could have stimulated $VEGF_{165}$ secretion from ADMSCs. To investigate this theory the macrophage secretomes were investigated further and profiled for angiogenic proteins and cytokines. This study investigated the response of macrophages to TIPS materials after only 10 days (and the *in vivo* studies ended after 21 days), it would be interesting to study further the implications of macrophages on angiogenesis through the interactions with the TIPS-processed materials, especially as the materials degrade and the initial immune response is resolved. M1 macrophages are implicated in the early stages of angiogenesis, through the secretion of nitric oxide that is known to stimulate angiogenesis, where nitric oxide stimulates VEGF production. [32, 449] M2 activated macrophages are known to secrete VEGF and TGF-b. VEGF is essential throughout the majority of the angiogenic process, whereas TGF-β is implicated in later phases, through the differentiation of pre-curser cells into pericytes that support the newly formed vessels. [450] This suggests that M2 macrophages could be involved in the mid/late stages of angiogenesis. There have been numerous pre-clinical studies that have demonstrated that angiogenesis was achieved through the secretion of a variety of factors growth factors and cytokines from both M1 and M2 macrophages, from initial capillary sprouting to vessel maturation. [451, 452] In addition, it has been proffered by Corliss *et al.,* 2016, that as monocytes prefer to migrate through capillaries in areas with lower ECM levels (where lower ECM levels occur during the early stages of angiogenesis through degradation of the basement membrane) and that monocytes differentiate into macrophages, (that in turn secrete ECM remodelling proteins), that early-stage differentiated macrophages can also support capillary sprouting. [453]

As macrophages seeded onto PLGA 7507 TIPS polymer films had shown to have superior pro-angiogenic activity, it was decided that the secretomes from M1 and M2 macrophages seeded onto 7507 PLGA TIPS films would be investigated further using an angiogenic profiler, that screens for 55 different

angiogenic-related proteins (Figure 7.10). There were distinct increases in pro-angiogenic factors between M1 cells seeded onto TIPS polymer films in comparison to M1 cells on smooth control films, signifying that the TIPS films influenced the secretion of pro-angiogenic proteins. However, the factors detected (FGFR2, MIP-1A and MMP9) are secreted by M2 macrophages, [454] suggesting that the M1 macrophages had differentiated into M2 macrophages in response to the TIPS surfaces. In addition, M2 macrophages on TIPS polymer films secreted higher levels of multiple pro-angiogenic factors such as; ANG, EG-VEGF, Endoglin, IGFB-1/-2/-3, MMP-8, PDGF-AA, PIGF, Prolactin, Serpin E1 and uPA compared to M1 macrophages on TIPS polymer films and control PLGA surfaces suggesting the M2 macrophages seeded onto TIPS films had increased pro-angiogenic behaviour which is promising for implantation of the materials to promote angiogenesis.

A human Cytokine Proteome Profiler array was used to measure 36 cytokines from the secretomes from M1 and M2 macrophages seeded onto 7507 TIPS polymer films and 7507 control polymer films. Figure 7.11 revealed that M1 macrophages secreted chemokine (C-C Motif) ligand 1 inflammatory cytokine-309 (CCL1/I-309), complement component 5/5a (C5/C5a), chemokine (C-C motif) ligand 2/monocyte chemoattraction protein-1 (CCL2/MCP-1) and growth related alpha protein ligand 1 (CXCL1/GROa), that are known cytokines secreted by M2 macrophages. [422, 455-457] It was also discovered that M1 macrophages secreted IL-4, a factor that induces M2 macrophage differentiation. [458] In addition, M1 macrophages secreted G-CSF, that promotes M-CSF and also induces M2 macrophage differentiation. [459] These finding suggested that the M1 macrophages seeded onto PLGA polymer films began to show signs of M2 differentiation and behaviour, however there was evidence of the presence of M1 cells due to the detection of M1 markers IL-5 and GM-CSP that induces M1 differentiation. [459, 460] As these factors were not found in M2 cell samples signifying that once seeded onto the PLGA polymer films, M2 cells did not exhibit pro-inflammatory activity. STRING analysis [247] revealed that M2 macrophages seeded onto 7507 TIPS polymer films showed links to blood vessel development, regulation of angiogenesis and vascular development (supplementary Figure S7.1),

whereas control groups and films seeded with M1 macrophages revealed no such links.

These findings suggest that PLGA 7507 TIPS polymer films regulated macrophage behaviour away from the pro-inflammatory response and towards the promotion of angiogenesis. This is promising for future studies involving the implantation of PLGA 7507 TIPS polymer films as a potential therapy for PAD.

7.5 Summary

This chapter explored the biological mechanism responsible for the pro-angiogenic effect of TIPS polymer films seen in Chapter 5 and Chapter 6 by focussing on macrophage response associated with TIPS polymer films.

Staining of tissue sections from the implantation of 7507 TIPS polymer films into the hindlimb ischaemia model revealed evidence of macrophage attachment to the materials (Figure 7.1). Identification of M1 and M2 macrophages was attempted, where M1 macrophages have been shown to be pro-inflammatory and M2 macrophages have roles in resolving the immune response and angiogenesis. Preliminary results were negative for M1 cells and there was some evidence for M2 cells, however further staining was required to definitively identify the inflammatory cells present around the TIPS film implant.

In vitro experiments revealed an increase in $VEGF_{165}$ secretion from M2 macrophages when seeded onto 7507 TIPS polymer films. In addition, there was evidence of M1 differentiation into M2 macrophages when exposed to TIPS-processed PLGA with links to blood vessel development, regulation of angiogenesis and vascular development uncovered through protein profiling.

The results suggested that PLGA TIPS films may increase pro-angiogenic M2 macrophage activity in comparison to smooth and non-degradable polymers. This is promising for the proposed application of TIPS films as an implant to treat ischemic disease.

7.6 Supplementary Information

Figure S7.1: STRING analysis data identifying the links between the proteins secreted from M2 macrophages seeded onto 7507 TIPS polymer films. Regulation of angiogenesis (5 genes, 2.4e-14 FD), cellular process (16 genes), blood vessel development (5 genes, 4.32e-14 FD), vasculature development (5 genes, 5.43e-15 FD) and ECM organisation (6 genes, 3.93e-18) biological processes were highlighted.

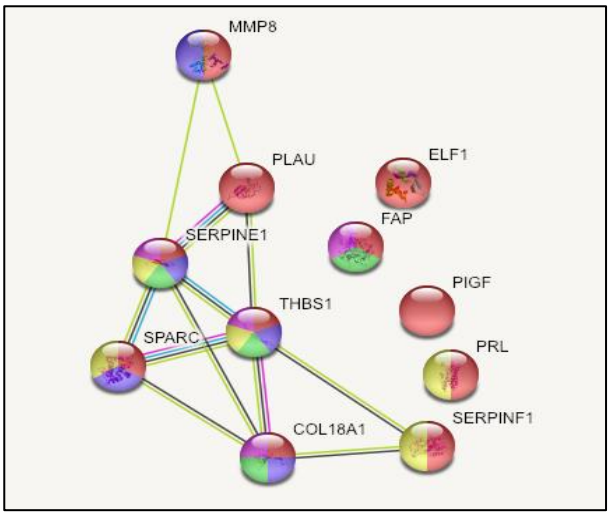

Part II. Evaluation of TIPS-Processed Microparticles

1. Introduction

It is commonly recognised that to truly understand a biological process or an effect, one should strive to recreate *in vivo* conditions as closely as possible. However, this may not always be feasible, especially in the early stages of research. Culturing cells in 2D conditions provides many advantages for research purposes, including cost-effective opportunities for reproducibility, long-term culture with unrestricted access to oxygen, nutrients and constant temperatures. Nonetheless, the simplicity of 2D culture conditions may not reflect cells in their natural state. This can result in alterations in cellular differentiation and gene expression. [167, 461] Culturing cells in 3D environments may overcome the shortcomings associated with 2D cell culture, as they are thought to more accurately represent *in vivo* conditions by providing a larger surface area to volume ratio, affecting the spatial orientation of cells on the surfaces, which can result in more representative cell-cell contacts and allow the formation of cellular niches. 3D culture is a broad term that can refer to culturing cells in suspension, in gels or hydrogels and on scaffolds such as microparticles or fibres. [461, 462] When culturing cells in suspension adherent cells can cluster, often forming spheroids. Necrotic cores may form with spheroids, from the innermost cells not receiving enough nutrients and oxygen. Therefore, culturing cells on 2D or 3D substrates can increase their chance of survival. [462] In this instance, the 3D substrate investigated is in the form of microparticles. Despite the difficulty that can occur with 3D culture methods due to issues with handling, reproducibility and expense, [461] microparticles are an attractive option as they not only provide

larger surface area to volume ratios than 2D surfaces, they can be easily administered *in vivo* and have been shown to have superior cell attachment and proliferation in comparison to other biomaterials. [463] For example, Patel *et al.*, 2019, discovered that microparticles exhibited superior cell attachment and colonisation in comparison to phosphate glass discs for the application in bone tissue engineering. [464]

Part II of this thesis explores the manufacture and characterisation of TIPS-processed microparticles and the subsequent culture of ADMSCs onto the surface microparticles. The angiogenic behaviour of cells was explored using a pre-clinical model of peripheral artery disease (PAD).

Part II.

Chapter 2: Preparation of TIPS-Processed Microparticles

2.1 Introduction

The TIPS process has been described in Part I. Section 1.3 and 2D TIPS processed polymer films were produced and characterised in Part I. Chapters 2 and 3. This chapter describes the fabrication of 3D TIPS microparticles and reports the physical characterisation of the materials using microscopy techniques and roughness measurements.

2.2 Methods

2.2.1 TIPS Microparticle Preparation

To produce TIPS microparticles PLGA 7502 (PURASORB PDLG 7502, 75:25 DL-lactide/glycolide copolymer, inherent viscosity 0.22 dl/g, Corbion Biomaterials, Gornchem, Netherlands) and PLGA 7507 (PURASORB PDLG 7507, 75:25 DL-lactide/glycolide copolymer, inherent viscosity 0.70 dl/g, Corbion Biomaterials, Gornchem, Netherlands) 10 wt% polymer solutions were prepared as described in Part I. Section 2.2.1.

The polymer solution was fed into a Var D Nisco encapsulation unit (Nisco Engineering, Zurich, Switzerland) and ejected through a sapphire tipped nozzle with a 150 μm orifice using a syringe pump (Pump 11, Harvard Apparatus, UK) at a flow rate of 3 mL/min. The polymer droplets were dropped from 80 cm and collected into 250 mL liquid nitrogen in a 1000 mL polypropylene straight-sided beaker (10349324, Fisher Scientific, UK) to thermally induce phase separation. In order to ensure the residual DMC did not exceed its melt temperature (2-4^{o}C) and dissolve the polymer microparticles, the samples were then transferred into a 50 mL Falcon tube (352070, BD Biosciences, USA) and placed into a -80^{o}C freezer. The materials were lyophilised (Edwards Freeze-dryer, EF03, Edwards, West Sussex, UK) for 18 hours to allow the sublimation of residual DMC from within the material. This procedure removed the solvent and formed the unique hierarchical and porous structure the TIPS materials. Microparticles were sieved to a size range of 250 – 355 μm using Endecotts brass sieves (200.BIW.250 and 200bBOW.255, Fisher Scientific, UK).

Solid microparticles composed of PLGA 7502 (PURASORB PDLG 7502, 75:25 DL-lactide/glycolide copolymer, inherent viscosity 0.22 dl/g, Corbion Biomaterials, Gornchem, Netherlands) and PLGA 7507 (PURASORB PDLG 7507, 75:25 DL-lactide/glycolide copolymer, inherent viscosity 0.70 dl/g, Corbion Biomaterials, Gornchem, Netherlands) and polystyrene of an identical

size range (250 – 355 μm) were prepared by Phosphorex, (PS300K, Phosphorex, USA).

2.2.2 Ultrastructural Imaging of Microparticles Using Scanning Electron Microscopy

The surface topographies of the PLGA 7507 TIPS, PLGA 7502 TIPS, PLGA 7507 control and polystyrene control microparticles were visualised under a scanning electron microscope (SEM). The full methodology was described in Part I. Section 3.2.4.

2.2.3 Internal Structure Imaging of TIPS Microparticles using Focused Ion Beam Scanning Electron Microscopy

To assess the internal structure of TIPS microparticles a Carl Zeiss XB1540 cross beam focused ion beam microscope (FIB) was used. FIB used a charged focused ion beam which was able to mill samples in order to visualise beyond the surface. [465] This occurs through ions that are created from a liquid metal source from within the instrument, which are accelerated down an ion column at high voltage under vacuum onto the surface of the material. [466] 7507 TIPS microparticles were mounted onto aluminium stubs via carbon tabs and allowed to completely dry. Prior to imaging each sample was sputter coated with gold/palladium alloy in an argon atmosphere to prevent charging of the specimen that can affect the image quality. Samples were imaged under vacuum with SEM before milling to locate the area of interest. SEM was used to monitor the milling and take images afterwards. The focused ion beam was used to mill a 3 μm x 3 μm x 3 μm area into the microparticles.

2.2.4 Internal Structure Analysis using X-ray Nano Computed Tomography

Nano Computed Tomography (NanoCT) was used to analyse the internal structure of TIPS microparticles composed of PLGA 7502 and 7507. Zeiss 800 Ultra Xradia nanoCT-S100 system was used to visualise the internal structure of a 60 μm segment (maximum area) of the microparticles at a resolution of 50 nm. Single microparticles were mounted onto needles, using epoxy

adhesive (14260, Devcon, Ireland) and placed onto the stage within the X-ray nanoCT. 160 projections were taken of each microparticle with exposure set to 10 and bin at 2. Images were produced from x-ray beams generated by a rotating copper anode at 8 keV. It was able to penetrate into the material, passing through the sample and was detected, resulting in a phase contrast images that were stacked to create 3D reconstructions.

2.2.5 TIPS Microparticle Analysis Using Morphologi G3

Morphologi G3 particle characteriser (Malvern, UK) was used to characterise the size and circularity of PLGA 7507 and 7502 TIPS microparticles, PLGA 7507 control microparticles and polystyrene microparticles. The samples were loaded into the dispersion chamber and were scattered onto a clean glass slide. The slide was positioned under a microscope, where the entire sample was visualised, and an image was taken. From this, parameters were set including size and circularity filters, and the Morphologi G3 software analysed the microparticles. A size filter of 250 – 400 μm was applied as the microparticles had been pre-sieved to a size range of 250 – 355 μm, therefore anything detected by the instrument outside of this range would be either fragments, microparticles touching or other artefacts/noise. For these reasons, a circularity filter of >0.95 was also applied, with a filter of 1 representing a perfect sphere. As the goal was to determine the average size of the microparticles it was important to exclude artefacts that would have disrupted the true average measurements. The software counted all of the microparticles analysed as well as imaged each individual microparticle, that also allowed for additional manual filtering and assessment.

2.2.6 In Vitro Degradation Analysis of TIPS Microparticles

An *in vitro* degradation study was conducted by aliquoting 30 mg of microparticles into pre-weighed glass vials. The rubber stoppers on the vials were loosened and the samples placed in a in a desiccator to provide a dry environment until a constant mass was measured indicating residual moisture had been removed. Phosphate buffer solution pH 7.4 (1294-0724, VWR) was added to each vial containing microparticles to produce a final ratio of volume

of the buffer solution of 10 mL:30 mg of microparticles. The vials were placed onto a tube roller and placed inside a dry incubator at 37°C at constant rotation. To determine mass loss, filter paper (Grade 303; 150 mm, VWR) was dried to achieve a constant mass using a desiccator containing silica gel beads under vacuum at room temperature. After 3 weeks, the PBS was removed from the first five samples and stored in separate sterile 50 mL Falcon tubes (352070, BD Biosciences, USA). The pH was measured (after calibration of the pH meter using pH 4 and 7 buffers). The vials containing the microparticles were rinsed twice with 10 mL analytical grade water (7732-18-5, Fisher Scientific, UK). The wash water was passed through the filter paper to retain any degradation products within the water. The total contents of each vial were added to individual filter papers. The degraded sample and filter paper were dried in a desiccator containing silica gel beads at room temperature to remove residual water before the mass of each sample was measured using an analytical balance. Samples were weighed to constant mass. The process was repeated with samples collected at 6, 12, 18, 24 and 30 weeks.

2.2.7 Statistical Analysis

The data was input into GraphPad Prism 8 software (GraphPad Software, USA) for analysis and presented as mean values with error bars depicting the standard deviation. To analyse two or more groups with one variable, ordinary one-way ANOVA tests were used. For two or more groups with two or more variables a Two-way ANOVA was used with Geisser-Greenhouse correction applied. For comparison between two groups the data were first tested for normality through a Kolmogorov-Smirnov test. If normally distributed, a parametric unpaired Welch Student *t*-test was performed. If not normally distributed, a nonparametric Wilcoxon Student *t*-test was performed. P values of <0.05 indicated statistical significance and were shown as *, with $P<0.01$ = **, $P<0.001$ = *** and $P<0.0001$ = ****.

2.3 Results

2.3.1 Ultrastructural Imaging of Microparticles Using Scanning Electron Microscopy

SEM was used to visualise the topography and structure of the PLGA 7507 TIPS, PLGA 7502 TIPS, PLGA 7507 control and polystyrene microparticles. Images were taken at a range of magnifications (x50-x3000). Imaging revealed that PLGA microparticles produced using the TIPS process had very porous and rough surfaces, in contrast to the PLGA control and polystyrene microparticles which had smooth, non-porous surfaces. SEM images (Figure 2.1) showed the 7507 TIPS and 7502 TIPS microparticles were similar in size to each other and within a size range of 250 – 355 μm and included a single large radial pore on the surface of the microparticles (Figure 2.7). High magnification imaging has revealed that PLGA 7502 TIPS microparticles have larger pore sizes compared to PLGA 7507 TIPS microparticles. The size of the microparticles were measured using a Morphologi G3 particle analyser.

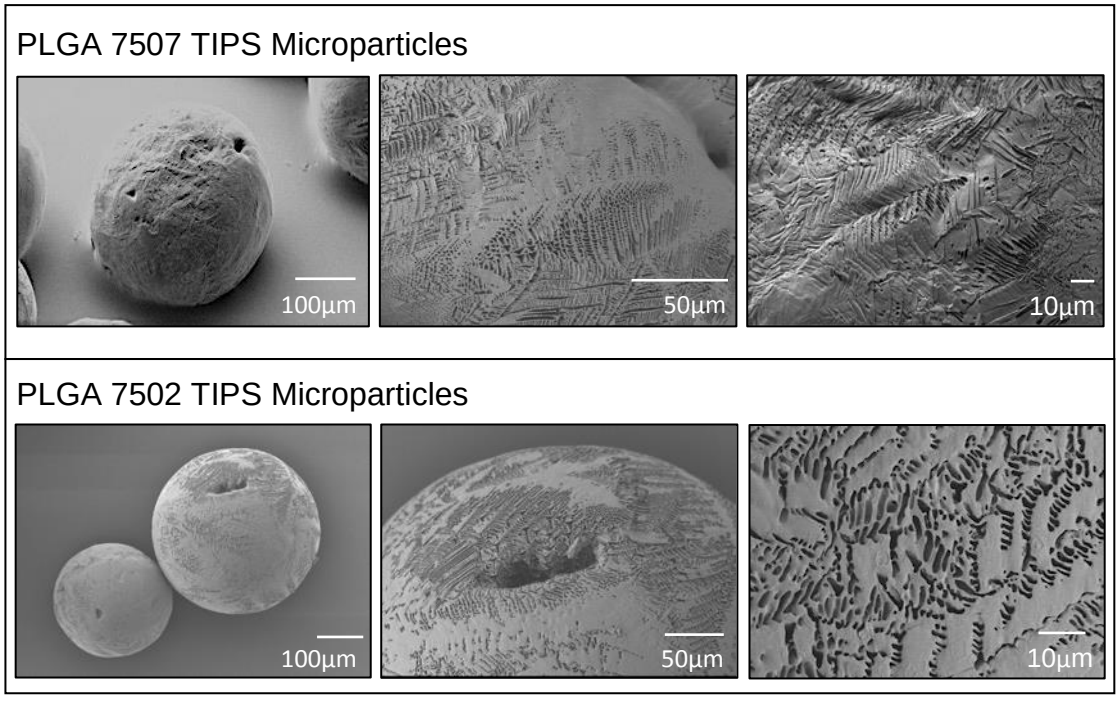

Figure 2.1: SEM images of PLGA 7507 TIPS microparticles and PLGA 7502 TIPS microparticles.

	Number of Microparticles	Mean Diameter (μm)	Circularity
PLGA 7507 TIPS	223	367.1 ±34	> 0.95
PLGA 7502 TIPS	604	298.5 ±32	> 0.95
PLGA 7507 Control	147	306.5 ±32	> 0.8
Poly- styrene	562	306.2 ±30	> 0.8

Table 2.1: Morphologi G3 results of PLGA 7507 TIPS microparticles, PLGA 7502 TIPS microparticles, PLGA 7507 control microparticles and polystyrene control microparticles.

Results in Table 2.1 display that PLGA 7507 TIPS microparticles were found to have a mean diameter of 376 microns and PLGA 7502 TIPS microparticles had a mean diameter of 299 microns.

2.3.2 Degradation of 7507 TIPS Microparticles

As the PLGA 7507 TIPS microparticles began to degrade, they showed a loss in circularity (Figure 2.2), and surface porosity and roughness. This change in morphology was most drastic between days 0 to 1. As with the polystyrene films, polystyrene microparticles showed no signs of degradation. The PLGA 7507 control microparticles showed little evidence of degradation, with some subtle changes in circularity seen.

The *in vitro* degradation of 7507 TIPS microparticles was evaluated further over 30 weeks with pH and mass loss measured at weeks 3, 6, 12, 18, 24 and 30 (n=5). Samples were prepared as outlined in section 3.2.11. The pH of the supernatant was measured and shown in Figure 2.4, where it can be seen that

pH significantly decreased over time from 6.91 ±0.06 after 3 weeks to 2.82 ±0.38 at 30 weeks. There was no further change in pH between 24 and 30 weeks. Figure 2.5 shows the mass loss as the microparticles degrade. After 3 weeks 15.5% of the starting mass of the material was lost, with only 12.8% of the original mass remaining after 30 weeks.

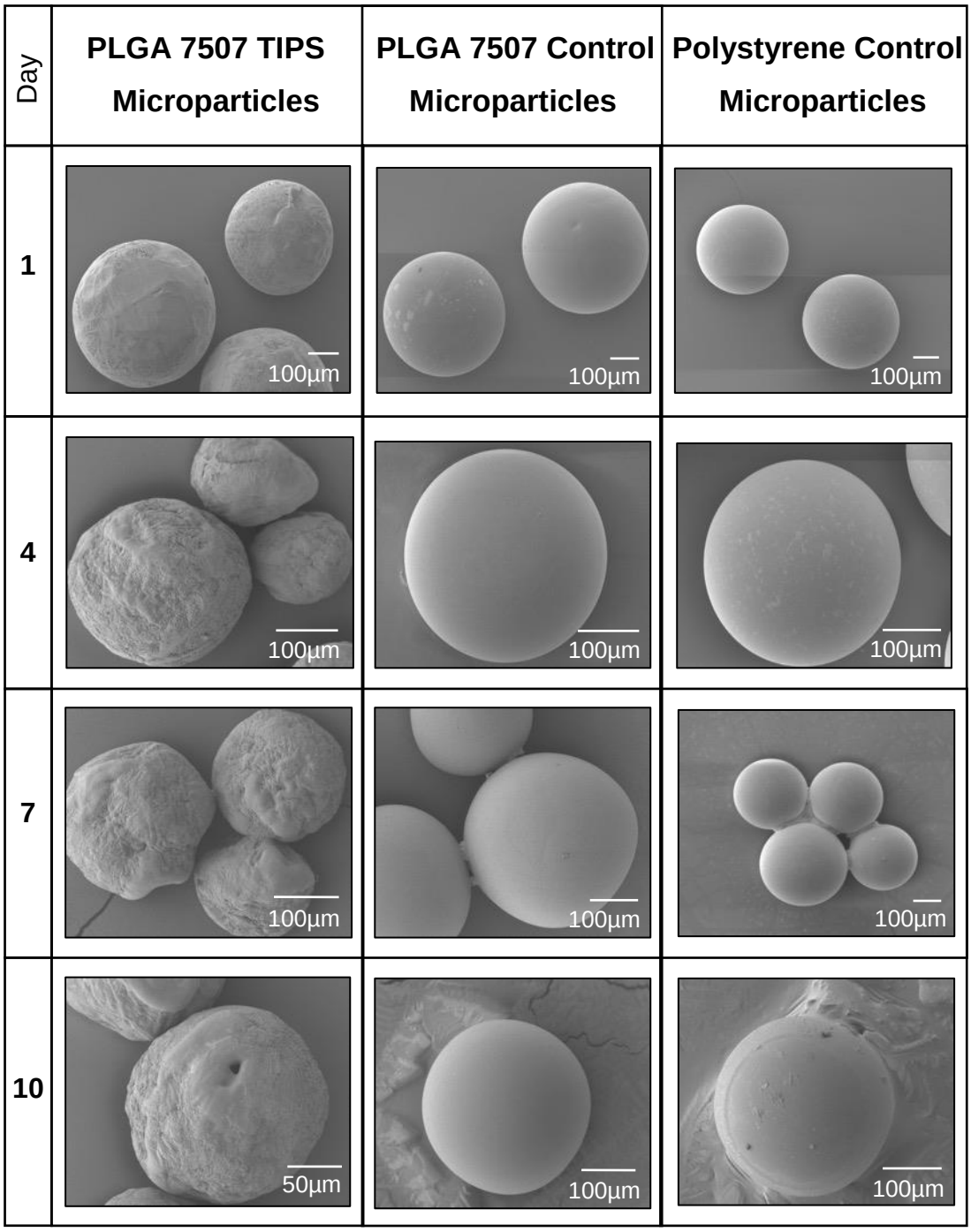

Figure 2.2: SEM images of PLGA 7507 TIPS microparticles, PLGA 7507 control microparticles and polystyrene control microparticles at day 1, 4, 7 and 10.

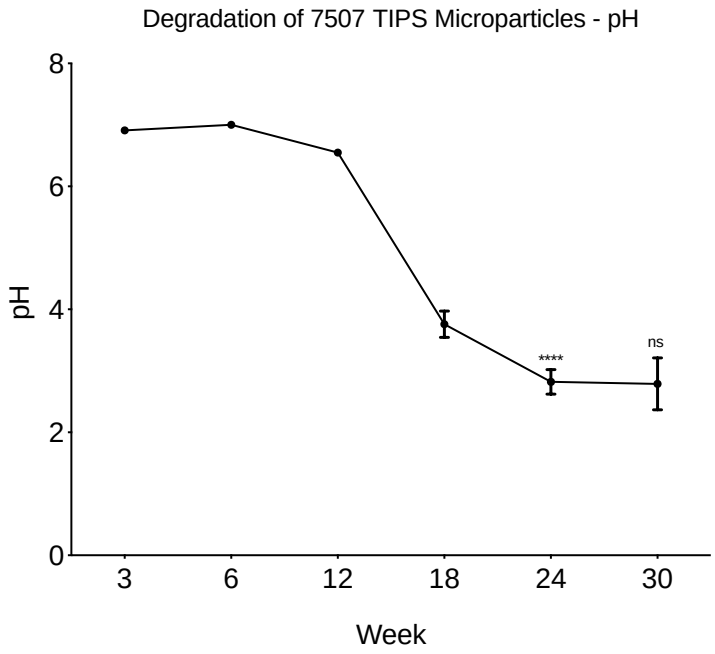

Figure 2.4: a) pH measurements of PLGA 7507 TIPS microparticles. (n=5) pH at week was 3 statistically higher than week 24 (P<0.0001 = ****)

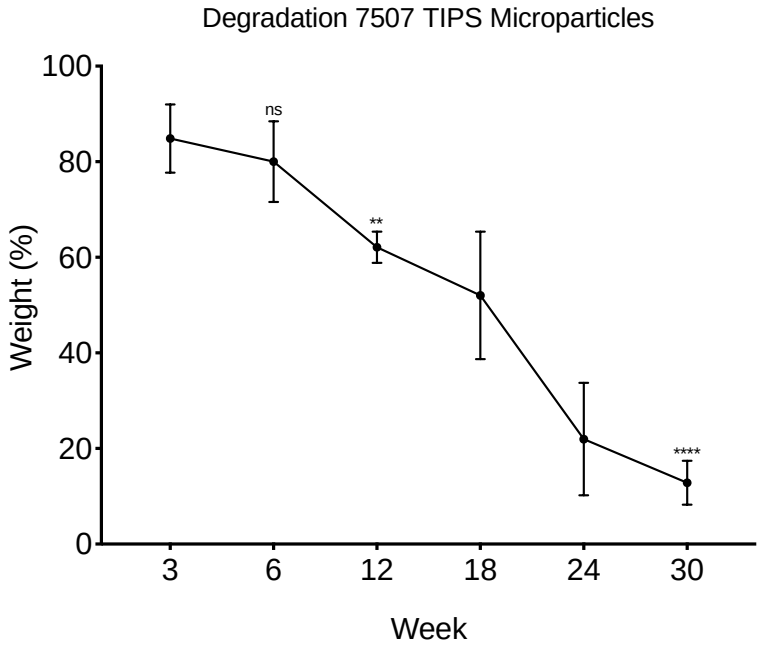

Figure 2.5: b) degradation of PLGA 7507 TIPS microparticles as weight percentage loss (n=5). Weight loss at week 6 was statistically lower (P<0.01 = **) at week 6 from week 3 and at week 30 lower than week 3 (P<0.0001 = ****)

2.3.3 Investigating the Internal Structure of TIPS Microparticles

The internal structure of PLGA 7507 and 7502 TIPS microparticles were studied using X-ray NanoCT techniques. Reconstructed images (Figure 2.6) reveal that TIPS processed polymers had interconnected porous networks beyond the surfaces of the samples.

FIB was able to capture images beyond the surface of the materials by milling 3 µm deep into the microparticle. Images reveal that 7507 TIPS processed microparticles were porous beyond the surface, with micro and nano pores visible. In addition, high-magnification microscopy showed the large radiating surface pore typically associated with the TIPS manufacturing process. The large surface pore opened into a cavity within the microparticles. Radial channels were visible throughout the internal structure of the microparticles. (Figure 2.7)

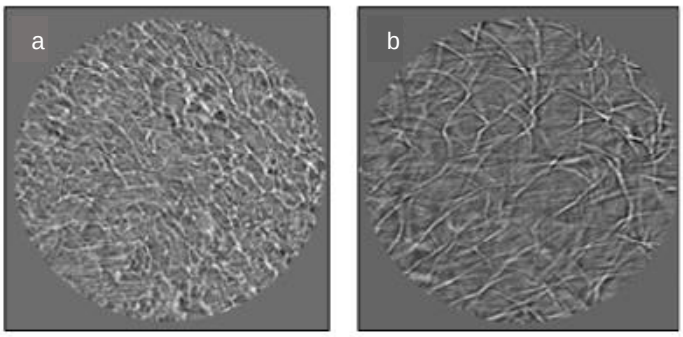

Figure 2.6: NanoCT images a) z-stack of PLGA 7507 TIPS microparticle b) z-stack of PLGA 7502 TIPS microparticle

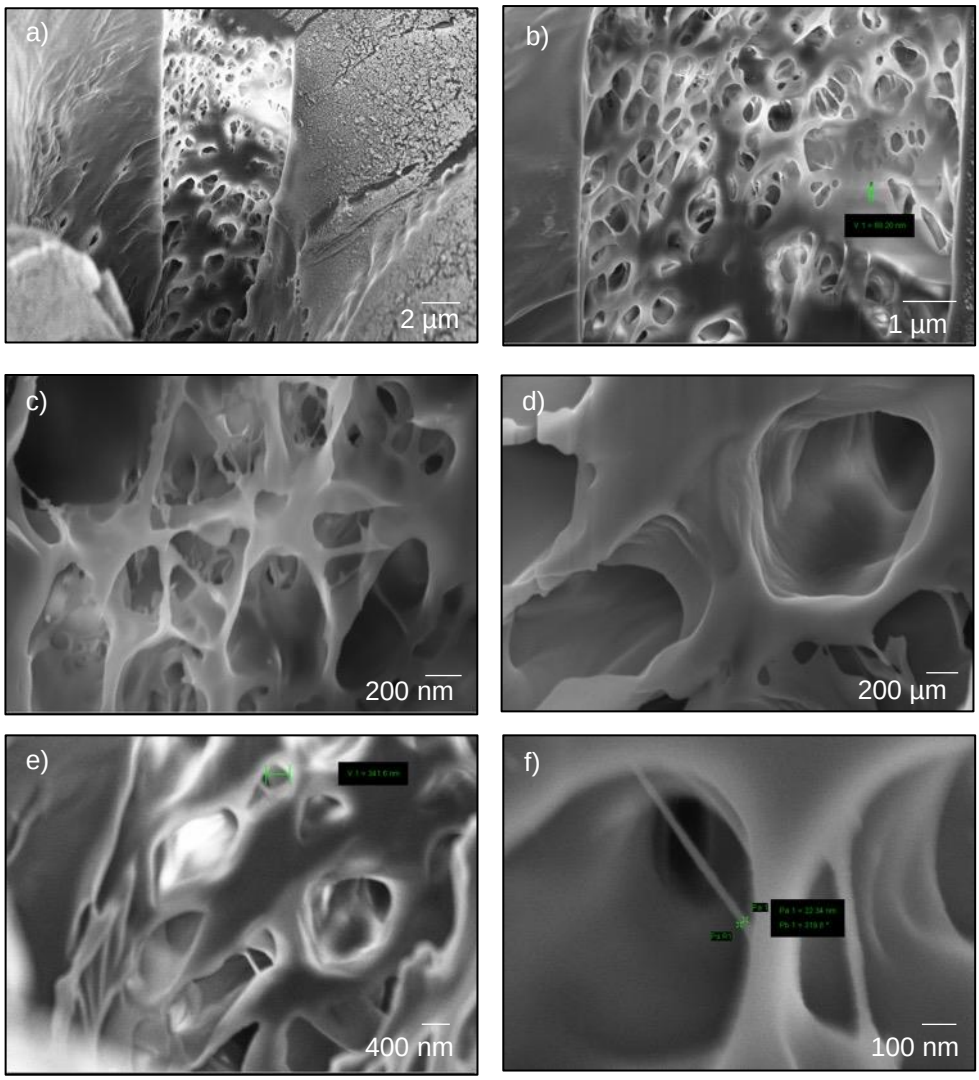

Figure 2.7: FIB-SEM images of PLGA 7507 TIPS microparticles a) 3µm mill into the radial pore of the microparticle b-f) internal structure of microparticles.

2.4 Discussion

This chapter explored the production and characterisation of TIPS PLGA microparticles. Microscopy techniques were used to visualise the structure of the TIPS microparticles and the subsequent degradation rate of the materials were investigated. SEM revealed that PLGA microparticles manufactured through TIPS processing had produced structures with highly rough and porous surfaces (Figure 2.1). These findings were similar to those in Part I. Section 2.3.1 where the surface topographies of TIPS-processed polymer films were produced and characterised. This highlights that the TIPS technique can be used to produce a range of biomaterial structures. This is beneficial as the manufacture of materials can be tuned to the optimal size for the desired application.

The degradation of PLGA 7507 TIPS microparticles were investigated through SEM, mass loss and pH changes. SEM imaging (Figure 2.2) revealed that the 7507 TIPS microparticles began to degrade at early time points as did the PLGA 7507 TIPS polymer films. The TIPS 7507 TIPS microparticles degraded at a much faster rate than control PLGA and polystyrene microparticles that showed little sign of degradation after 10 days. The difference in porosity between the TIPS microparticles and control microparticles was a driving factor in the degradation rate. Porosity provided a larger surface area to volume ratio for the contact of H_2O on the surface of the material, which broke down the polymer chains through hydrolysis of the ester bonds resulting in faster degradation rates. [105, 122, 204] The degradation of a biomaterial is a beneficial property as it negates the need for removal surgeries and eliminates the risk of a prolonged immune response. The advantage of PLGA is that its degradation products are lactic acid and glycolic acid, which are metabolised naturally by the body. [105, 467, 468] In addition, the TIPS process can be tuned to allow the polymer to degrade in time to the healing process and new tissue formation. [469, 470]

The internal structure of TIPS microparticles were investigated using FIB. FIB revealed that the microparticles were porous beyond their surfaces. High magnification images (Figure 2.7) showed pores on the nanoscale, indicating a hierarchical structure of the microparticles, with evidence of nano-size features (Figures 2.7d and 2.7e) within the structure. The internal structure of the TIPS microparticles was further assessed using NanoCT. NanoCT has been developed from established computed topography techniques, most commonly used for medical imaging that can image with spatial resolutions in the millimetre range. From this, microCT was developed that can produce images with a spatial resolution in the micron range, and then nanoCT was developed that has resolution in the nano range. Computed topography is primarily used as a non-destructive internal imaging technique. [471] In comparison to FIB, NanoCT was non-destructive and did not require drying of the sample, coating or placement under vacuum. [472] The 3D reconstructions of the TIPS microparticles revealed an internal interconnected highly porous network suggesting that the TIPS microparticles would remain porous as they degraded. This allows for cell and tissue ingrowth and importantly transfer of nutrients and waste products. The difference between 7502 TIPS microparticle and 7507 TIPS microparticle nanoCT reconstructions (Figure 2.6) were because of the larger pores seen with 7502 TIPS microparticles (Figure 2.1). The difference in pore size is due to the higher inherent viscosity of PLGA 7507 compared to PLGA 7502 as, during TIPS processing phase separation is slowed through decreased motility of the molecules within the polymer resulting in smaller pore size. [473] Pore size influences cell attachment, cell proliferation and tissue ingrowth. With larger pores hindering cell migration and proliferation and smaller pores hindering nutrient diffusion, [474, 475] suggesting that the 7507 TIPS microparticles would improve the response of cells in comparison to 7502 TIPS microparticles.

2.5 Summary

The TIPS process was utilised to produce PLGA microparticles with rough surface topographies and interconnected porous structures. The 7507 TIPS microparticles were shown to degrade steadily over time and at a faster rate than 7507 PLGA and polystyrene control microparticles, due to their increased porosity. To investigate the effect of the TIPS structure on cellular behaviour, the TIPS microparticles were studied further for their effect on ADMSC attachment, proliferation and angiogenic behaviour in comparison to smooth controls, with a view to explore how surface topography and porosity can influence cell behaviours.

Part II.

Chapter 3 Biological Characterisation of TIPS Microparticles

3.1 Introduction

A major limitation of cell therapy is the delivery and retention of viable cells at the implant site. [5, 74, 89-91] To overcome this, cells can be seeded onto a scaffold before delivery *in vivo* with a view to improve cell retention. Before this, the behaviour of the cells on the materials must be established. This chapter explored the attachment of ADMSCs on TIPS microparticles, that were chosen due to their pro-angiogenic behaviour. [76-79, 240] The angiogenic response of the ADMSCs to the unique structure of the TIPS-processed materials were also investigated.

3.2 Methods

3.2.1 Adipose Derived Mesenchymal Stem Cell Culture

ADMSCs culture protocol and media preparation was carried out as described in Part I. Section 4.2.1.

3.2.2 Verifying the Plasticity of Adipose Derived Mesenchymal Stem Cells

To assess if the cells used during the project retained their plasticity after passaging, cell differentiation towards adipogenic, osteogenic and chondrogenic phenotype was performed. To detect osteogenic cells, Alizarin Red was used. Alizarin red stains extracellular calcium deposits by binding to calcium in a chelation process that precipitates and stains red. Stained osteocytes were imaged using light microscopy. LipidTOX was used to identify adipocytes as the stain has a high affinity phospholipidosis within cells and fluoresces green (emission 505 nm). DAPI was used as a nuclear and chromosome counterstain for the adipogenic cells. [476] Alician blue was used to detect cells differentiated towards chondrocytic lineages as it stains acidic glycosaminoglycans in cartilage. [477]

3.2.3 Attaching Cells onto TIPS Microparticles

Before use, TIPS microparticles were prepared for cell attachment. 7 mL 100% absolute ethanol was added to 3 mL sterile deionised water. 1 mL of the 70% absolute ethanol (E10600/05, Fisher Scientific, UK) was added to 4 mL MesenPro RS^{TM} reduced serum medium. Using a spoon-ended spatula (micro 185/7 mm, 2310470, VWR, UK), two scoops of microparticles were added to a glass vial. 1 mL of the ethanol/media solution was added gently to the glass vial. The vial was sealed with a rubber stopper and wrapped in Parafilm (BRND701611, VWR, UK). The vial was vortexed (Vortex Genie 2) for 10-15 seconds and centrifuged at 3,000 rpm for 5 minutes. The samples were incubated in a hybridisation oven for 24 hours at 37^{o}C at constant rotation. The wetting media was removed and microparticles were washed in 1 mL 1X PBS.

Approximately 10 mg of the wetted TIPS microparticles were transferred to a 96 well flat bottomed ultra-low attachment plate (CLS3474, Corning, UK) in 50 µL complete MesenPro RS^{TM} media. The plate was incubated for 12 hours using a microplate shaker (SciQuip Microplate mixer) that shook the microplate for 10 seconds every hour at low speed (approximately 100 rpm) at 37^{o}C 5% CO_2. The cell attachment and proliferation were monitored via light microscopy. The culture medium was removed, and the samples washed twice with 1X PBS to remove any unattached cells and residual culture media.

3.2.3.1 Attaching Cells to TIPS Microparticles Using the Hanging Drop Method

Perfecta3D 96-well Hanging drop plates (HDP1096-8, 3D Biomatrix, USA) were used to attach cells to individual microparticles. The hanging drop plates were disassembled and both reservoirs of the bottom plate were filled with 1 mL sterilised deionised water and the reservoirs of the middle plate were filled with 2 mL sterilised deionised water to create a humidified atmosphere. The plates were reassembled and single hydrophilised 7502 PLGA TIPS, 7507 PLGA TIPS, 7507 PLGA control and polystyrene microparticles in 35 µL prewarmed MesenPro RS^{TM} reduced serum were pipetted into each well at a 45-degree angle to produce a hanging droplet. 10 µL of 5 x 10^4 cells/mL cell suspension were added to each well. If hanging drops had not formed, a sterile 200 µL pipette tip was gently pushed through the well at a 90^{o} angle, ensuring not to completely push through the droplet. Plates were incubated at 37^{o}C/5% CO_2 for 24 hours.

To collect the supernatants from hanging drop plates, 40 µL of media from each well was pipetted up by pressing a sterile 200 µL pipette tip against the wall of the well at a 45^{o} angle, to avoid pipetting up the microparticle and disrupting the cells on the microparticle. This was carried out at days 1, 4, 7 and 10. The supernatants were frozen for further evaluation and replaced with 45 µL fresh pre-warmed complete MesenPro RS^{TM} medium. Cellularised microparticles were harvested from hanging drop plates by placing the middle well of the plate on top of a sterile ultra-low attachment 96 well plate (CC229,

Appleton Woods, UK). Using a multichannel pipette (P200 Pipetman, Glison, UK), 100 μL of 1X PBS (P5493-1L, Sigma, UK) was pipetted into each well of the hanging drop plate to push through the microparticles into the wells of the 96 well plate, resulting in one microparticle per well.

3.2.4 Quantifying Cells Attached to Microparticles and Polymer Films

3.2.4.1 Cell Counting with a Haemocytometer

Hanging drops with one PLGA 7507 TIPS microparticle or PLGA 7502 TIPS microparticle were seeded with 1000, 500, 250, 125 ADMSCs per well in 45 μL complete MesenPro RS™ media. Plates were incubated for 24 hours at 37ºC/5% CO_2. Hanging drops were retrieved in 96 well plate and gently washed with 100 μL 1X PBS (P5493-1L, Sigma, UK). The 1X PBS was discarded and 50 μL 0.25% sterile filtered 1X Trypsin-EDTA solution (pH 7.0 -7.6, T4049, Sigma, UK) was added. Plates were incubated at 37ºC and 5% CO_2 for 5 minutes. 100 μL of complete MesenPro RS™ media was added to each well to neutralise the trypsin. The media from each well was placed into a haemocytometer for counting.

3.2.4.2 Measuring Cell Proliferation with CyQUANT NF Cell Proliferation Assay

CyQUANT NF assay (C35006, Molecular Probes, UK) procedure for adherent cells was followed. The dye was prepared by first diluting the provided x5 HBSS stock buffer to x1 HBSS buffer with deionised water in accordance with the manufacturer's instructions. 22 μL of CyQUANT NF dye reagent (protected from light) was added to 10 mL x1 HBSS buffer.

A standard curve was produced for experiments using cells in hanging drop plates to calculate cell numbers from fluorescence from unknown samples. In a sterile, 96 well hanging drop plate, serial dilutions of ADMSCs from 2000 cells/well to 8 in 45 μL of complete MesenPro RS™ medium were seeded into each well in triplicate. The plates were incubated at 37ºC/5% CO_2 for 24 hours to allow cell spheroid development. 35 μL of the culture medium was removed and the samples were gently washed twice with 35 μL of 1X PBS (P5493-1L,

Sigma, UK). 35µl of the prepared CyQUANT NF dye solution was added to each well and the plate was incubated for 1 hour. From each sample 45 µL of supernatant was transferred to a Corning 96 well black wall with a clear flat bottom tissue culture plate in triplicate (CLS3603, Sigma-aldrich, UK) (n=5). The fluorescence intensity was measured using a fluorescence microplate reader (TECAN SPECTRAFLUOR Fluorescence and Absorbance microplate reader, BETAFTC program, Tecan, Switzerland) at 485 nm excitation and 530 nm emission detection. The same procedure for the standard curve was followed to calculate cell number attached to each microparticle.

3.2.4.3 Measuring Cell Proliferation with PrestoBlue® Cell Viability Reagent

PrestoBlue® Cell viability reagent (A13261, Molecular Probes, UK) had to first be optimised before used to calculate cell numbers attached to microparticles. An optimisation experiment was carried out to determine the most appropriate detection method and incubation time. Absorbance at 570 nm excitation and 620 emission was compared to fluorescence at 535 nm excitation and 612 nm emission. ADMSCs (8000 to 16 cells/well) were seeded into hanging drop plates in 45 µL of complete MesenPro RS™ media and incubated at 37°C/5% CO_2 for 24 hours. 4.5 µL of PrestoBlue® was added directly to each well of the hanging drop plate. Samples were measured for absorbance and fluorescence at 0.1, 0.5, 1, 2, 4, 5, 21 and 24 hours.

To calculate cell numbers on cellularised microparticles 4.5 µL PrestoBlue® reagent was added directly into each well and incubated for 21 hours at 37°C 5% CO_2 avoiding exposure to direct light. Samples were transferred into a black wall/clear flat bottom 96 well tissue culture plate and read using a fluorescence microplate reader at 530 nm excitation and 612 nm emission detection. (n=8)

3.2.4.4 Measuring Cell Proliferation with CellTox Green

CellTox green cytotoxicity assay (G8741, Promega, UK) was used to measure numbers of cells attached to microparticles. The assay dye enters dead cells

through compromised cell membranes and binds to the DNA. A lysis solution was added to the samples, to induce death and allow for detection through fluorescence. [478] To produce a standard curve ADMSCs were harvested and resuspended in 1 mL fresh medium and counted using 0.4% trypan blue (11538886, Fisher Scientific, UK) and haemocytometer. Cell concentrations were adjusted to 200,000 viable cells/mL in at least 4 mL fresh medium. The cell suspensions were divided equally in half. To the first tube, 80 μL lysis solution for every 2 mL suspension was added to create a cytotoxicity control. To the other cell suspension, 80 μL fresh media was added for every 2 mL suspension. To a black well plate 100 μL of fresh MesenPro RS™ media was added to each well. 100 μL of the cytotoxicity control was added to the first 4 wells of column 1 in the plate. Serial dilutions were created along the plate. With the last 4 wells of column 1, the same process was repeated with the viable cell suspension. To all wells 100 μL of CellTOX green 2x reagent was added. The plate was mixed for 30 seconds by orbital shaking 500-700 rpm and incubated for 15 minutes at room temperature. Fluorescence at excitation 485 nm and emission 535 nm was measured.

Hanging drops with one 7507 microparticle were seeded with 500 ADMSCs per well in 45 μL complete MesenPro RS™ media. Plates were incubated for 24 hours at 37°C/5% CO_2. Hanging drops were retrieved in 96 well plate and gently washed with 100 μL 1X PBS. A lysis solution was created by combining 8 μL lysis stock to 200 μL MesenPro RS™ media. 20 μL of the lysis solution was added to each well and incubated for 30 minutes at 37°C/5% CO_2. CellTOX green solution was created by adding 10 μL CellTOX green stock to 5 mL MesenPro RS™ media. 20 μL of the solution was added to each well, incubated for 15 minutes at 37°C and 5% CO_2 while being protected from the light. Plates were read with a plate reader at 490/535 nm.

3.2.5 Staining Cell Nuclei with DAPI

To stain the nuclei of cellularised microparticles 20-40 μL of cellularised microparticles in suspension were pipetted onto a glass microscope slide. The

residual cell culture medium removed, leaving only the microparticles. Two drops of DAPI mountant medium (VECTASHEILD Antifade mounting medium, H-1200, Vector Laboratories, UK) was added and the sample was covered with a glass cover slip. The slides were imaged using a Lecica Microsystems fluorescence microscope.

3.2.6 Staining Cell Cytoskeleton with Alexa Fluor 488 Phalloidin

To visualise ADMSC attachment to 7507 TIPS microparticles, ADMSCs were seeded onto 7507 TIPS microparticles in hanging drops and retrieved as described in section 3.2.14. The cellularised microparticles were gently washed twice with 100 µL prewarmed 1X PBS (P5493-1L, Sigma, UK). The samples were fixed in 100 µL 2.5% formaldehyde (HT501128, Sigma-Aldrich, UK) for 10 minutes at room temperature. The samples were washed in prewarmed 1X PBS twice and incubated in 0.1% Triton X-100 (T8787, Sigma, UK) in 1X PBS for 5 minutes at room temperature. The samples were washed in prewarmed 1X PBS twice and incubated in 250 µL 1% BSA (>96%, 05482, Sigma, UK) in 1X PBS for 30 minutes at room temperature. Alexa Fluor 488 phalloidin stain (A1239, ThermoFisher, UK) was diluted at a ratio of 1:4 in 1X PBS. The stain was added to each sample and incubated at room temperature for 20 minutes whilst protected from light. Samples were washed twice with 1X PBS and transferred to microscope slides, counterstained and mounted with 4', 6-diamidino-2-phenylindole (DAPI) mountant (VECTASHEILD Antifade mounting medium, H-1200, Vector Laboratories, UK). Images were taken with an SPE1 fluorescence microscope under 495 nm excitation and 518 nm emission.

3.2.7 Statistical Analysis

Statistical Analysis methodology was described in Chapter 2 Section 2.2.7.

3.3 Results

3.3.1 Verifying the Plasticity of Adipose Derived Mesenchymal Stem Cells

To assess if the cells used during the project retained their plasticity after passaging and cell culture, cell differentiation towards adipogenic, osteogenic and chondrogenic phenotype was performed. Staining and imaging revealed that the cells seeded in monolayers were capable of differentiation into all three linages, although some cells remained undifferentiated in the adipogenic and osteogenic cultured (Figures 3.1a-d). To ensure consistency only cells between passages 3 and 6 were used in all experiments. In addition, ADMSCs seeded onto 7507 TIPS microparticles were allowed to migrate off the microparticles, and were differentiated into adipogenic, osteogenic and chondrogenic phenotypes to assess if attachment to the TIPS microparticles affected ADMSC plasticity. Figures 3.1 (e - g) showed that ADMSCs successfully differentiated into adipogenic and osteogenic lineages, but differentiation into chondrogenic phenotype was unsuccessful.

3.3.2 Imaging Cellularised Microparticles

ADMSCs seeded onto microparticles were imaged under light microscopy and stained with DAPI that binds to A-T bases in live cells. Images revealed that microparticles clustered together as cells attached to microparticles had bridged together, indicated by arrows in Figure 3.2.

3.3.3 Imaging Microparticles Cellularised in Hanging Drop Plates

Cell attachment to TIPS microspheres was visualised using light and fluorescence microscopy. Light microscopy images of ADMSCs attached to 7507 TIPS polymers in hanging drop plates showed that cells after 1 day had successfully adhered and covered the TIPS microparticle and that proliferation continued to day 10 with outgrowth visible. Figure 3.3 revealed that ADMSCs

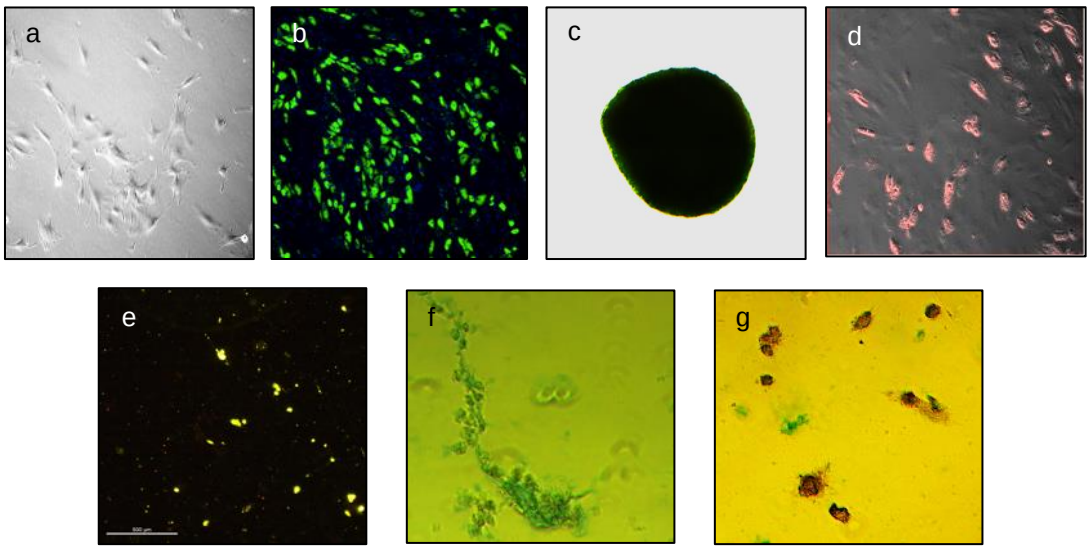

Figure 3.1: a) undifferentiated ADMSCs b) fluorescent image of LipidTOX green staining for adipogenic differentiation of ADMSCs c) optical image of alcian blue staining for chondrogenic differentiation of ADMSCs d) optical image of alizarin red staining for osteogenic differentiation of ADMSCs e) fluorescent image of LipidTOX green staining for adipogenic differentiation of ADMSCs from 7507 TIPS microparticles f) optical image of alcian blue staining for chondrogenic differentiation of ADMSCs from 7507 TIPS microparticles g) optical image of alizarin red staining for osteogenic differentiation of ADMSCs from 7507 TIPS microparticles.

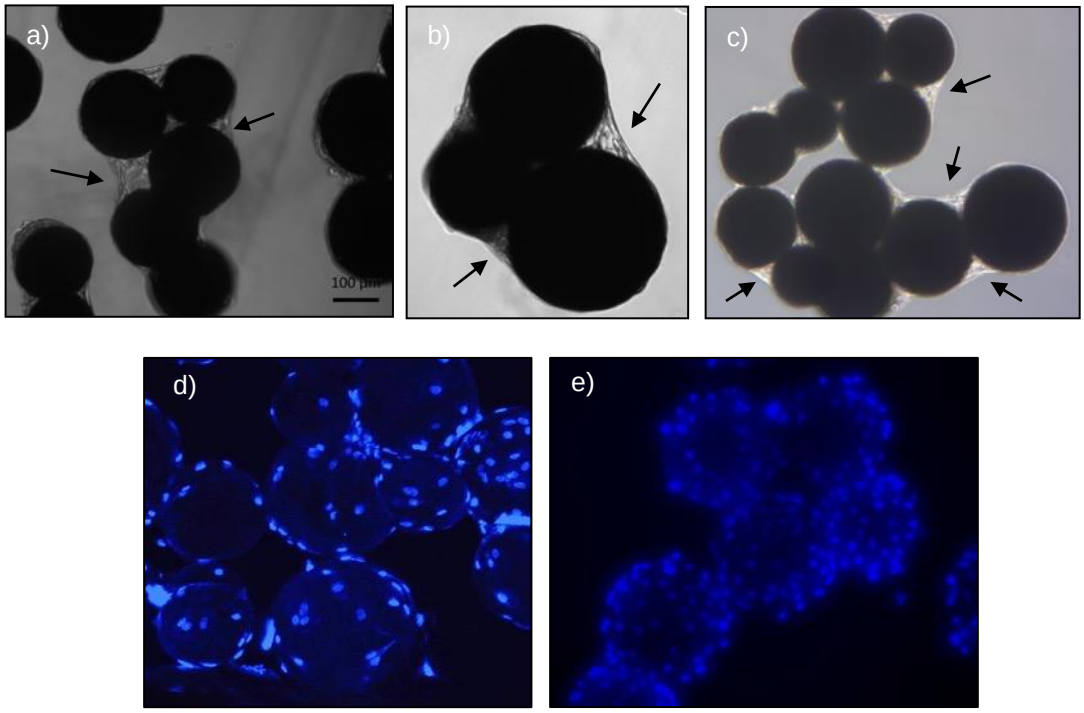

Figure 3.2: a-c) Light microscopy images of 7507 TIPS microparticles seeded with ADMSCs d-e) Fluorescent images of DAPI stained ADMSCs seeded onto 7507 TIPS microparticles.

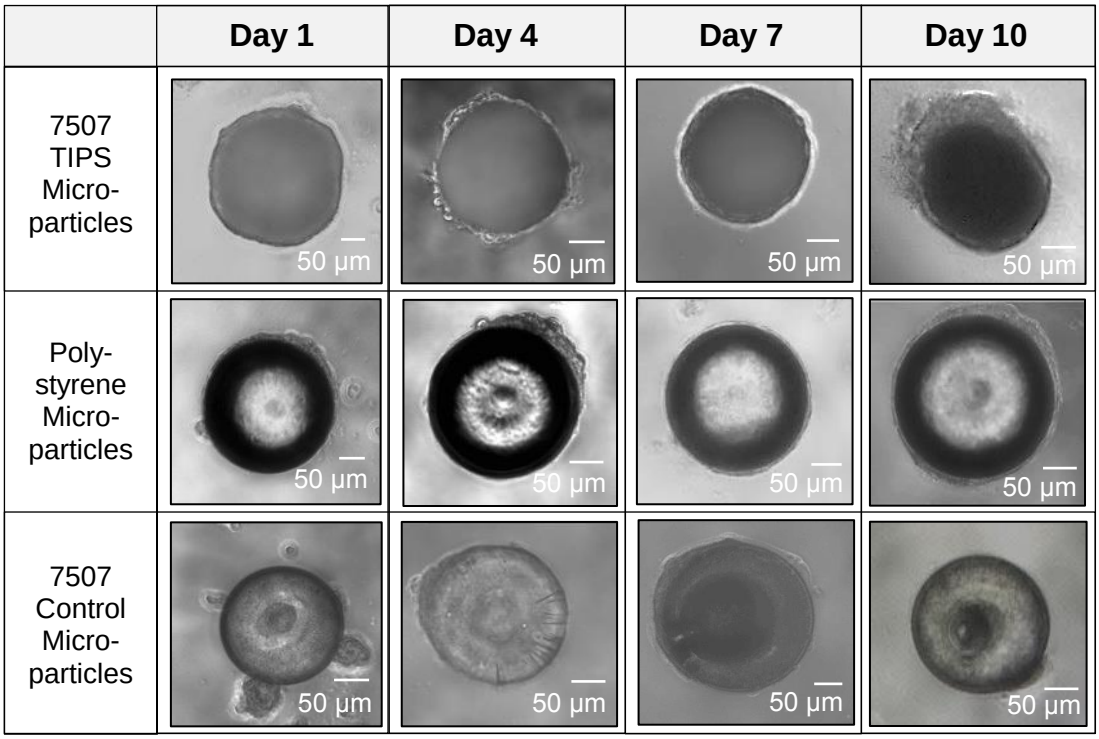

Figure 3.3: Optical imaging of ADMSCs seeded onto 7507 TIPS microparticles, 7507 control microparticles and polystyrene control microparticles at days 1, 4, 7 and 10.

successfully attached to polystyrene microparticles with some proliferation seen at day 10. At day 1 cells had less successfully attached to control PLGA 7507 microparticles, with clusters of cells visible. After 4 days the ADMSCs had appeared to spread more evenly around the smooth microparticle but less cell proliferation was seen in comparison to 7507 TIPS microparticles.

Alexa Fluor 488 phalloidin was used to stain the actin cytoskeleton of ADMSCs and DAPI was used as a nucleic counterstain. Figure 3.4 displays fluorescent images of individual microparticles with higher numbers of ADMSCs seen on TIPS 7507 microparticles in comparison to control PLGA microparticles. Figure 3.4d shows a high density of ADMSCs surrounding 7507 TIPS microparticles 4 days after seeding.

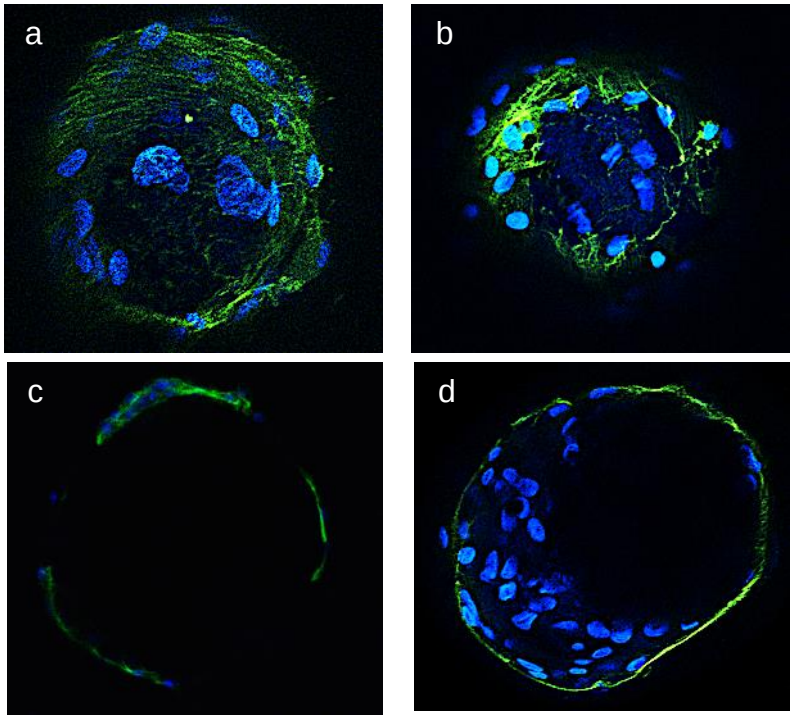

Figure 3.4: Alexa Fluor 488 phalloidin and DAPI fluorescent images of ADMSCs seeded onto microparticles in hanging drops. a-b) Cellularised 7507 TIPS microparticles at day 1 c) Cellularised 7507 control microparticles at day 1 d) Cellularised 7507 TIPS microparticles at day 4.

3.3.4 Determining Cell Number and Measuring Cellular Proliferation

3.3.4.1 Measuring Cell Proliferation with CyQUANT NF Cell Proliferation Assay

When first utilising hanging drop plates to cellularise microparticles CyQUANT NF was used to determine the number of cells attached to 7507 and 7502 TIPS microparticles. ADMSCs were seeded from 1000 to 8 cells/well using serial dilutions. The CyQUANT NF optimisation experiments (Figure 3.5) revealed no significant difference between microparticles seeded with 1000 or 500 cells. There was a significantly higher fluorescence expression for 500 cells seeded onto PLGA 7507 TIPS microspheres in comparison to PLGA 7502 microspheres and cells only.

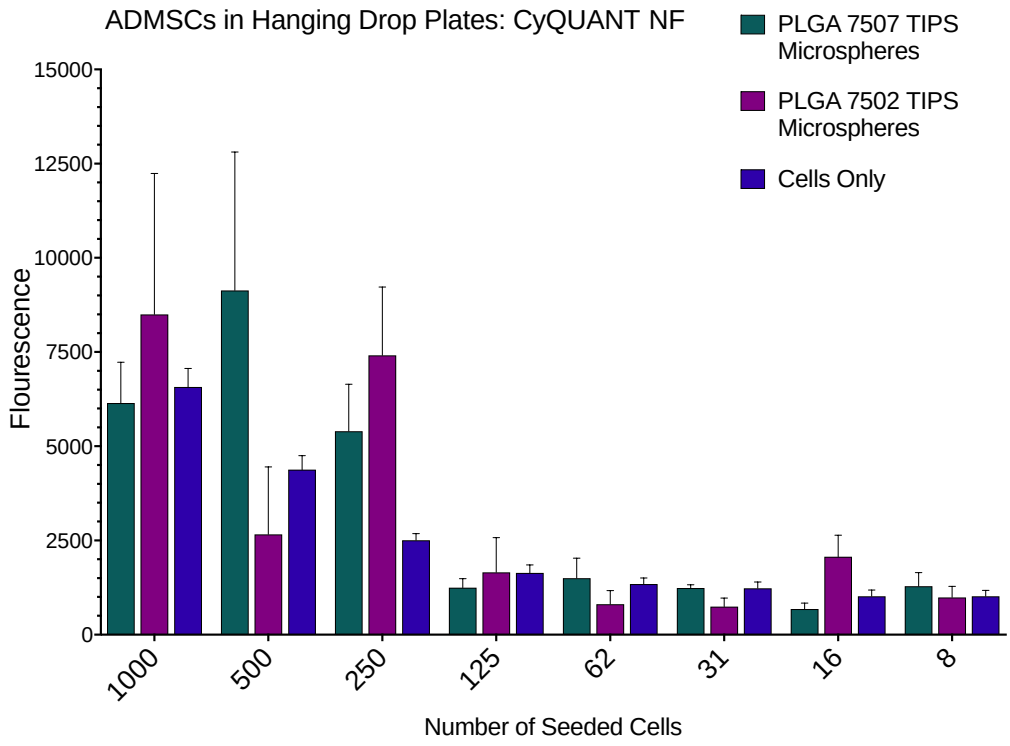

Figure 3.5: Quantification of ADMSCs seeded at concentrations of 1000-8 cells/microparticle onto 7507 TIPS and 7502 TIPS microparticles in hanging drop plates compared to cell only controls calculated using CyQUANT NF cell proliferation assay. (n=5) Two-way ANOVA with Geisser-Greenhouse correction = ** (P=0.0024)

3.3.4.2 Measuring Cell Proliferation with CellTox Green

CellTox Green dye binds to the DNA of lysed cells. With the use of a lysis buffer, cell concentration was determined. Figure 3.6 shows that there were lower cell numbers detected on 7507 TIPS microparticles in comparison to cell only groups at 2000 and 1000 cells. However, below 500 cells, cell concentrations were not significantly different, therefore low cell numbers could not be distinguished and this assay was not used in further studies.

3.3.4.3 Measuring Cell Proliferation with PrestoBlue® Viability Reagent

PrestoBlue® was first optimised by adding the viability reagent to serial dilutions of ADMSCs from 2000 to 8 cells/well within a hanging drop plate. The plates were read for fluorescence (n=3) and absorbance (n=5) after 0.1, 0.5, 1, 1.5, 2, 3, 4, 5, 6, 18 and 24 hours. Results (Figure 3.7) revealed that

an incubation time of 24 hours had the strongest fluorescent readings and significantly significant results and was therefore determined to be the optimal incubation time.

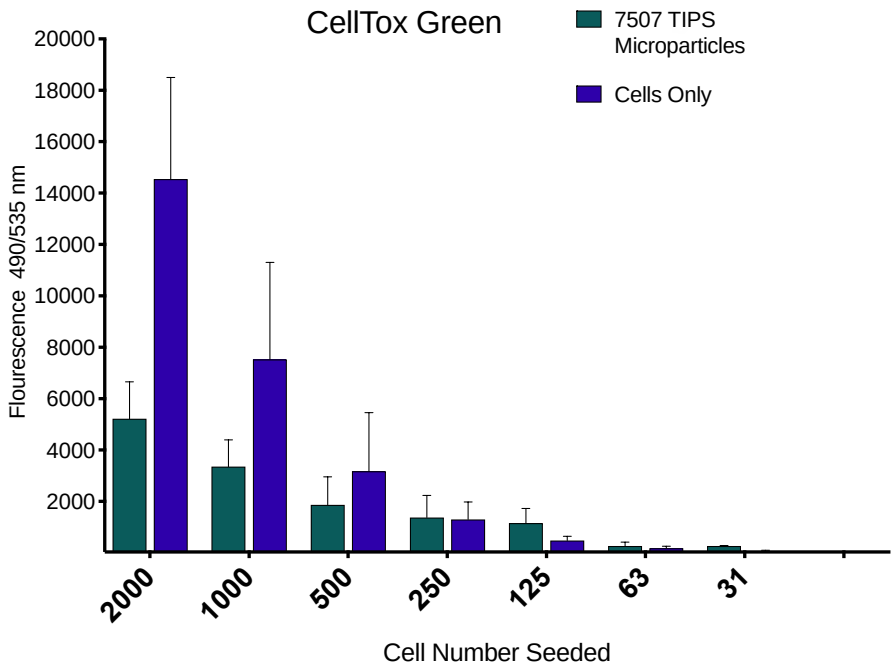

Figure 3.6: ADMSCs seeded at concentrations of 2000-31 cells/microparticle onto 7507 TIPS microparticles in hanging drop plates compared to cell only controls quantified with CellTox Green. (n=3) Two-way ANOVA with Geisser-Greenhouse correction = **** (P<0.0001)

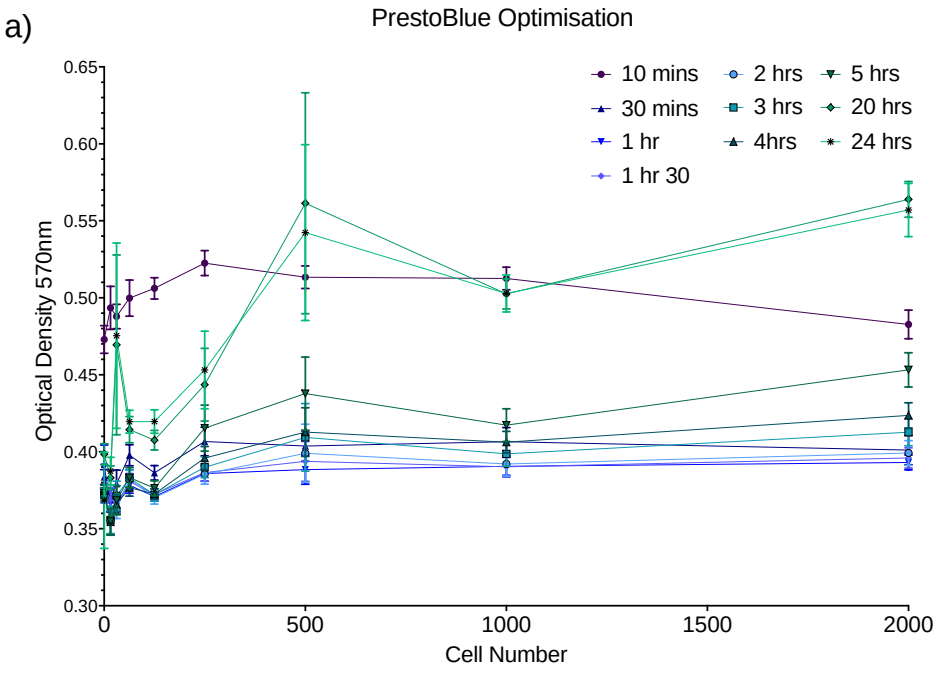

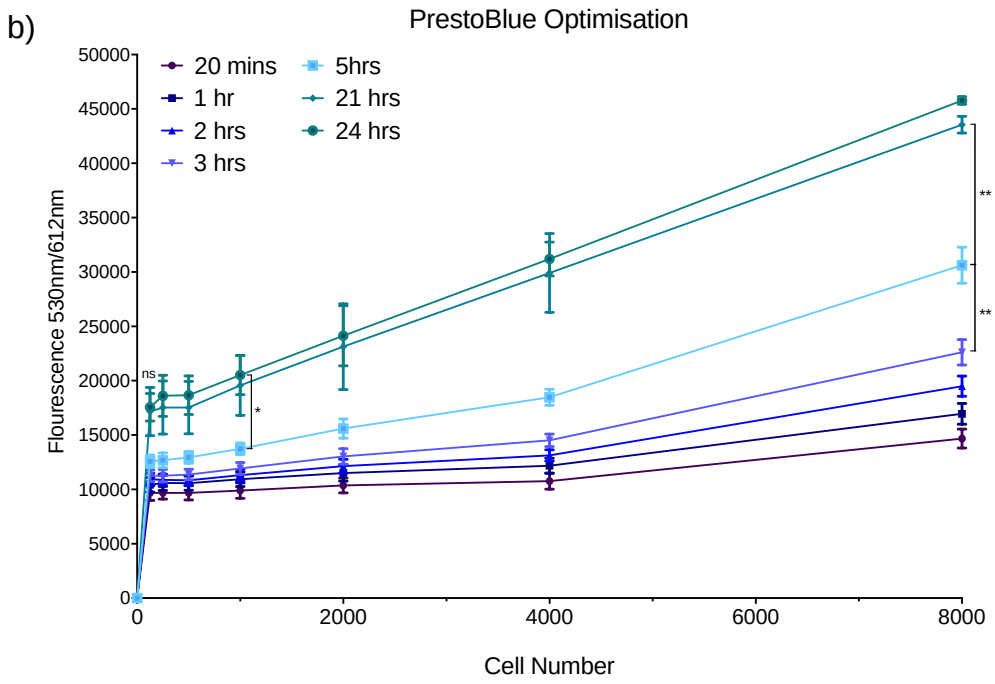

Figure 3.7: PrestoBlue® cell viability assay optimisation experiments a) absorbance readings b) fluorescence (n=3) Where * = P<0.05, ** = P<0.01 and **** = P<0.0001.

PrestoBlue® was able to detect considerably lower cell numbers compared to CyQUANT NF and CellTox Green assays when cells were seeded onto TIPS microparticles. PrestoBlue® was able to show significant difference of detection between 125 and 62 cells seeded onto 7507 TIPS microparticles. In addition, Figure 3.8 revealed that 7507 TIPS microparticles had higher cell numbers in comparison to 7502 TIPS microparticles and polystyrene microparticles (up to 500 cells/well), suggesting that the 7507 TIPS microparticles facilitated cell attachment. Similarly, to measurements with the CyQUANT NF assay, there was no significant difference in detection between 1000 and 500 cells/microparticle, suggesting that 500 cells had saturated the microparticles inhibiting further attachment. As PrestoBlue® was found to be a more sensitive assay, it was selected to determine cell proliferation over 10 days.

Figure 3.9 shows that cells seeded onto 7507 TIPS microparticles had higher attachment (571 ±204 cells/microparticle) compared to PLGA and polystyrene control microparticles (178 ±46 cells/well and 302 ±81 cells/well). The

proliferation of cells was higher on 7507 TIPS microparticles (1769 ±397 cells/microparticle) compared to 7507 control and polystyrene microparticles from day 1 to 10. 7507 TIPS microparticles supported the highest proliferation rates after 10 days, with 1769 ±397 cells per microparticle (in comparison to PLGA control microparticles 868 ±267 cells/well and polystyrene microparticles 1417 ±294 cells/well). Polystyrene microparticles had significantly higher numbers of cells at all the time points compared with smooth PLGA microparticles, which had the overall lowest cell attachment and proliferation numbers. This suggests that smooth PLGA control microparticles did not facilitate cell attachment.

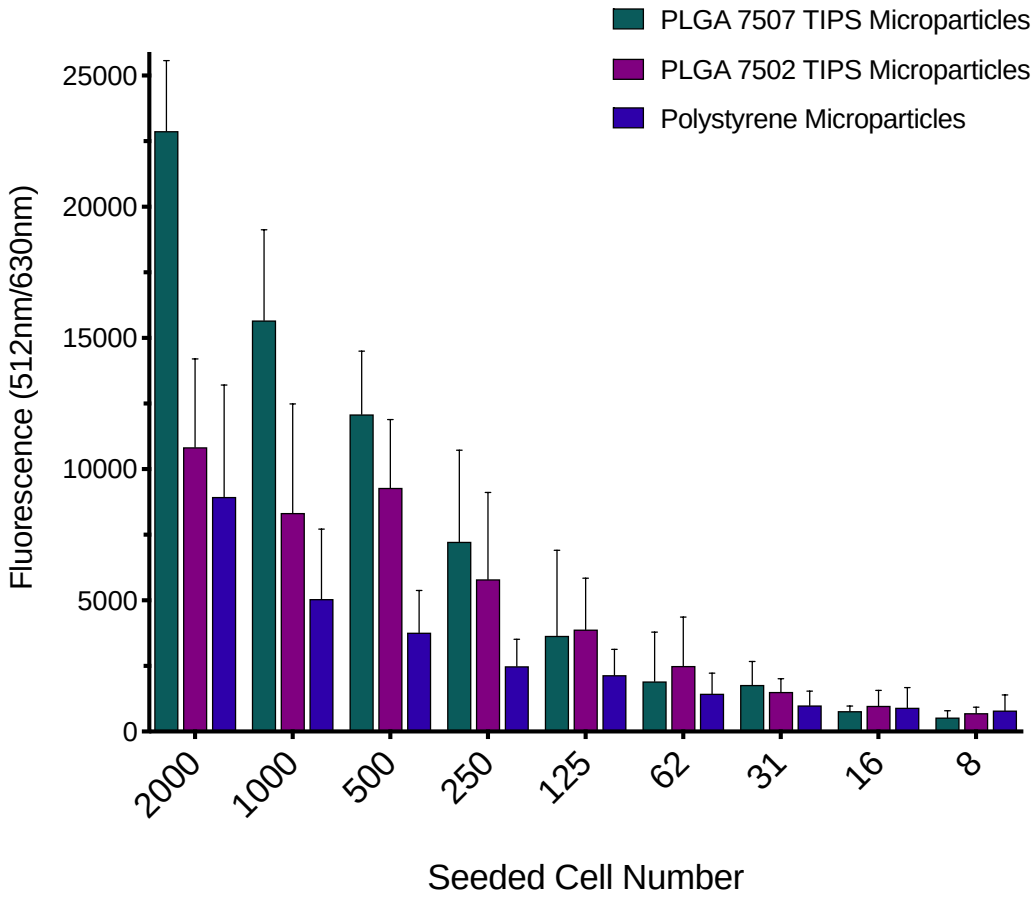

Figure 3.8: PrestoBlue® results of ADMSCs seeded at concentrations of 2000-8 cells/microparticle onto 7507 and 7502 TIPS microparticles in hanging drop plates compared to cell only controls. (n=3) Two-way ANOVA with Geisser-Greenhouse correction

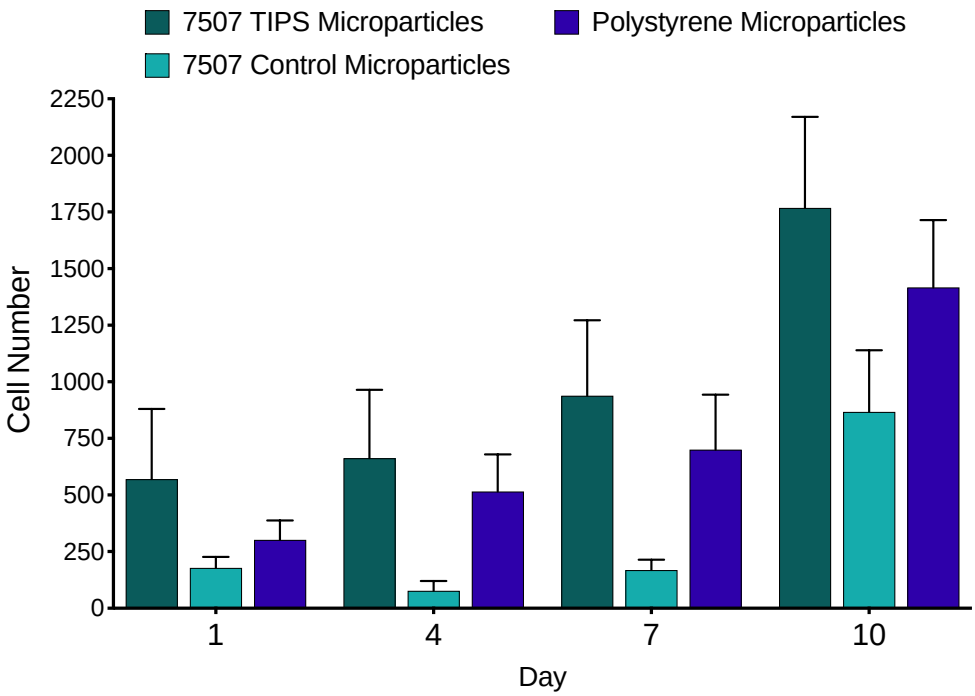

Figure 3.9: PrestoBlue® results of ADMSCs seeded onto 7507 TIPS microparticles, 7507 control microparticles and polystyrene control microparticles. (n=8) Two-way ANOVA with Geisser-Greenhouse correction = ** (P<0.0046)

3.3 Discussion

To assess the plasticity of the ADMSCs used, the cells at passage 9 were differentiated into osteo-, adipo- and chondro-cyte lineages. Cells successfully differentiated into all three lineages and from this it was decided that ADSMCs were used up to a maximum passage of 9 (Figure 3.1). It has been discovered that on occasion stem cells can spontaneously differentiate when exposed to biomaterials. For example, materials with higher stiffnesses have been shown to promote osteogenic differentiation. [181, 479] As the purpose of this study was to exploit the pro-angiogenic behaviour of ADMSCs (attached to TIPS-processed materials) for therapeutic angiogenesis, spontaneous differentiation would be undesirable and may hinder the angiogenic behaviour of the cells. Therefore, ADMSCs were attached to 7507 TIPS microparticles and were allowed to migrate off the TIPS microparticles and incubated in conditions to promote differentiation into osteo-, adipo- and chondro-cyte lineages to assess if the TIPS microparticles effected the plasticity of the stem cells. Staining revealed that the ADMSCs had successfully differentiated into osteo- and adipo-cyte linages. Unfortunately, the differentiation into chondrocytes was unsuccessful as to the differentiation process for chondrocytes required a high density of cells in a pellet to induce spheroid formation. The cells that migrated off the microparticles were in a monolayer and were not available at a high enough concentration to induce chondrocyte formation. Future studies could pool samples together to achieve a high concentration of cells to allow for chondrocyte differentiation. Since the cells did differentiate into osteo- and adipo-cytes, it was concluded that attachment on TIPS 7507 microparticles did not affect the plasticity of the ADMSCs.

Hanging drop plates were originally designed to induce spheroid formation, with an adherent cell suspensions added to each well and forced into a spheroid by eliminating the opportunity for cellular adherence to a surface. This technique was modified to attach ADMSCs to individual microparticles as by using the hanging drop method, the cells could only attach to the microparticles, thus, (after the retrieval of the microparticles from the plate and the removal of any unattached cells), any differences in cellular behaviour seen between TIPS and control microparticles could be attributed to the

differences in the structure and topographies of the microparticles (Part II. Chapter 2). In addition, the use of hanging drop plates eliminated clumping effects seen between microparticles (Figure 3.2) that resulted in the incomplete cellular coverage of the microparticles. Envisaging the delivery of cellularised microparticles as a treatment for PAD in future studies, more microparticles would be required (if clumped together) to deliver the same number of cells. This would be less cost-efficient and influence the ease of administration. Moreover, by seeding individual microparticles the number of cells per microparticle were more accurately determined. This is important for *in vivo* studies where it is vital to know the number of cells administered to avoid any negative side effects from over-administering a stem cell therapy. [45] One limitation of this method is its ability to be high-throughput. The seeding of individual microparticles is time consuming, especially when considering that it has been proposed that for cell therapies that tens to millions to billions of cells are required. [480] However the advantages of this method may out way this shortcoming, and it opens up the possibility of developing automated systems that can be used with a variety of microparticles and cells.

ADMSCs were seeded onto PLGA 7507 TIPS, PLGA 7502 TIPS, control PLGA 7507 and control polystyrene microparticles in the hanging drop plates. Figure 3.8 revealed that 7507 TIPS microparticles had superior cell attachment than PLGA 7502 TIPS microparticles, most likely due to the difference in pore size and degradation rate. Due to the fast degradation rate of the PLGA 7502 TIPS microparticles, after hydrophilisation (that was required to allow for cellular attachment due to the hydrophobic nature of PLGA) the microparticles had degraded into an extremely small size and became difficult to handle and visualise, especially when handling individual microparticles. Therefore, 7502 TIPS microparticles were not investigated within the hanging drop plate studies beyond optimisation experiments.

Multiple methods were investigated to accurately determine cell numbers on microparticles. Counting cells with a haemocytometer is a long-standing established method to count cells in suspension. It is quick, cheap and only requires a small amount of cell suspension (10-30 µL). [478] A

haemocytometer was initially used to count cell numbers (detached using trypsin-EDTA) from microparticles. However, haemocytometers are not suitable for counting low cell numbers, as they require scaling up all cell counts by 10^4, therefore if a count is misread by even one cell, the overall cell concentration would be incorrect by 10^4 cells/mL, making the overall error high. Despite the low cost and speed of running haemocytometer counts, the low accuracy and the low cell numbers used for hanging drop experiments meant that this method was only used to determine seeding densities for culturing and passaging cells. Therefore, assays were employed to accurately determine cell numbers.

CyQUANT NF cell proliferation assay was first used determine cell numbers on microparticles from hanging drop plates. CyQUANT NF results (Figure 3.6) indicated that there was no significant difference between 1000 and 500 cells per microparticle, suggesting that 500 cells were sufficient to saturate the microparticles and incubating the microparticles with more than 500 cells would be would not result in further cell attachment. However, as the recommended initial seeding density for ADMSCs is 3-5x10^3 cells/cm^2, [481] and as the Morphologi G3 data (Chapter 2 Table 2.1) had shown that the average size of the 7507 TIPS microparticles to be 300 µm (surface area = 0.028 cm^2), the seeding density for a single microparticle would be calculated as 8-14 cells. As CyQUANT NF assay results (Figure 3.5) were unable to detect significant differences in cell numbers lower than 125 cells, alternative cell proliferation assays (that were capable of detecting lower cell numbers) were explored.

CellTOX Green cytotoxicity assay was considered as it claims sensitivity of 19 cells/well, as well as being quick to perform, with a total assay time of 45 minutes. [482] Despite this, results (Figure 3.6) revealed that in this case, the assay was not capable of detecting cell numbers below 1000 cells/well. In addition, as the assay required a destructive lysis step, therefore it was decided that it would not be used further.

PrestoBlue® cell viability reagent was investigated as it has been shown to have excellent sensitivity, with capabilities to detect cell numbers as low as 12

cells/well, [190, 233] it is a live cell assay (where the dye can be added and removed from cells with no toxic effects) and can be completed in less than 10 minutes. [483] The PrestoBlue® reagent had to first be optimised for use with ADMSCs (stem cells had not been tested or cited by the manufacture) and in the hanging drop plates with microparticles. In addition, it can be read for absorbance and fluorescence, therefore both were investigated for optimal readings at a range of time points from 10 minutes up to 24 hours, as it was reported by Lall *et al.,* 2013, that incubation times of 24 hours may be required for low cell numbers. [234] From the results (Figure 3.7) it was determined that fluorescence (530 nm/612 nm) was the superior method to quantify the colorimetric changes. Fluorescence readings revealed that (Figure 3.7b), cells were detected after 20 minutes, however there was no significant difference between 16 cells/well and 8000 cells/well, suggesting that this was not a long enough incubation time to differentiate between cell densities. When comparing 8000 cells/well fluorescence readings after 20 minutes and 24 hours, there was a significant difference in detection readings. It can be seen that (Figure 3.7b) there was an increase in fluorescence readings that correlated with an increased incubation time. As there was no significant difference between incubation for 21 and 24 hours, it was determined that incubation times of 21 hours was optimal. Optimisation experiments of cells seeded onto 7507 TIPS microparticles show that PrestoBlue® was capable of detecting higher cell numbers compared to PLGA 7502 TIPS and polystyrene microparticles. This trend was also seen in Figure 3.3 and 3.9, where increased numbers of ADMSCs seeded onto 7507 TIPS microparticles were found over 10 days. This suggests that cell attachment was superior on 7507 formulation of TIPS microparticles, which can be attributed to the rough and porous nature of the material.

As stated, the recommended seeding density per microparticle was calculated as 8-14 cells. Unfortunately, none of the assays investigated were able to accurately determine such low cell numbers. In addition, with the error that can occur with accurately seeding such low cell numbers, it was decided that cell seeding numbers of 500 cells per microparticle would be used, as this was

determined to be the optimal initial seeding density (Figures 3.3, 3.5 and 3.8). In addition, on a practical level, attaching 8-14 cells per microparticle would prolong cell culture times and required higher numbers of cellularised constructs for implantations, resulting in increased costs (through increased cell culture times and biomaterials required) and a potential negative immune response from the implantation of a large volume of material. PrestoBlue® was chosen as the optimal assay to determine cell numbers attached to TIPS microparticles (with a 21-hour incubation time) as it had shown superior sensitivity over the other assays investigated.

Part I. Chapter 4 explored TIPS polymer films, and it was shown that similarly to 7507 TIPS microparticles, the 7507 TIPS polymer films had superior cell attachment and proliferation in comparison to 7507 PLGA TIPS films and smooth control films. These findings highlight how different characteristics of various formulations of PLGA can influence cell behaviour. Specifically, Part I. Chapter 3 determined that 7507 TIPS polymer films have increased stiffness and roughness in comparison to 7502 PLGA TIPS films and smooth PLGA controls, where these properties have been shown to positively influence cell attachment and proliferation. [219, 225] Therefore, it could be proffered that the superior cell attachment found on 7507 TIPS microparticles is due to the increase in roughness and stiffness of the 7507 PLGA, however quantification experiments with the microparticles to accurately determine this are required. These were not possible due to the limitations of the AFM. It has been recognised that it is difficult to image and analyse microparticles using AFM, due to the curvature of the particles resulting in artefacts and only small scan areas are possible. [484, 485] An alternative to AFM that could be explored in future studies is optical profilometry, that rather than a cantilever or stylus, uses light to measure surface morphology and is capable of analysing 3D structures. [486]

Nevertheless, the distinctive physical differences between TIPS processed 7507 and 7502 PLGA have influenced ADMSC behaviour through attachment and proliferation, whether manufactured into 2D polymer films or 3D

microparticles. To investigate the cellular behaviour further, the angiogenic response of ADMSCs attached to TIPS microparticles was explored in subsequent chapters.

3.5 Summary

This chapter explored the cellularisation of TIPS processed microparticles through a novel hanging drop technique. The hanging drop method cellularised individual microparticles, allowing for more control over cellularisation and eliminated the effects of tissue culture surfaces. Cell numbers were quantified through the optimisation of a number of assays, where PrestoBlue® cell viability reagent was chosen as the most suitable quantification method. Superior attachment of ADMSCs was seen on 7507 TIPS microparticles through PrestoBlue® readings and optical and fluorescent imaging. This response can be attributed to the increased roughness, porosity and stiffness of TIPS microparticles. This effect was also found with TIPS-processed polymer films, where the 7507 PLGA formulation resulted in increased cell attachment and proliferation (Part I. Chapter 4).

The angiogenic behaviour of ADMSCs seeded onto 7507 TIPS microparticles in hanging drop plates compared to smooth polymer control microparticles were studied in Part II. Chapter 5.

Part II.

Chapter 4 Investigation of Biological Mechanism Responsible for the Observed *In Vitro* Pro-Angiogenic Effect of TIPS-Processed ADMSC Substrates

4.1 Introduction

The angiogenic activity of ADMSCs attached to polymer films was explored in Part I. Chapter 5, with an increase in pro-angiogenic behaviour seen from PLGA 7507 TIPS polymer films compared to PLGA 7502 TIPS polymer films and smooth polymer film controls. This chapter explores if the observed pro-angiogenic effect was also seen with ADMSCs attached to PLGA 7507 TIPS microparticles in hanging drop plates. *In vitro* angiogenesis assays and angiogenic protein profiling were used to investigate the biological mechanism responsible for any angiogenic responses found.

4.2 Methods

4.2.1 Measuring Cell Proliferation of Adipose Derived Mesenchymal Stem Cells on TIPS Microparticles

Cell numbers were measured with PrestoBlue® cell viability reagent as described in Part I. Chapter 4 Section 3.4.2.3 at days 1, 4, 7 and 10.

4.2.3 Measuring In Vitro Angiogenic Activity of Adipose Derived Mesenchymal Stem Cells on TIPS surfaces

4.2.3.1 Measuring Vascular Endothelial Growth Factor$_{165}$ Secretion using Enzyme-linked Immunosorbent Assay

The secretion of $VEGF_{165}$ from ADMSCs seeded onto 7507 TIPS microparticles, 7507 PLGA microparticles and polystyrene microparticles in hanging drop plates at days 1, 4, 7 and 10 (n=7) was analysed by $VEGF_{165}$ ELISA (DY293B, R&D Systems, UK) described in Part I. Section 5.2.2.1.

4.2.3.2 Screening for Angiogenic Protein Secretion from Adipose Derived Mesenchymal Stem Cells Using Human Proteome Profiler Angiogenesis Array

The supernatants from ADMSCs attached onto 7507 TIPS microparticles, 7507 PLGA microparticles and polystyrene microparticles were screened for 55 different angiogenic-related growth factors using a Proteome Profiler angiogenesis array (ARY007, R&D Systems, UK) as described in Part I. Section 5.2.2.2 (n=2).

4.2.3.3 In Vitro Evaluation of Angiogenesis Using a Vasculogenesis to Angiogenesis Array

The supernatants from ADMSCs seeded onto 7507 TIPS microparticles, 7507 PLGA microparticles and polystyrene microparticles were investigated in an *in*

vitro angiogenesis array (V2a array, ZHA-4000, Cellworks, UK) as described in Part I. Section 5.2.2.3.

To assess the effect of pro-angiogenic growth factors and anti-angiogenic factors on the secretion of angiogenic growth factors from ADMSCs cultured on 7507 TIPS microparticles, the V2a array was carried out as described in Part I. Section 5.2.2.3 with the addition of a pro- or anti-angiogenic factor selected from the pro- and anti-angiogenic factors highlighted from the human angiogenic proteome profiler array. 0.1μg of VEGF (ZHA-1300) or 0.2 μg/mL Serpin F1/PEDF Protein (1177-SF-025, R&D, UK) was added to the supernatants from 7507 TIPS microparticles in V2a growth medium. Media changes occurred every 2-3 days for 14 days and tubules were stained with anti-human CD31 antibody and imaged.

4.2.4 Statistical Analysis

Statistical Analysis methodology was described in Chapter 2 Section 2.2.7.

4.3 Results

4.3.1 Vascular Endothelial Growth Factor Secretion from Adipose Derived Mesenchymal Stem Cells on TIPS Microparticles

Figure 4.1 shows the number of ADMSCs attached onto microparticles, with PLGA 7507 TIPS microparticles supporting higher cell attachment and proliferation up to day 10 determined in Chapter 3. The VEGF secretion from ADMSCs seeded onto microparticles were measured and displayed in Figure 4.2a. ADMSCs seeded onto 7507 TIPS microparticles showed an increase of VEGF secretion from day 1 to 10 (283 ±90 pg/mL to 1415 ±490 pg/mL), with the highest VEGF secretion from 7507 TIPS microparticles at day 10 at 1415 ±490 pg/mL in comparison to PLGA 7507 control and polystyrene microparticles (670 ±120 pg/mL and 1186 ±95 pg/mL respectively).

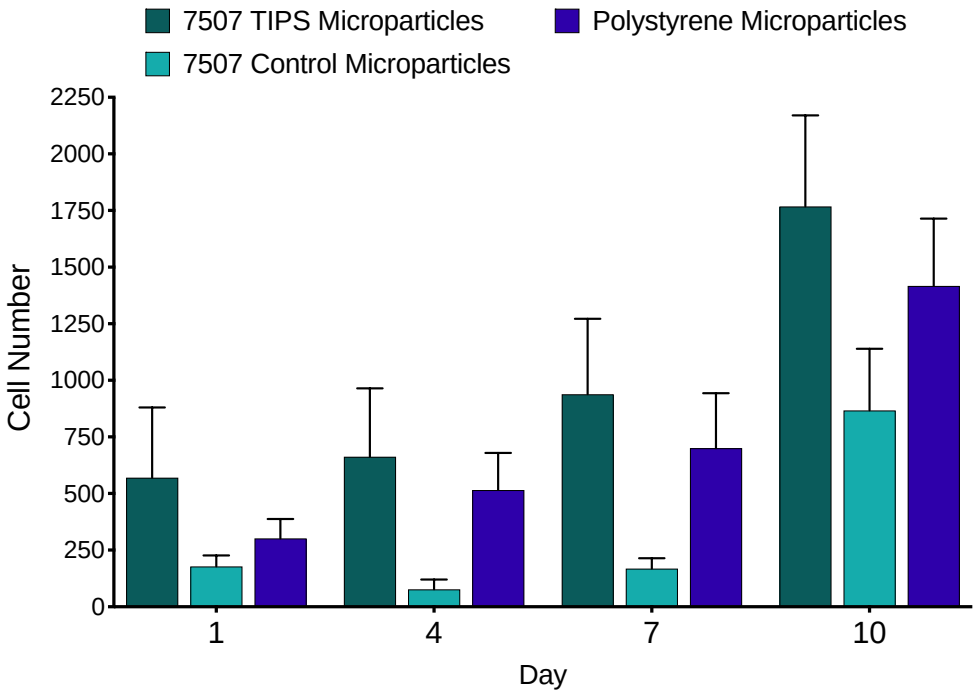

Figure 4.1: Quantification of ADMSCs attached to 7507 TIPS microparticles, control micro-particles and polystyrene control microparticles (n=8). Two-way ANOVA with Geisser-Greehouse correction = ** (P=0.0046)

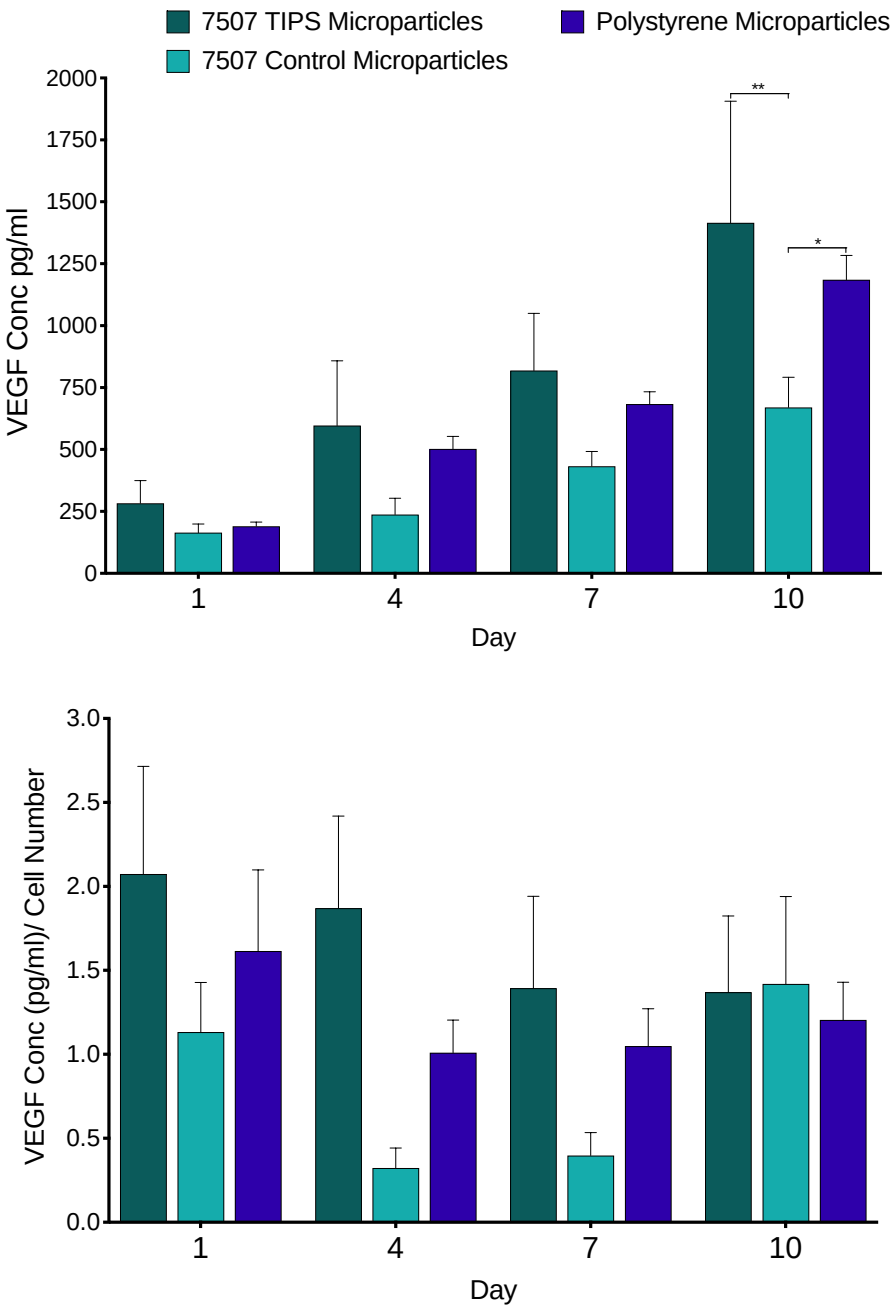

Figure 4.2 a) $VEGF_{165}$ secretion (pg/mL) from ADMSCs attached to 7507 TIPS microparticles, 7507 PLGA control microparticles and polystyrene microparticles (n=7) b) Normalised results showing the amount of VEGF (pg/mL) secreted per cell. Two-way ANOVA with Geisser-Greenhouse correction = ** (P<0.00445)

Normalised results in Figure 4.2b show that at the earlier time points and up to day 7 7507 TIPS microparticles had significantly higher VEGF secretion per cell compared to 7507 control microparticles and polystyrene microparticles (1.9 ±0.5 pg/mL/cell, 0.3 ±0.1 pg/mL/cell, 1.0 ±0.2 pg/mL/cell respectively).

4.3.2 Screening for Angiogenic Protein Secretion from Adipose Derived Mesenchymal Stem Cells Using Human Proteome Profiler Angiogenesis Array

Supernatants from ADMSCs seeded onto microparticles in hanging drop plates were screened using an angiogenic proteome profiler array. Results presented show proteins that had a 2-fold increase/decrease when compared to polystyrene microparticles. Figure 4.3 revealed distinct differences in the secretion of angiogenic related proteins between 7507 TIPS microparticles and 7507 control microparticles normalised to polystyrene control microparticles. Notably, Angiopoietin-2, Amphiregulin, EG-VEGF, IGFBP-1/-3, PD-ECGF, PDGF-AA were down-regulated on 7507 control microparticles and up-regulated on 7507 TIPS microparticles. There were also higher levels of VEGF, PIGF, HGF, IL-1b/-8 and Persephin secreted from ADMSCs seeded onto 7507 TIPS microparticles compared to 7507 PLGA and polystyrene control microparticles.

Supernatants were screened at different time points to assess differences in the secretion of angiogenic growth factors from ADMSCs day 1 to 10. Figures 4.4 – 4.6 shows that at day 1, 20 pro-angiogenic proteins were down. regulated on 7507 PLGA smooth control microparticles and upregulated on 7507 TIPS PLGA microparticles compared with polystyrene smooth microparticles. Of these, there were high levels of VEGF, uPA and PDGF-AB/BB detected and pro-inflammatory Serpin E1, MMP-9, IL-8 and IL-1b detected. After day 1, profilers show that the difference between the pro-angiogenic factors secreted from ADMSCs on microparticles decreased when compared to polystyrene, with the exception of VEGF, uPA, PDGF-AA/AB, persephin, PDGF-AA and PD-ECGF that increased after 10 days on PLGA smooth and TIPS microparticles compared with polystyrene. Throughout the timepoints only a few anti-angiogenic proteins were identified, with the potency of proteins such as Serpin F1, TSP and TIMP-1 decreasing over time on the TIPS 7507 microparticles compared to polystyrene. In addition, the anti-angiogenic proteins CVCL16, Endostatin, PF4 and LAP were found in higher quantities

on cells seeded onto polystyrene microparticles when compared to PLGA microparticles. When the proteome profiler results were further analysed using the 'STRING' database, the TIPS microparticle samples strong links to the angiogenesis pathway (14 genes, 2.28e-14 false discovery rate), blood vessel and vasculature development pathway (15 genes, 1.4e-13 false discovery rate) and the tissue development pathway (19 genes, 9.95e-11) were highlighted. These pathways were also identified for the PLGA control microparticles (supplementary Figure S4.3).

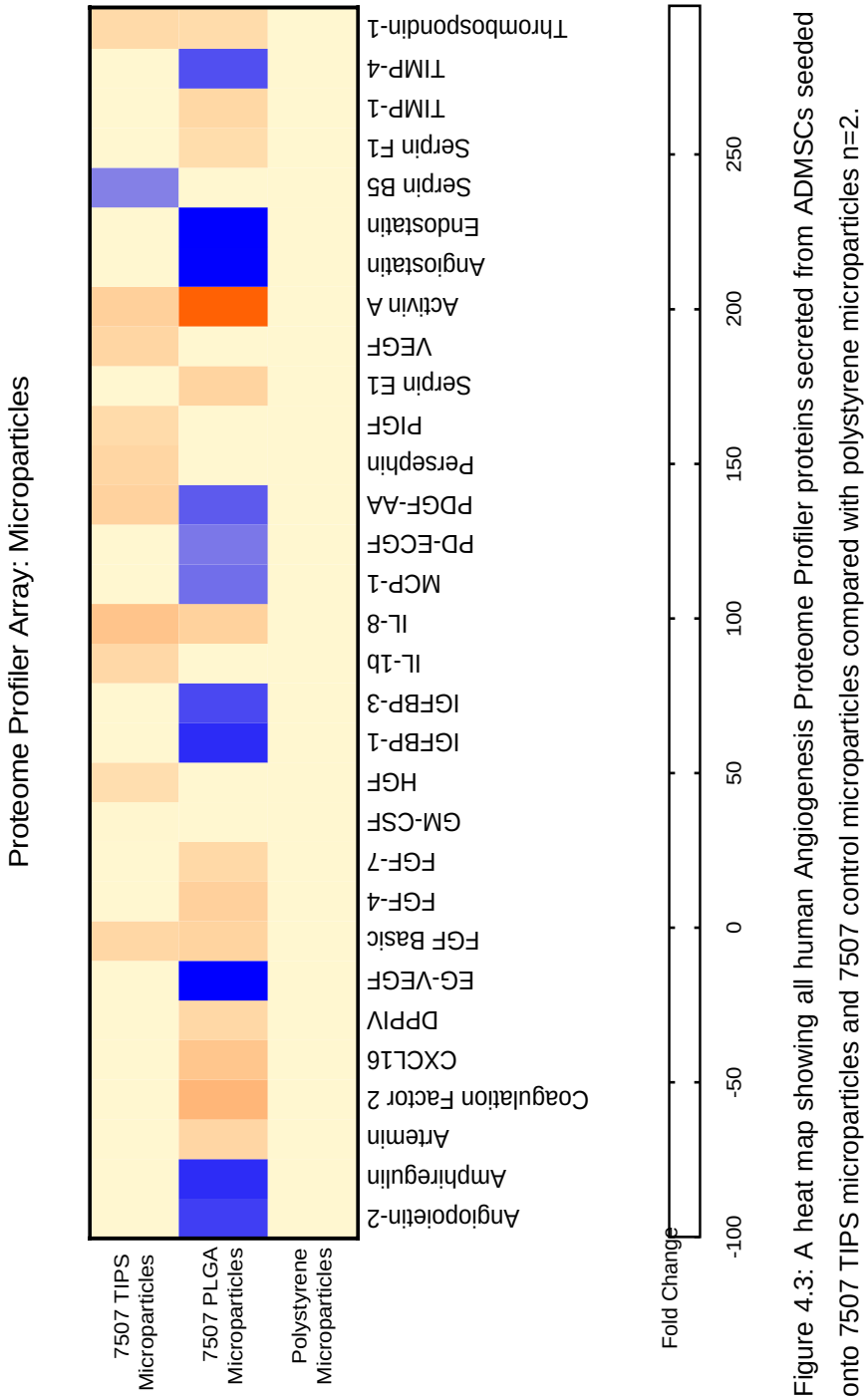

Figure 4.3: A heat map showing all human Angiogenesis Proteome Profiler proteins secreted from ADMSCs seeded onto 7507 TIPS microparticles and 7507 control microparticles compared with polystyrene microparticles n=2.

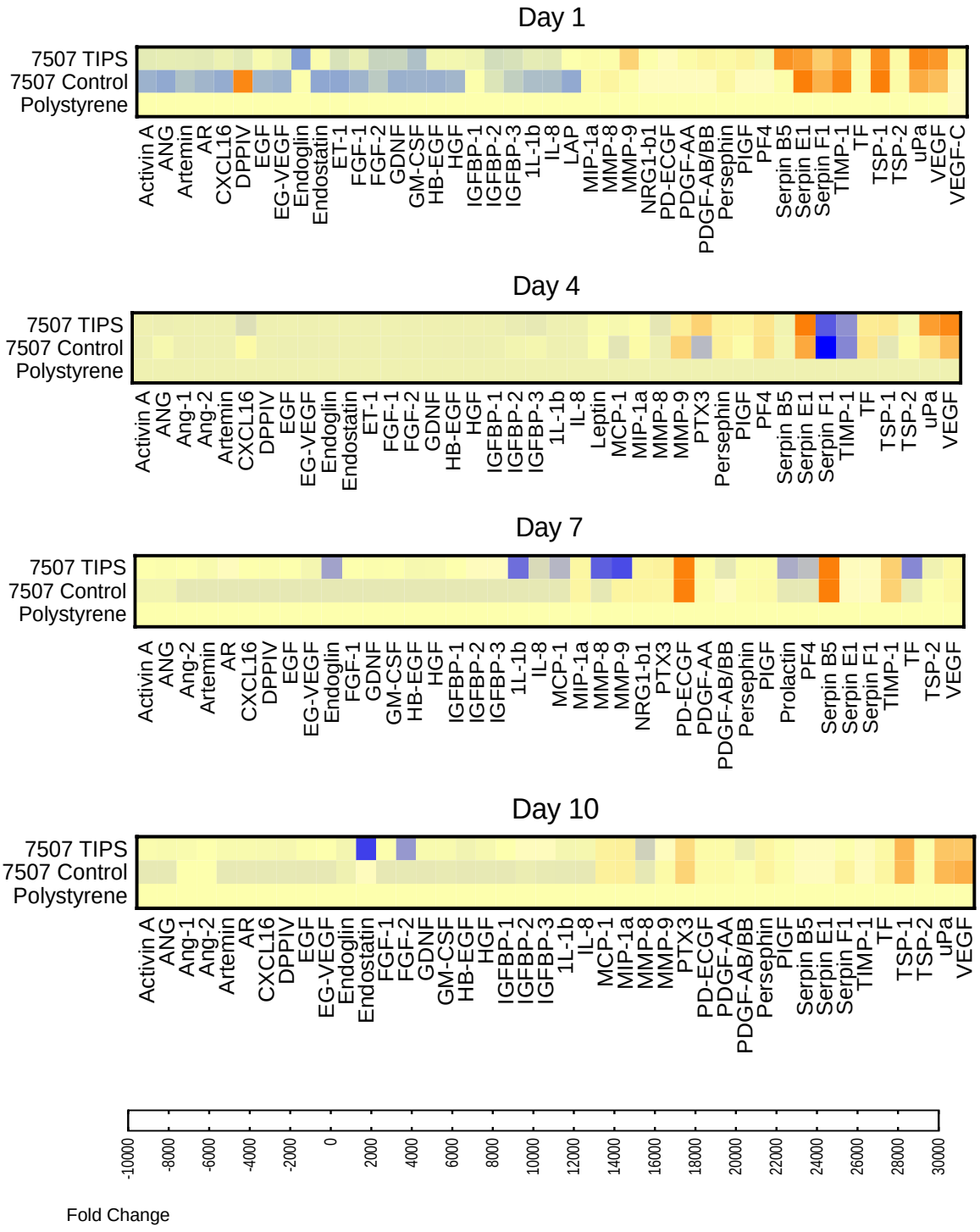

Figure 4.4: Heat maps showing human angiogenesis proteome profiler proteins secreted from ADMSCs seeded onto 7507 TIPS microparticles and 7507 control microparticles compared with polystyrene microparticles at days 1, 4, 7 and 10.

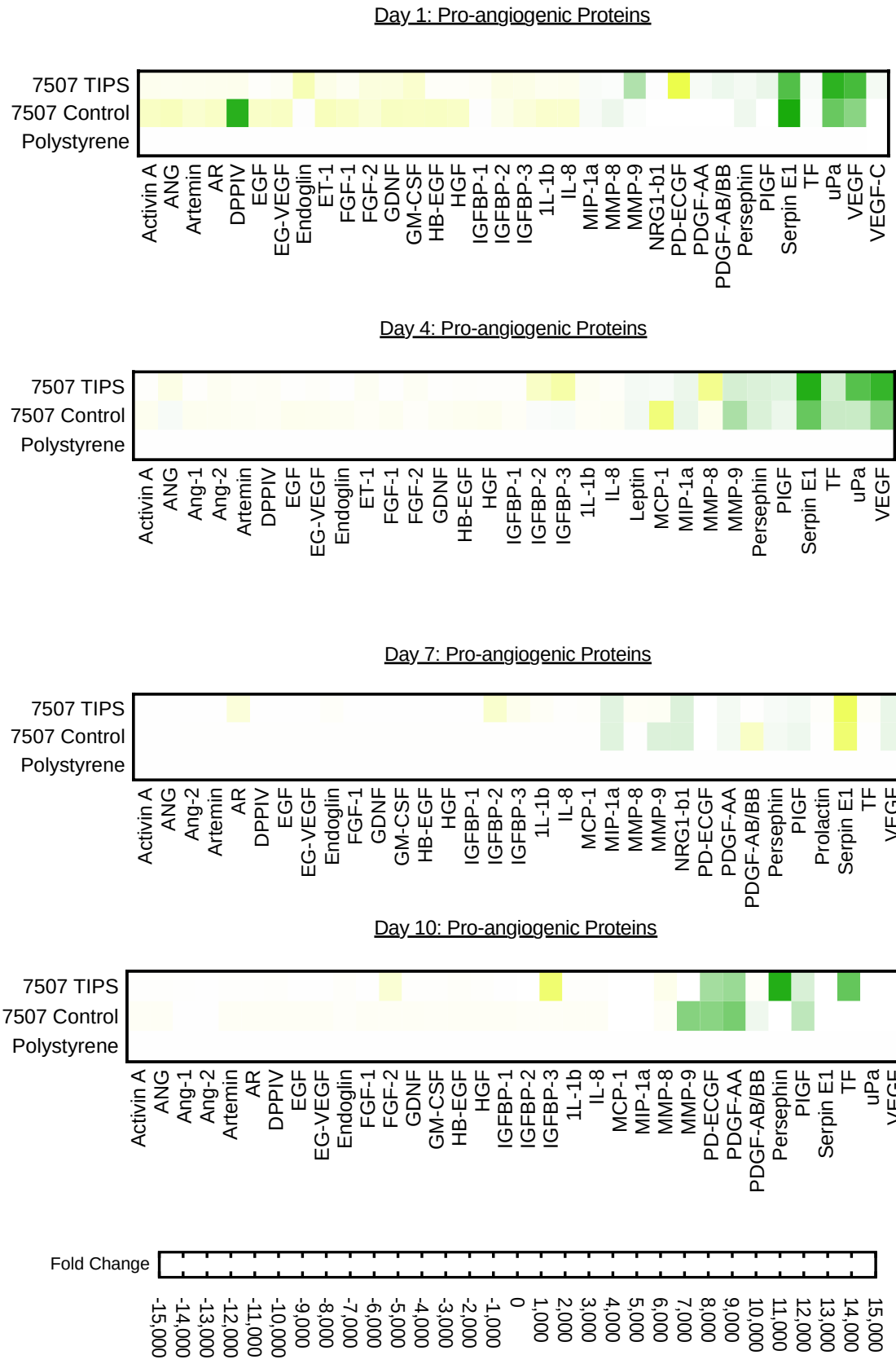

Figure 4.5: Heat maps showing human pro-angiogenesis proteome profiler proteins secreted from ADMSCs seeded onto 7507 TIPS microparticles and 7507 control microparticles compared with polystyrene microparticles at days 1, 4, 7 and 10.

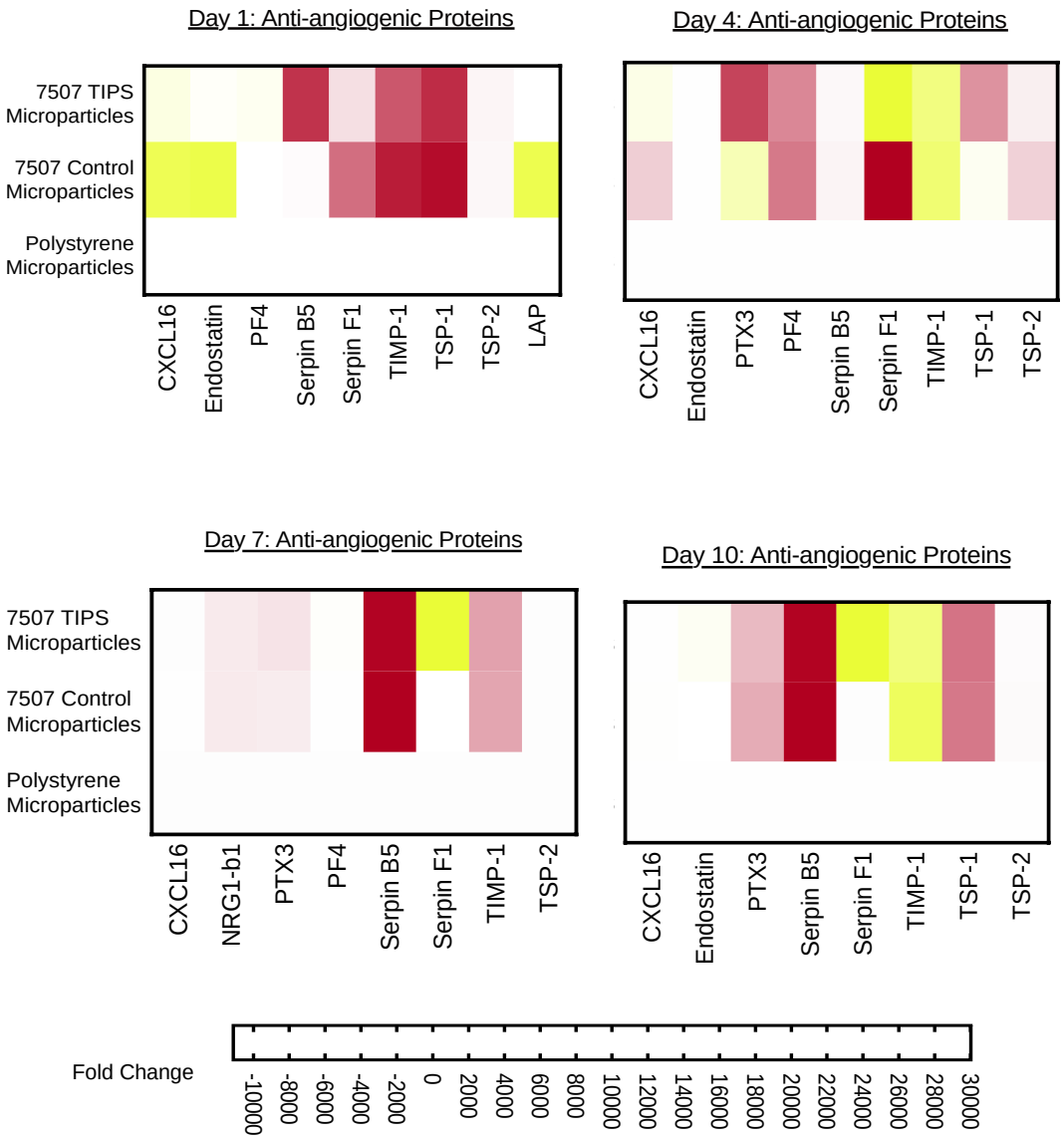

Figure 4.6: Heat maps showing human anti-angiogenesis proteome profiler proteins secreted from ADMSCs seeded onto 7507 TIPS microparticles and 7507 control microparticles compared with polystyrene microparticles at days 1, 4, 7 and 10.

4.3.3 In Vitro Evaluation of Angiogenesis Using a Vasculogenesis to Angiogenesis Array

The V2a array was also used for to assess the effect of ADMSCs cultured on microparticles on *in vitro* angiogenesis. Co-cultures were exposed to conditioned media containing the supernatants of ADMSCs seeded onto 7507 TIPS, 7507 control and polystyrene microparticles. After 14 days samples

were stained for anti-CD31, imaged and analysed using Angio.Sys.2.0 software. 7507 TIPS microparticles had significantly higher average tubule length, branches and junctions compared to 7507 control microparticles. There were no significant differences between 7507 TIPS microparticle samples length, branches and junctions and polystyrene microparticle samples.

The V2a array was used in an additional experiment to investigate how the addition of a pro-angiogenic and anti-angiogenic growth factor to the

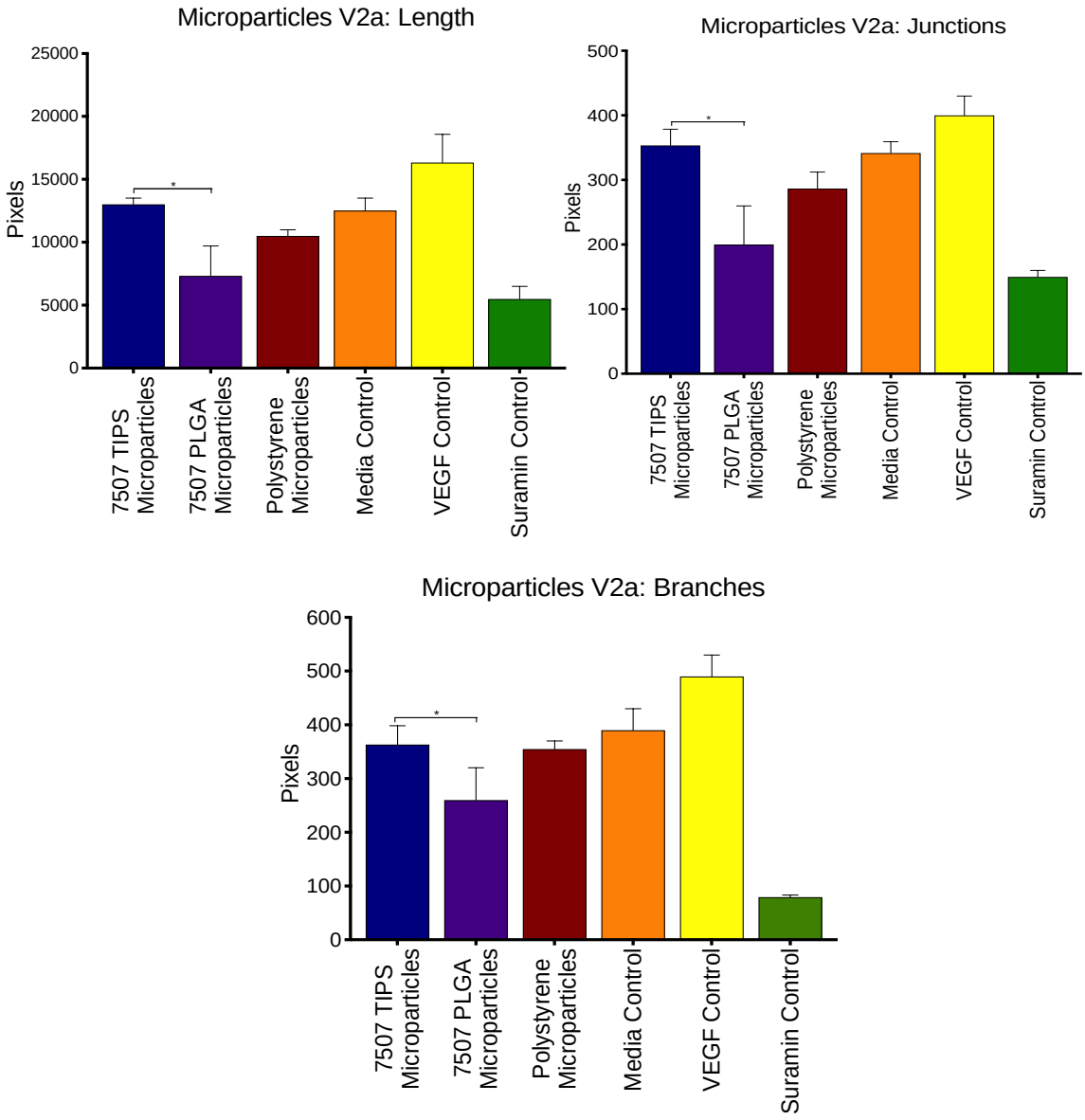

Figure 4.7: Quantification of the V2a array from the secretomes from ADMSCs attached to PLGA 7507 TIPS microparticles, PLGA 7507 microparticles, and polystyrene microparticles a) tubule length b) tubule junctions c) tubule branches. (n=1) Where * = P<0.05, ** = P<0.01, *** = P<0.001 and **** = P<0.0001. Ordinary One-way ANOVA = **** (P<0.0001)

conditioned media of ADMSCs cultured on 7507 TIPS microparticles could affect angiogenesis in vitro. VEGF was chosen as the pro-angiogenic factor as it had previously been studied using ELISA (Figure 4.2), was shown to be positively secreted in the proteome profiler (Figures 4.3 - 4.6) and was the internal positive control for the V2a array. Serphin F1/PEDF was selected to inhibit angiogenesis as it actively blocks VEGF and was shown in the proteome profilers to be down regulated from TIPS microparticle samples (Figures 4.3 - 4.6). Results show that the addition of VEGF to the conditioned media of ADMSCs seeded onto 7507 TIPS microparticles increases tubule length, and the addition of PEDF significantly decreases the tubule length and junctions of tubules compared with to 7507 TIPS microparticle supernatants.

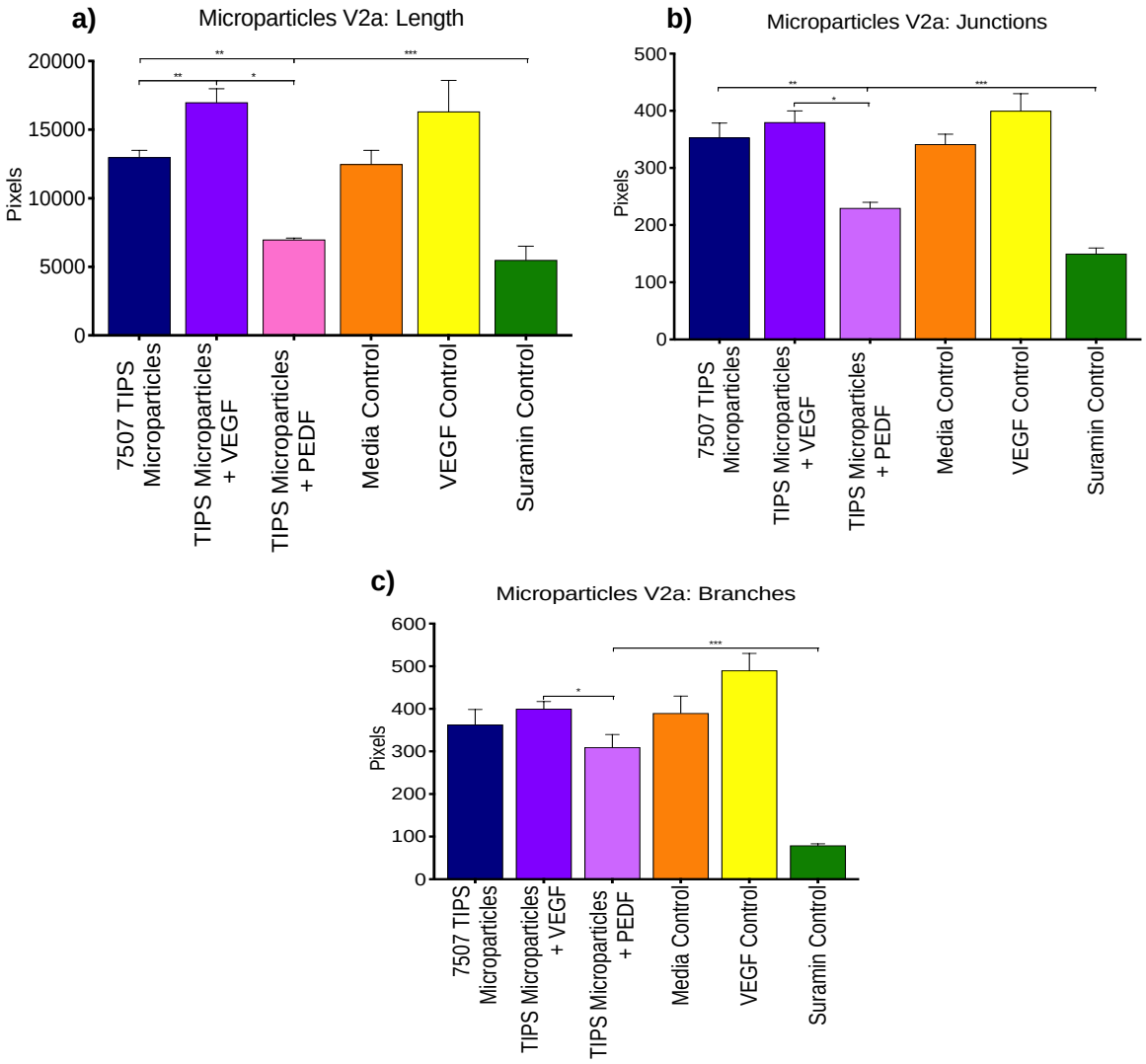

Figure 4.8: Quantification of the V2a array from the secretomes from ADMSCs attached to PLGA 7507 TIPS microparticles with the addition of the pro-angiogenic factor VEGF and anti-angiogenic factor PDGF a) tubule length b) tubule junctions c) tubule branches (n=1). Where * = P<0.05, ** = P<0.01, *** = P<0.001 and **** = P<0.0001. Ordinary One-way ANOVA = **** (P<0.0001)

4.4 Discussion

One of the driving factors angiogenesis is VEGF, that induces vascular leakage, vasodilation, endothelial cell migration, endothelial cell proliferation and tubule formation. [248-250] Consequently, VEGF concentration was selected to be measured as a primary indicator of angiogenic activity through ELISA, specifically $VEGF_{165}$. $VEGF_{165}$ is the most potent isoform of VEGF-A, a subset of VEGF that is crucial in angiogenesis through the stimulation of blood vessel sprouting and vascular regeneration. [487]

The PLGA 7507 TIPS microparticles had an increased $VEGF_{165}$ release per ADMSC up to day 7 (1.4 ±0.5 pg/mL/cell) compared to PLGA 7507 control microparticles (0.4 ±0.1 pg/mL/cell) and polystyrene microparticles (1.05 ±0.2 pg/mL/cell). Interestingly, the ADMSCs seeded onto PLGA 7507 smooth microparticles had their highest secretion of $VEGF_{165}$ at days 1 and 10, with the secretion reducing significantly at days 4 and 7. This behaviour could be due to poor cell attachment onto the smooth surface, cellular apoptosis, the potential secretion of other growth factors, the secretion of anti-angiogenic factors or inflammatory proteins. [488, 489] The ADMSCs seeded onto the smooth polystyrene microparticles did not have any significant changes in $VEGF_{165}$ concentrations per cell through the time points.

When considering how topography can influence the secretion of angiogenic growth factors, and the non-degradable smooth characteristics of polystyrene and the smooth surfaces of the PLGA control microparticles, it can be hypothesised that non-degradable and smooth materials do not improve the secretion of the proangiogenic growth factor $VEGF_{165}$ from ADMSCs. At day 10 there was no significant difference in the secretion of $VEGF_{165}$ from 7507 TIPS microparticles, 7507 control microparticles and polystyrene microparticles, as the control groups began to secrete higher levels of $VEGF_{165}$ compared with the earlier time points. When looking ahead into the *in vivo* implantation of the cellularised microparticles as a treatment for tissue ischaemia, it would be most effective to culture ADMSCs on TIPS 7507

microparticles for 1-4 days before implantation, as between these time points the cells secreted the highest levels of $VEGF_{165}$. Having shorter incubation times will also benefit downstream treatments, as the product would be more readily available. Furthermore, shortened tissue culture times would also reduce costs.

It has been established that to induce angiogenesis, concentrations of 0.05-0.6 pg/mL of VEGF/cell is required, [266-268] as ADMSCs naturally secrete 0.003-0.04 pg/mL of VEGF per cell. [269, 270] Figure 4.2b shows a $VEGF_{165}$ secretion of 2.1 ±0.6 - 1.4 ±0.4 pg/mL/cell on 7507 TIPS microparticles, which suggest that these levels would be capable of promoting angiogenesis *in vivo.* This also demonstrates that cell attachment to TIPS 7507 microparticles enhanced the $VEGF_{165}$ secretion per ADMSC compared with smooth microparticles. These results are encouraging as it has been shown that $VEGF_{165}$ secretion can be increased without the use of genetic modification of the cells. Many studies involving the increase in secretion of angiogenic growth factors from stem cells involve genetically modifying the cells to do so, resulting in improved *in vitro* and *in vivo* angiogenic outcomes. [28, 157, 158, 490] By negating the use of this technology, the hazardous consequences such as uncontrolled gene mutations, uncontrolled growth factor expression and oncogenic effects are eliminated. [491-493]

From Figures 4.2b it can be observed that the ADMSCs seeded onto microparticles had overall higher $VEGF_{165}$ levels (pg/mL) per cell compared with the polymer films manufactured from the same material (Part I. Figure 4.1b). It has been established that cells behave differently on 2D and 3D cultures with regards to spreading, morphology, differentiation and survival. [167] In this case, the cells responded differently to the different culture conditions by altering the levels of growth factors secreted, with microparticle culture favouring $VEGF_{165}$ secretion. 3D environments are thought to be more representative of *in vivo* conditions, as cells do not naturally occur as monolayers as they do in 2D culture. Cells can thus grow beyond monolayers in 3D culture and in turn have improved proliferation, gene expression and growth factor release. [247] This behaviour can be exploited for tissue

engineering applications, where 7507 TIPS microparticles can be used to promote angiogenic behaviour of ADMSCs to treat ischemic disease.

To further assess the release of angiogenic growth factors from ADMSCs seeded onto 7507 TIPS microparticles in comparison to controls, an angiogenic proteome profiler array was used to screen for 55 angiogenic related proteins. Further analysis using the STRING database [247] revealed that there were strong associations with angiogenesis, blood vessel and vascular development and tissue development processes. There were 14 linked genes and proteins associated with the angiogenesis pathway detected from the secretomes of ADMSCs seeded onto TIPS and control 7507 microparticles and 11 genes and proteins were secreted from ADMSCs seeded onto polystyrene microparticles. This suggests that 7507 PLGA could have an influence in increasing angiogenic responses compared with polystyrene. It was uncovered in Part I. Chapter 3 that polystyrene had much higher stiffness measurements than PLGA. Over-stiff surfaces can cause changes in cellular morphology, [178] that in turn effects cell behaviour. In this instance the stiffness of polystyrene microparticles could have contributed in less $VEGF_{165}$ from being secreted from the attached ADMSCs.

The proteome profiler array (Figure 4.3) revealed MCP1 to be upregulated from TIPS samples and downregulated on PLGA control samples. MCP1 is a pro-angiogenic factor that is secreted by mesenchymal stem cells. It has been shown to promote angiogenesis *in vitro* through the promotion of endothelial cell migration, proliferation and angiogenic factor gene expression. [494] In addition, it has been shown to induce capillary formation and restore blood flow in pre-clinical models of hindlimb ischemia through the expression of VEGF and HIF-α. [495, 496] It would be interesting to explore the role of MCP1 further considering the large difference in expression between TIPS and PLGA control groups and the links to VEGF expression and angiogenesis. Furthermore, MCP1 has also been identified as a proinflammatory cytokine that can induce senescence in MSCs through expression of CCR2 that facilitates monocyte chemotaxis. [497] Despite this, MCP1 has been shown to

be pro-angiogenic in *in vitro* in combination with a pro-inflammatory response. Therefore, an increase in inflammation through the secretion of MCP1 can still result in a pro-angiogenic response as well as an increase in proliferation. [498, 499]

ADMSCs are known to secrete multiple factors including and not limited to; VEGF, HGF, IGF-1, FGF, IL-8, G-CSF, EGF, TGF, IL-1b, MCP-1 and PDGF. [76, 77, 79, 92, 500] The proteome profiler array highlighted multiple pro-angiogenic factors secreted from the ADMSCs when attached to TIPS microparticles, including: VEGF-A, FGF-a, FGF-b, epidermal growth factor (EGF), angiopoietin-2, angiogenin prolactin and persephin. Angiopoietin-2, prolactin and persephin are not typically associated with the secretomes of ADMSCs, where angiopoietin-2 binds to receptors on endothelial cells and in combination with VEGF, influences cell migration and proliferation, [280] and prolactin and persephin interact with ERK pathways that ultimately influence endothelial cell tubule formation. [317, 320, 321] Therefore, the production of these pro-angiogenic factors from ADMSCs could be in response to the exposure to TIPS microparticles. When comparing how these interactions differ from day 1 to day 10, there was an increase in genes associated with angiogenesis from ADMSCs on 7507 TIPS microparticles on day 1 from 10 genes (FD 4.02e-09) to 13 genes (FD 9.56e-13) on day 10. This increase was seen with the 7507 PLGA control microparticles with day 1, showing 10 genes (FD 5.52e-09) increase to 11 genes (FD 1.31e-10) at day 10. In addition, there was an increase in the blood vessel development pathway from 7507 TIPS microparticle samples on day 1, from 11 genes (FD 4.76e-09) to 14 genes (FD 3.27e-12) on day 10. This same effect was seen with the 7507 PLGA control microparticles (day 1; 11 genes FD 8.39e-09 and day 10; 14 genes 2.2e-12). These findings begin to suggest that the behaviour of ADMSCs begin to change over time with regards to biological processes occurring, such as blood vessel development. Also, there were differences between the proteins associated with angiogenesis, with at 10 day more proteins secreted from ADMSCs seeded onto 7507 TIPS microparticles, suggesting that the TIPS microparticles could influence an increase in pro-angiogenic activity compared with the 7507 PLGA control microparticles. The difference in topography and

structure between these materials could have contributed to the different responses of ADMSCs observed.

To further understand the effect of the TIPS microparticles on the angiogenic behaviour of ADMSCs, an *in vitro* angiogenesis array was performed. The V2a array measures the length, junctions and branches of tubules formed after exposure to the secretomes from ADMSCs attached to 7507 TIPS and control microparticles. The findings revealed that tubule length, junctions and branches were increased from TIPS 7507 microparticle samples compared to 7507 control microparticles and polystyrene microparticles. This is the same effect seen with TIPS-processed polymer films, (Part I. Chapter 5) where PLGA 7507 TIPS polymer films had the highest *in vitro* angiogenic response. The advanced angiogenic behaviour from ADMSCs attached to 7507 TIPS-processed polymers have also been highlighted in the proteome profiler arrays, where the increase in tubule formation is due to the increase in pro-angiogenic factors secreted from ADMSCs on TIPS surfaces (as shown by the proteome profiler arrays and VEGF ELISA) in comparison to controls. This response can be attributed to the superior in stiffness, porosity and roughness provided by the TIPS-processed 7507 PLGA.

To investigate if $VEGF_{165}$ was a driving force in the promotion of tubule formation (Figure 4.7), the V2a was performed with the addition of a pro-angiogenic and anti-angiogenic factor to the secretomes of ADMSCs cultured on 7507 TIPS microparticles. $VEGF_{165}$ was included as a positive control, where the addition of $VEGF_{165}$ to the secretomes from ADMSCs seeded onto 7507 TIPS microparticles resulted in a significant increase in the length, branches and junctions of the tubules compared with the 7507 TIPS microparticle secretome only group, demonstrating the role of $VEGF_{165}$ in increasing *in vitro* angiogenic behaviour. There was no significant difference between the VEGF positive control group and the 7507 TIPS microparticle with $VEGF_{165}$ group, signifying that culturing ADMSCs on 7507 TIPS microparticles did not negatively affect how $VEGF_{165}$ interacts with endothelial cells to produce tubules, by perhaps secreting anti-angiogenic proteins that would block $VEGF_{165}$ binding to endothelial cells. The proteome profiler (Figure 4.6)

showed that there were a small number of anti-angiogenic factors secreted from ADMSCs on PLGA control microparticles that were shown to be down regulated when seeded on TIPS microparticles. Anti-angiogenic factors included pigment epithelium-derived growth factor (PEDF), TIMP-1, endostatin and maspin. For the purpose of this study, a factor that specifically interacted with VEGF was desired. As maspin and endostatin interfere with endothelial cell proliferation without directly blocking VEGF and [322, 501] TIMP-1 inhibits angiogenesis via inhibiting MMPs that are involved in the degradation of the ECM, these factors were not selected. [502] PEDF (also known as serpin F1) was chosen as it was down-regulated on TIPS microparticles in the proteome profilers (Figures 4.6). PEDF has been shown to obstruct angiogenesis by directly inhibiting VEGF binding to VEGF-receptor 1 [503, 504] that blocks the MAPK/ERK pathway, inhibiting migration and proliferation of endothelial cells. [505] MAPK/ERK pathway plays a role in angiogenesis by stimulating endothelial cell (angiogenic) activity in response to growth factors such as VEGF. [506] The addition of PEDF to the secretomes from ADMSCs on TIPS microparticles significantly hindered the number of junctions and the length of tubules in the V2a assay compared with the secretome only samples (Figure 4.8). From this it can be said that VEGF is a key regulator of angiogenesis and may be acting through the MAPK/ERK pathway. Although, compared to the suramin negative control (suramin actively blocks VEGF [274]) the ADMSCs secretomes from TIPS microparticles with PEDF had significantly higher tubule length, junctions and branches. Therefore, as tubules had formed, there must be other angiogenic factors within the secretome stimulating angiogenesis in addition to VEGF, that is not able to be blocked by PEDF. This assumption is supported by the proteome profiler data that highlights a host of proteins present that can promote angiogenesis, suggesting an additional pathway may be activated. In order to uncover the underlying cellular mechanisms in which angiogenesis is promoted from ADMSCs seeded onto TIPS surfaces future work is required.

4.5 Summary

This chapter explored the angiogenic effect of ADMSCs attached to TIPS microparticles and investigated the biological mechanism responsible for the observed effect. ADMSCs attached to TIPS microparticles secreted higher quantities of $VEGF_{165}$ per cell compared with controls, suggesting that the unique hierarchical, porous and rough structure of the TIPS microparticles resulted in an increase in angiogenic growth factor secretion. To investigate the underlying mechanism responsible for the increase in $VEGF_{165}$ secretion seen on TIPS microparticles, proteome profiler arrays and V2a arrays were performed. As with ADMSCs attached to 7507 TIPS polymer films, the proteome profiler array and subsequent analysis was able to highlight multiple pathways were promoted on TIPS microparticles, such as angiogenesis and the blood vessel development pathway. Pro- (VEGF) and anti- (PEDF) angiogenic growth factors were added to the secretomes of ADMSCs seeded onto 7507 TIPS microparticles and the angiogenic response was investigated with the V2a array. The addition of PEDF significantly hindered *in vitro* angiogenesis through actively blocking VEGF, compared with the increase in tubule formation from the addition of VEGF. This highlighted that VEGF was a key regulator inducing angiogenesis from ADMSCs seeded 7507 TIPS microparticles, most likely through the MAPK/ERK pathway. [505] There were also indications of activation of additional pathways through the secretion of multiple growth factors, however further exploration of this theory is required.

4.6 Supplementary Information

S4.1 $VEGF_{165}$ secretion (pg/mL) per ADMSC seeded onto 7507 TIPS microparticles, 7507 control microparticles and polystyrene microparticles at days 1, 4, 7 and 10. The highest secretion of $VEGF_{165}$ where from ADMSCs seeded onto 7507 TIPS microparticles at day 1.

pg/mL/cell	Day 1	Day 4	Day 7	Day 10
7507 TIPS microparticles	2.1	1.9	1.4	1.4
7507 control microparticles	1.1	0.3	0.4	1.4
Polystyrene microparticles	1.6	1.0	1.1	1.2

S4.2 Proteome profiler proteins from ADMSCs on 7507 TIPS microparticles were analysed through STRING Analysis for connections to biological processes. Images show the connections between the secreted genes and proteins. Strong connections were found between angiogenesis, blood vessel and vasculature development and tissue development pathways.

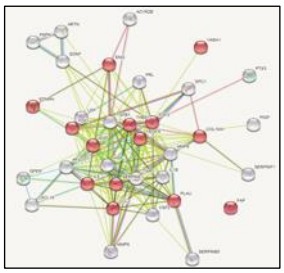

Angiogenesis pathway *(14 genes – false discovery rate 2.28e-14)*

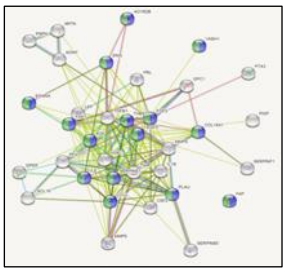

Blood vessel and vasculature development pathway *(15 genes – false discovery rate 1.4e-13/2.24e-13)*

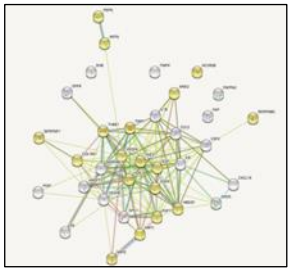

Tissue development pathway *(18 genes – false discovery rate 4.15e-11)*

S4.3 Proteome profiler proteins from ADMSCs on 7507 control microparticles were analysed through STRING Analysis for connections to biological processes. Images show the connections between the secreted genes and proteins. Strong connections were found between angiogenesis, blood vessel and vasculature development and tissue development pathways.

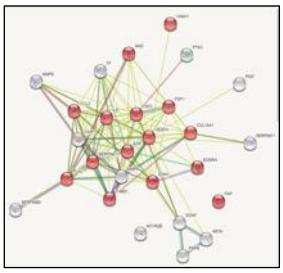

Angiogenesis pathway *(14 genes – false discovery rate 9.54e-16)*

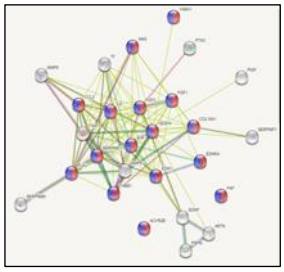

Blood vessel and vasculature development pathway *(15 genes – false discovery rate 2.18e-15/2.24e-13)*

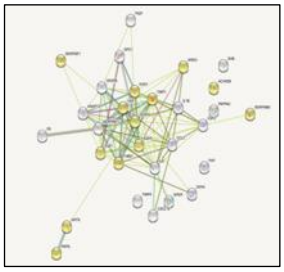

Tissue development pathway *(13 genes – false discovery rate 4.43e-06)*

S4.4 Proteome profiler proteins from ADMSCs on polystyrene microparticles were analysed through STRING Analysis for connections to biological processes. Images show the connections between the secreted genes and proteins. Strong connections were found between angiogenesis, blood vessel and vasculature development and tissue development pathways.

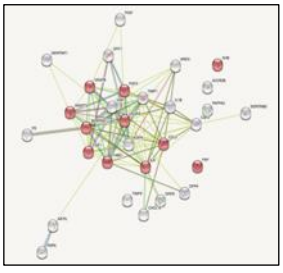

Angiogenesis pathway *(11 genes – false discovery rate 1.2e-10)*

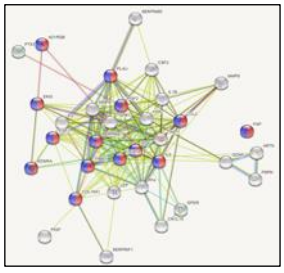

Blood vessel and vasculature development pathway *(14 genes – false discovery rate 1.23e-15/2.24e-13)*

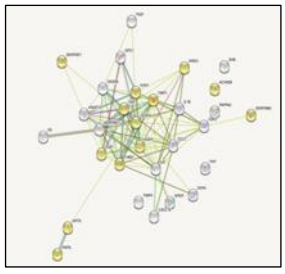

Tissue development pathway *(13 genes – false discovery rate 4.32e-06)*

S4.5 Images from the V2a array tubules stained with anti-CD31. Images were analysed through Angio.Sys software and tubule length, branches and junctions were quantified.

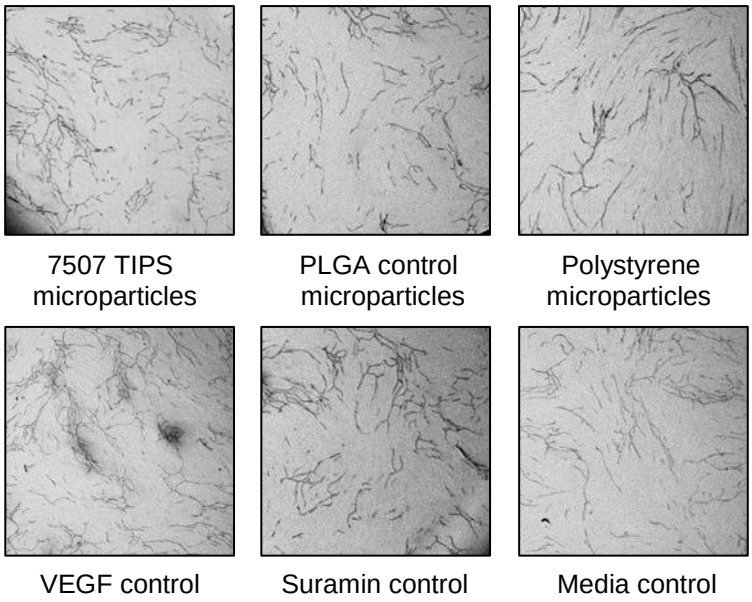

S4.6 Images from the V2a array tubules stained with anti-CD31 where a pro- and anti- angiogenic factor was added to the 7507 TIPS microparticle sampels. Images were analysed through Angio.Sys software and tubule length, branches and junctions were quantified. The addition of VEGF increased tubule formation from samples exposed to 7507 TIPS secretomes and tubule formation was hindered by the addition of PEDF.

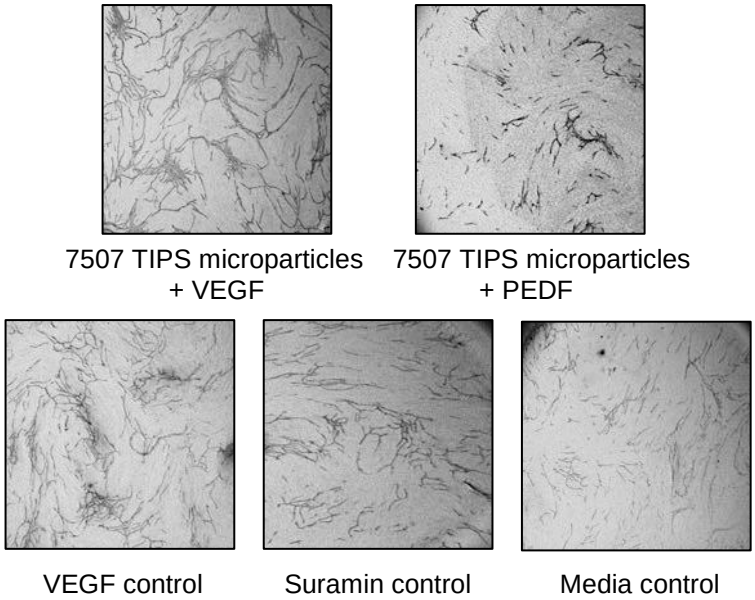

Part II.

Chapter 5 Pre-Clinical Evaluation of Acellular TIPS-Based Microparticles

5.1 Introduction

The hindlimb ischaemia model has been established as a valuable pre-clinical model of peripheral artery disease [17, 46, 50, 71, 242, 334, 341] (PAD) as discussed in Part I. Chapter 6. The procedure to induce ischaemia was optimised in previous chapters, where unilateral femoral artery ligation was selected as the optimal method to induce ischaemia in mice.

Biomaterials can be a useful tool to aid the delivery of cells *in vivo* for therapeutic angiogenesis, as many studies have shown that promising cell therapies are unable to remain at the implant site when administered in suspension. [4, 5, 71, 73, 77, 91-94] To investigate the response of TIPS microparticles *in vivo,* they were administered into the hindlimb ischaemia model through a non-invasive method. The behaviour of the TIPS microparticles and the effect on angiogenesis in comparison to controls were evaluated with laser doppler imaging and histology methods.

5.2 Methods

5.2.1 Inducing Ischaemia in a Preclinical Model of Peripheral Arterial Disease

A murine hindlimb ischaemia model was used a pre-clinical model of PAD. A full description of the procedure used to induce hindlimb ischaemia was outlined in Part I. Section 6.2.1.

5.2.2 Blood Flow Evaluation Using Laser Doppler Imaging

Laser doppler imaging was used to evaluate blood flow in the murine hindlimbs immediately after surgeries and at days 7, 14 and 21. The technique has been described in Part I. Section 6.2.2.

5.2.3 Implantation of Microparticles into the Hindlimb Ischaemia Model

Before the implantation studies microparticles were prepared by hydrophilisation outlined in Chapter 3 Section 3.2.3, washed twice with 3 mL sterile 1X PBS and combined with Aquaform hydrogel (1418C, Aspen Medical, UK) at a concentration of 100 mg/mL in order to create an injectable material. The number of microparticles was determined by weighing 100 mg of the microparticles and combining this with 1 mL of gel. 100 µL of this mixture was pipetted onto glass slides (631-1551, VWR, UK) and imaged against a black background to provide a reproduceable background for images. The microparticles within these samples were manually counted, with the average microparticle number per 100 µL being 1803 ±178 (n=6). Unilateral femoral artery ligation was used to create ischaemia in the hindlimb of c57bl/6 mice. After ischaemia was induced, 50 µL of 7507 TIPS microparticles in Aquaform gel was pipetted around the occluded bundle (n=2) using a positive displacement pipette (P50-250, Gilson Microman). The incision was closed using 5-0 coated Vicryl absorbable sutures (J409G, Ethicon, USA) This was repeated with 50 µL 7507 PLGA control microparticles in Aquaform gel (100 mg/mL), 50 µL of Aquaform gel only to assess the effects of the gel *in vivo* (n=2) and a no treatment control (n=1).

Another hydrogel, GranuGEL, was also investigated (n=3) and the effects of both gels evaluated. GranuGEL (ELM054, Convatec, UK) was combined with hydrophilised microparticles at a concentration of 200 mg/mL. Unilateral femoral artery ligation was induced in the hindlimb of c57bl/6 mice and 100 µL 7507 TIPS microparticles and GranuGEL mixture was pipetted around the site of ischaemia (n=2) using a positive displacement pipette (P50-250, Gilson Microman). This was repeated with 7507 PLGA control microparticles at a concentration of 200mg/mL with GranuGEL (n=2), GranuGEL only control (n=1) and no treatment (n=1). All incisions were closed with 3-4 5-0 coated Vicryl absorbable sutures (J409G, Ethicon, USA) and cleaned, then the animals were placed into a recovery chamber until consciousness was regained. All incision sites were checked after 24 hours to ensure the sutures had not broken. If this had occurred, the sites were re-sutured as outlined in Part I. Section 6.2.2. The animals were monitored for or signs of infection or suffering every 6-7 days. The efficiency of the surgeries was assessed by laser doppler imaging immediately after surgery, and the blood reperfusion was measured weekly up to 21 days with laser doppler imaging. The surgeries were repeated three times.

5.2.4 Evaluating the Effect of the Hindlimb Ischaemia Model on the Degradation of 7507 TIPS Microparticles

7507 TIPS microparticles were prepared by hydrophilisation, washed twice with 1X PBS and combined with GranuGEL (ELM054, Convatec, UK) at a concentration of 200 mg/mL. Unilateral femoral artery ligation was induced in the hindlimb of c57bl/6 mice and 100 µL 7507 TIPS microparticles and Granugel mixture was pipetted around the occluded bundle (n=8) using a positive displacement pipette (P50-250, Gilson Microman). The incisions were closed with 3-4 coated Vicryl absorbable sutures (J409G, Ethicon, USA) and cleaned, then animals were placed into a recovery chamber until recovered. All incision sites were checked after 24 hours to ensure the sutures had not broken. If this occurred, the sites were re-sutured and the animals were monitored for or signs of infection or suffering every 6-7 days efficiency of the surgeries was assessed by laser doppler imaging immediately after surgery, the degradation of the microparticles was evaluated at 6, 12, 18 and 24 weeks.

5.2.5 Evaluation of Implanted TIPS-Based Materials

5.2.5.1 Preparing Microscope Slides

The preparation of TESPA slides was described in Part I. Section 6.2.3.1.

5.2.5.2 Histological Analysis of Tissues

Histology methodology was described in Part I. Section 6.2.3.2.

5.2.5.3 Haematoxylin and Eosin staining of Tissue Sections

Haematoxylin and Eosin (H&E) cellular stain was used to stain tissue sections. The staining procedure was described in Part I. Section 6.2.3.3.

5.2.5.4 Immunohistochemical Staining of Tissue Sections

Tissues were stained with the endothelial cell marker Von Willebrand factor (VWF) to evaluate blood vessel development. The staining procedure was described in Part I. Section 6.2.3.4.

5.2.5.5 Evaluation of Arteriogenesis

H&E stained tissue sections were evaluated for arteriogenesis. The full methodology was described in Part I. Section 6.2.4.

5.2.6 Evaluation of Angiogenesis Related Gene Expression from Ischemic Limbs Treated with TIPS Microparticles

A full description of the procedures used in the evaluation of gene expression from tissues treated with TIPS-based materials was outlined in Part I. Section 6.2.5. This includes the methodology for RNA extraction (Part I. Section 6.2.5.1), reverse transcription of RNA to cDNA (Part I. Section 6.2.5.2), design of primers (Part I. Section 6.2.5.3) and relative qPCR (Part I. Section 6.2.5.4).

5.2.7 Statistical Analysis

Statistical Analysis methodology was described in Chapter 2 Section 2.2.7.

5.3 Results

5.3.2.1. Evaluation of Implanted TIPS Microparticles into the Hindlimb Ischaemia Model

7507 PLGA TIPS microparticles were implanted after the induction of ischaemia in the hindlimbs of mice via injection with the aid of Aquaform. Aquaform is a biocompatible hydrogel used to rehydrate dry tissue consisting of propylene glycol and grafted starch polymer. [507] Post-operative laser doppler imaging confirmed ischaemia had been successfully induced and was repeated at days 7, 14 and 21 (supplementary Figure S5.1). There were no significant differences in reperfusion ratios between all groups. 7507 TIPS microparticles and 7507 control microparticles were also implanted in GranuGEL (a hydrogel and hydrocolloid gel) [508] to assess if the Aquaform gel effected the reperfusion rate. There were no significant differences between the reperfusion rates of TIPS microparticles, and control treated limbs

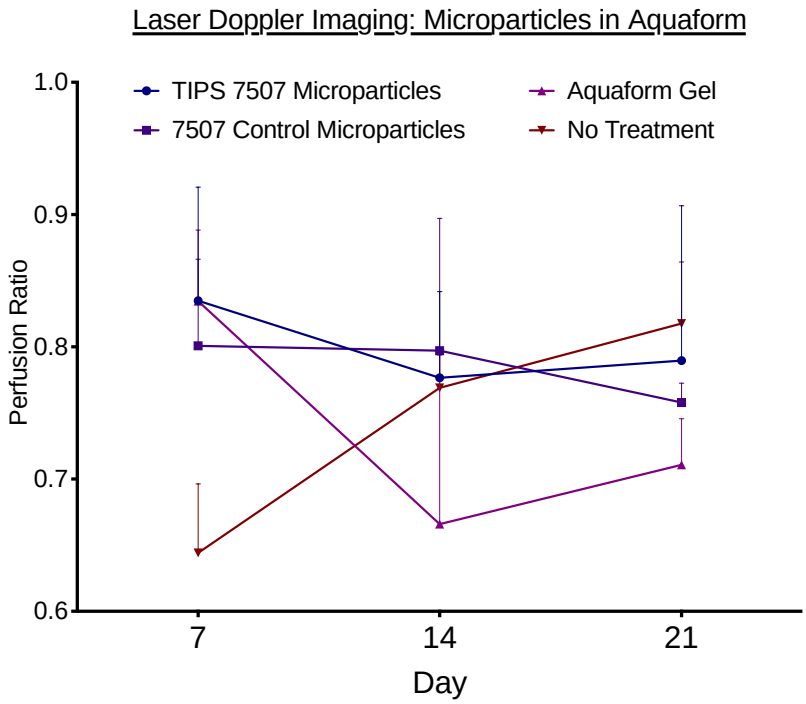

Figure 5.1: Quantification of laser-doppler imaging from hindlimbs from mice impanated with 7507 PLGA TIPS microparticles in Aquaform, control 7507 PLGA microparticles in Aquaform, Aquaform only and no treatment. Results are shown as perfusion ratio at days 7, 14 and 21 (n=1)

at days 7 and 14. At day 21 the 7507 TIPS microparticle group had significantly increased reperfusion ratios after 21 days (1.38 ±0.5 perfusion ratio) compared to 7507 control microparticles, GranuGEL and a no treatment control (0.89 ±0.2, 0.8 ±0.14, and 0.86 ±0.2 perfusion ratio respectively).

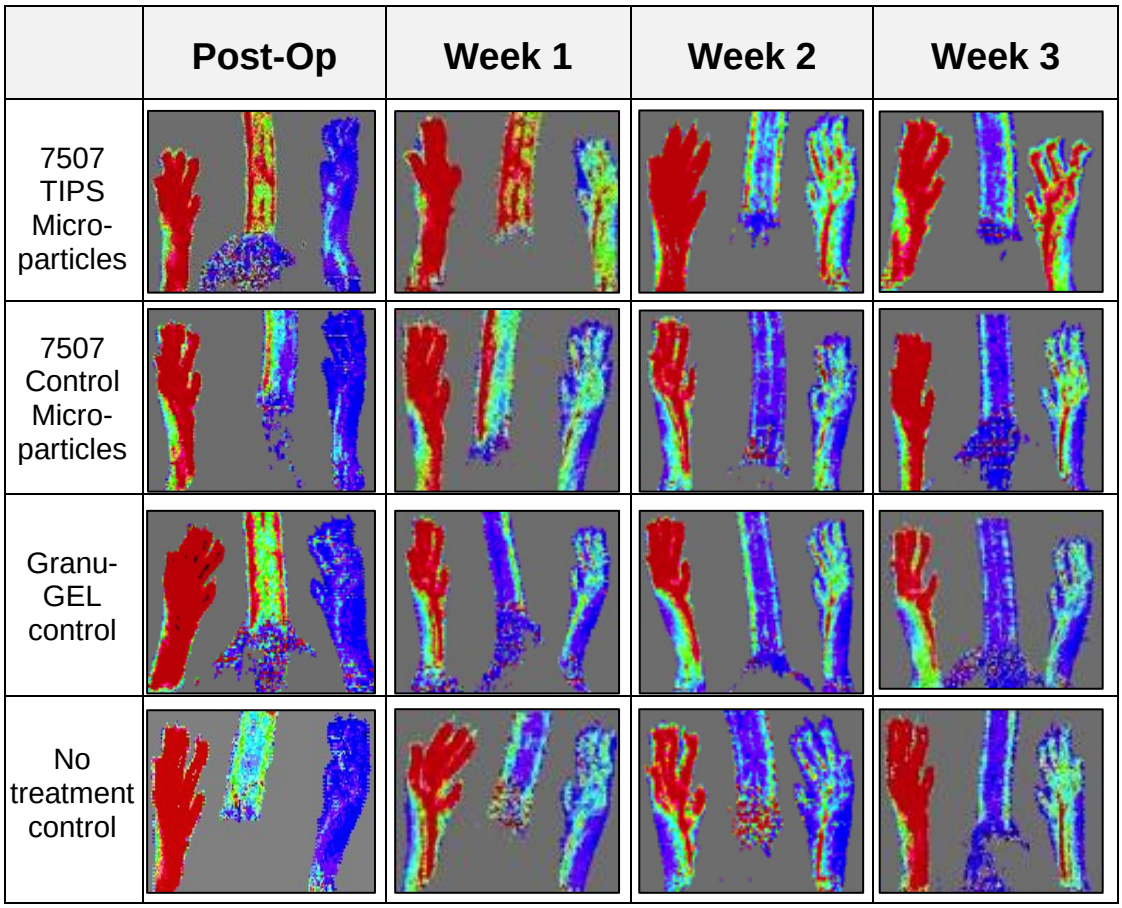

Figure 5.2: Laser-doppler imaging from hindlimbs from mice impanated with 7507 PLGA TIPS microparticles in GranuGEL, control 7507 PLGA microparticles in GranuGEL, GranuGEL only and no treatment. Images were taken post-operatively and at days 7, 14 and 21.

5.3.4 Histological Analysis Evaluation of Implanted TIPS Microparticles

H&E staining showed that a large granuloma had formed in the groups with the Aquaform implant (Figure 5.4). To assess if this was an effect from the surgery or the Aquaform, another gel, GranuGEL, was investigated. The H&E images (Figure 5.5) from the GranuGEL only controls show that granulomas had not formed to the same extent as the Aquaform gel. From these findings

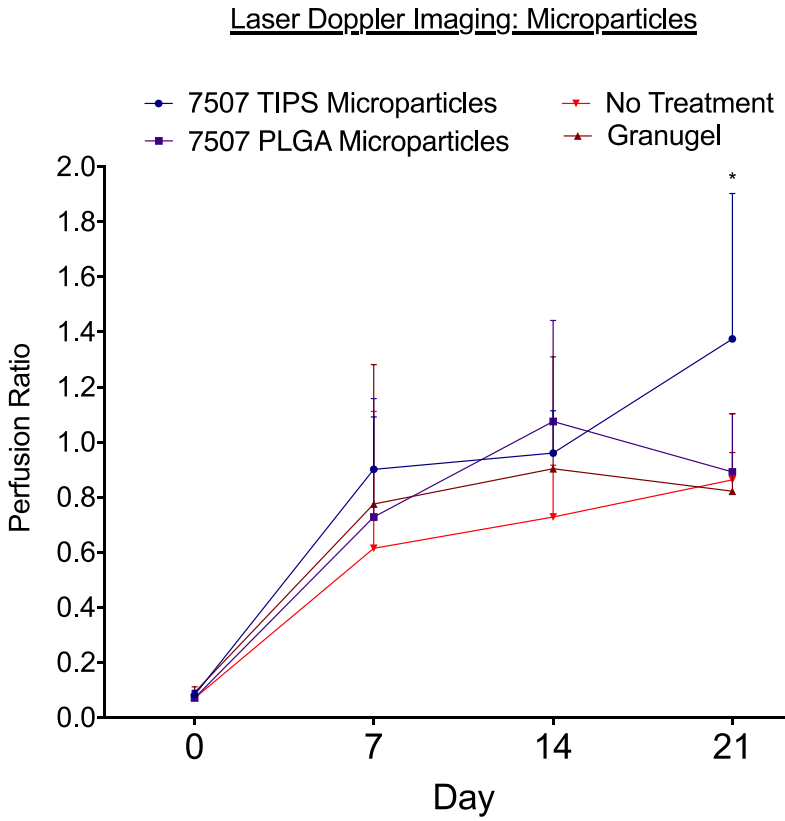

Figure 5.3: Quantification of laser-doppler imaging of the paws of mice that had undergone unilateral femoral artery ligation and subsequent implantation of 7507 PLGA TIPS processed microparticles in GranuGEL, control 7507 PLGA microparticles in GranuGEL, GranuGEL only and no treatment. Results are shown as perfusion ratio at days 7, 14 and 21. (n=3) Two-way ANOVA with Geisser-Greenhouse correction = *. (P=0.015)

GranuGEL was chosen as the delivery vehicle for microparticle implantation. H&E staining (Figure 5.6) revealed that the 7507 TIPS and control microparticles remained at the implant site and showed signs of degradation and deformation. The TIPS structure was visible as well as the attachment of cells on the TIPS and control surfaces. In addition, there was an indication of attachment of giant multinucleated cells indicated by blue arrows in Figure 5.6d. These cells were a sign of the immune response reacting to the implantation of the biomaterial. This response was studied further in Part II. Chapter 6. There was also evidence of blood vessel formation around the 7507 TIPS microparticles, indicated by black arrows in Figure 5.6. This was further highlighted with VWF positive staining in Figure 5.8, where blood vessels were visible around the implanted 7507 TIPS microparticles.

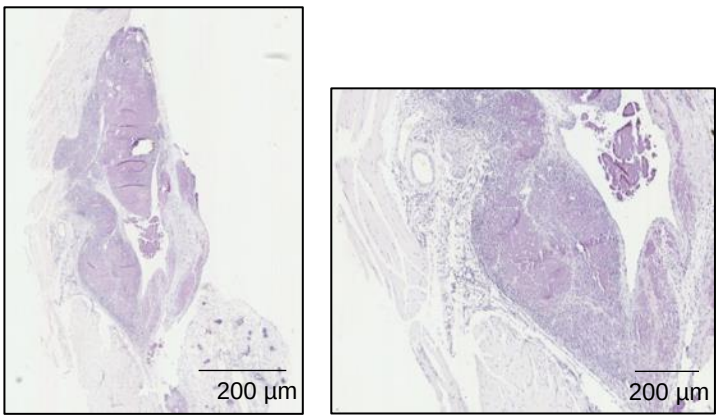

Figure 5.4: H&E staining of tissue sections showing the implantation of Aquaform gel in the hindlimb ischaemia model.

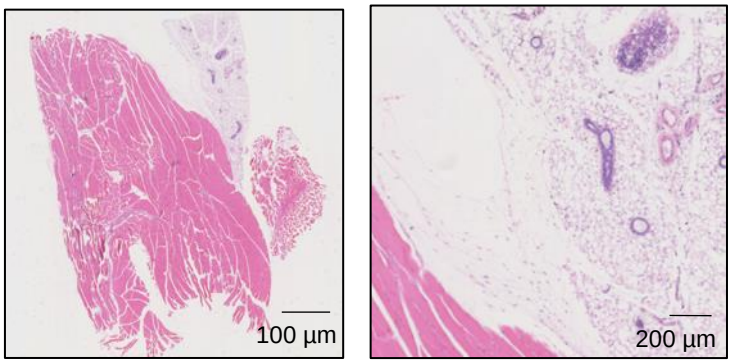

Figure 5.5: H&E staining of tissue sections showing the implantation of GranuGEL in the hindlimb ischaemia model.

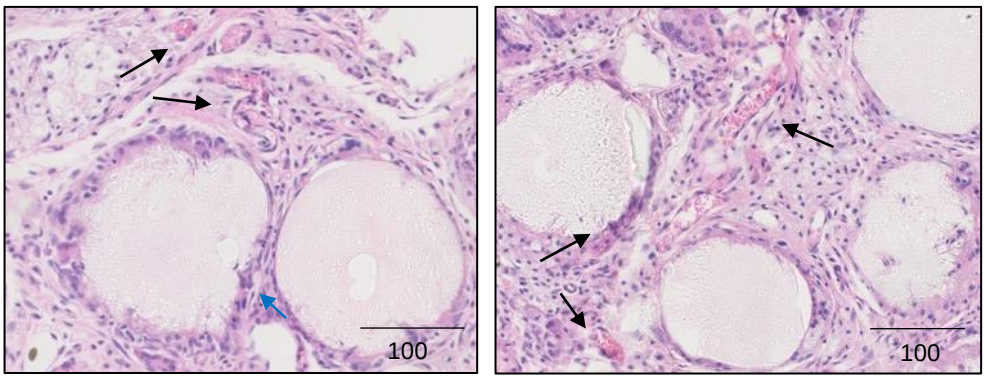

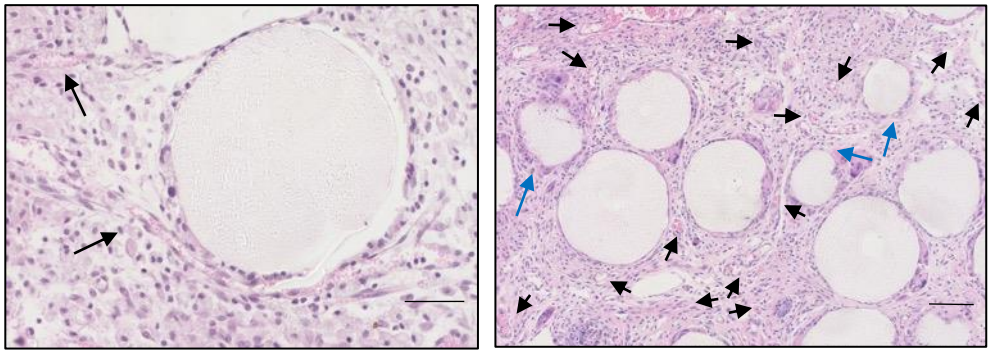

Figure 5.6: H&E staining of tissue sections showing the implantation of PLGA 7507 TIPS microparticles into the hindlimb ischaemia model. Black arrows indicate evidence of blood vessel formation around the microparticles. Blue arrows indicate giant multinucleated cells.

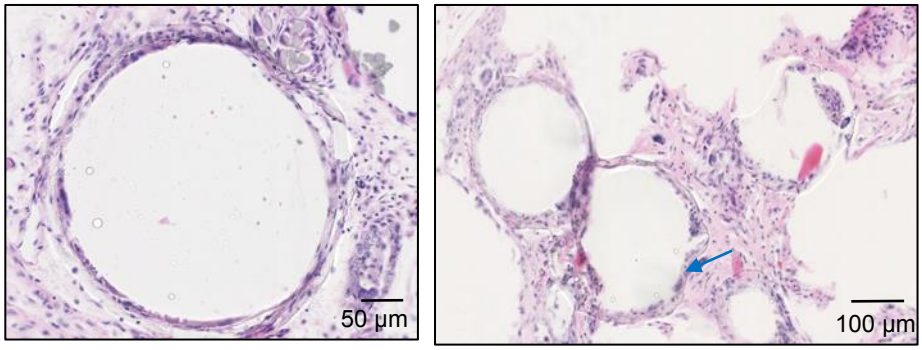

Figure 5.7: H&E staining of tissue sections showing the implantation of PLGA 7507 control microparticles into the hindlimb ischaemia model.

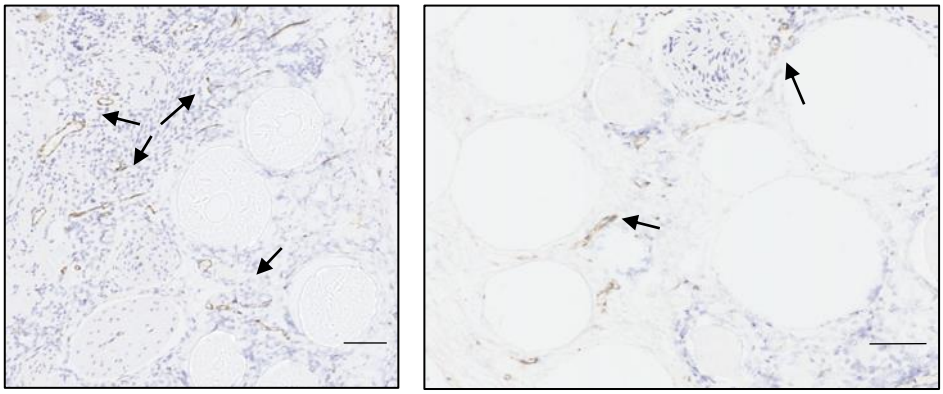

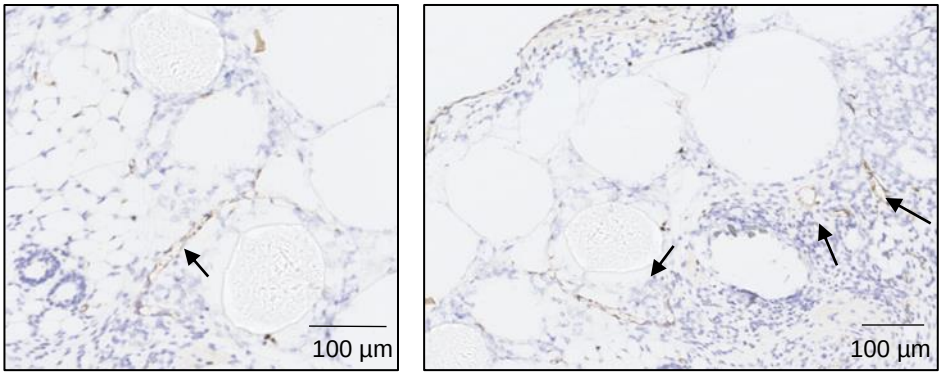

Figure 5.8: VWF staining of tissue sections showing the implantation of PLGA 7507 TIPS microparticles hindlimb ischaemia model. Black arrows highlight positive staining and indicate evidence of blood vessel formation.

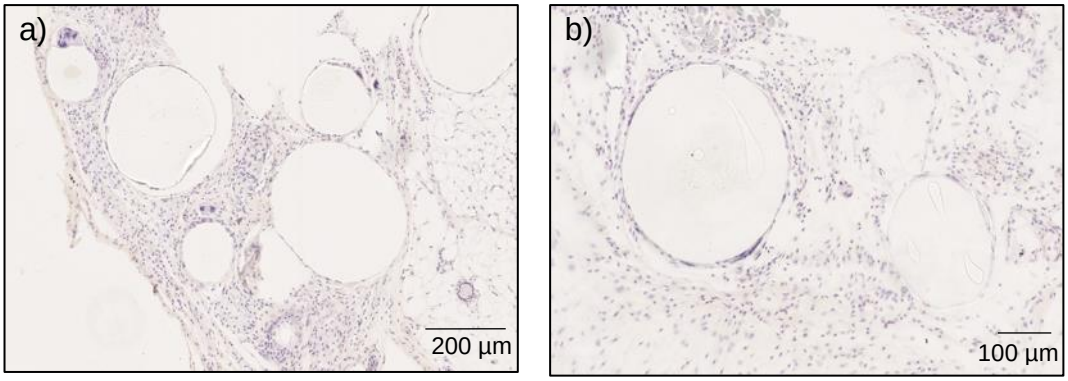

Figure 5.9: VWF staining of tissue sections showing the implantation of PLGA 7507 control microparticles hindlimb ischaemia model.

PLGA control microparticles were H&E stained and images (Figure 5.7) revealed that the microparticles had not migrated from the implant site and as with the TIPS microparticles, showed signs of degradation and deformation. The PLGA control microparticle sections were also stained for VWF, however no positive staining could be seen.

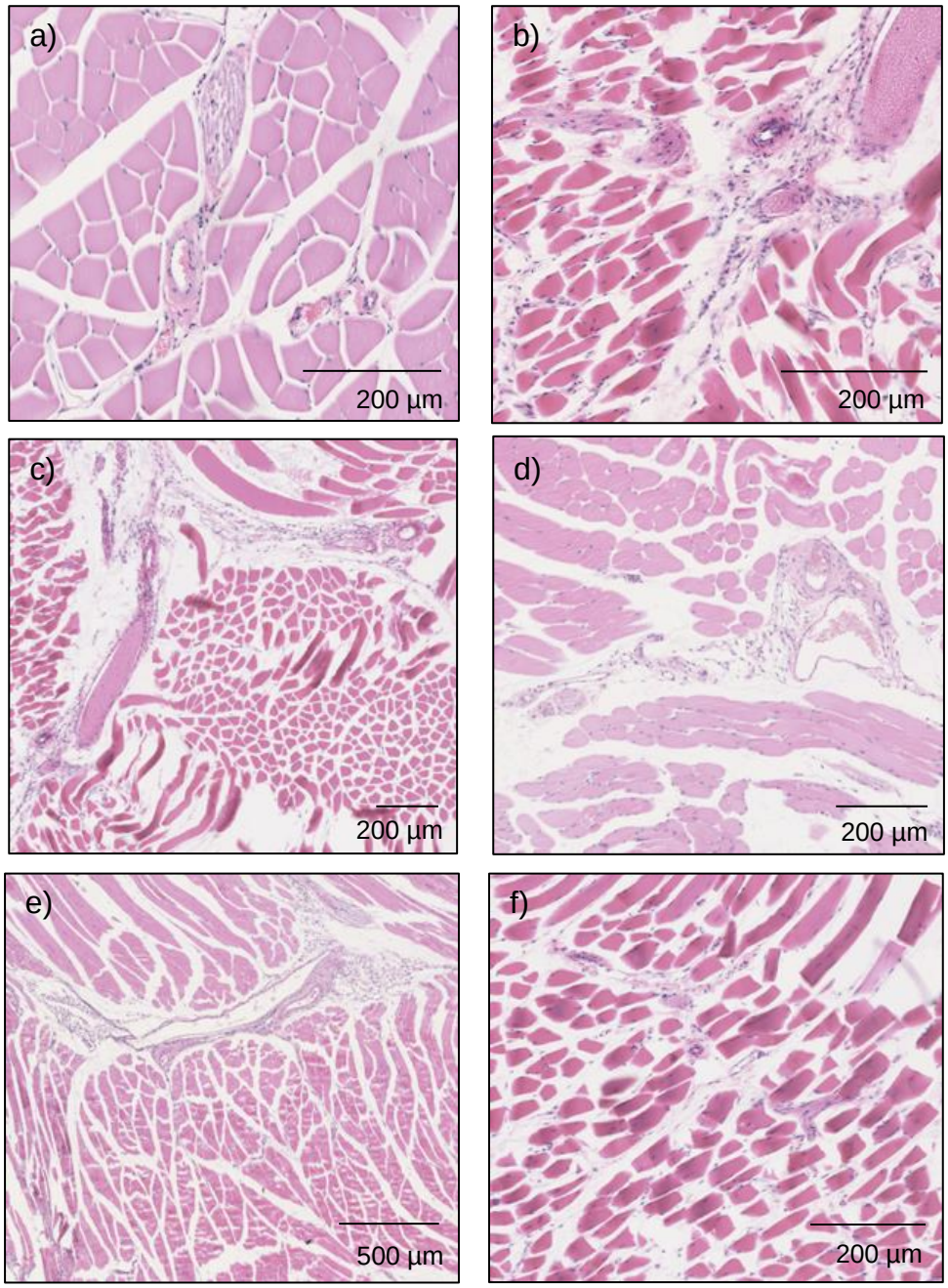

Figure 5.10: H&E stained tissue sections showing collateral blood vessels within the gastrocnemius muscle from each *in vivo* condition a) 7507 TIPS microparticle implantation b-c) 7507 PLGA control microparticle implantation d) granugel only control e) no treatment control f) no ischaemia and no treatment control.

H&E stained sections were examined for evidence of arteriogenesis. This was achieved by identifying collateral blood vessel formations in the gastrocnemius muscle and quantifying the vessel area, lumen area and vessel area/lumen area. Figure 5.10 shows images of representative collaterals and Figure 5.11 shows the quantification of blood vessels (n=3). Results show that ischemic

limbs receiving no treatment had significantly larger collateral vessel size and lumen size. Ischemic limbs treated with TIPS 7507 PLGA microparticles had significantly smaller collateral vessel size and lumen compared with PLGA smooth control microparticles, granugel and no treatment controls. There was a large significant difference in both the vessel area and lumen area between ischemic limbs with no treatment and non-ischemic controls.

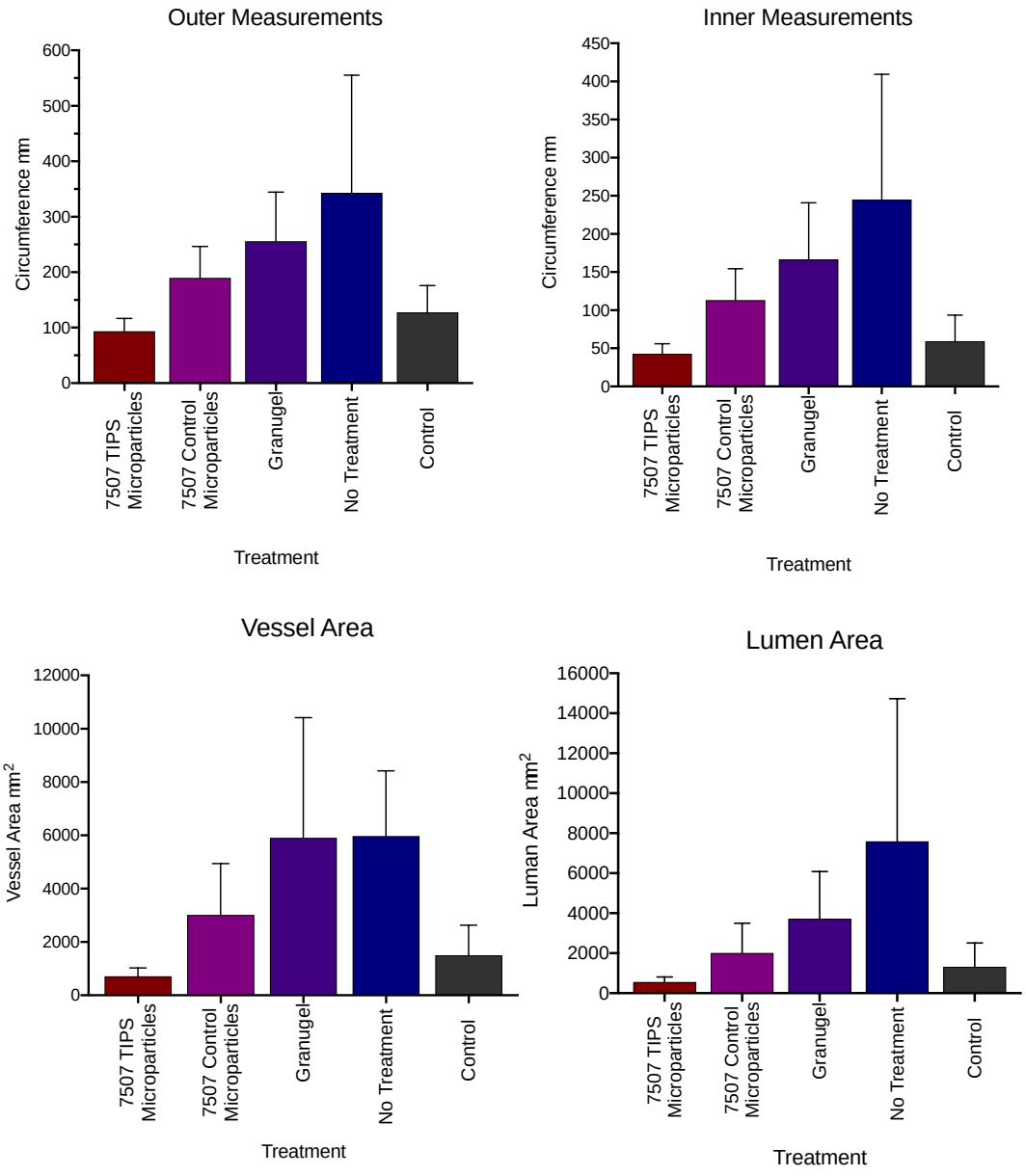

Figure 5.11: Quantification of collaterals from H&E staining a) outer vessel circumference measurements (µm) b) lumen circumference measurements (µm) c) vessel area (µm^2) d) lumen area (µm^2). (n=5) Ordinary one-way ANOVA = **** (P<0.0001).

To assess how the 7507 TIPS microparticles degraded *in vivo* and if the hindlimb ischaemia model effected the degradation rate of the material, 7507 TIPS microparticles were implanted into the hindlimb ischemic model and limbs were harvested at 1, 3, 6, 12 and 24 weeks for evaluation. H&E images in Figure 5.12 display the TIPS microparticles at the different timepoints. Images reveal that the microparticles degraded over time, with only a few particles still visible after 24 weeks. The images show that the microparticles remain at the implant site even as they degraded. H&E stained tissue sections at 3 and 6 weeks reveal evidence of giant multinucleated cell attachment around the microparticles, but after 24 weeks these can no longer be seen. After 6 weeks muscle had started to form around the microparticles.

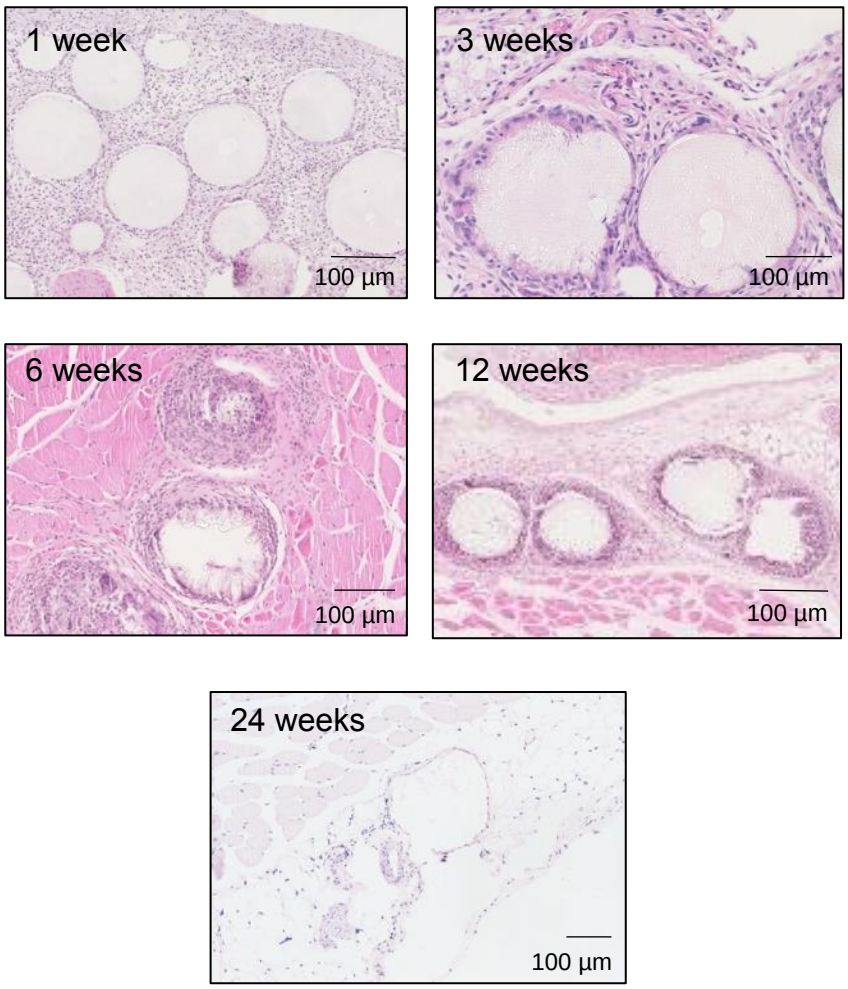

Figure 5.12: H&E staining of tissue sections showing the implantation of PLGA 7507 TIPS microparticles into the hindlimb ischaemia model at weeks 1, 3, 6, 12 and 24 (n=1).

5.3.6 Analysis of in vivo Gene Expression

The gene expression within samples that had undergone ischemic surgery and treated with TIPS PLGA microparticles were analysed for VEGF-A, FGF2, PDGFRA, PDGF and NRP1 expression. The samples were run through a series of thermal cycles and results normalised to Actin that acted as a reference gene. Results (Figure 13) reveal that there was a significant decrease in expression of VEGF-A and PDGFRA from mice with hindlimb ischaemia treated with PLGA control microparticles compared to TIPS PLGA microparticles. There were no other differences in expression between groups and tested genes. These experiments required further optimisation and protocol development.

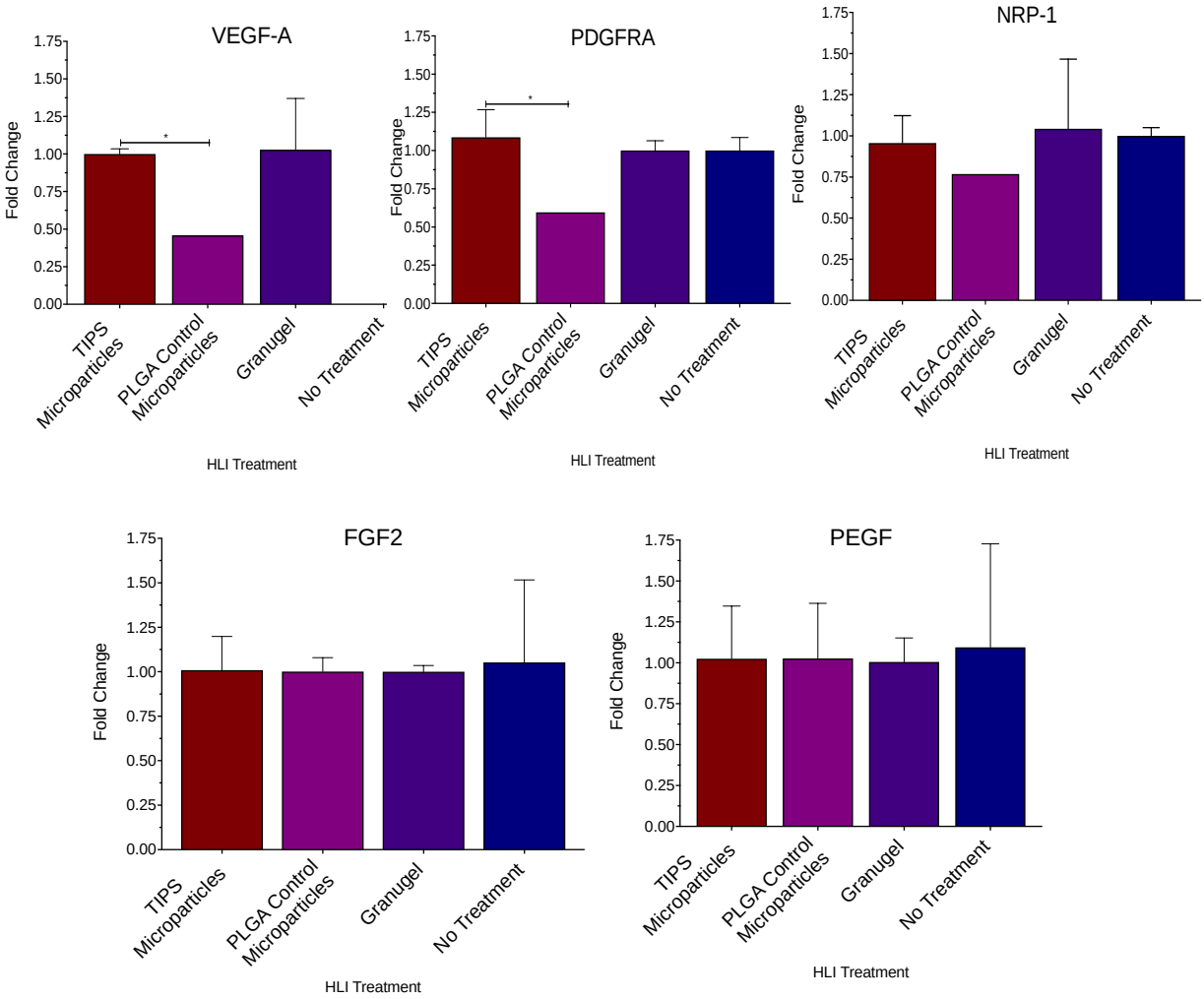

Figure 5.13: Quantification of VEGF-A, PDGFA, PEGF, FGF2 and NRP-1 expression from qPCR (n=1). Where * = P<0.05, ** = P<0.01, *** = P<0.001 and **** = P<0.0001.

5.4 Discussion

The hindlimb ischaemia model is a well-established pre-clinical model of PAD and is often utilised to investigate potential therapies. [66, 71, 91, 146, 334-337, 339, 342, 344, 353-355] As with the pre-clinical polymer film studies (Part I. Chapter 6), pilot studies were performed to investigate the delivery of the biomaterials and their effect on revascularisation through laser doppler imaging and histological analysis.

On order to administer the microparticles via a minimally invasive method, they had to be combined with a hydrogel. Aquaform gel was chosen as it is approved for clinical use as a wound healing gel, consisting of biocompatible and biodegradable polymers (grafted starch polymer and propylene glycol). [507] The Aquaform gel successfully aided delivery of the microparticles *in vivo* through injection. Laser doppler imaging and quantification revealed that there were no significant differences in reperfusion between groups treated with TIPS microparticles, PLGA control microparticles, Aquaform only and no treatment after 21 days (Figure 5.1). Tissues were processed through histology for further analysis. H&E staining (Figure 5.4) revealed that the limbs treated with Aquaform gel had developed large granulomas after 21 days. This could have contributed to the lack of revascularisation observed. To investigate this further, an alternative delivery vehicle was trailed. GranuGEL was selected as it is a clinically approved wound dressing that is comprised of a hydrogel and hydrocolloid (specifically pectin, sodium carboxy-methlycellulose and proplene glycol). It is sterile, easily injectable and has been shown to remain at administration sites within wound care applications. [508, 509] Laser doppler analysis revealed that GranuGEL had not appeared to negatively affect the reperfusion of the limbs. H&E staining of the tissue sections showed no adverse effects of the hydrogel, advocating its safety for this use. Therefore, GranuGEL was selected to deliver microparticles in further *in vivo* studies.

Quantification of laser doppler imaging results show that there were significantly higher reperfusion rates of ischemic limbs treated with TIPS

microparticles in comparison to control microparticles, no treatment and GranuGEL only controls after 21 days. This suggested that TIPS microparticles did not hinder revascularisation, but in fact aided it. Histological staining of the tissues revealed that the TIPS microparticles had remained at the implant site, highlighting their safety *in vivo* as they did not migrate. H&E staining (Figure 5.6) shows that host cellular infiltration had occurred, due to the high porosity of TIPS microparticles. This aided the ability of the microparticles to remain at the implant site, which in turn was promising when looking forward to future studies delivering cellularised constructs, as the chance of the cells remaining at the implant site and eliciting their therapeutic effect would be increased. In addition, safety concerns regarding the migration of microparticles [510] are addressed through histology images, revealing that the microparticles remained at the implant site even as they degraded, with microparticles visible up to 24 weeks (Figure 5.12).

To further assess how the implantation of TIPS microparticles improved the reperfusion rate of the ischemic limbs, the tissues were processed through histology and stained for VWF, an endothelial cell marker. H&E staining (Figure 5.6) had indicated blood vessel formation around the TIPS microparticles and VWF staining (Figure 5.8) revealed positive staining for endothelial cells and thus blood vessel development. The implantation of control PLGA microparticles, GranuGEL and no treatment did not reveal evidence of blood vessel formation (Figure 5.9 and supplementary Figure 5.1). Additional evaluation could involve quantifying the capillaries as a ratio of capillary density to myofibers as this account for the differences in reperfusion rates seen between the ischemic limbs, as an increase in capillary to muscle fibres would allow an increase in blood perfusion of the muscle. [364] Higher capillary to myofiber ratios have been linked to an increase in angiogenesis and reperfusion of ischemic limbs in pre-clinical and clinical studies. [365-367] Despite this, these results, in combination with the laser doppler analysis, suggested that the implantation of 7507 TIPS microparticles promoted revascularisation in a pre-clinical model of PAD through promotion of angiogenesis. This was a promising result from what was intended as a proof

of concept pilot study to assess the feasibility of implanting these materials.

It has been shown that reperfusion of ischemic limbs occurs through angiogenesis (the formation of capillaries from pre-existing vessels initiated through ischaemia) or arteriogenesis (the enlargement of arteries from pre-existing arterioles through vasodilation). [369, 370] Preliminary investigations into the extent of arteriogenesis (Figure 5.10) indicated that the implantation of TIPS 7507 microparticles had a less evidence for arteriogenesis due to smaller vessel and lumen diameters compared to 7507 PLGA control microparticles, GranuGEL, no treatment and no ischaemia controls. This finding suggests that the implantation of 7507 TIPS microparticles increased reperfusion in ischemic limbs through angiogenesis, as however further studies (discussed Part I. Chapter 6) are required to confirm this. As arteriogenesis and angiogenesis occurs as a result from the activation of different pathways from different stimuli, simply angiogenesis is initiated by hypoxia and is driven by endothelial cells, and arteriogenesis is initiated by nitric oxide and an increase in shear stress. [369, 370, 450] The cellular interaction with the control materials could have increased shear stress, resulting in an increase in arteriogenesis, whereas contact with the rough, porous topography of TIPS-processed materials could have initiated the recruitment of endothelial cells, and thus blood vessel development via angiogenesis.

The implantation of both TIPS microparticles and polymer films displayed an increase in reperfusion 21 days after ischaemia compared with controls (Figures 5.3). From Figure 6.4 in Part I. Chapter 6, it can be seen that the TIPS polymer films had a much greater increase in perfusion compared with control polymer films and no treatment controls in comparison to the implantation of TIPS microparticles compared to control microparticles groups. Despite this, when looking at the perfusion ratios of the TIPS microparticles at day 21 (1.4 ±0.5) and TIPS polymer films (0.9 ±0.2) the results are comparable, suggesting that both TIPS-processed materials increase reperfusion to similar levels. However, the control materials had different effects, with 7507 PLGA control polymer films having the least beneficial effect on reperfusion in the

hindlimb ischaemia model, with no increase in reperfusion seen after 7 days. PLGA control microparticles had an increase in perfusion ratio up to day 14, then a slight decrease measured at day 21. This could have been due to vasodilation effects, that often increase reperfusion up to 14 days in hindlimb ischaemia models. These results suggest that TIPS processed materials as either polymer films or microparticles can successfully induce angiogenesis *in vivo*.

The presented *in vivo* work began as a proof of concept study, with the view to implant cellularised TIPS microparticles into the hindlimb ischaemia model for therapeutic angiogenesis. However, due to pro-angiogenic response of the acellular TIPS microparticles seen, they were evaluated further through qPCR in order to understand if there were differences in pro-angiogenic gene expression within the tissues.

qPCR was utilised to analyse the expression of VEGF-A, PDGFRA, FGF2, PEDF, NRP-1 from ischemic tissues receiving TIPS microparticles, control microparticles, GranuGEL and no treatment. The optimisation of RNA extraction and qPCR techniques was discussed in Part I. Chapter 6.4. There was a significant difference between the expression of VEGF-A and PDGFRA, with lower levels expressed by PLGA 7507 control microparticle groups in comparison to TIPS 7507 microparticle groups. No further conclusions could be drawn from qPCR results as unfortunately, due to time constraints as well as a limited number of samples, additional qPCR experiments were not possible. Ideally the qPCR would be optimised, and further testing performed.

There is evidence that the implantation of acellular biomaterials alone can be an effective treatment for ischemic disease. It has been shown that fibrin microparticles implanted into a rabbit hindlimb ischaemia model by Fan *et al.*, 2006, resulted in increased capillary density determined through angiography. [61] DeQuach *et al.*, 2012, administered a skeletal muscle matrix derived hydrogel into a preclinical model of PAD. It was reported that after 14 days there was an increase in arteriole and capillary density compared with controls. [345] Similarly, Ungerleider *et al.*, 2016, administered an ECM based

hydrogel into a murine hindlimb ischaemia model. After 35 days treated limbs resembled healthy tissue and transcriptional studies showed an increase in blood vessel and muscle development after exposure to the biomaterial.

The proposed mechanism of how acellular materials aid in regeneration is through providing mechanical support to the damaged tissue. [511] In addition, by providing an artificial niche *in vivo* the proximal cells can be encouraged to behave as the surrounding tissue would through mechanical, chemical and biochemical support from the material. [512] Specifically, biomaterials that mimic the ECM with high porosity and nano/micro topological surface features have been shown to improve *in vivo* cell behaviours by providing an anchor site for implanted cells, allow host cell attachment, for tissue integration and mechanical support. [513] When analysing the increase in the pro-angiogenic response from TIPS microparticles in comparison to control microparticles, the roughness and porosity of the TIPS microparticles can be accredited to the increase in reperfusion, as this characteristic is the primary difference between these two biomaterials. Furthermore, the implantation of a biomaterial could recruit cells to the implant site through the release of cell homing agents, perhaps through inflammation markers (as the implantation of biomaterials causes an inflammatory response). [396]

Biodegradable materials can support tissue regrowth up to the point that they degrade, and ideally until new functional tissue is formed and the material is no longer required. [512] Hence it is vital to select a material that has a degradation profile tuned to degrade at the rate required. PLGA processed through the TIPS procedure allows for this, as the porous TIPS structure degrades at a faster rate than smooth controls (Figure 2.2). As previously discussed, PLGA can be tuned through adjusting lactic acid and glycolic acid ratios to control the degradation rate and the TIPS process can be adjusted to produce materials with varying porosity that in turn can affect mechanical integrity. An *in vivo* degradation study of 7507 TIPS microparticles implanted into the hindlimb ischaemia model performed over 24 weeks revealed through H&E stained sections that the TIPS microparticles not only degraded from 1 to 24 weeks, but also cell infiltration into the microparticles increased along

with the formation of muscle around the microparticles that was seen over time (Figure 5.12). This suggests there is little risk of the TIPS microparticles migrating after implantation and that they have integrated into the host tissue. This was promising as it suggests that the microparticles do not elicit a prolonged, chronic immune reaction after 24 weeks. Future work could explore the possibility of implanting alternative formulations of PLGA TIPS microparticles into the hindlimb ischemia model to explore the effects of different degradation rates on tissue regrowth and revascularisation of the ischemic limbs.

The unique surface topography and structure of TIPS-based PLGA biomaterials have been shown to elicit a pro-angiogenic response without the addition of biological agents or cells in a pre-clinical model of PAD. The use of an acellular treatment in the clinic would provide an 'of the shelf product' that could be immediately available, kept in long-term storage and prepared when needed. This, in turn, would be more economical than a cell-based therapy that would require isolation, culture and attachment of cells. In addition, by eliminating the introduction of a cell therapy to the body risks of tumorgenicity, emboli formation and uncontrolled differentiation of stem cells would not be considered risk factors with acellular treatments. [514, 515]

5.5 Summary

This chapter was a pilot study that investigated the administration of PLGA 7507 TIPS microparticles in a pre-clinical model of PAD. TIPS microparticles were successfully implanted into the hindlimb ischaemia model via minimally invasive injection with the aid of a hydrogel. Laser doppler imaging revealed that the TIPS microparticles resulted in a significantly higher reperfusion rate of the ischemic limb after 21 days in comparison to smooth PLGA and polystyrene control microparticles.

Histological analysis revealed that the microparticles remained at the implant site, indicating that in future studies involving the implantation of cellularised constructs, the cells would be able to remain at the implant site and have their therapeutic effect. Further evaluation has indicated blood vessel formation around the TIPS microparticles through positive VWF staining as well as cellular cell infiltration into microparticles through the radiating pores.

H&E stained tissue sections were analysed for evidence of arteriogenesis. Preliminary results revealed that there was more evidence of arteriogenesis within control groups in comparison to TIPS microparticle group, indicating that the increase in revascularisation seen with the TIPS microparticles is more likely from the formation of capillaries through the angiogenesis.

The unique surface topography and structure of acellular TIPS based PLGA constructs have been shown to support the host tissue, promote revascularisation, facilitate cell infiltration and activate pathways that result in capillary formation and illicit a pro-angiogenic response through the host tissue reaction to the nano and micro surface characteristics. These findings open up the possibility of utilising TIPS-processed polymers for a non-invasive treatment of PAD.

5.6 Supplementary Information

S5.1 Laser doppler imaging of the paws of mice. Hindlimb ischemia performed in the right limbs and images taken immediately surgery and at weeks 1 and 3. Post-operative images reveal that ischemia was successfully induced. Week 3 images show that TIPS and control microparticles had rates reperfusion in comparison to aquaform gel and no treatment controls.

	Post-Op	**Week 1**	**Week 3**
7507 TIPS Micro-particles	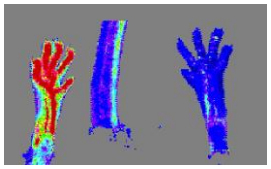	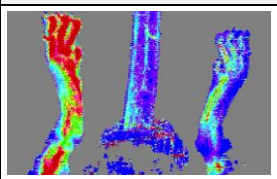	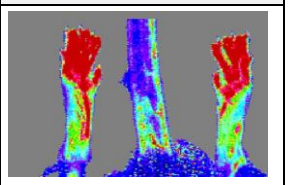
7507 Control Micro-particles	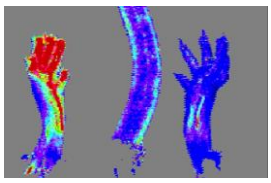	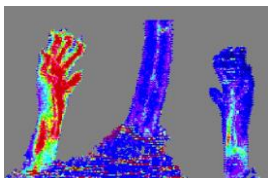	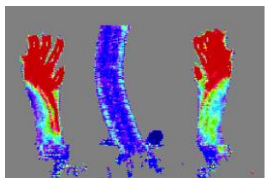
Aquaform gel control	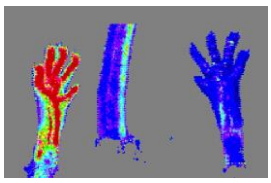	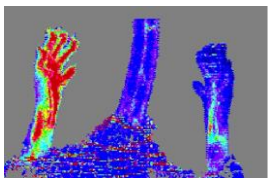	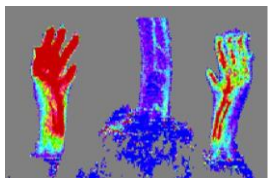
No treatment control	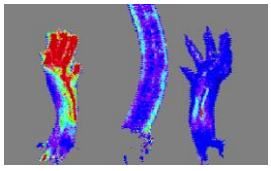	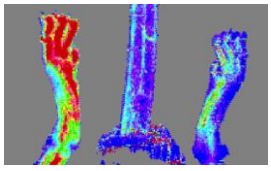	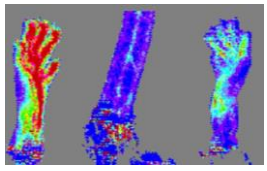

S5.2 VWF staining of a-b) No treatment control c-d) GranuGEL only control e-f) No ischaemia control. No positive staining was seen in any of the control groups.

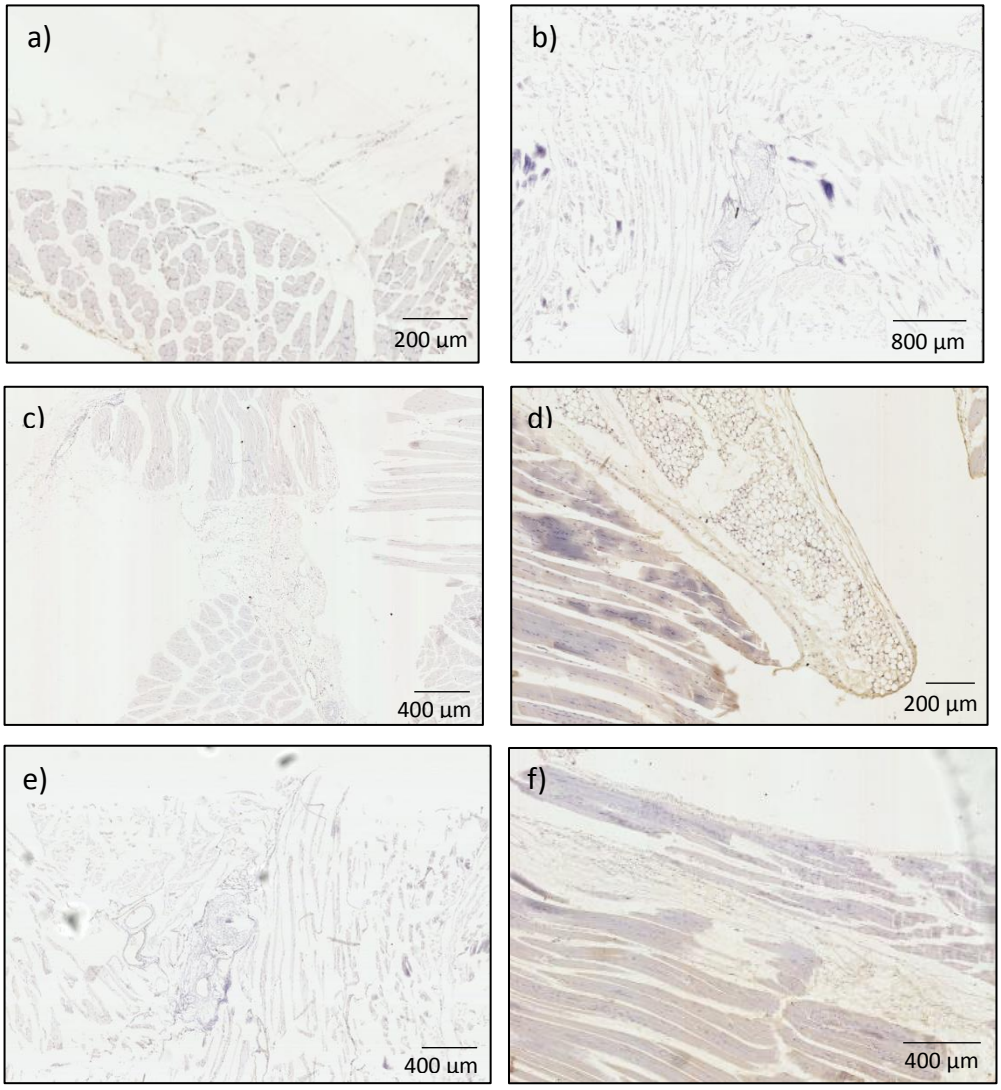

Part II.

Chapter 6: Investigation of Putative Biological Mechanisms Responsible for the *In Vivo* Pro-Angiogenic Effect of Acellular TIPS-Processed Substrates

6.1 Introduction

The immune response to biomaterials was described in Part I. Section 7.1.1. Briefly, an immune response will always occur upon the implantation of a biomaterial, especially if it is an allograft or synthetic material that the body recognises as foreign. [396] This response will usually resolve or develop into a prolonged chronic immune response through the differentiation of macrophages into type 1 (M1) or type 2 (M2), where M1 cells promote inflammation and M2 cells promote regeneration and angiogenesis. [396-403] The outcome of the immune response is dependent on many factors, including the physical characteristics of the biomaterial. These characteristics include; degradability, porosity, roughness, hydrophobicity and stiffness. [396, 402, 409-411, 445] This chapter explores the immune response to 7507 PLGA TIPS microparticles through the examination of *in vivo* implanted acellular TIPS microparticles from Part I. Chapter 5 and the study of the *in vitro* response of M0/M1/M2 macrophages seeded onto TIPS microparticles in hanging drop plates.

6.2 Methods

6.2.1 Histological Analysis of Tissue Sections

Immunohistochemistry for anti-CD163 (1:500, ab182422, Abcam, UK) and anti-CD80 (1:50, ab64116, Abcam, UK) on tissue sections from the *in vivo* implantation of 7507 PLGA TIPS microparticles (Part I. Chapter 5) was carried out as described in Part I. Section 6.2.3.2.

6.2.2 TCP-1 Cell Culture

Human monocytic THP-1 cells were cultured as described in Part I. Section 7.2.2.

6.2.3 Differentiation of TCP-1 Cells into Macrophages

TCP-1 cells were differentiated into macrophages (M0) as described in Part I. Section 7.2.3.

6.2.4 Differentiation of Macrophages into Classical Macrophage Type 1 Phenotype

M0 cells were differentiated into type 1 phenotype (M1) macrophages as described in Part I. Section 7.2.4.

6.2.5 Differentiation of Macrophages into Alternative Macrophage Type 2 Phenotype

M0 cells were differentiated into type 2 phenotype (M2) macrophages as described in Part I. Section 7.2.5.

6.2.6 Cellularising PLGA TIPS Microparticles

7507 TIPS microparticles were prepared as described in Part I. Section 2.2.1. Macrophages were combined with TIPS microparticles as described in in hanging drop plates as described in Part I. Section 3.2.3.

Each 7507 TIPS microparticle was cultured with 500 M1 or M2 cells in 45 µL of M1 or M2 differentiation medium. 35 µL of the supernatants were removed

from each well at days 1, 4, 7 and 10, frozen and each well was replenished with 45 µL of fresh M1 or M2 differentiation media.

To assess how seeding onto TIPS microparticles effected the differentiation of M0 cells, 7507 TIPS microparticles were seeded with 500 M1 or M2 cells in 45 µL of differentiation medium and cultured for 24 hours in complete RMPI-1640 media. After 24 hours 40 µL of the media was removed and 40 µL M1 or M2 media was added. 35 µL of the supernatants of each well was removed at days 1, 4, 7 and 10, frozen and each well was replenished with 45 µL fresh differentiation media.

To investigate the effect of M1 and M2 supernatants of ADMSCs, 7507 TIPS microparticles were cultured with 500 ADMSCs in 45 µL complete MesenPro RS media and cultured for 24 hours. After 24 hours the 35 µL of MesenPro RS media was removed and 35 µL of supernatants collected from M1 or M2 cells was added. The supernatants collected from each well were removed at days 1, 4, 7 and 10, frozen and each well was replenished with 45 µL M1 or M2 supernatants.

6.2.7 Assessing Macrophage Behaviour on TIPS Microparticles

Enzyme-linked Immunosorbent Assay (ELISA) (DY293B, R&D Systems, UK) was used to determine the extent of the M1 and M2 differentiation, as well as the amount of IL-12 p70 released into the supernatants of the samples from and microparticles (n=3).

$VEGF_{163}$ ELISA (DY293B, R&D Systems, UK) was carried out as described in Part I. Section 5.2.2.1.

6.2.8 Statistical Analysis

Statistical Analysis methodology was described in section Part I. Section 2.2.11.

6.3 Results

6.3.1 Histological Analysis of Tissue Sections

Implantation of 7507 TIPS microparticles into the hindlimb ischemia model showed evidence of multinucleated giant cell formation at the surface of the materials, highlighted by H&E staining (black arrows) in Figure 6.1. To investigate the identity of these cells, anti-CD163 immunostaining was used to identify the presence of type 1 phenotype macrophages (M1) and anti-CD80 immunostaining was used to identify the presence of type 2 macrophages (M2). Figure 6.2 showed no evidence of positive anti-CD80 staining around

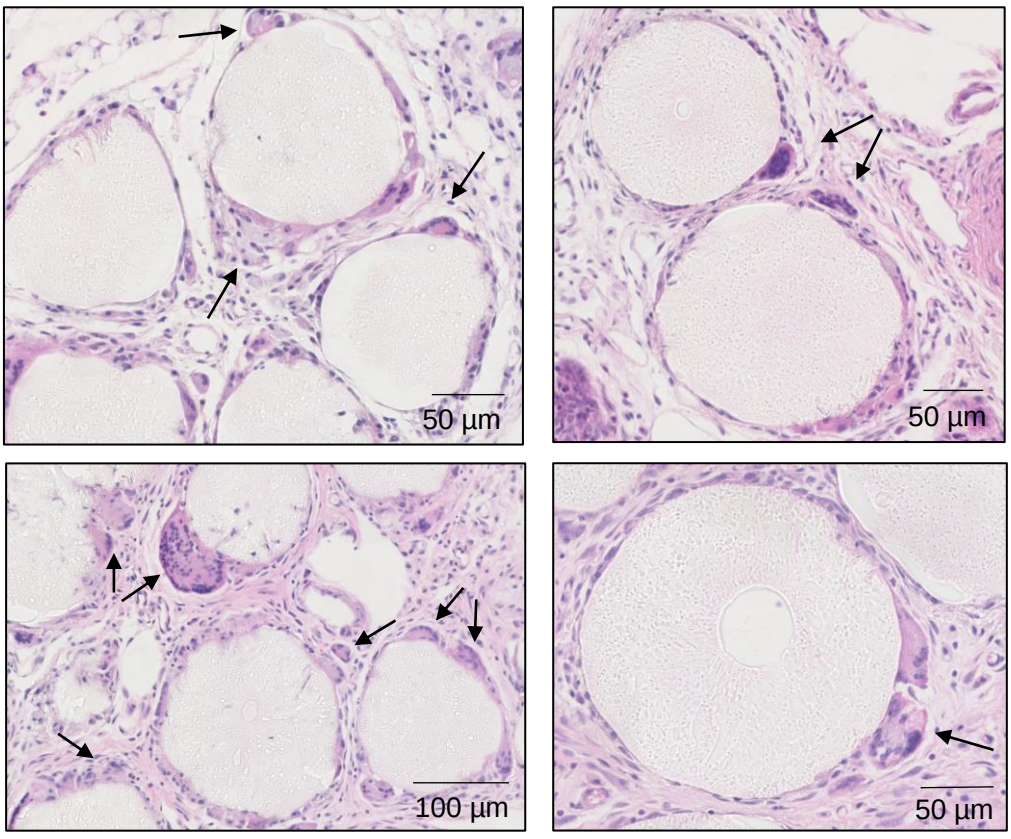

Figure 6.1: Macrophage Cell Evidence around 7507 TIPS Microparticles implanted into a pre-clinical models of peripheral artery disease.

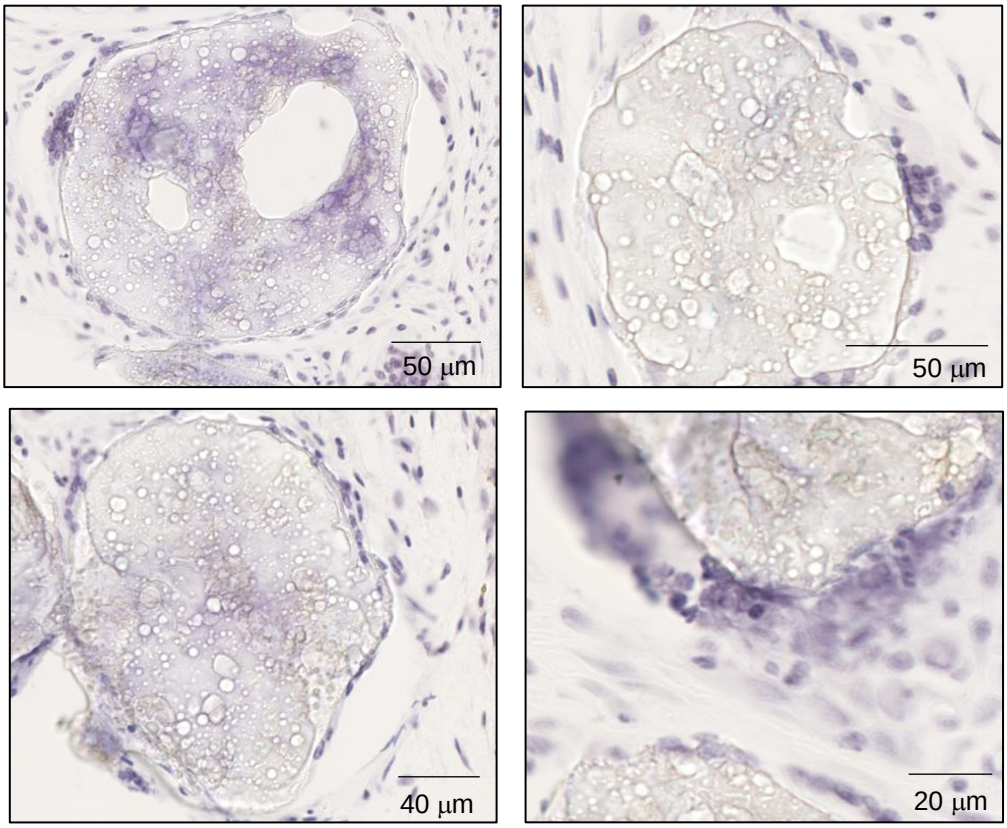

Figure 6.2: Anti-CD80 staining on 7507 TIPS Microparticles implanted into a pre-clinical models of peripheral artery disease.

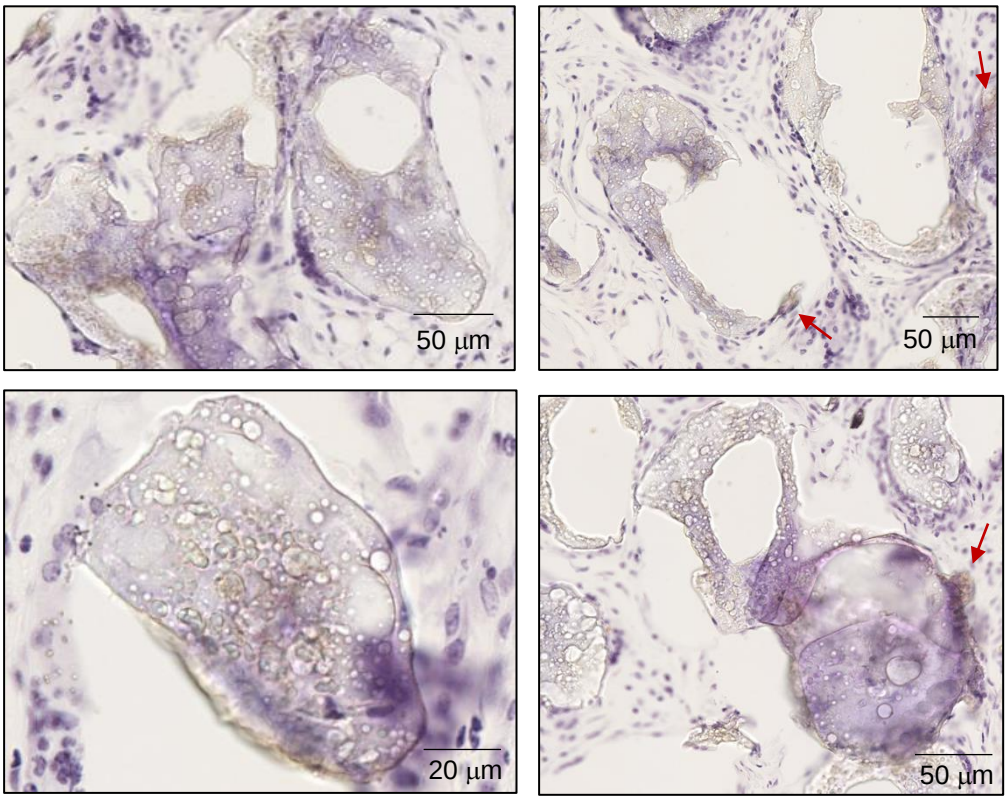

Figure 6.3: Anti-CD163 staining on 7507 TIPS Microparticles implanted into a pre-clinical models of peripheral artery disease.

7507 TIPS microparticles. Tissue sections stained for anti-CD163 (Figure 6.3) revealed inconclusive positive staining. Red arrows indicate possible positively stained anti-CD163 cells.

6.3.2 Differentiation of TCP-1 Cells into Macrophages

THP-1 cells were differentiated into macrophages and then into M1 and M2 phenotypes. To ascertain if the differentiation had been successful an IL-12 p70 ELISA was performed. M1 (and not M2) macrophages secrete IL-12 p70. Figure 6.4 revealed successful differentiation through increased expression of IL-12 p70 from M1 cells.

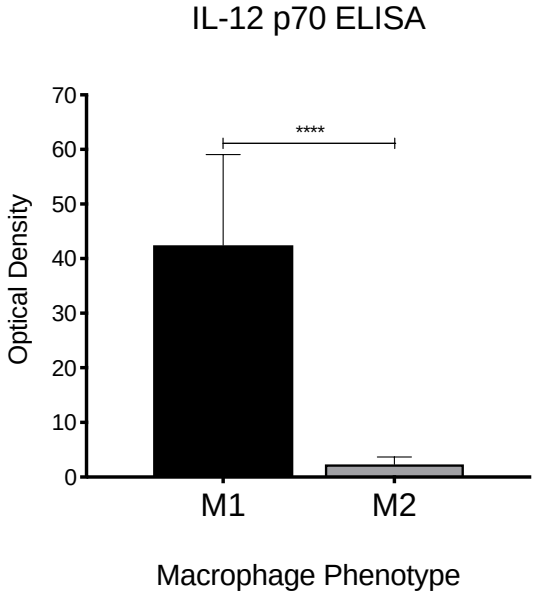

Figure 6.4 : IL-12 p70 secretion from M1 and M2 phenotype macrophages (n=5) Where * = P<0.05, ** = P<0.01, *** = P<0.001 and **** = P<0.0001.

7.3.3. Assessing Macrophage Behaviour on TIPS Microparticles

M0 macrophages were seeded on 7507 PLGA TIPS microparticles in hanging drop plates. The M0 cells were differentiated into either M1 or M2 phenotype macrophages to assess how the materials affected the ability of the cells to differentiate. The supernatants from each sample was measured for IL-12

levels. Figure 6.5 revealed that attachment to 7507 PLGA microparticles did not hinder the differentiation of M0 macrophages as high levels of IL-12 were secreted from M1 cells, which also increased over time. The low secretion of IL-12 from M2 cells confirms this phenotype.

The supernatants were measured for VEGF secretion to assess the angiogenic activity of the macrophages seeded onto 7507 TIPS microparticles in hanging drop plates. Figure 6.6 revealed high levels of VEGF secreted from M2 like macrophages, with higher concentrations of VEGF detected from cells after 10 days in comparison to day 4 (1100 ±99 pg/mL and 720 ±46 pg/mL respectively). M1 macrophages had very low secretion of VEGF at day 1 and 4, with an increase after 10 days (30 ±14 pg/mL and 340 ±3 pg/mL respectively), with a lower secretion from M1 like macrophages in comparison to M2 like macrophages.

To assess how exposure to macrophage secretomes affected the TIPS microparticles cellularised with ADMSCs, the microparticles were seeded with ADMSCs and exposed to the supernatants from M1 or M2 cells. When

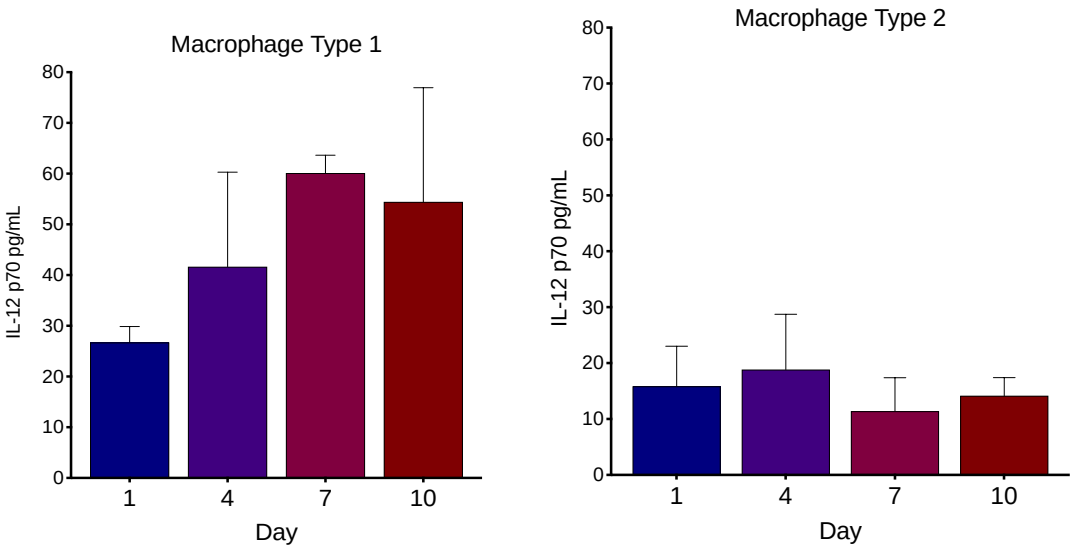

Figure 6.5: IL-12 p70 secretion (pg/mL) from M0 macrophages differentiated into M1 (One-way ANOVA = **** (P<0.0001) and M2 phenotype macrophages attached to PLGA 7507 TIPS microparticles at days 1, 4, 7 and 10. (n=5)

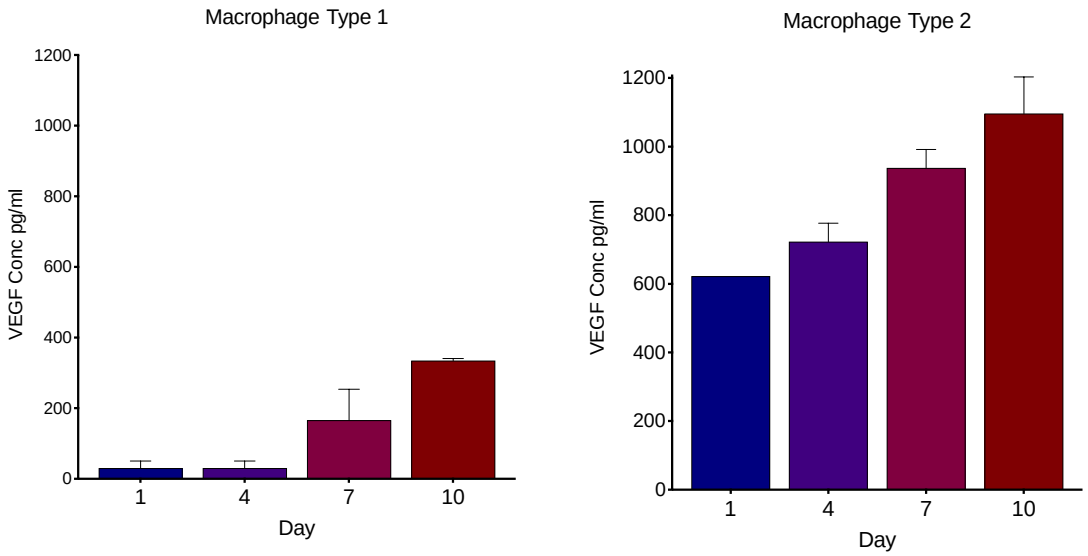

Figure 6.6: $VEGF_{165}$ secretion (pg/mL) from M1 and M2 (One-way ANOVA = ** (P=0.001) phenotype macrophages attached to PLGA 7507 TIPS microparticles at days 1, 4, 7 and 10. (n=5)

exposed to M2 secretomes, ADMSCs secreted increased levels of VEGF from day 1 to 10 (1800 ±300 pg/mL and 4300 pg/mL respectively). The ADMSCs seeded onto 7507 TIPS microparticles exposed to M1 secretomes secreted much lower levels of VEGF that did not vary over the time points, with an overall VEGF concentration after 10 days of 1300 pg/mL.

Figure 6.8 compares the VEGF secretion from ADMSCs seeded onto 7507 TIPS microparticles at day 10 determined in Part II. Section 4.3.1 to the secretion of VEGF from ADMSCs exposed to M1 or M2 secretomes after 10 days seeded onto 7507 TIPS microparticles. There was a significant increase in the VEGF secreted from ADMSCs exposed to M2 secretomes in comparison to standard culture conditions (ADMSC complete media) and M1 secretomes (4300 ±5 pg/mL, 1415 ±490 pg/mL and 1325 ±15 pg/mL respectively). The addition of M1 secretomes had not influenced the secretion of VEGF from ADMSCs in comparison to standard culture conditions.

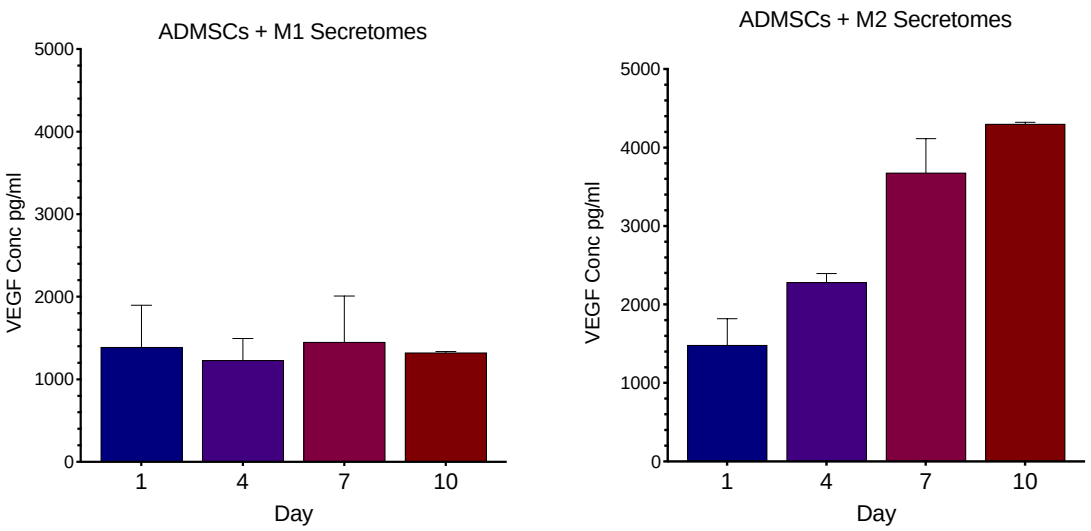

Figure 6.7: $VEGF_{165}$ secretion (pg/mL) from ADMSCs attached to PLGA 7507 TIPS microparticles at days 1, 4, 7 and 10 exposed to M1 (One-way ANOVA = ** (P=0.0072)) and M2 (One-way ANOVA = * (P=0.033)) macrophage secretomes. (n=5)

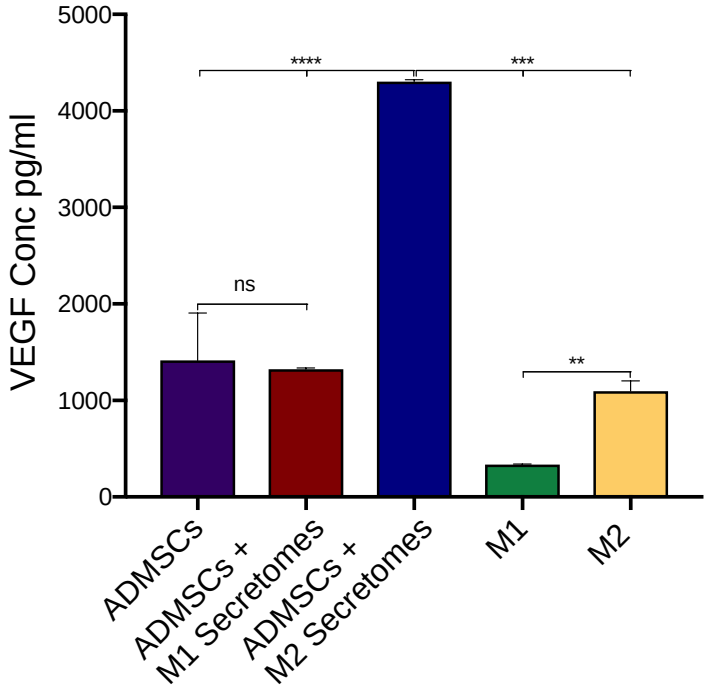

Figure 6.8: $VEGF_{165}$ secretion (pg/mL) from ADMSCs attached to PLGA 7507 TIPS microparticles at day 10 in hanging drop plates in ADMSC culture media and exposed to M1 or M2 macrophage secretomes. M1 and M2 cells seeded onto 7507 TIPS microparticles VEGF secretion at day 10. Where * = P<0.05, ** = P<0.01, *** = P<0.001 and **** = P<0.0001. Ordinary one-way ANOVA = **** (P<0.0001)

6.4 Discussion

Examination of implanted 7507 PLGA TIPS microparticles into a pre-clinical model of PAD revealed the attachment of multinucleated giant cells to the surfaces of the TIPS microparticles (Figure 6.1). To identify these cells, two stains for M1 and M2 macrophages were utilised. As with the studies involving the implantation and examination of TIPS polymer films, (Part I. Chapter 7 Figure 7.3) tissue staining with TIPS microparticles revealed no indication of positive anti-CD80 staining (Figure 6.2). Tissue sections implanted with TIPS polymer films did show some evidence of anti-CD163 positive staining, (Part I. Figure 7.2) however anti-CD163 staining on tissue sections with TIPS microparticles was inconclusive (Figure 6.3). To conclusively identify the multinucleated giant cells attached to the implanted TIPS microparticles (Figure 6.1) further staining is required. Further staining could be performed to identify if the cells are macrophages using anti-CD86, [516, 517] F4/80 [518] or anti-CD11, [519] and if confirmed alternative antibodies for differentiated macrophages could be explored, such as CD68 for M1 [520] and CD206 for M2. [521] It has been established that identifying macrophage phenotype can be difficult due to the large number of similar proteins expressed by both M1 and M2 cells, such as CD86 or major histocompatibility complex II (MCH-II). [521-523] In addition, M2 macrophages have four subtypes (M2a, M2b, M2c and M2d). [422, 442, 459] The subtypes of M2 macrophages express different markers. M2a and M2c express CD163 and CD206, M2b expresses CD86 and M2d cells express VEGF. [422, 524, 525] Therefore, the cells seen around the TIPS microparticles in Figure 6.1 could be subtype of M2 macrophages that was not detected by anti-CD163. The data from the VEGF ELISA also suggest that the cells present could be M2d cells as this subtype of M2 macrophages are known to secrete VEGF, which would support data from Part II. Chapter 5 that revealed that the implantation of TIPS microparticles led to improved reperfusion of ischemic limb. Thus, these data provide a tentative mechanism for the pro-angiogenic effect of TIPS microparticles *in vivo.*

In vitro analysis provided evidence that M0 macrophages successfully

differentiated into M1 and M2 phenotypes through the increased secretion of the M1 marker IL-12 from M1 cells (Figure 6.4). [424] Figure 6.5 revealed that the secretion of IL-12 increased over time when seeded onto 7507 TIPS microparticles, suggesting that the material did not inhibit M1 cell behaviour or proliferation. It has been established that M1 activity can be maintained and stimulated through the attachment to porous materials. [427-430] Therefore, an increase in IL-12 secretion was not unexpected considering that the TIPS microparticles maintain a porous topography after 10 days (SEM images in Part II. Chapter 2).

The increase in a pro-inflammatory response, seen through an increase in M1 like cell activity (increase in IL-12p70 secretion in Figure 6.5) to the TIPS microparticles may not be a negative reaction, as it has been shown that porous materials resolve pro-inflammatory responses more successfully than smooth materials. [431-435] This resolution is promoted by the presence of M2 cells. Figure 6.5 showed that M2 phenotype was maintained (through low IL-12 secretion). In addition, M2 cells secreted high levels of VEGF that increased from day 1 to day 10, suggesting that attachment to TIPS microparticles promoted proliferation and the pro-angiogenic behaviour of M2 cells. There was also an increase in the VEGF produced from M1 cells over time, suggesting that M1 cells could have differentiated into M2 cells in response to the TIPS microparticles, where it has been shown that macrophages can switch between phenotypes in response to external conditions. [526] This is promising for the administration of TIPS microparticles *in vivo* as if M2 cells are able to survive once attached to the microparticles and if M1 cells differentiate into M2 cells, the inflammatory response will resolve quiker therefore reducing the risk of infection or failure of the implant.

Chapter 4 revealed that ADMSCs seeded onto 7507 TIPS microparticles exhibited pro-angiogenic properties *in vitro* in comparison to smooth microparticle controls. To investigate how the secretomes from M1 and M2 macrophages effected ADMSCs angiogenic behaviour, 7507 TIPS microparticles cellularised with ADMSCs were exposed to M1 and M2 secretomes and the VEGF secretion was measured. ADMSCs exposed to M2

secretomes showed an increase in VEGF expression, which can be attributed to the additional VEGF secreted from the M2 cells (Figure 6.6) or other factors secreted by M2 macrophages could have stimulated VEGF secretion from ADMSCs. It has been shown that M2 macrophages secrete additional pro-angiogenic factors such as PDGF-AA, uPA and MMP-9, [423, 527] where PDGF has been shown to regulate the secretomes from ADMSCs, [528] specifically the expression of VEGF. [267, 529] The large increase in VEGF secretion from ADMSCs exposed to M2 secretomes was higher than both ADMSCs alone and M2 alone VEGF concentrations at day 10 (Figure 6.8), this suggests that the increase in VEGF was due to a paracrine effect of the M2 macrophages stimulating pro-angiogenic behaviour of ADMSCs. This is promising for future studies administrating cellularised TIPS microparticles *in vivo* to treat ischemic disease, as the ADMSCs, TIPS topography and the macrophage response associated with tissue implantation could be an ideal combination to initiate blood vessel formation through promotion of VEGF.

When comparing the amount of VEGF secreted from ADMSCs in hanging drop plates measured in Chapter 4 Figure 4.2b it can be seen in Figure 6.8 that there was no significant difference between ADMSCs exposed to M1 secretomes and ADMSCs maintained in standard culture conditions, suggesting that M1 macrophages did not hinder ADMSC pro-angiogenic behaviour. When considering the use of cellularised TIPS microparticles *in vivo* to promote angiogenesis, these results are encouraging because exposure to M1 secretomes did not block the VEGF secretion from ADMSCs. In fact, M1 cell behaviour increased in response to TIPS microparticles, through an increase in secretion of IL-12p70 seen in Figure 6.5. There was evidence that M1 macrophages had begun to differentiate into M2 macrophages after exposure to TIPS microparticles (as indicated by increase in VEGF secretion in Figure 6.6). To confirm this, further investigation would be required to identify the presence of M2 cells.

Figure 6.8 had revealed that ADMSCs exposed to M2 secretomes produced high levels of VEGF, it is hypothesised that when implanted *in vivo,* the initial immune response comprising of M1 cells could become pro-angiogenic.

6.5 Summary

This chapter explored the putative biological mechanism responsible for the *in vivo* pro-angiogenic effect of acellular TIPS microparticles. Initial work involved investigating the identity of multi-cellular giant cells that had attached to the TIPS microparticles *in vivo* (Figure 6.1). Immunostaining for anti-CD80 as a marker for M1 cells (Figure 6.2) and anti-CD163 for M2 cells (Figure 6.3) was inconclusive, and further investigations using different antibodies to alternative markers is required. M2 macrophages have four subtypes and M2d macrophages are not detected by anti-CD163, but by VEGF secretion. It is postulated that the cells found attached to the implanted TIPS microparticles were M2d cells and this in turn contributed to the pro-angiogenic response seen in Chapter 5 through increased reperfusion rates and blood vessel formation.

In vitro studies examining the effect of TIPS microparticles on M1 and M2 behaviour revealed that exposure to the unique TIPS surfaces did not obstruct macrophage behaviour, where M1 cells produced high levels of IL-12 and M2 cells produced increased quantities of VEGF over time. There was also an increase in VEGF secretion from M1 cells, suggesting that they may have begun to differentiate into M2 phenotype.

The immune response to TIPS microparticles cellularised with ADMSCs was investigated. It was discovered that M2 secretomes had a stimulatory effect on the secretion of VEGF from ADMSCs through paracrine effects. These finding suggest the foreign body response observed with the implantation of TIPS microparticles could contribute to a pro-angiogenic effect that might be beneficial. The impact of the angiogenic response on arteriogenesis and functional vasculature requires further investigation.

Conclusions

To address the hypothesis of this project, that ‘hierarchical textured surface topographies promote the secretion of angiogenic growth factors for therapeutic angiogenesis’, multiple strategies were employed. Firstly, a range of biomaterials were manufactured through the TIPS process into 2D polymer films. After initial physical and biological characterisation, where it was revealed that TIPS-processed PLGA had superior roughness and stiffness than smooth controls and had an interconnected porous structure, it was determined that 7507 and 7502 PLGA would be studied further in comparison to controls to evaluate how surface topography effected cell behaviour.

Initially the strategy of this study was to begin investigations with 2D polymer films as they provided advantages such as ease of manufacture, reproducibility and were able to be characterised with a range of techniques, then the focus of the project would have shifted to microparticles, that can be delivered *in vivo* via minimally invasive methods. However, as it was uncovered that ADMSCs (selected due to their pro-angiogenic properties) elicited an increased pro-angiogenic response when attached to TIPS films over smooth controls, the polymer films were studied further.

Pilot studies involving the implantation of the TIPS polymer films originally aimed to investigate the ease of implantation, migration, degradation and host response to the material, revealed unexpected results. The implantation of acellular 7507 PLGA TIPS films increased the revascularisation of ischemic limbs, and subsequent immunohistochemistry identified the presence of blood vessels around the implants. These findings open up the possibility of utilising 2D polymer films to treat PAD, without the addition of biological agents.

Studies into the *in vitro* pro-angiogenic response of ADMSCs attached to TIPS-processed polymers uncovered that ADMSCs attached to 7507 TIPS microparticles had the highest VEGF secretion per cell overall, indicating that this may be the optimal material for therapeutic angiogenesis. TIPS microparticles were cellularised using a novel hanging drop method, that

allowed for more control over cellularisation and eliminated the effects of tissue culture surfaces. 7507 TIPS microparticles were successfully administered into a pre-clinical model of PAD via minimally invasive injection, and as with the TIPS films, acellular TIPS microparticles stimulated a pro-angiogenic response *in vivo* where blood vessels had formed around the implants. Histological analysis revealed that TIPS-processed substrates had not migrated, highlighting their safety *in vivo* and indicating that in future studies involving the implantation of cellularised constructs, the cells would be able to remain at the implant site and have their therapeutic effect.

From the pre-clinical studies, the inflammatory response towards the implanted biomaterials was investigated. Evidence of inflammatory cells were seen around the implanted TIPS materials, and their identification was attempted. Preliminary results were negative for pro-inflammatory M1 macrophages and there was some evidence for pro-angiogenic M2 macrophages around the TIPS-processed substrates. It is proposed that the cells found attached to the implanted TIPS materials were M2d cells (that secrete VEGF) and this in turn contributed to the pro-angiogenic responses seen through increased reperfusion rates of the ischemic limbs and blood vessel development. *In vitro* studies revealed that exposure to the unique TIPS surfaces did not obstruct macrophage behaviour. There was also an increase in VEGF secretion from M1 cells upon exposure to 7507 PLGA TIPS-processed substrates, suggesting that they may have begun to differentiate into M2 phenotype, with links to blood vessel development, regulation of angiogenesis and vascular development uncovered through protein profiling, however further work is required to establish this.

In conclusion, it has been shown that hierarchical textured surface topographies resulted in the increase in secretion of angiogenic growth factors from ADMSCs. it has been demonstrated that the TIPS process can be utilised to make a range of substrates, that can be used for tissue engineering applications. In addition, the pro-angiogenic behaviour of the acellular TIPS-processed substrates were demonstrated in a pre-clinical model of PAD, indicating the potential use of biomaterials for therapeutic angiogenesis.

Future Work

From the results presented from this project, there are various directions future research could investigate. This work primarily focused on characterising the physical properties of PLGA 7507 10 wt% films and microparticles (selected from initial screening of polymers in Part I. Chapter 2), the response of ADMSCs to this composition of PLGA as well as the effect in a pre-clinical model of PAD. However, there are numerous formulations of PLGA, therefore future work could focus on screening a wider range of TIPS processed polymers to assess the optimum properties for therapeutic angiogenesis. Such properties include lactic acid to glycolic acid ratios, inherent viscosity, material shape, mechanical integrity, porosity and degradation rate, that can in turn influence the therapeutic potential. There are additional methodologies that can be employed to characterise the TIPS-processed structures. For example, due to the limitations of AFM, the roughness and stiffness of microparticles was not possible, therefore they could be analysed through optical profilometry. [486] Porosity can also be quantified through mercury intrusion porosimetry, nitrogen adsorption and helium porosimetry. [530, 531] However, further Nano-CT analysis would also yield quantitative information on the porosity of the TIPS polymer films and microparticles.

An experiment utilising the NanoCT scans was planned, however because of time constraints it was not possible to execute. The NanoCT scans of the surface of the 7507 TIPS polymer films were obtained, with increasing levels of smoothness created through manipulation of the images. The intention was to 3D print the structures with a non-degradable material. From this, ADMSCs would be attached to the films and the angiogenic response assessed. The rational from this study would have been to uncover if the pro-angiogenic response seen from ADMSCs seeded onto TIPS surfaces was from the topography, how decreasing the topography effected cell behaviour and if the pro-angiogenic response was induced by the biodegradable PLGA.

Investigations into the *in vitro* effect of ADMSCs seeded onto TIPS polymer films (Part I. Chapter 5) and TIPS microparticles (Part II. Chapter 4) revealed

pro-angiogenic responses to 7507 TIPS-processed substrates. Proteome profiler arrays and angiogenesis arrays were utilised to identify the underlying mechanism of action. Several biological processes were discovered, and it was concluded that multiple pathways may be involved in promoting the increase in $VEGF_{165}$ secreted from ADMSCs when seeded onto TIPS-processed substrates. Further work is required to discover the pathways activated to further understand the effect of TIPS-processed substrates on ADMSCs, that can be achieved through blocking specific kinases with inhibitors, using intracellular fluorescent indicators, biochemically analysing signal transduction, [532] RNA interference screening [533] and functional genomics. [534]

There is also increasing evidence suggesting that subjecting ADMSCs to hypoxic conditions can improve their proliferation, differentiation and pro-angiogenic properties. [535-538] Therefore, it would be interesting to consider the effects of hypoxia on the behaviour of ADMSCs when attached to TIPS-processed PLGA. To achieve this, a hypoxia chamber can be utilised to induce hypoxia *in vitro.* In addition, by subjecting the cells to hypoxic conditions it would be more representative of the ischemic environment found *in vivo* allowing for a more accurate study and understanding of cellular responses.

A novel methodology for cellularising microparticles was divulged in Part II. Chapter 3. The hanging drop method allowed for a higher degree of control over cell attachment to microparticles. The development of this method opens up the possibility for engineering automated technology to allow for the scaling up of this process. This would be beneficial for streamlining the preparation of ADMSCs attached to TIPS microparticles a potential therapeutic for PAD.

The initial aims of pre-clinical studies (Part I. Chapter 6 and Part II. Chapter 5) were to implant cellularised constructs into the hindlimb ischaemia model. However, the positive response seen from pilot studies involving the implantation of acellular constructs in the reperfusion of ischemic limbs were focused on. Consequently, due to time constraints, the implantation of cellularised constructs was not possible. Despite this, it would be noteworthy

to assess the effects of cellularised constructs *in vivo,* especially considering the *in vitro* pro-angiogenic response from ADMSCs seeded onto both 7507 TIPS polymer films and microparticles. To achieve this, immunocompromised mice would be used with appropriate controls, such as the implantation of ADMSCs in suspension, to identify if the addition of a biomaterial effected cell retention at the implant site, as well as cellular behaviour *in vivo.* One of the key questions to be answered from the *in vivo* implantation of cellularised constructs is if the ADMSCs will differentiate into endothelial cells or recruit endothelial cells through secretion of angiogenic growth factors to promote angiogenesis. This would result in a better understanding of how the cells respond in the hindlimb ischaemia model and how angiogenesis is promoted in this environment. In addition, the ADMSCs can be modified with bioluminescence and tracked *in vivo* to monitor cell migration. [539] This would not only address safety concerns (of stem cell migration, uncontrolled proliferation and differentiation) [540] but would also be vital as one of the rationales for using biomaterials in combination with cell therapy is that they will allow the cell to remain at the implant site and to have their therapeutic effect.

Preliminary evaluation into the extent of arteriogenesis were explored (Part I. Chapter 6 and Part II. Chapter 5). However, to fully assess arteriogenesis in comparison to angiogenesis (that is studied through endothelial cell staining), further surgery is required where probes are implanted into the hindlimbs of mice to stimulate the gascilis anterior muscle with subsequent blood pressure measurements performed. [373, 377-379] These experiments can help establish if any improvement in reperfusion observed (through laser doppler imaging) is due to arteriogenesis or angiogenesis, and through this the mechanism of action can begin to be understood.

As discussed in Part I. Chapter 6 and Part II. Chapter 5, the genetic analysis of tissues from the pre-clinical studied required optimising. This was not possible due to a limited number of samples and time restraints. It would be worthwhile to explore the differences in (angiogenesis related) gene expression between ischemic tissues treated with TIPS and control materials,

as there were significant differences between the reperfusion rates between these groups to further understand the increased reperfusion seen in the ischemic limbs from the implantation of TIPS biomaterials.

In Part I. Chapter 6, Wars2 was identified as a gene that was promoted in ischemic limbs treated with 7507 TIPS polymer films in comparison to control PLGA polymer films. Wars2 has been shown to promote angiogenesis through increasing endothelial cell migration, proliferation and capillary formation. [393-395] Therefore, future work could focus on ascertaining how TIPS surfaces influence Wars2, and if in turn this is a key factor in the observed pro-angiogenic responses seen *in vitro* and *in vivo*.

Finally, there is a large scope for research opportunities that can come from work investigating the inflammatory response to TIPS-processed materials in Part I. Chapter 7 and Part II. Chapter 6. Stained tissue sections from pre-clinical *in vivo* studies revealed evidence of an immune response to the implanted acellular TIPS-processed materials. Staining was attempted to identify the cells involved, however additional staining for either different macrophage markers or other immune cells was required. The *in vitro* response of macrophages to TIPS-processed PLGA was examined and preliminary results suggested that TIPS-processed substrates may be more advantageous than smooth and non-degradable polymers as an effective treatment for ischemic diseases through the promotion of pro-angiogenic M2 macrophage activity. However, further experimentation is required including M0 only controls and flow cytometry analysis to ascertain if the differentiation of M0 cells to M1 and M2 phenotypes was completely successful. Understanding the immune response to an implant can determine its success or failure, and in this case perhaps TIPS-processed materials can exploit the inevitable immune response to avoid chronic inflammation and promote angiogenesis.

References

1. Foundation, B.H. *Heart Statistics - BHF Statistics Factsheet*. Heart and Circulatory Diseases Statistics 2018 04/02/2019]; Available from: https://www.bhf.org.uk/what-we-do/our-research/heart-statistics.
2. Organization, W.H. *Cardiovascular diseases (CVDs)*. 2017 04/02/2019]; Available from: https://www.who.int/news-room/fact-sheets/detail/cardiovascular-diseases-(cvds).
3. Foundation, B.H. *Focus on: Peripheral arterial disease*. 02/02/2019]; Available from: https://www.bhf.org.uk/informationsupport/heart-matters-magazine/medical/peripheral-arterial-disease.
4. Stuckey, D.J., *Stem Cell Therapy – MRI for In Vivo Monitoring of Cell and Tissue Function*. 2011: Elsevier B.V.
5. Stuckey, D., et al., *In vivo tracking of mesenchymal stem cells in the infarcted rat heart by magnetic resonance imaging.* HEART, 2006. **92**(2).
6. Merten, O.W., *Advances in cell culture: anchorage dependence. Philos Trans R Soc Lond B Biol Sci* . 2015. **370**(1661): p. 20140040.
7. Avolio, E., et al., *Combined intramyocardial delivery of human pericytes and cardiac stem cells additively improves the healing of mouse infarcted hearts through stimulation of vascular and muscular repair.* Circulation Research, 2015. **116**(10): p. 81-94.
8. BMJ, *Diagnosis and management of peripheral arterial disease.* BMJ, 2012. **345**: p. e5208.
9. Ouriel, K., *Peripheral arterial disease.* The Lancet, 2001. **358**(9289): p. 1257-1264
10. Fowkes, F.G., et al., *Comparison of global estimates of prevalence and risk factors for peripheral artery disease in 2000 and 2010: a systematic review and analysis.* Lancet, 2013. **382**(9901): p. 1329-1340.
11. Allen, J., et al., *Comparison of lower limb arterial assessments using color-duplex ultrasound and ankle/brachial pressure index measurements.* Angiology, 1996. **47**(3): p. 225-232.
12. Gornik, H.L. and J.A. Beckman, *Peripheral Arterial Disease.* Circulation, 2005. **111**(3): p. 169-172.
13. Criqui, M.H., et al., *Mortality over a period of ten years in patients with peripheral arterial disease.* N Engl J Med, 1992. **326**(6): p. 381–386.
14. Selvin, E. and T.P. Erlinger, *Prevalence of and Risk Factors for Peripheral Arterial Disease in the United States.* Circulation, 2004. **110**(6): p. 738-743.
15. Dhaliwal, G. and D. Mukherjee, *Peripheral arterial disease: Epidemiology, natural history, diagnosis and treatment. The International Journal of Angiology : Official Publication of the International College of Angiology, Inc* . 2007. **16**(2): p. 36-44.

16. NICE. *Peripheral arterial disease: Quality Standard* NICE Guidance 2014 01/08/18]; Available from: www.nice.org.uk/guidance/qs52/chapter/introduction.
17. Shishehbor, M.H., *Acute and critical limb ischemia: When time is limb.* Cleveland Clinic Journal of Medicine, 2014. **81**(4): p. 209-216.
18. Wolfe, J.N., *Defining the outcome of critical ischaemia: a one year prospective study.* Br . J . Surg . 1986. **73**(321).
19. Howard, D.P.J., et al., *Population- Based Study of Incidence, Risk Factors, Outcome, and Prognosis of Ischemic Peripheral Arterial Events* Circulation, 2015 **132**(19): p. 1805–1815
20. Bennet, M. and J. Davidson. *All about blocked arteries*. 2016 28/08/19]; Available from: https://www.bhf.org.uk/heart-matters-magazine/medical/blocked-arteries.
21. Gornik, H.L. and J.A. Beckman, *Cardiology patient page. Peripheral Arterial Disease.* Circulation, 2005. **111**(13): p. 169-172.
22. Hinkle, J.L. and L. Bowman, *Neuroprotection for ischemic stroke* J Neurosci Nurs, 2003. **35**(2): p. 1 14-118.
23. Stramer, B.M., R. Mori, and P. Martin, *The inflammation-fibrosis link? A Jekyll and Hyde role for blood cells during wound repair.* J Invest Dermatol., 2007. **127**(5): p. 1009-1017.
24. Fraye, E., *Acquired Mitochondropathy - A New Paradigm in Western Medicine explaining Chronic Diseases: The Safety Guide for Prevention and Therapy of Chronic Ailments* . . 2 ed. 2011: Springer.
25. Sims, N.R. and H. M uyderman, *Mitochondria, oxidative metabolism and cell death in stroke.* Biochimica et Biophysica Acta, 2010. **1802**(1): p. 80–91.
26. Mount, N.M., et al., *Cell-based therapy technology classifications and translational challenges* P*hilosophical Transactions of the Royal Society B: Biological Sciences*, 2015. **370**(1680): p. 20150017.
27. Tan, R.P.C., A.H.P. Lennartsson, K. Miravet, M.M. Lee, B.S.L. Rnjak-Kovacina, J. Clayton, Z.E. Cooke, J.P. Ng, M.K.C. Patel, S. Wise, S.G., *Integration of induced pluripotent stem cell-derived endothelial cells with polycaprolactone/gelatin-based electrospun scaffolds for enhanced therapeutic angiogenesis.* Stem Cell Research & Therapy, 2018. **9**(70).
28. Deveza, L., J. Choy, and F. Yang, *Therapeutic Angiogenesis for Treating Cardiovascular Diseases.* Theranostics, 2012. **2**(8): p. 801-814.
29. Lanza, R., R. Langer, and J.P. Vacanti, *Principles of Tissue Engineering*. 2000, Oxford: Elevier Academic Press.
30. JA, E. and N. S, *The extracellular matrix of blood vessels.* Curr Pharm Des. , 2009. **15**(12): p. 1385-1400.
31. P, C., *Mechanisms of angiogenesis and arteriogenesis.* Nature Medicine, 2000. **6**(4): p. 389-95.

32. Cross, M. and L. Claesson-Welsh, *FGF and VEGF function in angiogenesis: signalling pathways, biological responses and therapeutic inhibition. .* TRENDS in Pharmacological Sciences, 2001. **22**(4): p. 201-207.
33. Kit Yue, P., et al., *Pharmacogenomics and the Yin/ Yang actions of ginseng: anti-tumor, angiomodulating a nd steroid-like activities of ginsenosides.* Chinese Medicine, 2007. **2**(6): p. 1-21.
34. Selvaprithviraj , V., et al., *Pro-Angiogenic Molecules for Therapeutic Angiogenesis* Current Medicinal Chemistry, 2017. **24**: p. 3413-3432
35. Welti, J., et al., *Recent molecular discoveries in angiogenesis and antiangiogenic therapies in cancer.* J Clin Invest, 2013. **123**(8): p. 3190-3200.
36. Pepper, M., S. Mandriota, and R. Montesano, *The New Angiotherapy. Angiogenesis-Regulating Cytokines.* 2002, Totowa, New Jersey: Humana Press.
37. Moon, J.J. and J.L. West, *Vascularization of Engineered Tissues: Approaches to Promote Angio-genesis in Biomaterials.* Curr Top Med Chem, 2008. **8**(4): p. 300-310.
38. Simons, M. and J.A. Ware, *Therapeutic angiogenesis in cardiovascular disease.* Nature Review Drug Discovery, 2003. **2**(3): p. 863-871.
39. Layman , H., et al., *The effect of the controlled release of basic fibroblast growth factor from ionic gelatin-based hydrogels on angiogenesis in a murine critical limb ischemic model Author links open overlay panel.* Biomaterials, 2007. **28**(16): p. 2646-2654.
40. Rajagopalan, et al., *Regional Angiogenesis With Vascular Endothelial Growth Factor in Peripheral Arterial Disease A Phase II Randomized, Double-Blind, Controlled Study of Adenoviral Delivery of Vascular Endothelial Growth Factor 121 in Patients With Disabling Intermittent Claudication.* Circulation, 2003. **108**: p. 1933–1938.
41. Sun , Q.C., R.R. Shen , Y. Mooney, D.J. Rajagopalan, S. Grossman , M.P, *Sustained Vascular Endothelial Growth Factor Delivery Enhances Angiogenesis and Perfusion in Ischemic Hind Limb.* Pharmaceutical Research, 2005. **22**(7): p. 1110-1116.
42. Simón-Yarza, T., et al., *Vascular endothelial growth factor-delivery systems for cardiac repair: an overview.* Theranostics, 2012. **2**(6): p. 541-552.
43. Shima, D.T., U. Deutsch, and P.A. D'Amore, *Hypoxic induction of vascular endothelial growth factor (VEGF) in human epithelial cells is mediated by increases in mRNA stability.* FEBS Letters, 1995. **370**(3): p. 203-208.
44. Koike, N., et al., *Creation of long-lasting blood vessels. .* Nature, 2005. **428**(6979): p. 138-139.
45. Herberts, C.A., M.S. Kwa, and H.P. Hermsen, *Risk factors in the development of stem cell therapy.* Journal of Translational Medicine, 2011. **9**(29): p. 9-29.

46. Kanematsu, A., et al., *Type I collagen can function as a reservoir of basic fibroblast growth factor.* Journal of Control Release, 2004. **99**(2): p. 281-292.
47. Marui, A., et al., *A novel approach to therapeutic angiogenesis for patients with critical limb ischemia by sustained release of basic fibroblast growth factor using biodegradable gelatin hydrogel - An initial report of the phase I-IIa study.* Circulation, 2007. **71**(8): p. 1181-1186.
48. Madrigal, M., K.S. Rao, and N.H. Riordan, *A review of therapeutic effects of mesenchymal stem cell secretions and induction of secretory modification by different culture methods* Journal of Translational Medicine, 2014. **12**(230): p. 1-14.
49. Silva, E.A. and D.J. Mooney, *Effects of VEGF temporal and spatial presentation on angiogenesis.* Biomaterials, 2010. **31**(6): p. 1235-1241.
50. Mäkinen, K., et al., *Increased vascularity detected by digital subtraction angiography after VEGF gene transfer to human lower limb artery: a randomized, placebo-controlled, double-blinded phase II study.* Molecular Therapy, 2002. **6**(1).
51. Shimamura, M., et al., *Gene Therapy and Cell-Based Therapies for Therapeutic Angiogenesis in Peripheral Artery Disease.* BioMed Research International, 2013. **2013**: p. 1-8.
52. Morishita, R., et al., *Phase I/IIa clinical trial of therapeutic angiogenesis using hepatocyte growth factor gene transfer to treat critical limb ischemia.* Arteriosclerosis, Thrombosis, and Vascular Biology, 2011. **31**(3): p. 713–720.
53. Stein, R., et al., *Limitation of the resting ankle-brachial index in symptomatic patients with peripheral arterial disease.* Vascular Medicine, 2003. **11**(1): p. 29-33.
54. Yoon, C.H., et al., *Synergistic neovascularization by mixed transplantation of early endothelial progenitor cells and late outgrowth endothelial cells: the role of angiogenic cytokines and matrix metalloproteinases .* Circulation, 2005. **112**(11): p. 1618-1627.
55. Yang, C., et al., *Enhancement of neovascularization with cord blood CD133+ cell-derived endothelial progenitor cell transplantation.* Thromb Haemost. , 2004. **91**(6): p. 1202-1212.
56. Bronzino, J., et al., *Tissue Engineering and Artificial Organs*. 1 ed, ed. J.D. Bronzino and D.R. Peterson. Vol. 4. 2006: Boca Raton: CRC Press.
57. Kinnaird, T., et al., *Local delivery of marrow-derived stromal cells augments collateral perfusion through paracrine mechanisms.* Circulation, 2004. **109**(12): p. 1543-1549.
58. Alvino, V.V., et al., *Transplantation of Allogeneic Pericytes Improves Myocardial Vascularization and Reduces Interstitial Fibrosis in a Swine Model of Reperfused Acute Myocardial Infarction.* Journal of the American Heart Association, 2018. **7**(2).
59. Madeddu, P.R., *Stem cell therapy for cardiovascular regeneration: the beginning or the end of all hearts' hopes '.* Pharmacology and Therapeutics, 2011. **129**: p. 1-2.

60. Kumar, D., T.J. Kamp, and M.M. LeWinter, *Embryonic stem cells: differentiation into cardiomyocytes and potential for heart repair and regeneration.* Coronary Artery Disease, 2005. **16**(12): p. 111-117.
61. Ungerleider, J.L. and K.L. Christman, *Concise Review: Injectable Biomaterials for the Treatment of Myocardial Infarction and Peripheral Artery Disease: Translational Challenges and Progress.* STEM CELLS Translational Medicine, 2014. **3**: p. 1090-1099.
62. Lee, K.B. and D.I. Kim, *Clinical Application of Stem Cells for Therapeutic Angiogenesis in Patients with Peripheral Arterial Disease.* International Journal of Stem Cells, 2009. **2**(1): p. 11-17.
63. Lachmann, N. and S. Nikol, *Therapeutic angiogenesis for peripheral artery disease: stem cell therapy.* Vasa, 2007. **36**(4): p. 241-251.
64. Jadczyk, T., A. Faulkner, and P. Madeddu, *Stem cell therapy for cardiovascular disease: the demise of alchemy and the rise of pharmacology.* British Journal of Pharmacology, 2013. **169**: p. 247-268.
65. Mason, C. and P. Dunnil, *Assessing the value of autologous and allogeneic cells for regenerative medicine.* Regenerative Medicine, 2009. **4**(6).
66. Rufaihah, A.J., et al., *Endothelial Cells Derived From Human iPSCS Increase Capillary Density and Improve Perfusion in a Mouse Model of Peripheral Arterial Disease.* Arteriosclerosis, Thrombosis, and Vascular Biology, 2011(31): p. 72-79.
67. Ishida , A., et al., *Autologous Peripheral Blood Mononuclear Cell Implantation for Patients With Peripheral Arterial Disease Improves Limb Ischemia.* Circulation Journal, 2005. **69**(10): p. 1260-1265.
68. Cathery, W., et al., *Concise Review: The Regenerative Journey of Pericytes Toward Clinical Translation.* Stem Cells, 2018. **36**(9): p. 1295–1310.
69. Chen, W.C., et al., *Human myocardial pericytes: multipotent mesodermal precursors exhibiting cardiac specificity.* Stem Cells, 2015. **33**(2): p. 557-573.
70. Campagnolo , P., et al., *Pericyte seeded dual peptide scaffold with improved endothelialization for vascular graft tissue engineering.* Advanced Healthcare Materials, 2016. **5**(23): p. 3046–3055.
71. Carrabba, M., et al., *Design, fabrication and perivascular implantation of bioactive scaffolds engineered with human adventitial progenitor cells for stimulation of arteriogenesis in peripheral ischemia.* Biofabrication, 2016. **8**(1): p. 15-20.
72. Avolio, E. and P. Madeddu, *Discovering cardiac pericyte biology: From physiopathological mechanisms to potential therapeutic applications in ischemic heart disease.* Vascular Pharmacology, 2016. **86**: p. 53–63.
73. Frangogiannis, N.G., *Cell therapy for peripheral artery disease.* 2018. **39**: p. 27-34.
74. Jones, M., et al., *Genetic stability of bone marrow-derived human mesenchymal stromal cells in the Quantum System.* Cytotherapy. **15**(11): p. 1323-1339.

75. Griffin, M.D., et al., *Anti-donor immune responses elicited by allogeneic mesenchymal stem cells: what have we learned so far?* Immunol Cell Biology, 2013. **91**(1): p. 40-51.
76. Couffinhal, T., et al., *Mouse Model of Angiogenesis.* Am J Pathol, 1998. **152**(6): p. 1667–1679.
77. Hong, K.U., et al., *A highly sensitive and accurate method to quantify absolute numbers of c-kit+ cardiac stem cells following transplantation in mice.* Basic Res Cardiol., 2013. **108**(3): p. 346.
78. Zeng, L.H., Q. Wang, X. Mansoor, A. Lee, J. Feygin, J. Zhang, G. Suntharalingam, P. Boozer, S. Mhashilkar, A., et al., *Bioenergetic and Functional Consequences of Bone Marrow–Derived Multipotent Progenitor Cell Transplantation in Hearts With Postinfarction Left Ventricular Remodeling.* Circulation, 2007. **115**(14): p. 1866-1875.
79. Rehman, J., et al., *Secretion of Angiogenic and Antiapoptotic Factors by Human Adipose Stromal Cells.* Circulation, 2004. **109**(10): p. 1292-1298.
80. McCarthy, M.E., et al., *Therapeutic Applications for Adipose-Derived Stem Cells in Wound Healing and Tissue Engineering.* Current Stem Cell Reports 2018. **4**(2): p. 127–137.
81. Deng, C., et al., *Extracellular matrix/stromal vascular fraction gel conditioned medium accelerates wound healing in a murine model.* Wound Repair Regeneration, 2017. **25**(6): p. 923-932.
82. Phelps, J., et al., *Bioprocessing of Mesenchymal Stem Cells and Their Derivatives: Toward Cell-Free Therapeutics.* Stem Cells International, 2018. **2018**: p. 23.
83. Ellison-Hughes, G.M. and P. Madeddu, *Exploring pericyte and cardiac stem cell secretome unveils new tactics for drug discovery.* Pharmacology and Therapeutics, 2017. **117**: p. 1-12.
84. Gangadaran, P., et al., *Extracellular vesicles from mesenchymal stem cells activates VEGF receptors and accelerates recovery of hindlimb ischemia Author links open overlay panel.* Journal of Controlled Release, 2017. **264**(28): p. 112-126.
85. Volarevic , V., et al., *Ethical and Safety Issues of Stem Cell-Based Therapy. International Journal of Medical Sciences*, 2018. **15**(1): p. 36-45.
86. Tsuji, W., J.P. Rubin, and K.G. Marra, *Adipose-derived stem cells: Implications in tissue regeneration.* World Journal Stem Cells, 2014. **6**(3): p. 312-321.
87. Xue, C., et al., *Exosomes Derived from Hypoxia-Treated Human Adipose Mesenchymal Stem Cells Enhance Angiogenesis Through the PKA Signaling Pathway.* 2018. **27**(7).
88. Park, H., et al., *Extracellular Vesicles Derived from Hypoxic Human Mesenchymal Stem Cells Attenuate GSK3β Expression via miRNA-26a in an Ischemia-Reperfusion Injury Model.* Yonsei Medical Journal, 2018. **59**(6): p. 736-745.

89. Almerey , T., et al., *The Effect of Ischemia on Adipose-Derived Mesenchymal Stem Cells Expression In Vivo.* Journal of Vascular Surgery, 2018. **67**(6).
90. Tsuji, W., J.P. Rubin, and K.G. Marra, *Adipose-derived stem cells: Implications in tissue regeneration.* World Journal Stem Cells, 2014. **6**(3): p. 312-321.
91. Vu, N.B., et al., *Allogeneic Adipose-Derived Mesenchymal Stem Cell Transplantation Enhances the Expression of Angiogenic Factors in a Mouse Acute Hindlimb Ischemic Model*, in *Advances in Experimental Medicine and Biology*. 2017, Springer: Boston, MA.
92. Zeng, L., et al., *Bioenergetic and Functional Consequences of Bone Marrow–Derived Multipotent Progenitor Cell Transplantation in Hearts With Postinfarction Left Ventricular Remodeling.* Circulation, 2007. **115**(14): p. 1866-1875.
93. A., K., *Mesenchymal Stem Cell Delivery Routes and Fate.* International Journal of Stem Cells 2008. **1**(1): p. 1-7.
94. Stuckey, D.J., et al., *Iron particles for noninvasive monitoring of bone marrow stromal cell engraftment into, and isolation of viable engrafted donor cells from, the heart.* Stem Cells, 2006. **24**(8): p. 1968-1975.
95. Lia, Y., et al., *Primed 3D injectable microniches enabling low-dosage cell therapy for critical limb ischemia.* PNAS, 2014. **111**(37): p. 13511–13516.
96. Ludwinski, F.E., et al., *Encapsulation of macrophages enhances their retention and angiogenic potential. <i data-test="journal*-title" style="color: rgb(34, 34, 34); font-family: "Source Sans Pro", arial, helvetica, sans-serif; font-size: 22.4px; letter-spacing: 0.17px; background-color: rgb(255, 255, 255);">Regenerative Medicine, 2019. **4**(6).
97. Capoccia, B.J., et al., *Revascularization of ischemic limbs after transplantation of human bone marrow cells with high aldehyde dehydrogenase activity.* Blood, 2009. **113**(21): p. 5340-5351.
98. Putman, D.M., et al., *Umbilical cord blood-derived aldehyde dehydrogenase-expressing progenitor cells promote recovery from acute ischemic injury.* Stem Cells., 2012. **30**(10): p. 2248-2260.
99. Re , F., et al., *Inhibition of anchorage-dependent cell spreading triggers apoptosis in cultured human endothelial cells.* Journal of Cell Biology, 1994. **127**(2): p. 537.
100. Ratner, B.D., *Biomaterials Science: An Interdisciplinary Endeavor*, in *Biomaterials Science*, B.D. Ratner, et al., Editors. 1996, Academic Press. p. 1-8.
101. Jacques Caton, J.L.P., *Over 25 years survival after Charnley's total hip arthroplasty.* Int Orthop . 2011. **35**(2): p. 1 85–188.
102. Cionca Norbert , H.D., Mombelli Andrea, *Zirconia dental implants: where are we now, and where are we heading?* Periodontology, 2000. **73**(1).
103. EW, N., *Synthetic polymers as drug-delivery vehicles in medicine.* Met Based Drugs, 2008(1): p. 469-531.

104. Vats A, T.N., Polak JM , Gough JE, *Scaffolds and biomaterials for tissue engineering: a review of clinical applications, , Volume 28, Issue 3.* Clinical Otolaryngology & Allied Sciences, 2003. **28**(3).
105. Makadia, H.K. and S.J. Siegel, *Poly Lactic-co-Glycolic Acid (PLGA) as Biodegradable Controlled Drug Delivery Carrier.* Polymers (Basel) 2011. **1**(3): p. 1377-1397.
106. Lü, J.M., et al., *Current advances in research and clinical applications of PLGA-based nanotechnology.* Expert review of molecular diagnostics, 2009. **9**(4): p. 325-341.
107. Rocha FG, S.C., Krebs NJ, Leach JK, Mooney DJ, Ashley SW, Vacanti JP, Whang EE, *The effect of sustained delivery of vascular endothelial growth factor on angiogenesis in tissue-engineered intestine.* Biomaterials, 2008. **29**(19): p. 2884-2890.
108. Ahmadi R, M.N., Forbes A, Day RM, *Enhanced attachment, growth and migration of smooth muscle cells on microcarriers produced using thermally induced phase separation.* Acta Biomaterialia, 2011. **7**(4): p. 1542-1549
109. Da i W, K.e.N., Li n X, Don g J, Ch en G, *The influence of structural design of PLGA/collagen hybrid scaffolds in cartilage tissue engineering.* Biomaterials, 2010. **31**(8): p. 2141-2152.
110. Blacker JJ, K.J., Day RM, *Novel fabrication techniques to produce microspheres by thermally induced phase separation for tissue engineering and drug delivery.* Acta Biomaterials, 2008. **4**(2): p. 264-272.
111. Makadia HK , S.S., *Poly Lactic-co-Glycolic Acid (PLGA) as Biodegradable Controlled Drug Delivery Carrier.* Polymers (Basel), 2012. **3**(3): p. 1377–1397.
112. Makadia, H. and S. Siegel, *Poly Lactic-co-Glycolic Acid (PLGA) as Biodegradable Controlled Drug Delivery Carrier.* Polymers (Basel), 2012. **3**(3): p. 1377–1397.
113. Jayasinghe, S.N., *Cell electrospinning: a novel tool for functionalising fibres, scaffolds and membranes with living cells and other advanced materials for regenerative biology and medicine.* Analyst, 2013. **138**(8): p. 2215-2223.
114. A, J., *Micro and nanoparticle production.* Powder Technology, 2007. **176**(1): p. 18-35.
115. Kim, K. and D.W. Pack, *Microspheres for Drug Delivery.* Biomedical Nanotechnology, 2006. **7**(8): p. 19-50.
116. Le , J.Y., J. An , and C. Kai Chua *Fundamentals and applications of 3D printing for novel materials Author links open overlay panel.* Applied Materials Today, 2017. **7**: p. 120-133.
117. Aldaadaa, A., N. Owji, and J. Knowles, *Three-dimensional Printing in Maxillofacial Surgery: Hype versus Reality.* Journal of Tissue Engineering. **9**: p. 1–5

118. Dongting , L., et al., *Patient-Specific 3D Printed Models of Renal Tumours Using Home-Made 3D Printer in Comparison with Commercial 3D Printer.* Journal of Medical Imaging and Health Informatics, 2018. **8**(2): p. 303-308.
119. Rose, A.S., et al., *Pre-operative Simulation of Pediatric Mastoid Surgery with 3D-Printed T emporal Bone Models.* International Journal of Pediatric Otorhinolaryngology, 2015. **79** p. 740–744
120. Jacobs, S., et al., *3D-Imaging of cardiac structures using 3D heart models for planning in heart surgery: a preliminary study* Interactive CardioVascular and Thoracic Surgery, 2008. **7**(1): p. 6-9.
121. Martínez-Pérez, C.A., et al., *Scaffolds for Tissue Engineering Via Thermally Induced Phase Separation.* Advances in Regenerative Medicine, 2011: p. 276-294.
122. Blacker, J., J. Knowels, and R. Day, *Novel fabrication techniques to produce microspheres by thermally induced phase separation for tissue engineering and drug delivery.* Acta Biomaterials, 2008. **4**(2): p. 264-272.
123. Nam, Y.S. and T.G. Park, *Porous biodegradable polymeric scaffolds prepared by thermally induced phase separation.* J Biomed Mater Res., 1999. **47**(1): p. 8-17.
124. Dai, W., et al., *The influence of structural design of PLGA/collagen hybrid scaffolds in cartilage tissue engineering.* Biomaterials, 2010. **31**(8): p. 2141-2152.
125. Hutmacher, D.W., *Scaffolds in tissue engineering bone and cartilage : Applications of Biodegradables.* Orthopaedic Polymeric Biomaterials, 2000. **21**(24): p. 2529–2543.
126. Holzwarth , J.M. and P.X. Ma *Biomimetic nanofibrous scaffolds for bone tissue engineering.* Biomaterials, 2011. **32**(36): p. 9622-9629.
127. Sofokleous, P., M.H.W. Chin, and R.M. Day, *Phase-separation technologies for 3D scaffold engineering* in *Functional 3D Tissue Engineering Scaffolds Materials, Technologies, and Applications Woodhead Publishing Series in Biomaterials*, Y. Deng and J. Kuiper, Editors. 2018, Woodhead Publishing: An imprint of Elsevier: The Officers' Mess Business Centre, Royston Road, Duxford, CB22 4QH, United Kingdom. p. 101-122.
128. Chen , J., et al., *Conductive nanofibrous composite scaffolds based on in-situ formed polyaniline nanoparticle and polylactide for bone regeneration.* Journal of Colloid and Interface Science, 2018. **514**: p. 517-527.
129. Zare-Mehrjardi , N., et al., *Differentiation of Embryonic Stem Cells into Neural Cells on 3D Poly (D, L-Lactic Acid) Scaffolds versus 2D Cultures.* The International Journal of Artificial Organs, 2011. **34**(10): p. 1012-1023.
130. Hollister, S.J., *Porous scaffold design for tissue engineering.* Nature Materials, 2005. **4**(7): p. 518–524.
131. Rezwan , K., et al., *Biodegradable and bioactive porous polymer/inorganic composite scaffolds for bone tissue engineering Author links open overlay panel.* Biomaterials, 2006. **27**(18): p. 3413-3431.

132. Sarkar , S., et al., *Development and characterization of a porous micro-patterned scaffold for vascular tissue engineering applications.* Biomaterials, 2006. **27**(27): p. 4775-4782.
133. Grémare, A., et al., *Characterization of printed PLA scaffolds for bone tissue engineering.* Journal of Biomedical Materials Research Part A, 2017. **106**(4).
134. Wanga, Y.F., et al., *Systematic characterization of porosity and mass transport and mechanical properties of porous polyurethane scaffolds Systematic characterization of porosity and mass transport and mechanicalSystematic characterization of porosity and mass transport and mechanical properties of porous polyurethane scaffolds.* Journal of the Mechanical Behavior of Biomedical Materials, 2017. **65**: p. 657–664.
135. Vozzi , F., et al., *Biomimetic engineering of the cardiac tissue through processing, functionalization, and biological characterization of polyester urethanes.* Biomedical Materials, 2018. **13**(5).
136. Mauro Rigato, M., M. Monami, and G.P. Fadini, *Autologous Cell Therapy for Peripheral Arterial Disease. Systematic Review and Meta-Analysis of Randomized, Nonrandomized, and Noncontrolled Studies.* Circulation Research, 2017. **120**: p. 1326-1340.
137. El-Sherbiny, I.M. and M.H. Yacoub, *Hydrogel scaffolds for tissue engineering: Progress and challenges.* Global Cardiology Science & Practice, 2013. **2013**(3): p. 316-342.
138. Katare, et al., *Perivascular Delivery of Encapsulated Mesenchymal Stem Cells Improves Postischemic Angiogenesis Via Paracrine Activation of VEGF-A.* Arteriosclerosis, Thrombosis, and Vascular Biology, 2013. **33**: p. 1872–1880.
139. Chow, A., et al., *Human Induced Pluripotent Stem Cell-Derived Cardiomyocyte Encapsulating Bioactive Hydrogels Improve Rat Heart Function Post Myocardial Infarction.* Stem Cell Reports, 2017. **9**: p. 1415–1422.
140. Speidel, A.T., et al., *Multimodal Hydrogel-Based Platform To Deliver and Monitor Cardiac Progenitor/Stem Cell Engraftment.* American Chemical Society, 2017. **3**: p. 338−348.
141. Noukeu, L.C., et al., *Nanoparticles for Detection and Treatment of Peripheral Arterial Disease.* Small, 2018. **14**.
142. Resnik, D.B. and S.S. Tinkle, *Ethical issues in clinical trials involving nanomedicine.* Contemporary Clinical Trails, 2007. **28**(4): p. 433-441.
143. Kapnisi, M.M., C Marijon, C. Guex, A.G., et al., *Auxetic Cardiac Patches with Tunable Mechanical and Conductive Properties toward Treating Myocardial Infarction* Advanced Functional Materials, 2018. **28**: p. 1800618.
144. Mirabella, T., et al., *3D-printed vascular networks direct therapeutic angiogenesis in ischaemia.* Nature Biomedical Engineering, 2017. **1**.

145. style="mso-margin-top-alt:auto, p.c.M., et al., *3D-printed vascular networks direct therapeutic angiogenesis in ischaemia. Nature Biomedical Engineering*, 2017. **1**.
146. Mima, Y., et al., *Enhancement of Cell-Based Therapeutic Angiogenesis Using a Novel Type of Injectable Scaffolds of Hydroxyapatite-Polymer Nanocomposite Microspheres.* PLoS ONE, 2012. **7**(4): p. 351-399.
147. Dhandayuthapani , B., et al., *Polymeric Scaffolds in Tissue Engineering Application: A Review.* International Journal of Polymer Science, 2011. **2011**: p. 19.
148. Gentile , P., et al., *An Overview of Poly(lactic- co -glycolic) Acid (PLGA)-Based Biomaterials for Bone Tissue Engineering. Int. J. Mol. Sci.* , 2014. **15**(3): p. 3640-3659.
149. Agrawal, C.M., and R.B. Ray, *Biodegradable polymeric scaffolds for musculoskeletal tissue engineering.* Journal of Biomedical Materials Research, 2001. **55**(2): p. 141-150.
150. Pan, Z. and J. Ding, *Poly(lactide- co -glycolide) porous scaffolds for tissue engineering and regenerative medicine.* Interface Focus, 2012. **2**(3): p. 366–377.
151. Swider , E., et al., *Customizing poly(lactic-co-glycolic acid) particles for biomedical applications.* Acta Biomaterialia, 2018. **73**: p. 38-51.
152. Huang, C.C., et al., *Injectable PLGA porous beads cellularized by hAFSCs for cellular cardiomyoplasty.* Biomaterials, 2012. **33**: p. 4069-4077.
153. Hoareau, L., et al., *Combined therapy for critical limb ischaemia: Biomimetic PLGA microcarriers potentiates the pro-angiogenic effect of adipose tissue stromal vascular fraction cells.* Journal of Tissue Engineering and Regenerative Medicine, 2018. **12**(6).
154. Saif, J., et al., *Combination of Injectable Multiple Growth Factor–Releasing Scaffolds and Cell Therapy as an Advanced Modality to Enhance Tissue Neovascularization.* Arteriosclerosis Thrombosis Vascular Biology, 2010. **30**: p. 1897-1904.
155. Richardson, T.P., et al., *Polymeric system for dual growth factor delivery.* Nature Biotechnologies, 2001. **19**: p. 1029-1034.
156. Deveza, L., J. Choi, and F. Yang, *Therapeutic angiogenesis for treating cardiovascular diseases. .* Theranostics, 2012. **2**(8): p. 801-814.
157. Yang , F., et al., *Genetic engineering of human stem cells for enhanced angiogenesis using biodegradable polymeric nanoparticles.* PNAS, 2010. **107**(8): p. 3317–3322.
158. Matsumoto, R., et al., *Vascular endothelial growth factor-expressing mesenchymal stem cell transplantation for the treatment of acute myocardial infarction.* Arterioscler Thromb Vasc Biol., 2005. **25**(6): p. 1168-1173.
159. Chen, S.Y., et al., *Autologous transplantation of EPCs encoding FGF1 gene promotes neovascularization in a porcine model of chronic myocardial ischemia.* Int J Cardiol., 2009. **135**(2): p. 223-232.

160. Karam , J.P., C. Muscari , and C.N. Montero-Menei *Combining adult stem cells and polymeric devices for tissue engineering in infarcted myocardium.* Biomaterials, 2012. **33**(23): p. 5683-5695.
161. Saghiri, M.A., et al., *The role of angiogenesis in implant dentistry part I: Review of titanium alloys, surface characteristics and treatments.* Medicina Oral, Patología Oral y Cirugía Bucal, 2016. **21**(4): p. e514-e525.
162. Yu , Y., et al., *Multifunctions of dual Zn/Mg ion co-implanted titanium on osteogenesis, angiogenesis and bacteria inhibition for dental implants.* Acta Biomaterialia, 2017. **49**: p. 590-603.
163. De Luca, A.C., et al., *Effect of microgrooved surface topography on osteoblast maturation and protein adsorption.* Journal of Biomedical Materials Research Part A, 2015. **103**(8).
164. Bobbert, F.S.L. and A.A. Zadpoor, *Effects of bone substitute architecture and surface properties on cell response, angiogenesis, and structure of new bone.* Journal of Material Chemistry Part B, 2017. **5**(5): p. 6175-6192.
165. Yoon, et al., *In Vivo Osteogenic Potential of Human Adipose-Derived Stem Cells/Poly Lactide-Co-Glycolic Acid Constructs for Bone Regeneration in a Rat Critical-Sized Calvarial Defect Model.* Tissue Engineering, 2007. **13**(3).
166. Johnson, M.T., et al., *Evaluating methods for isolating total RNA and predicting the success of sequencing phylogenetically diverse plant transcriptomes.* PloS one, 2012. **7**(11): p. e50226.
167. Baker, B.M. and C.S. Chen, *Deconstructing the Third Dimension – How 3D Culture Microenvironments Alter Cellular Cues.* Journal of Cell Science, 2012. **125**: p. 1-10.
168. Yun Kim, H., et al., *Effect of pore sizes of PLGA scaffolds on mechanical properties and cell behaviour for nucleus pulposus regeneration in vivo.* Journal of Tissue Engineering and Regenerative Medicine, 2014. **11**(1).
169. Lloyd, A., *Engineering surfaces to enhance cell adhesion : Surface engineering.* Materials Today, 2003. **6**(11): p. 1-19.
170. Janson, I.A. and A.J. Putnam, *Extracellular matrix elasticity and topography: Material-based cues that affect cell function via conserved mechanisms.* Biomedical Materials Research Part A, 2015. **103**: p. 1246–1258.
171. Gittensa, R.A., et al., *The effects of combined micron-/submicron-scale surface roughness and nanoscale features on cell proliferation and differentiation.* Biomaterials, 2011. **32**(13): p. 3395–3403.
172. Kim, T.H., et al., *Nanografted Substrata and Triculture of Human Pericytes, Fibroblasts, and Endothelial Cells for Studying the Effects on Angiogenesis.* Tissue Engineering Part A, 2016. **22**(7-8): p. 698-706.
173. Sangsanoh, P., et al., *Effect of the surface topography and chemistry of poly(3-hydroxybutyrate) substrates on cellular behavior of the murine neuroblastoma Neuro2a cell line.* Polymer Bulletin, 2017. **74**(10): p. 4101-4118.

174. Guilak, F., et al., *Control of stem cell fate by physical interactions with the extracellular matrix.* Cell Stem Cell, 2009. **5**(1): p. 17-26.
175. Bellas , E. and S.S. Chen *Forms, Forces and Stem Cell Fate.* Current Opinion in Cell Biology, 2014. **31**: p. 92-97.
176. Clause , K.C., L.J. Liu , and K. Tobita, *Directed stem cell differentiation: the role of physical forces.* Cell Commun Adhes, 2010. **17**(2): p. 48–54.
177. Jang, K.J., et al., *Two Distinct Filopodia Populations at the Growth Cone Allow to Sense Nanotopographical Extracellular Matrix Cues to Guide Neurite Outgrowth.* PLoS ONE, 2010. **5**(12): p. 15966.
178. Breuls , R.G.M., T.U. Jiya , and T.H. Smit, *Scaffold Stiffness Influences Cell Behavior: Opportunities for Skeletal Tissue Engineering.* Open Orthop J, 2008. **2**: p. 103–109.
179. Krishnan, L., et al., *Manipulating the Microvasculature and its Microenvironment.* Crit Rev Biomed Eng., 2013. **41**(2): p. 91-123.
180. Phillips, J.E., et al., *Human mesenchymal stem cell differentiation on self-assembled monolayers, presenting different surface chemistries.* Acta Biomaterialia, 2010. **6**(1): p. 12–20.
181. Halder, G., S. Dupont, and S. Piccolo, *Transduction of mechanical and cytoskeletal cues by YAP and TAZ.* Nature Reviews Molecular Cell Biology volume 2012. **13**: p. 591 – 600.
182. Koch, L., et al., *Laser bioprinting of human induced pluripotent stem cells—the effect of printing and biomaterials on cell survival, pluripotency, and differentiation.* Biofabrication, 2018. **10**.
183. Carpenter, et al., *Efficient Differentiation of Human Induced Pluripotent Stem Cells Generates Cardiac Cells That Provide Protection Following Myocardial Infarction in the Rat.* Stem Cells and Development, 2012. **21**(6).
184. Hazeltine, L.B., et al., *Effects of Substrate Mechanics on Contractility of Cardiomyocytes Generated from Human Pluripotent Stem Cells.* International Journal of Cell Biology, 2012: p. 1-13.
185. Thavandiran, N.N., S.S. Xiao, Y. Radisic, M., *Topological and electrical control of cardiac differentiation and assembly, .* Stem Cell Research & Therapy, 2013. **4**(14): p. 1-9
186. Zhao , Q., H. Ren , and Z. Han, *Mesenchymal stem cells: Immunomodulatory capability and clinical potential in immune diseases.* Journal of Cellular Immunotherapy, 2016. **2**(1): p. 3-20.
187. Jaiswal, N., et al., *Osteogenic differentiation of purified, culture-expanded human mesenchymal stem cells in vitro.* Journal of Cellular Biology, 1997. **64**.
188. Kiliana, K.A., et al., *Geometric Cues for Directing the Differentiation of Mesenchymal Stem Cells.* Proceedings of the National Academy of Sciences, 2010. **107**(11): p. 4872-4877.

189. Eng, C.C., et al., *Enhancement of Mechanical and Thermal Properties of Polylactic Acid/Polycaprolactone Blends by Hydrophilic Nanoclay.* Indian Journal of Materials Science, 2013. **2013**: p. 11.
190. Stoddart, M.J., *Cell Viability Assays: Introduction*, in *Mammalian Cell Viability. Methods in Molecular Biology (Methods and Protocols)*, M.J. Stoddart, Editor. 2011: Humana Press.
191. Joy, D.C. and D.G. Howitt, *Scanning Electron Microscopy*. 3rd ed. Encyclopedia of Physical Science and Technology, ed. R. Meyers. 2003.
192. Butt , H., B. Cappella , and M. Kappl *Force measurements with the atomic force microscope: Technique, interpretation and applications.* Surface Science Reports, 2005. **59**(1-6): p. 1-152.
193. Meyer, E., *Atomic Force Microscopy.* Progress in Surface Science, 1992. **41**: p. 3-49.
194. Valente, C.A., et al., *Design and optimization of biocompatible polycaprolactone/poly(L-lactic-co-glycolic acid) scaffolds with and without microgrooves for tissue engineering applications.* Journal of Biomedical Materials Research Part A, 2018. **106**(6).
195. Ghasemi-Mobarakeh, L. and S. Ramakrishna, *Electrospun poly(ε-caprolactone)/gelatin nanofibrous scaffolds for nerve tissue engineering.* Biomaterials, 2008. **29**(34): p. 4532-4539.
196. Tang, Z.G., N.P. Rhodes, and J.A. Hunt, *Control of the Domain Microstructures of PLGA and PCL Binary Systems: Importance of Morphology in Controlled Drug Release.* Design, 2007. **85**(7): p. 1044-1050.
197. Idris, A., et al., *Effects of Phase Separation Behavior on Morphology and Performance of Polycarbonate Membranes.* Membranes, 2017. **7**(21): p. 1-18.
198. Thesleff, A., et al., *Biomechanical Characterisation of Bone-anchored Implant Systems for Amputation Limb Prostheses: A Systematic Review. .* Annals of biomedical engineering, 2018. **46**(3): p. 377-391.
199. Webb, K., V. Hlady, and P.A. Tresco, *Relative importance of surface wettability and charged functional groups on NIH 3T3 fibroblast attachment, spreading, and cytoskeletal organization.* Journal of biomedical materials research, 1998. **41**(3): p. 422-430.
200. **Ryan** , J.A., *Evolution of Cell Culture Surfaces.* BioFiles, 2008. **3.8**(21).
201. Lee, J.H., et al., *Interaction of Different Types of Cells on Polymer Surfaces with Wettability Gradient.* Journal of Colloid and Interface Science, 1998. **205**: p. 323–330.
202. Wright, B., et al., *A Simple and Robust Method for Pre-wetting Poly (lactic-co-glycolic) Acid Microspheres.* Journal of Biomaterials Applications, 2015. **30**(2): p. 147–159.

203. Mikos, A.G., et al., *Wetting of poly(L-lactic acid) and poly(DL-lactic-co-glycolic acid) foams for tissue culture.* Biomaterials, 1994. **15**(1): p. 55-58.
204. Chew, S.A., M.A. Arriaga, and V.A. Hinojosa, *Effects of surface area to volume ratio of PLGA scaffolds with different architectures on scaffold degradation characteristics and drug release kinetics.* Journal of Biomedical Materials Research Part A, 2016. **104**(5): p. 1202-1211.
205. Wells, R.G., *The Role of Matrix Stiffness in Regulating Cell Behavior* Hepatology, 2008. **47**(4): p. 1394-1400.
206. Cao , Y., et al., *The influence of architecture on degradation and tissue ingrowth into three-dimensional poly(lactic- co -glycolic acid) scaffolds in vitro and in vivo.* Biomaterials, 2006. **27**(14): p. 2854-2864.
207. Karageorgiou , V.K., D., *Porosity of 3D biomaterial scaffolds and osteogenesis.* Biomaterials, 2005. **26**(27): p. 5474-5491.
208. Wu , L. and J. Ding, *In vitro degradation of three-dimensional porous poly(d , l -lactide- co -glycolide) scaffolds for tissue engineering.* Biomaterials, 2004. **25**(27): p. 5821-5830.
209. Krebs a, M.D., et al., *Injectable poly(lactic-co-glycolic) acid scaffolds with in situ pore formation for tissue engineering.* Acta Biomaterialia, 2009. **5**(8): p. 2847-2859.
210. Lancerotto , L. and D.P. Orgill, *Mechanoregulation of Angiogenesis in Wound Healing.* Adv Wound Care (New Rochelle), 2014. **3**(10): p. 626–634.
211. Reinhart-King, C.A., *How Matrix Properties Control the Self-Assembly and Maintenance of Tissues.* Ann Biomed Eng, 2011. **39**(7): p. 1849-1856.
212. Das, R.K. and O.F. Zouani, *A review of the effects of the cell environment physicochemical nanoarchitecture on stem cell commitment.* Biomaterials, 2014. **35**(20): p. 5278-5293.
213. Chen, L., C. Yan, and Z. Zheng, *Functional polymer surfaces for controlling cell behaviors.* Materials Today, 2018. **21**(1): p. 38-59.
214. Sun, M., et al., *Extracellular matrix stiffness controls osteogenic differentiation of mesenchymal stem cells mediated by integrin α5.* Stem cell research & therapy, 2018. **9**(1): p. 52.
215. Sun, M., et al., *Effects of Matrix Stiffness on the Morphology, Adhesion, Proliferation and Osteogenic Differentiation of Mesenchymal Stem Cells.* International journal of medical sciences, 2018. **15**(3): p. 257-268.
216. Xu, J., et al., *Effect of matrix stiffness on the proliferation and differentiation of umbilical cord mesenchymal stem cells.* Differentiation, 2017. **96**: p. 30-39.
217. Le´vesquea, S.G., R.M. Lima, and M.S. Shoichet, *Macroporous interconnected dextran scaffolds of controlled porosity for tissue-engineering applications.* Biomaterials, 2005. **26**: p. 7436–7446.

218. Loh, Q.L. and C. Choong, *Three-dimensional scaffolds for tissue engineering applications: role of porosity and pore size* Tissue engineering. Part B, Reviews, 2013. **19**(6): p. 485-502.
219. Duval, K., et al., *Modeling Physiological Events in 2D vs. 3D Cell Culture.* Physiology (Bethesda), 2017. **32**(4): p. 266–277.
220. Kolind, K., et al., *Guidance of stem cell fate on 2D patterned surfaces.* Biomaterials, 2012. **33**(28): p. 6626-6633.
221. ThermoFisher. *StemPro™ Human Adipose-Derived Stem Cells*. 31/10/18]; Available from: https://www.thermofisher.com/order/catalog/product/R7788115?SID=srch-srp-R7788115.
222. Boroujeni, M.E., et al., *The Proliferation and Differentiation Capacity of Bone Marrow Derived- Human Mesenchymal Stem Cells in Early and Late Doubling.* Asian Journal of Biochemistry, 2012. **7**: p. 27-36.
223. Eslaminejad, M.B., S. Mardpour, and M. Ebrahimi, *Growth Kinetics and in Vitro Aging of Mesenchymal Stem Cells Isolated From Rat Adipose Versus Bone Marrow Tissues.* Iranian Journal of Veterinary Surgery, 2008. **3**(2): p. 9-20.
224. Alberts , B., et al., *Integrins*, in *Molecular Biology of the Cell*. 2002, Garland Science: New York.
225. Zareidoost, A., et al., *The relationship of surface roughness and cell response of chemical surface modification of titanium.* J Mater Sci Mater Med . 2012. **23**(3): p. 1479-1488.
226. Biazar, E., et al., *The relationship between cellular adhesion and surface roughness in polystyrene modified by microwave plasma radiation.* Int J Nanomedicine . 2011. **6**: p. 631-639.
227. Sunarso, et al., *Effect of micro-roughening of poly(ether ether ketone) on bone marrow derived stem cell and macrophage responses, and osseointegration.* Journal of Biomaterials Science, Polymer Edition, 2018. **29**(12): p. 1375-1388.
228. Soundararajan, A., et al., *Surface topography of polylactic acid nanofibrous mats: influence on blood compatibility.* Journal of Materials Science: Materials in Medicine, 2018. **29**(145).
229. Gittens, R.A., et al., *The effects of combined micron-/submicron-scale surface roughness and nanoscale features on cell proliferation and differentiation.* Biomaterials, 2011. **32**(13): p. 3395-3403.
230. Chen, W., Y. Sun, and J. Fu, *Microfabricated nanotopological surfaces for study of adhesiondependent cell mechanosensitivity.* Small, 2013. **9**(1): p. 81-90.
231. Scholz, W.K. *Cell Adhesion and Growth on Coated or Modified Glass or Plastic Surfaces*. 2010 02/01/19]; Available from: https://www.thermofisher.com/document-connect/document-connect.html?url=https://assets.thermofisher.com/TFS-Assets/LSG/Application-Notes/D00253.pdf.

232. Wang, P., S.M. Henning, and D. Heber, *Limitations of MTT and MTS-Based Assays for Measurement of Antiproliferative Activity of Green Tea Polyphenols.* PLoS ONE 2010. **5**(4): p. e10202.
233. Xu , M., D.J. McCanna , and J.G. Sivak *Use of the viability reagent PrestoBlue in comparison with alamarBlue and MTT to assess the viability of human corneal epithelial cells.* Journal of Pharmacological and Toxicological Methods, 2015. **71**: p. 1-7.
234. Lall, N., et al., *Viability Reagent, PrestoBlue, in Comparison with Other Available Reagents, Utilized in Cytotoxicity and Antimicrobial Assays.* International journal of microbiology, 2013. **2013**: p. 420601.
235. Scientific, T. *CyQUANT™ NF Cell Proliferation Assay Kit*. Cell Proliferation Assay Kits 02/01/19]; Available from: https://www.thermofisher.com/order/catalog/product/C35006.
236. Sanganalmath, S.K. and R. Bolli, *Cell Therapy for Heart Failure: A Comprehensive , Overview of Experimental and Clinical Studies, Current Challenges, and Future Directions.* Circulation Research, 2013. **113**(6): p. 810-834.
237. Pūtaiao, S.L.H.P.A. *Bone marrow transplants - timeline*. *Adaptations of marine organisms* 2014 18/11/18]; Available from: www.sciencelearn.org.nz/resources/142-adaptations-of-marine-organisms.
238. *The Cell and Gene Therapy Catapult UK clinical trials database*. 2017 18/11/18]; Available from: https://ct.catapult.org.uk/resources/cell-and-gene-therapy-catapult-uk-clinical-trials-database.
239. McCune, J.S., *Rapid Advances in Immunotherapy to Treat Cancer.* Immunotherapy, 2018. **103**(4): p. 540-544.
240. Timmers, L., et al., *Human mesenchymal stem cell-conditioned medium improves cardiac function following myocardial infarction.* Stem Cell Research, 2011. **6**(3): p. 206-214.
241. Kuhbier, J.W., et al., *Isolation, Characterization, Differentiation, and Application of Adipose-Derived Stem Cells*, in *Bioreactor Systems for Tissue Engineering II. Advances in Biochemical Engineering / Biotechnology*, C. Kasper, M. van Griensven, and R. Pörtner, Editors. 2010, Springer: Berlin, Heidelberg
242. Liew, A. and T. O'Brien, *Therapeutic potential for mesenchymal stem cell transplantation in critical limb ischemia.* Stem cell research & therapy, 2012. **3**(4): p. 1-28.
243. Guillén, M.I., et al., *Paracrine Anti-inflammatory Effects of Adipose Tissue-Derived Mesenchymal Stem Cells in Human Monocytes.* Frontiers in Physiology, 2018. **9**(661): p. 1-10.
244. Suzuki, H. and Y. Iso, *Clinical application of vascular regenerative therapy for peripheral artery disease.* BioMed Research International, 2013: p. 6.

245. Lee, J.S.H., J.M., et al., *A long-term follow-up study of intravenous autologous mesenchymal stem cell transplantation in patients with ischemic stroke.* Stem Cells, 2010. **28**(6): p. 1099-1106.
246. Tao, H., et al., *Proangiogenic Features of Mesenchymal Stem Cells and Their Therapeutic Applications.* Stem Cells International, 2016. **2016**: p. 1-11.
247. Szklarczyk, D., et al., *The STRING database in 2017: quality-controlled protein-protein association networks, made broadly accessible.* Nucleic Acids Res, 2017. **45**: p. D362-68.
248. Wagner, P.D., *The critical role of VEGF in skeletal muscle angiogenesis and blood flow.* Biochem Soc Trans., 2011. **39**(6): p. 1556-1559.
249. Shibuya, M., *Structure and Function of VEGF/VEGF-receptor System Involved in Angiogenesis.* Cell Structure and Function, 2001. **26**: p. 25-35.
250. Dvorak, H.F., *Vascular Permeability Factor/Vascular Endothelial Growth Factor: A Critical Cytokine in Tumor Angiogenesis and a Potential Target for Diagnosis and Therapy.* Journal of Clinical Oncology, 2002. **20**(21): p. 4368-4380.
251. Duffy, A.M., D.J. Bouchier-Hayes, and J.H. Harmey, *Vascular Endothelial Growth Factor (VEGF) and Its Role in Non-Endothelial Cells: Autocrine Signalling by VEGF*, in *Madame Curie Bioscience*. 2013, Landes Bioscience: Austin, Texas.
252. Helotera, H. and K. Alitalo, *The VEGF Family, The Inside Story.* Cell, 2007. **130**(4): p. 591-592.
253. Ge, Q., et al., *VEGF secreted by mesenchymal stem cells mediates the differentiation of endothelial progenitor cells into endothelial cells via paracrine mechanisms.* Mol Med Rep., 2018. **17**(1): p. 1667-1675.
254. Shibuya, M., *Vascular Endothelial Growth Factor (VEGF) and Its Receptor (VEGFR) Signaling in Angiogenesis: A Crucial Target for Anti- and Pro-Angiogenic Therapies.* Genes Cancer, 2011. **2**(12): p. 1097-1105.
255. Carmeliet, P. and D. Collen, *Molecular Basis of Angiogenesis: Role of VEGF and VE-Cadherin.* Annals New York Academy of Sceince, 2006. **902**(1): p. 249-264.
256. Ferra, N.G., H.P. and J. LeCouter, *The Biology of VEGF and its Receptors.* Nature Medicine, 2003. **9**(6): p. 669-676.
257. Ferrara, N. and R.S. Kerbel, *Angiogenesis as a therapeutic target.* Nature, 2005. **438**(7070): p. 967-974.
258. Shalaby , F., et al., *Failure of blood-island formation and vasculogenesis in Flk-1 deficient mice.* Nature, 1995. **35**.
259. Cébe Suarez, S., et al., *A VEGF-A splice variant defective for heparan sulfate and neuropilin-1 binding shows attenuated signaling through VEGFR-2. Cellular and Molecular Life Sciences* 2006. **63**(17): p. 2067–2077.
260. Peach, C.J., et al., *Molecular Pharmacology of VEGF-A Isoforms: Binding and Signalling at VEGFR2. . Int. J. Mol. Sci.* , 2018. ***19***: p. 1264.

261. M., P.-P., *The role of VEGF 165b in pathophysiology.* Cell adhesion & migration, 2012. **6**(6): p. 561-568.
262. Lerman, M.J., et al., *The Evolution of Polystyrene as a Cell Culture Material.* Tissue Engineering Part B: Reviews, 2018. **24**(5).
263. Song, S.Y., H.M. Chung, and J.H. Sung, *The pivotal role of VEGF in adipose-derived-stem-cell-mediated regeneration.* Expert Opinion on Biological Therapy, 2010. **10**(11): p. 1529-1537.
264. Grützkau, A., et al., *A. Synthesis, storage, and release of vascular endothelial growth factor/vascular permeability factor (VEGF/VPF) by human mast cells: implications for the biological significance of VEGF206. . Mol Biol Cell*, 1998. **9**(4): p. 875-884.
265. Wang, C.Q., et al., *Amphiregulin enhances VEGF-A production in human chondrosarcoma cells and promotes angiogenesis by inhibiting miR-206 via FAK/c-Src/PKCδ pathway.* Cancer Letters, 2017. **28**(385): p. 261-270.
266. Tsuji, W., J.P. Rubin, and K.G. Marra, *Adipose-derived stem cells: Implications in tissue regeneration.* World journal of stem cells, 2014. **6**: p. 312-321.
267. Gianni-Barrera, R., et al., *Split for the cure: VEGF, PDGF-BB and intussusception in therapeutic angiogenesis.* Biochemical Society Transactions 2016. **42**(6): p. 1637-1642.
268. Groppa, E., et al., *VEGF dose regulates vascular stabilization through Semaphorin3A and the Neuropilin-1+ monocyte/TGF-β1 paracrine axis.* EMBO Molecular Medicine, 2015. **7**(10): p. 1366-1384.
269. Li, C.Y., et al., *Comparative analysis of human mesenchymal stem cells from bone marrow and adipose tissue under xeno-free conditions for cell therapy.* Stem Cell Res Ther., 2015. **6**(1): p. 55.
270. Lee, E.Y., et al., *Hypoxia-enhanced wound-healing function of adipose-derived stem cells: Increase in stem cell proliferation and up-regulation of VEGF and bFGF.* Wound Repair and Regeneration, 2009. **17**(4).
271. Xu , L., D. Fukumura, and R.K. Jain, *Acidic Extracellular pH Induces Vascular Endothelial Growth Factor (VEGF) in Human Glioblastoma Cells via ERK1/2 MAPK Signaling Pathway MECHANISM OF LOW pH-INDUCED VEGF*.* The Journal of Biological Chemistry, 2002. **277**: p. 11368-11374.
272. Benjamini, Y. and Y. Hochberg, *Controlling the false discovery rate: a practical and powerful approach to multiple testing.* Journal of the Royal Statistical Society Series B, 1995. **57**: p. 289-300.
273. Ribatti , D., *The chick embryo chorioallantoic membrane (CAM) assay.* Reproductive Toxicology, 2017. **70**: p. 97-101.
274. Waltenberger, J., et al., *Suramin is a potent inhibitor of vascular endothelial growth factor. A contribution to the molecular basis of its antiangiogenic action.* J Mol Cell Cardiol., 1996. **28**(7): p. 1523- 1529.

275. Kathir , K.M., et al., *Understanding the Mechanism of the Anti-angiogenic Activity of Suramin.* Biophysical Journal, 2009. **96**(3): p. 600-601.
276. Gittens, R.A., et al., *The effects of combined micron-/submicron-scale surface roughness and nanoscale features on cell proliferation and differentiation.* Biomaterials, 2011. **32**(13): p. 3395–3403.
277. Song, S.Y., H.M. Chung, and J.H. SUng, *The pivotal role of VEGF in adipose-derived-stem cell-mediated regeneration.* Expert Opin. Biol. Ther., 2010. **10**(11).
278. Ervolino de Oliveira , C., et al., *Activin A induces vascular endothelial cell proliferation and angiogenesis in oral cancer.* AACR Special Conference: Tumor Angiogenesis and Vascular Normalization: Bench to Bedside to Biomarkers, 2015.
279. Porter, S., et al., *The ADAMTS metalloproteinases.* Biochemical Journal, 2005. **368**(1): p. 15-27.
280. Fagiani, E. and G. Christofori, *Angiopoietins in angiogenesis.* Cancer Letters, 2013. **328**(1): p. 18-26.
281. Felcht, M.L., R. Schering, A.Seidel, P. Srivastava, K. Hu, J.Bartol, A.Kienast, Y.Vettel, C.Loos, E.K.Kutschera, S.Bartels, S.Appak, S.Besemfelder, E.Terhardt, D.Chavakis, E.Wieland, T.Klein, C.Thomas, M.Uemura, A.Goerdt, S.Augustin, H.G., *Angiopoietin-2 differentially regulates angiogenesis through TIE2 and integrin signalling.* J Clin Invest., 2012. **122**(6): p. 1991-2005.
282. Cao, Y. and L. Xue, *Angiostatin.* Semin Thromb Hemost. , 2004. **30**(1): p. 83-93.
283. Banerjee, A., et al., *ARTEMIN Promotes De Novo Angiogenesis in ER Negative Mammary Carcinoma through Activation of TWIST1-VEGF-A Signalling.* PLoS ONE, 2012. **7**(11).
284. Ruf, W., N. Yokota, and F. Schaffner, *Tissue factor in cancer progression and angiogenesis.* Thromb Res, 2010. **125**: p. 36-38.
285. Chu, A.J., *Tissue Factor, Blood Coagulation, and Beyond: An Overview.* International Journal of Inflammation, 2011. **2011**: p. 30.
286. Yu, X., et al., *CXCL16 induces angiogenesis in autocrine signaling pathway involving hypoxia-inducible factor 1α in human umbilical vein endothelial cells.* Oncol Rep, 2016. **35**(3): p. 1557-1565.
287. Chen, W.T., *DPPIV and Seprase in Cancer Invasion and Angiogenesis*, in *Dipeptidyl Aminopeptidases in Health and Disease. Advances in Experimental Medicine and Biology*, N. Back, et al., Editors. 2004, Springer: Boston, MA.
288. Guillamo , J.S., et al., *Molecular Mechanisms Underlying Effects of Epidermal Growth Factor Receptor Inhibition on Invasion, Proliferation, and Angiogenesis in Experimental Glioma.* American Association for Cancer Research, 2009. **15**(11).
289. Brouillet, S., et al., *Molecular characterization of EG-VEGF-mediated angiogenesis: differential effects on microvascular and macrovascular endothelial cells.* Mol Biol Cell. , 2010. **21**(16): p. 2832-2843.

290. Nassiri, F., et al., *Endoglin (CD105): a review of its role in angiogenesis and tumor diagnosis, progression and therapy.* Anticancer Res. , 2011. **31**(6): p. 2283-2290.
291. Pufe, T., et al., *Endostatin/collagen XVIII--an inhibitor of angiogenesis--is expressed in cartilage and fibrocartilage.* Matrix Biology, 2004. **23**(5): p. 267-276.
292. Zatterstrom, U.K., et al., *Collagen XVIII/endostatin structure and functional role in angiogenesis.* Cell Struct Function, 2000. **25**(2): p. 97-101.
293. Knowles, J., M. Loizidou, and I. Taylor, *Endothelin-1 and angiogenesis in cancer.* Curr Vasc Pharmacol., 2005. **3**(4): p. 309-314.
294. Yun, Y.R., et al., *Fibroblast growth factors: biology, function, and application for tissue regeneration.* Journal of tissue engineering, 2010: p. 218142
295. Gillis, P., et al., *Keratinocyte growth factor induces angiogenesis and protects endothelial barrier function.* J Cell Sci., 1999. **112**: p. 2049-2057.
296. Chen, M., et al., *Glial Cell Line-Derived Neurotrophic Factor (GDNF) Promotes Angiogenesis through the Demethylation of the Fibromodulin (FMOD) Promoter in Glioblastoma.* Med Sci Monit,, 2018. **24**: p. 6137-6143.
297. Valdembri, D., et al., *In vivo activation of JAK2/STAT-3 pathway during angiogenesis induced by GM-CSF.* FASEB J., 2002.
298. Mehta, V.B. and G.E. Besner, *HB-EGF promotes angiogenesis in endothelial cells via PI3-kinase and MAPK signaling pathways.* Growth Factors, 2007. **24**(4): p. 253-263.
299. Bussolino, E., et al., *Hepatocyte Growth Factor Is a Potent Angiogenic Factor Which Stimulates Endothelial Cell Motility and Growth.* The Journal of Cell Biology, 1992. **119**(3): p. 629-641.
300. Morishita, R., et al., *Therapeutic angiogenesis using hepatocyte growth factor (HGF).* Current Gene Therapy, 2004. **4**(2): p. 199-206.
301. Zhong, Z., et al., *GDNF secreted from adipose-derived stem cells stimulates VEGF-independent angiogenesis.* Oncotarget, 2014. **7**(24): p. 1-13.
302. Azar, W.J., et al., *IGFBP-2 enhances VEGF gene promoter activity and consequent promotion of angiogenesis by neuroblastoma cells.* Endocrinology, 2011. **152**(9): p. 3332-3342.
303. Granata, R., et al., *Insulin-like growth factor binding protein-3 induces angiogenesis through IGF-I- and SphK1-dependent mechanisms.* J Thromb Haemost., 2007. **5**(4): p. 835-845.
304. Voronov, E., Y. Carmi, and R.N. Apte, *The role IL-1 in tumor-mediated angiogenesis.* Frontiers in physiology, 2014. **5**(114).
305. Heidemann, J., et al., *Angiogenic effects of interleukin 8 (CXCL8) in human intestinal microvascular endothelial cells are mediated by CXCR2.* J Biol Chem. , 2003. **278**(10): p. 8508-8515.

306. Maroni, D. and J.S. Davis, *TGFB1 disrupts the angiogenic potential of microvascular endothelial cells of the corpus luteum.* Journal of Cell Science, 2011. **124**(14): p. 2501-2510.
307. Park, H.Y., et al., *Potential role of leptin in angiogenesis: leptin induces endothelial cell proliferation and expression of matrix metalloproteinases in vivo and in vitro.* Exp Mol Med. , 2001. **33**(2): p. 95-102.
308. Ma, J., et al., *MCP-1 mediates TGF-beta-induced angiogenesis by stimulating vascular smooth muscle cell migration.* Blood, 2007. **109**(3): p. 987-994.
309. Liao, Y.Y., et al., *CCL3 promotes angiogenesis by dysregulation of miR-374b/ VEGF-A axis in human osteosarcoma cells.* Oncotarget, 2015. **7**(4): p. 4310-4325.
310. Fang, C., et al., *An important role of matrix metalloproteinase-8 in angiogenesis in vitro and in vivo.* Cardiovascular Research, 2013. **99**(1): p. 146-155.
311. Mira, E., et al., *Secreted MMP9 promotes angiogenesis more efficiently than constitutive active MMP9 bound to the tumor cell surface.* J Cell Sci. , 2004. **117**: p. 1847-1857.
312. Guia, C., et al., *Neuregulin-1 Promotes Myocardial Angiogenesis in the Rat Model of Diabetic Cardiomyopathy.* Cell Physiol Biochem, 2018. **46**: p. 2325-2334.
313. Presta, M., et al., *Long Pentraxin-3 Modulates the Angiogenic Activity of Fibroblast Growth Factor-2.* Front. Immunol., 2018. **9**: p. 2327.
314. Fujimoto, J., et al., *Expression of platelet-derived endothelial cell growth factor (PD-ECGF) and its mRNA in uterine cervical cancers.* Br J Cancer. , 1999. **79**(7-8): p. 1249-1254.
315. Raica, M. and A.M. Cimpean, *Platelet-Derived Growth Factor (PDGF)/PDGF Receptors (PDGFR) Axis as Target for Antitumor and Antiangiogenic Therapy.* Pharmaceuticals (Basel), 2010. **3**(3): p. 572-599.
316. Burman, K.D., *Thyroid Cancer and Other Thyroid Disorders, An Issue of Endocrinology and Metabolism Clinics of North America*. 2014: Elsevier Health Sciences.
317. Mulligan, L.M., *RET revisited: expanding the oncogenic portfolio.* Nature Reviews Cancer, 2014. **14**: p. 173-186.
318. Aidoudi, S. and A. Bikfalvi, *Interaction of PF4 (CXCL4) with the vasculature: A role in atherosclerosis and angiogenesis.* Thrombosis and Haemostasis, 2010. **104**(5): p. 941-948
319. Luttun, A., M. Tjwa, and P. Carmeliet, *Placental growth factor (PlGF) and its receptor Flt-1 (VEGFR-1): novel therapeutic targets for angiogenic disorders.* Ann N Y Acad Sci., 2002. **979**: p. 80-93.
320. Corbacho, A.M., G. Martínez De La Escalera, and C. Clapp, *Roles of prolactin and related members of the prolactin/growth hormone/placental lactogen family in angiogenesis.* J Endocrinol., 2002. **173**(2): p. 219-238.

321. Reuwer, A.Q., et al., *Functional consequences of prolactin signalling in endothelial cells: a potential link with angiogenesis in pathophysiology?* J Cell Mol Med., 2012. **16**(9): p. 2035-2045.
322. Zhang, M., et al., *Maspin is an angiogenesis inhibitor.* Nature Medicine, 2000. **6**(2): p. 196-199.
323. Simone, T.M., et al., *SERPINE1: A Molecular Switch in the Proliferation-Migration Dichotomy in Wound-"Activated" Keratinocytes.* Advances in wound care, 2014. **3**(3): p. 281-290.
324. Bhutto, I.A., et al., *Pigment epithelium-derived factor (PEDF) and vascular endothelial growth factor (VEGF) in aged human choroid and eyes with age-related macular degeneration.* Exp Eye Res., 2006. **82**(1): p. 99-110.
325. Brew, K. and H. Nagase, *The tissue inhibitors of metalloproteinases (TIMPs): an ancient family with structural and functional diversity.* Biochimica et biophysica acta, 2010. **1803**(1): p. 55-71.
326. Pullen, N.A., et al., *Matrix metalloproteinase-1 expression enhances tumorigenicity as well as tumor-related angiogenesis and is inversely associated with TIMP-4 expression in a model of glioblastoma.* 2012. **106**(3): p. 461-471.
327. Lawler, J., *Thrombospondin-1 as an endogenous inhibitor of angiogenesis and tumor growth.* J Cell Mol Med. , 2002. **6**(1): p. 1-12.
328. Krady, M.M., et al., *Thrombospondin-2 modulates extracellular matrix remodeling during physiological angiogenesis. .* The American journal of pathology, 2008. **173**(3): p. 879-891.
329. Breuss, J.M. and P. Uhrin, *VEGF-initiated angiogenesis and the uPA/uPAR system.* Cell Adh Migr, 2012. **6**(6): p. 535-615.
330. Sato, Y., *The vasohibin family: a novel family for angiogenesis regulation.* J Biochem., 2013. **153**(1): p. 5-11.
331. Nör, J.E., et al., *Vascular endothelial growth factor (VEGF)-mediated angiogenesis is associated with enhanced endothelial cell survival and induction of Bcl-2 expression.* Am J Pathol, 1999. **154**(2): p. 375-384.
332. Hoeben , A., et al., *Vascular Endothelial Growth Factor and Angiogenesis.* Pharmacological Reviews 2004. **56**(4): p. 549-580.
333. Chien, M.H., et al., *Vascular endothelial growth factor-C (VEGF-C) promotes angiogenesis by induction of COX-2 in leukemic cells via the VEGF-R3/JNK/AP-1 pathway.* Carcinogenesis, 2009. **30**(12): p. 2005-2013.
334. Niiyama, H., et al., *Murine model of hindlimb ischemia.* Journal of visualized experiments : JoVE, 2009. **23**: p. 1035.
335. Suhar a, M., et al., *Targeting ability of self-assembled nanomedicines in rat acute limb ischemia model is affected by size.* Journal of Controlled Release, 2018. **286**(28): p. 394-401.

336. Pu, L.Q., et al., *A Persistent Hindlimb Ischemia Model in the Rabbit.* Journal of Investigative Surgery, 2009. **7**(1): p. 49-60.
337. Long , C.A., et al., *An endovascular model of ischemic myopathy from peripheral arterial disease.* Journal of Vascular Surgery, 2017. **66**(3): p. 891-901.
338. Margovsky, A., et al., *Small vessel ischaemia induced by microbead embolization in the sheep hind limb.* Aust N Z J Surg. , 1998. **68**(8): p. 592-598.
339. Helisch, A., et al., *Impact of Mouse Strain Differences in Innate Hindlimb Collateral Vasculature.* Arterioscler Thromb Vasc Biol., 2006. **26**(3): p. 520-526.
340. Hellingman, A.A., et al., *Variations in Surgical Procedures for Hind Limb Ischaemia Mouse Models Result in differences in Collateral Formation.* European Journal of Vascular and Endovascular Surgery, 2010. **40**(6): p. 796-803.
341. Brenes , R.A., et al., *Toward a mouse model of hind limb ischemia to test therapeutic angiogenesis.* Journal of Vascular Surgery, 2012. **56**(6): p. 1669-1679.
342. Padgett, M.E., et al., *Methods for Acute and Subacute Murine Hindlimb Ischemia.* Journal of visualized experiments : JoVE, 2016. **112**: p. 54166.
343. Liu, X., et al., *Osmotic drug delivery to ischemic hindlimbs and perfusion of vasculature with microfil for micro-computed tomography imaging. Journal of visualized experiments : JoVE*, 2013(76): p. 50364.
344. Mirebella, T., et al., *3D-printed vascular networks direct therapeutic angiogenesis in ischaemia. Nature Biomedical Engineering*, 2017. **1**.
345. DeQuach, J.A., et al., *Injectable skeletal muscle matrix hydrogel promotes neovascularization and muscle cell infiltration in a hindlimb ischemia model. European cells & materials* 2012. **23**(412): p. 400-412.
346. Stuckey, D.J., et al., *Magnetic resonance imaging evaluation of remodeling by cardiac elastomeric tissue scaffold biomaterials in a rat model of myocardial infarction.* Tissue Engineering Part A, 2010. **16**(11): p. 3395-3402.
347. Parmar, N. and R. Day, *TIPS to manipulate myogenesis: retention of myoblast differentiation capacity using microsphere culture.* European Cells and Materials, 2015. **30**: p. 41-50.
348. Ahmadi, R., et al., *Enhanced attachment, growth and migration of smooth muscle cells on microcarriers produced using thermally induced phase separation.* Acta Biomaterialia, 2011. **7**(4): p. 1542-1549
349. Mutter, G.L., et al., *Comparison of frozen and RNALater solid tissue storage methods for use in RNA expression microarrays.* BMC Genomics, 2004. **4**(88).
350. Fischer , A.H., et al., *Preparation of Cells and Tissues for Fluorescence Microscopy: Hematoxylin and Eosin Staining of Tissue and Cell Sections*, in *Basic Methods in Microscopy*, Spector and Goldman, Editors. 2006, Cold Spring Harbor Laboratory Press: Cold Spring Harbor, NY, USA.

351. Waters, R.E., et al., *Pre-Clinical Models of Human Peripheral Arterial Occlusive Disease: Implications for Investigation of Therapeutic Agents.* Journal of Applied Physiology, 2004. **97**(2): p. 773-780
352. Zhuang, Z.W., et al., *Challenging the surgical rodent hindlimb ischemia model with the miniinterventional technique.* Journal of vascular and interventional radiology : JVIR, 2011. **22**(10): p. 1437-1446.
353. Madeddu, P., et al., *Murine models of myocardial and limb ischemia: Diagnostic end-points and relevance to clinical problems.* Vascular Pharmacology, 2006. **45**(5): p. 281-301.
354. Parik h, P.P., et al., *A Reliable Mouse Model of Hind limb Gangrene.* Annals of Vascular Surgery, 2018. **48**: p. 222-232.
355. MacAskill, M.G., et al., *Robust Revascularization in Models of Limb Ischemia Using a Clinically Translatable Human Stem Cell-Derived Endothelial Cell Product.* Molecular Therapies, 2018. **26**(7): p. 1669-1684.
356. Sorrentino , S., et al., *Hindlimb Ischemia Impairs Endothelial Recovery and Increases Neointimal Proliferation in the Carotid Artery.* Scientific Reports, 2018. **8**(761).
357. Goto, T., et al., *Search for appropriate experimental methods to create stable hind-limb ischemia in mouse.* Tokai J Exp Clin Med. , 2006. **31**(3): p. 128-132.
358. Sönmez, T.T., et al., *A Novel Laser-Doppler Flowmetry Assisted Murine Model of Acute Hindlimb Ischemia-Reperfusion for Free Flap Research.* PLoS ONE 2013. **8**(3): p. e66498.
359. Greco, A., et al., *Repeatability, Reproducibility and Standardisation of a Laser Doppler Imaging Technique for the Evaluation of Normal Mouse Hindlimb Perfusion.* Sensors, 2013. **13**: p. 500-515.
360. Prabhakaran , M.P., et al., *Biomimetic material strategies for cardiac tissue engineering.* Materials Science and Engineering: C, 2011. **31**(3): p. 503-513.
361. Kim, B.S., et al., *Angiogenin-loaded fibrin/bone powder composite scaffold for vascularized bone regeneration.* Biomaterials Research, 2014: p. 1-9.
362. Pusztaszeri, M.P., W. Seelentag, and F.T. Bosman, *Immunohistochemical Expression of Endothelial Markers CD31, CD34, von Willebrand Factor, and Fli-1 in Normal Human Tissues.* Journal of Histochemistry & Cytochemistry, 2006. **54**(4): p. 385–395.
363. Starke, R.D., et al., *Endothelial von Willebrand factor regulates angiogenesis.* Blood, 2011. **117**(3): p. 1071-1080.
364. Shimizu-Motohashi, Y. and A. Asakura, *Angiogenesis as a novel therapeutic strategy for Duchenne muscular dystrophy through decrease ischemia and increased satellite cells.* Front. Physiol., 18 February 2014 2014. **5**(50).

365. Weel, V., et al., *Expression of Vascular Endothelial Growth Factor, Stromal Cell-Derived Factor-1, and CXCR4 in Human Limb Muscle With Acute and Chronic Ischemia.* Arterioscler Thromb Vasc Biol., 2007. **27** p. 1426-1432.
366. Olfert, I.M., et al., *Advances and challenges in skeletal muscle angiogenesis. American journal of physiology. Heart and circulatory physiology*, 2016. ***310***(3): p. 326–336.
367. Deveci, D., J.M. Marshall, and S. Egginton, *Relationship between capillary angiogenesis, fiber type, and fiber size in chronic systemic hypoxia.* Am J Physiol Heart Circ Physiol., 2001. **281**(1): p. 241-252.
368. Patan, S., *Vasculogenesis and angiogenesis.* Cancer Treat Res., 2004. **117**: p. 3-32.
369. Limbourg, A., et al., *Evaluation of Postnatal Arteriogenesis and Angiogenesis in a Mouse Model of Hind-Limb Ischemia.* Nature Protocols, 2009. **4**: p. 1737-1784.
370. Tahergorabi, Z. and M. Khazaei, *A review on angiogenesis and its assays.* Iranian journal of basic medical sciences, 2012. **15**(6): p. 1110-1126.
371. Caporali, A., et al., *Soluble ST2 Is Regulated by p75 Neurotrophin Receptor and Predicts Mortality in Diabetic Patients With Critical Limb Ischemia.* Arteriosclerosis, Thrombosis and Vascular Biology, 2012(32): p. 149-160.
372. Lee , S.L., W.C. Pevec , and R.C. Carlsen *Functional outcome of new blood vessel growth into ischemic skeletal muscle.* Journal of Vascular Surgery, 2001. **34**(6): p. 1096-1102.
373. Cardinal, T.R., et al., *Chronic hindlimb ischemia impairs functional vasodilation and vascular reactivity in mouse feed arteries.* Frontiers in physiology, 2011. **2**(91).
374. Cen, Y., et al., *Denervation in Femoral Artery-Ligated Hindlimbs Diminishes Ischemic Recovery Primarily via Impaired Arteriogenesis.* PLoS ONE, 2016. **11**(5): p. e0154941.
375. Aliya, S., *Effects of Vasodilation and Arterial Resistance on Cardiac Output.* J Clinic Experiment Cardiol 2011. **2**: p. 170.
376. Iglarz, M., et al., *Chronic Blockade of Endothelin Receptors Improves Ischemia-Induced Angiogenesis in Rat Hindlimbs Through Activation of Vascular Endothelial Growth Factor–NO Pathway.* Arterioscler Thromb Vasc Biol., 2001. **21**: p. 1598-1603.
377. Wang, C.H., et al., *Assessment of mouse hind limb endothelial function by measuring femoral artery blood flow responses.* J Vasc Surg., 2011. **53**(5): p. 1350-1358.
378. Heiss, C., et al., *In vivo measurement of flow-mediated vasodilation in living rats using high-resolution ultrasound.* Am J Physiol Heart Circ Physiol., 2008. **294**(8): p. 1086-1093.
379. Schuler , D., et al., *Measurement of Endothelium-Dependent Vasodilation in Mice—Brief Report.* Arterioscler Thromb Vasc Biol. **34**: p. 2651-2657.

380. Lloyd, et al., *Arteriogenesis and angiogenesis in rat ischemic hindlimb: role of nitric oxide.* American Journal of Physiology, 2001. **281**(6).
381. Laughlin, M.H., et al., *Training induces nonuniform increases in eNOS content along the coronary arterial tree.* J Appl Physiol, 2001. **90**: p. 501-510.
382. Boo, Y.C. and H. Jo, *Flow-dependent regulation of endothelial nitric oxide synthase: role of protein kinases.* Am J Physiol Cell Physiol, 2003. **285**: p. C499-C508.
383. Contreras , D.V., et al., *The role of nitric oxide in the post-ischemic revascularization process.* Pharmacology & Therapeutics, 2006. **112**(2): p. 554-563.
384. Davis, M.E., et al., *Shear stress regulates endothelial nitric-oxide synthase promoter activity through nuclear factor kappa B binding.* J Biol Chem, 2004. **279**: p. 163-168.
385. Bustin, S.A., *Why the need for qPCR publication guidelines? - The case for MIQE.* Methods, 2010. **50**(4): p. 217-226.
386. Desjardins, P. and D. Conklin, *NanoDrop microvolume quantitation of nucleic acids.* Journal of visualized experiments : JoVE, 2010(45): p. 2565.
387. Tataurov, A.V., Y. You, and R. Owczarzy, *Predicting ultraviolet spectrum of single stranded and double stranded deoxyribonucleic acids. Biophys. Chem*, 2008. **133**(1-3): p. 66–70.
388. Sambrook and Russell, *Molecular Cloning: A Laboratory Manual* 3rd ed. 2001: Cold Spring Harbor Laboratory Press.
389. Technology, O.G. *Understanding and measuring variations in DNA sample quality*. 2011 02/12/2018]; Available from: https://www.ogt.com/resources/literature/483_understanding_and_measuring_variations_in_dna_sample_quality.
390. Johnson, M.T., et al., *Evaluating methods for isolating total RNA and predicting the success of sequencing phylogenetically diverse plant transcriptomes.* PloS one, 2012. **7** (11): p. e50226.
391. Wadle, S., et al., *Real-time PCR probe optimization using design of experiments approach.* Biomolecular Detection and Quantification, 2016. **7**: p. 1-8.
392. Wong, M.L. and J.F. Medrano, *Real-time PCR for mRNA quantitation.* BioTechniques, 2005. **39**(1): p. 75-85.
393. Wang, M., et al., *Wars2 is a determinant of angiogenesis.* Nature Communications, 2016. **7**: p. 1-12.
394. Zeng , R., et al., *Effect of mini-tyrosyl-tRNA synthetase/mini-tryptophanyl-tRNA synthetase on ischemic angiogenesis in rats: proliferation and migration of endothelial cells.* Heart Vessels, 2011. **26**: p. 69–80.
395. Williams, T.F., et al., *Secreted Threonyl-tRNA synthetase stimulates endothelial cell migration and angiogenesis.* Scientific Reports, 2013. **3**(1317): p. 1-7.
396. Anderson, J.M., A. Rodriguez, and D.T. Chan g, *Foreign Body Reaction to Biomaterials.* Seminars in Immunology, 2008. **20**(2): p. 86-100.

397. Vishwakarma, A., et al., *Engineering Immunomodulatory Biomaterials To Tune the Inflammatory Response.* Trends in Biotechnology, 2016. **34**(6): p. 470-482.
398. Xia, Z. and J.T. Triffitt, *A review on macrophage responses to biomaterials.* Biomed. Mater., 2006. **1**: p. R1–R9.
399. Franz , S., et al., *Immune responses to implants – A review of the implications for the design of immunomodulatory biomaterials.* Biomaterials, 2011. **32**(28): p. 6692-6709.
400. Klopfleisch, R., *Macrophage reaction against biomaterials in the mouse model – Phenotypes, functions and markers.* Acta Biomaterialia, 2016. **43**(1): p. 3-13.
401. Chung, L., et al., *Key Players in the Immune Response to Biomaterial Scaffolds for Regenerative Medicine.* Advanced Drug Delivery Reviews, 2017. **114**: p. 184-192.
402. van Loon, S.L.M., et al., *The Immune Response in In Situ Tissue Engineering of Aortic Heart Valves*, in *Calcific Aortic Valve Disease*, E. Aikawa, Editor. 2012, IntechOpen.
403. Dondossola, E., et al., *Examination of the foreign body response to biomaterials by nonlinear intravital microscopy. .* Nature biomedical engineering 2016. **1**(0007).
404. Brown, B.N.R., B.D. Goodman, S.B. Amar, S. Badylak, S.F., *Macrophage polarization: an opportunity for improved outcomes in biomaterials and regenerative medicine. .* Biomaterials, 2012. **33**(15): p. 3792-3802
405. Martinez, F.O. and S. Gordon, *The M1 and M2 paradigm of macrophage activation: time for reassessment.* Prime Rep. , 2014. **6**(13).
406. Okazaki, T., et al., *Macrophage colony-stimulating factor induces vascular endothelial growth factor production in skeletal muscle and promotes tumor angiogenesis* J. Immunol. , 2005. **174** p. 7531–7538
407. Henson, P.M., *The immunologic release of constituents from neutrophil leukocytes. I. The role of antibody and complement on nonphagocytosable surfaces or phagocytosable particles.* J Immunol, 1971. **107**(6): p. 1535–1546.
408. Yu, Q., et al., *Anti-fouling bioactive surfaces.* Acta Biomateriala, 2011. **7**(4): p. 1550-1570.
409. Beningo, K.A. and Y.I. Wang, *Fc-receptor-mediated phagocytosis is regulated by mechanical properties of the target.* J. Cell Sci., 2002. **115**(4): p. 849-856
410. Blakney, A.K., M.D. Swartzlander, and S.J. Bryant, *The effects of substrate stiffness on the in vitro activation of macrophages and in vivo host response to poly(ethylene glycol)-based hydrogels.* J. Biomed. Mater. Res., 2012. **100**(6): p. 1375-1386
411. Patel, N.R., et al., *Cell Elasticity Determines Macrophage Function.* PLoS ONE, 2012. **7**(9): p. e41024.
412. Bota, P.C.S., et al., *Biomaterial topography alters healing in vivo and monocyte/macrophage activation in vitro.* Journal of Biomedical Materials Research Part A, 2010. **95A**(2).

413. Sridharan , R., et al., *Biomaterial based modulation of macrophage polarization: a review and suggested design principles.* Materials Today, 2015. **18**(6): p. 313-325.
414. Paul, N.E., et al., *Topographical control of human macrophages by a regularly microstructured polyvinylidene fluoride surface.* Biomaterials, 2008. **29**: p. 4056–4064.
415. Chen , S., et al., *Characterization of topographical effects on macrophage behavior in a foreign body response model.* Biomaterials, 2010. **31**(3): p. 3479-3491.
416. Waterfield, J.D., et al., *The effect of surface topography on early NFκB signaling in macrophages.* Journal of Biomedical Materials Research Part A, 2010. **95A**(3).
417. Jetten, N., et al., *Anti-inflammatory M2, but not pro-inflammatory M1 macrophages promote angiogenesis in vivo.* Angiogenesis, 2014. **17**(109).
418. Rundhaug, J.E., *Matrix metalloproteinases and angiogenesis.* J Cell Mol Med., 2005. **9**(2): p. 267-285.
419. Wu, W.K., et al., *IL-10 regulation of macrophage VEGF production is dependent on macrophage polarisation and hypoxia.* Immunobiology, 2010. **215**(9-10): p. 796-803.
420. Cooke, J.P., *NO and angiogenesis.* Atherosclerosis, 2003. **4**(4): p. 53-30.
421. Milde, R., et al., *Multinucleated Giant Cells Are Specialized for Complement-Mediated Phagocytosis and Large Target Destruction.* Cell reports, 2015. **13**(9): p. 1937-1948.
422. Chávez-Galán, L., et al., *Much More than M1 and M2 Macrophages, There are also CD169(+) and TCR(+) Macrophages.* Frontiers in immunology, 2015. **6**(263).
423. Corliss, B.A., et al., *Macrophages: An Inflammatory Link Between Angiogenesis and Lymphangiogenesis. .* Microcirculation, 2016. **23**(2): p. 95-121.
424. Ma, X., et al., *Regulation of IL-10 and IL-12 production and function in macrophages and dendritic cells.* 2015. **1**(4): p. F1000.
425. Mills, C.D. and K. Ley, *M1 and M2 macrophages: the chicken and the egg of immunity. Journal of innate immunity*, 2014. **6**(6): p. 7 16-726.
426. Zheng, X.F., et al., *Lipopolysaccharide-Induced M2 to M1 Macrophage Transformation for IL-12p70 Production Is Blocked by Candida albicans Mediated Up-Regulation of EBI3 Expression.* PLoS ONE, 2013. **8**(5): p. e63967.
427. Chehroudi, B., T.R. Gould, and D.M. Brunette, *A light and electron microscopic study of the effects of surface topography on the behavior of cells attached to titanium-coated percutanous implants.* Journal of Biomedical Materials Research, 1991. **25**: p. 387-405
428. Picha, G.J. and R.F. Drake, *Pillared-surface microstructure and soft-tissue implants: effect of implant site and fixation.* Journal of Biomedical Materials Research, , 1996. **30** p. 305-312.
429. Fontana, F., et al., *Bioengineered Porous Silicon Nanoparticles at Macrophages Cell Membrane as Composite Platforms for Rheumatoid Arthritis.* Advanced Functional Materials, 2018. **28**(22).

430. Piya , R., et al., *Micropatterning of porous silicon Bragg reflectors with poly(ethylene glycol) to fabricate cell microarrays: Towards single cell sensing.* Biosensors and Bioelectronics, 2019. **127**: p. 229-235.
431. Parker, J.A.T.C., et al., *Soft-tissue response to silicone and poly-L-lactic acid implants with a periodic or random surface micropattern.* Biomed Mater Res, 2001. **61**: p. 91–98.
432. Singhvi, R., G. Stephanopoulos, and D.I.C. Wang, *Review: Effects of substratum morphology on cell physiology.* Biotech Bioeng, 1994. **43**: p. 764–771.
433. Braber, E.T., J.E. de Ruijter, and J.A. Jansen, *The effect of a subcutaneous silicone rubber implant with shallow surface microgrooves on the surrounding tissues in rabbits.* Journal of Biomedical Material Research 1997. **37** p. 539–547.
434. Rosengren, A., et al., *Tissue reactions to polyethylene implants with different surface topography.* Journal of Materials Science: Materials in Medicine, 1992. **10**(2): p. 75-82.
435. Refai, A., et al., *Effect of titanium surface topography on macrophage activation and secretion of proinflammatory cytokines and chemokines.* August 2004Journal of Biomedical Materials Research Part A 2004. **70**(2): p. 194-205.
436. Boersema, G.S., et al., *The Effect of Biomaterials Used for Tissue Regeneration Purposes on Polarization of Macrophages. BioResearch open access* 2016. **5**(1): p. 6-14.
437. Sussman, E.M., et al., *Porous Implants Modulate Healing and Induce Shifts in Local Macrophage Polarization in the Foreign Body Reaction.* 2014. **42**(7): p. 1508-1516.
438. Toniolo, A., et al., *Alternative Activation of Human Macrophages Is Rescued by Estrogen Treatment In Vitro and Impaired by Menopausal Status.* J Clin Endocrinol Metab, 2015. **100**(1): p. E50 –E58.
439. Sakhno, L.V., et al., *The Phenotypic and Functional Features of Human M2 Macrophages Generated Under Low Serum Conditions.* Scandinavian Journal of Immunology, 2016. **83**: p. 151–159
440. Mendez-Samperio, P., A. Perez, and L. Rivera, *Mycobacterium bovis Bacillus Calmette-Guérin (BCG)-induced activation of PI3K/Akt and NF-kB signaling pathways regulates expression of CXCL10 in epithelial cells.* Cellular Immunology, 2009. **256**(1-2): p. 12-18.
441. Rocher, C. and D.K. Singla, *SMAD-PI3K-Akt-mTOR Pathway Mediates BMP-7 Polarization of Monocytes into M2 Macrophages.* PLoS ONE 2013. **8**(12): p. e84009.
442. Vergadi , E., et al., *Akt Signaling Pathway in Macrophage Activation and M1/M2 Polarization.* J Immunol, 2017. **198**(3): p. 1006-1014.
443. Mahajan, K. and N.P. Mahajan, *PI3K-independent AKT activation in cancers: A treasure trove for novel therapeutics.* Journal of Cellular Physiology, 2012. **227**(9).

444. Hemmings, B.A. and D.F. Restuccia, *PI3K-PKB/Akt pathway.* Cold Spring Harbor perspectives in biology, 2012. **4**(9): p. a011189.
445. Rostam, H.M., et al., *The impact of surface chemistry modification on macrophage polarisation.* Immunobiology, 2016. **221**(11): p. 1237-1246.
446. Anderson, J.M. and M.S. Shive, *Biodegradation and biocompatibility of PLA and PLGA microspheres.* Advanced Drug Delivery Reviews, 1997. **28**(1): p. 5-24.
447. Dobner , S., et al., *A Synthetic Non-degradable Polyethylene Glycol Hydrogel Retards Adverse Post-infarct Left Ventricular Remodeling.* Journal of Cardiac Failure, 2009. **15**(7): p. 629-636.
448. Sadtler , K., et al., *Divergent immune responses to synthetic and biological scaffolds Author links open overlay panel.* Biomaterials, 2019. **192**: p. 405-415.
449. Eble, J. and S. Niland, *The extracellular matrix of blood vessels.* Curr Pharm Des. , 2009. **15**(12): p. 1385-1400.
450. Carmeliet, P., *Mechanisms of angiogenesis and arteriogenesis.* Nature Medicine, 2000. **6**(4): p. 389-95.
451. Willenborg, S., et al., *CCR2 recruits an inflammatory macrophage subpopulation critical for angiogenesis in tissue repair.* Blood, 2012. **120**(3): p. 613-625.
452. Spiller, K.L., et al., *The role of macrophage phenotype in vascularization of tissue engineering scaffolds.* Biomaterials, 2014. **35**(15): p. 4477-4488.
453. Corliss, B.A., et al., *Macrophages: An Inflammatory Link Between Angiogenesis and Lymphangiogenesis.* Microcirculation, 2016. **23**: p. 95-121.
454. Mantovani, A., et al., *Macrophage polarization: tumor-associated macrophages as a paradigm for polarized M2 mononuclear phagocytes.* Trends in Immunology **23**(11): p. 549-555.
455. Jansen , M.F., et al., *CD40 in coronary artery disease: a matter of macrophages?* Basic Res Cardiol . 2016. **111**(38).
456. Khan, A.M., A.M. Assiri, and D.C. Broering *Complement and macrophage crosstalk during process of angiogenesis in tumor progression.* J Biomed Sci . 2015. **22**(1): p. 58.
457. Scapini , P., et al., *CXCL1/Macrophage Inflammatory Protein-2-Induced Angiogenesis In Vivo Is Mediated by Neutrophil-Derived Vascular Endothelial Growth Factor-A.* J Immunol 2004. **172**(8): p. 5034-5040.
458. Bonder , C.S., J.J. Finlay-Jones , and P.H. Hart, *Interleukin-4 regulation of human monocyte and macrophage interleukin-10 and interleukin-12 production. Role of a functional interleukin-2 receptor γ-chain.* Immunology, 1999. **96**(4): p. 529-536.
459. Martinez, F.O. and S. Gordon, *The M1 and M2 paradigm of macrophage activation: time for reassessment.* F1000Prime Rep . 2014. **6**(13).
460. Dirksen, U., et al., *Human pulmonary alveolar proteinosis associated with a defect in GM-CSF/IL-3/IL-5 receptor common beta chain expression. J Clin Invest*, 1997. **100**(9): p. 2211-2217

461. Kapałczyńska, M., et al., *2D and 3D cell cultures – a comparison of different types of cancer cell cultures.* Archives of Medical Science, 2016. **14**(4): p. 1-10.
462. Edmondson, R., et al., *Three-dimensional cell culture systems and their applications in drug discovery and cell-based biosensors.* Assay and drug development technologies, 2014. **12**(4): p. 207-218.
463. Hossain, K.M.Z., U. Patel, and I. Ahmed, *Development of microspheres for biomedical applications: a review.* Prog Biomaterials, 2015. **4**: p. 1-19.
464. Patel, U., et al., *In vitro cellular testing of Strontium/Calcium substituted phosphate glass discs and microspheres shows potential for bone regeneration.* The Journal of Tissue Engineering and Regenerative Medicine, 2019.
465. Volkert, C.A.M., A.M., *Focused Ion Beam Microscopy and Micromachining.* Materials Research Society, 2007. **32**(5): p. 389-399.
466. Brostow, W., B.P. Gorman , and O. Olea-Mejia, *Focused ion beam milling and scanning electron microscopy characterization of polymer + metal hybrids.* Materials Letters, 2007. **61**(6): p. 1333-1336.
467. Thueson, D.O., et al., *The roles of pH and concentration in lactic acid-induced stimulation of epidermal turnover.* Dermatol Surg, 1998. **24**(6): p. 641-645.
468. Usuki, A., et al., *The inhibitory effect of glycolic acid and lactic acid on melanin synthesis in melanoma cells.* Exp Dermatol, 2003. **12**(2): p. 43-50.
469. Azevedo, H.S. and R.L. Reis, *Understanding the Enzymatic Degradation of Biodegradable Polymers and Strategies to Control Their Degradation Rate*, in *Biodegradable Systems in Tissue Engineering and Regenerative Medicine*. 2005, CRC Press LLC p. 177-201.
470. Lyu, S. and D. Untereker, *Degradability of polymers for implantable biomedical devices.* International journal of molecular sciences 2009. **10**(9): p. 4033-4065.
471. Dierick , M., et al., *The use of 2D pixel detectors in micro- and nano-CT applications.* Nuclear Instruments and Methods in Physics Research Section A: Accelerators, Spectrometers, Detectors and Associated Equipment, 2008. **591**(1): p. 255-259.
472. Wargo, E.A., et al., *Comparison of focused ion beam versus nano-scale X-ray computed tomography for resolving 3-D microstructures of porous fuel cell materials.* Journal of Power Sources, 2013. **241**(1): p. 608-618.
473. Lee, J.S., et al., *Thermally Induced Phase Separation in Poly(lactic acid)/ Dialkyl Phthalate Systems.* Journal of Applied Polymer Science, 2003. **88**: p. 2224 –2232.
474. Murphy, C.M. and F.J. O'Brien, *Understanding the effect of mean pore size on cell activity in collagen-glycosaminoglycan scaffolds.* Cell Adhesion & Migration, 2010. **4**(3): p. 377-381.
475. Murphy, C.M., M.G. Haugh, and F.J. O'Brien, *The effect of mean pore size on cell attachment, proliferation and migration in collagenglycosaminoglycan scaffolds for tissue engineering.* Biomaterials, 2010. **31**(3): p. 461- 46 6.

476. Majka, S.M., et al., *Analysis and isolation of adipocytes by flow cytometry.* Methods in enzymology, 2014. **537**: p. 281-296.
477. Ullah, M., et al., *A reliable protocol for the isolation of viable, chondrogenically differentiated human mesenchymal stem cells from high-density pellet cultures.* Biores Open Access, 2012. **1**(6): p. 297-305.
478. Quent, V.M.C., et al., *Discrepancies between metabolic activity and DNA content as tool to assess cell proliferation in cancer research.* Journal of Cellular and Molecular Medicine, 2010. **14**(4).
479. Phadke, A., C.W. Chang, and S. Varghese, *Functional Biomaterials for Controlling Stem Cell Differentiation.* Stud Mechanobiol Tissue Eng Biomater, 2010. **2**: p. 19–44.
480. Qadura, M., et al., *Concise Review: Cell Therapy for Critical Limb Ischemia: An Integrated Review of Preclinical and Clinical Studies.* Regenerative Medicine, 2018. **36**: p. 161-171.
481. ThermoFisher. *MesenPRO RS™ Medium*. 2018 31/10/18]; Available from: https://assets.thermofisher.com/TFS-Assets/LSG/manuals/MesenProRSM_man.pdf.
482. Promega. *CellTox™ Green Cytotoxicity Assay*. 2015 06/01/2019]; Available from: file:///Users/eseellehendow/Downloads/celltox-green-cytotoxicity-assay-protocol.pdf.
483. Thermofisher. *PrestoBlue™ Cell Viability Reagent*. Cell Viability Kits 06/01/2019]; Available from: https://www.thermofisher.com/order/catalog/product/A13261.
484. Liu, K.M., et al., *Measurement of the adhesion between single melamine-formaldehyde resin microparticles and a flat fabric surface using AFM. .* Journal of Adhesion Science and Technology, 2013. **27**(9): p. 973–987.
485. van Zwol, P.J., et al., *Roughness of Microspheres for Force Measurements* Langmuir, 2008 **24**: p. 7528-7531.
486. Hu, Z., et al., *Fluorescent stereo microscopy for 3D surface profilometry and deformation mapping.* Optics Express, 2013. **21**(10): p. 11808-11818.
487. Fearnley , G.W., et al., *Vascular Endothelial Growth Factor A-Stimulated Signaling from Endosomes in Primary Endothelial Cells.* Methods in Enzymology, 2014. **535**: p. 265-292.
488. Mor, F., F.J. Quintana, and I.R. Cohen, *Secreted by Activated T Cells and Induces Is Angiogenesis-Inflammation Cross-Talk: Vascular Endothelial Growth Factor Th1 Polarization.* Journal of Immunology, 2004. **172**: p. 4618-4623.
489. Beckermann, B.M., et al., *VEGF expression by mesenchymal stem cells contributes to angiogenesis in pancreatic carcinoma.* British Journal of Cancer, 2008. **99**: p. 622-631.
490. Das, H., et al., *Stem cell therapy with overexpressed VEGF and PDGF genes improves cardiac function in a rat infarct model.* PloS one, 2009. **4**(10): p. e7325.
491. Gerecht-Nir, S. and J. Itskovitz-Eldor, *Cell therapy using human embryonic stem cells.* Transpl Immunol, 2004. **12**(3-4): p. 203–209.

492. Bethesda, M. *Use of Genetically Modified Stem Cells in Experimental Gene Therapies*. *Stem Cell Information* 2016 18/11/18]; Available from: www.stemcells.nih.gov/info/Regenerative_Medicine/2006Chapter4.htm.
493. Hodgkinson, C.P., et al., *Genetic engineering of mesenchymal stem cells and its application in human disease therapy.* Human gene therapy, 2010. **21**(11): p. 1513-1526.
494. Niu, J., et al., *Monocyte Chemotactic Protein (MCP)-1 Promotes Angiogenesis via a Novel Transcription Factor, MCP-1-induced Protein (MCPIP).* The journal of biological chemistry, 2008. **283**(21): p. 14542–14551.
495. Hayashi, Y., et al., *CXCL14 and MCP1 are potent trophic factors associated with cell migration and angiogenesis leading to higher regenerative potential of dental pulp side population cells* Stem Cell Research & Therapy, 2015. **6**(111): p. 1-19.
496. Boomsma, R.A. and D.L. Geenen, *Mesenchymal stem cells secrete multiple cytokines that promote angiogenesis and have contrasting effects on chemotaxis and apoptosis. PLoS One* . 2012. **7**(4): p. e35685.
497. Jin, H.J., et al., *Senescence-Associated MCP-1 Secretion Is Dependent on a Decline in BMI1 in Human Mesenchymal Stromal Cells. . Antioxid Redox Signal*, 2016 **24**(9): p. 471-485.
498. Salcedo, R., et al., *Human endothelial cells express CCR2 and respond to MCP-1: direct role of MCP-1 in angiogenesis and tumor progression* Blood, 2000. **96**(1): p. 34-40.
499. Hee Hong, K., J. Ryu, and K. Hoon Han, *Monocyte chemoattractant protein-1–induced angiogenesis is mediated by vascular endothelial growth factor-A* Blood, 2005. **105**: p. 1405-1407.
500. Kocan, B., et al., *Trophic Activity and Phenotype of Adipose Tissue-Derived Mesenchymal Stem Cells as a Background of Their Regenerative Potential.* Stem cells international, 2017. **2017**: p. 1653254.
501. Sorensen, D.R. and T.A. Read, *Delivery of endostatin in experimental cancer therapy.* International journal of experimental pathology, 2002. **83**(6): p. 265-274.
502. Ikenaka, Y., et al., *Tissue inhibitor of metalloproteinases-1 (TIMP-1) inhibits tumor growth and angiogenesis in the TIMP-1 transgenic mouse model.* Int J Cancer. , 2003. **105**(3): p. 340-346.
503. Ren , J.G., C. Ji e, and C. Talbo t, *How PEDF prevents angiogenesis: a hypothesized pathway.* Medical Hypothesis, 2005. **64**(1): p. 74-78.
504. Cai, J., W.G. Jiang, and M. Boulton, *Pigment Epithelium-derived Factor Inhibits Angiogenesis via Regulated Intracellular Proteolysis of Vascular Endothelial Growth Factor Receptor 1.* The Journal of Biological Chemistry, 2005. **281**(6): p. 3604 – 3613.

505. He, X., et al., *PEDF and its roles in physiological and pathological conditions: implication in diabetic and hypoxia-induced angiogenic diseases. Clinical science (London, England : 1979)*, 2015. **128**(11): p. 805-823.
506. Mavria, G., et al., *ERK-MAPK signalling opposes Rho-kinase to promote endothelial cell survival and sprouting during angiogenesis.* Cancer Cell, 2006. **9**: p. 33-44.
507. Timmons, J., et al., *Aquaform® hydrogel — a new formulation for an improved wound care performance.* Wounds UK, 2008. **4**: p. 69-73.
508. Williams, C., *Granugel: hydrocolloid gel. .* British Journal of Nursing, 1996. **5**(3): p. 188-190.
509. Convatec. *GranuGEL GEL*. Wounds 2019 19/11/18]; Available from: https://www.convatec.co.uk/wound-skin/duoderm-dressings/granugel/.
510. Doucet, J., et al., *Advances in Degradable Embolic Microspheres: A State of the Art Review.* J. Funct. Biomater., 2018. **9**(24): p. 1-24.
511. Gaetani, R., J. Ungerleider, and K.L. Christman, *Acellular Injectable Biomaterials for Treating Cardiovascular Disease Author links open overlay panel*, in *Stem Cell and Gene Therapy for Cardiovascular Disease*. 2016. p. 309-325.
512. Chen, F.M. and X. Liu, *Advancing biomaterials of human origin for tissue engineering.* Progress in polymer science 2015. **53**: p. 86-168.
513. Fathi, A., et al., *Elastin based cell-laden injectable hydrogels with tunable gelation, mechanical and biodegradation properties.* Biomaterials, 2014. **35**(21): p. 5425-5435.
514. Phan, J., et al., *Engineering mesenchymal stem cells to improve their exosome efficacy and yield for cell-free therapy.* Journal of Extracellular Vesicles, 2018. **7**(1): p. 1-11.
515. Vizoso, F.J., et al., *Mesenchymal Stem Cell Secretome: Toward Cell-Free Therapeutic Strategies in Regenerative Medicine.* Internation Journal of Molecular Sciences, 2017. **18**(1852): p. 1-24.
516. Lloyd , C.M., et al., *Three-colour fluorescence immunohistochemistry reveals the diversity of cells staining for macrophage markers in murine spleen and liver.* 2008. **334**(1-2): p. 70-81.
517. Lefkowitch, J.H.H., J.H.Regent, N., *Kupffer Cell Aggregation and Perivenular Distribution in Steatohepatitis. Modern Pathology*, 2002. **15**: p. 699 – 704.
518. Salazar-Mather, T.P., J.S. Orange, and C.A. Biron, *Early Murine Cytomegalovirus (MCMV) Infection Induces Liver Natural Killer (NK) Cell Inflammation and Protection Through Macrophage Inflammatory Protein 1a (MIP-1a)–dependent Pathways.* J. Exp. Med, 1998. **187**(1): p. 1–14.
519. Andrews, D.M., et al., *NK1.1+ Cells and Murine Cytomegalovirus Infection: What Happens In Situ?* The Journal of Immunology, 2001. **166**: p. 1796–1802.

520. Zhou, Y., et al., *Different distributions of M1 and M2 macrophages in a mouse model of laser-induced choroidal neovascularization. .* Molecular medicine reports 2017. **15**(6): p. 3949-3956.
521. Jablonski, K.A., et al., *Novel Markers to Delineate Murine M1 and M2 Macrophages.* PLoS ONE 2015. **10**(12): p. e0145342.
522. Raes, G., et al., *Differential expression of FIZZ1 and Ym1 in alternatively versus classically activated macrophages.* J Leukoc Biol, 2002. **71**: p. 597–602.
523. Xaus , J., et al., *The Expression of MHC Class II Genes in Macrophages Is Cell Cycle Dependent.* J Immunol, 2000. **165**(11): p. 6364-6371.
524. Rőszer, T., *Understanding the Mysterious M2 Macrophage through Activation Markers and Effector Mechanisms.* Mediators of inflammation, 2015: p. 816460.
525. Patel, U., et al., *Macrophage polarization in response to epigenetic modifiers during infection and inflammation.* Drug discovery today, 2016. **22**(1).
526. Al-Maawi , S., et al., *In vivo cellular reactions to different biomaterials—Physiological and pathological aspects and their consequences Author links open overlay panel.* Seminars in Immunology, 2017. **29**: p. 49-61.
527. Beyer, S., et al., *An In Vitro Model of Angiogenesis during Wound Healing Provides Insights into the Complex Role of Cells and Factors in the Inflammatory and Proliferation Phase.* International Journal of Molecular Science, 2018. **19**(2913).
528. Lopatina, T., et al., *Platelet-derived growth factor regulates the secretion of extracellular vesicles by adipose mesenchymal stem cells and enhances their angiogenic potential.* Cell, Communication and Signalling, 2014. **12**(26).
529. Jia, P.R., *Co-administration of PDGF-BB and VEGF with bladder acellular matrix enhance smooth muscle regeneration and vascularization for bladder augmentation in a rabbit model.* The Journal of Cell Therapy, 2018. **20**(5): p. 88.
530. Manickam, S.S. and J.R. McCutcheon, *Characterization of polymeric nonwovens using porosimetry, porometry and X-ray computed tomography.* Journal of Membrane Science, 2012. **407-408**: p. 108-115.
531. Pradanos, L.P. and C.A. Hernandez, *Porosity measurements by a gas penetration method and other techniques applied to membrane characterization.* Thin Solid Films, 1999. **248**(1-2): p. 22-29.
532. Svoboda, K.K. and W.R. Reenstra, *Approaches to studying cellular signaling: a primer for morphologists.* The Anatomical record 2002. **269**(2): p. 123-139.
533. Gitter, A. and Z. Bar-Joseph, *Identifying proteins controlling key disease signaling pathways. .* Bioinformatics 2013. **29**(13): p. 227-236.
534. Nijman, S.M., *Functional genomics to uncover drug mechanism of action.* <h4 aria-expanded="false" aria-haspopup="true" class="content_header send_to align_right jig-ncbipopper" data-jigconfig="triggerPosition:'bottom center', destPosition : 'top center',destSelector : '#send_to_menu', hasArrow : false, openEvent : 'click',closeEvent : 'click', isTriggerElementCloseClick: false, addCloseButton:true,

groupName: 'entrez_pg', adjustFit:'none'" id="sendto" role="button" style="font-size: 1em; margin: 0px 0.2em 1.1em 0px; color: rgb(89, 51, 31); text-align: right; float: right;">Nat Chem Biol ogy, 2015. **11**(12): p. 942-948.

535. He, J., et al., *Hypoxic adipose mesenchymal stem cells derived conditioned medium protects myocardial infarct in rat.* Eur Rev Med Pharmacol Sci., 2015. **19**(22): p. 4397-406.
536. Fotia, C., et al., *Hypoxia enhances proliferation and stemness of human adipose-derived mesenchymal stem cells.* Cytotechnology. , 2015. **67**(6): p. 1073-1084.
537. Feng, Y.Z., M . Dangelmajer, S . Lee, Y.M . Wijesekera, O . Castellanos, C.X . Denduluri, A . Chaichana, K.L . Li, Q . Zhang, H . Levchenko, A . Guerrero-Cazares, H . Quiñones-Hinojosa, A . *Hypoxia-cultured human adipose-derived mesenchymal stem cells are non-oncogenic and have enhanced viability, motility, and tropism to brain cancer.* Cell Death Dis., 2014. **11**(5): p. e1567.
538. Liu, L., et al., *Hypoxia preconditioned human adipose derived mesenchymal stem cells enhance angiogenic potential via secretion of increased VEGF and bFGF.* Cell Biol Int. , 2013. **37**(6): p. 551-560.
539. Cao, J., et al., *In Vivo Tracking of Systemically Administered Allogeneic Bone Marrow Mesenchymal Stem Cells in Normal Rats through Bioluminescence Imaging. . Stem cells international*, *2016*: p. 3970942.
540. Mousavinejad, M., P.W. Andrews, and E.K. Shoraki, *Current Biosafety Considerations in Stem Cell Therapy.* Cell journal, 2016. **18**(2): p. 281-287.